	METRIC/SI (ENGLISH)
NASA TECHNICAL HANDBOOK Office of the NASA Chief Engineer	NASA-HDBK-4002B
	Approved: 2022-06-07 Superseding NASA-HDBK-4002A

MITIGATING IN-SPACE CHARGING EFFECTS—A GUIDELINE

Trade names and trademarks are used in this NASA Technical Handbook for identification only. Their usage does not constitute an official endorsement, either expressed or implied, by NASA.

APPROVED FOR PUBLIC RELEASE – DISTRIBUTION IS UNLIMITED

DOCUMENT HISTORY LOG

Status	Document Revision	Change Number	Approval Date	Description
Baseline			1999-02-17	Initial Release
Revision	A		2011-03-03	General Revision: Merged NASA TP-2361 and NASA-HDBK-4002; reorganized and changed/updated particular design rules and recommendations; added solar array design rules; enhanced appendices with simple surface charging equations; enhanced environments descriptions and equations; and added index.
Revision	B		2022-06-07	Significant changes were made to this NASA Technical Handbook. It is recommended that it be reviewed in its entirety before implementation. Key changes: Updated many figures including Figures 1 and 2; corrected typos and errors in equations and tables; improved statistical details for the environmental descriptions; clarified the explanations based on inputs and questions on the previous version; and added the knowledge checks.

FOREWORD

This NASA Technical Handbook is published by the National Aeronautics and Space Administration (NASA) as a guidance document to provide engineering information; lessons learned; possible options to address technical issues; classification of similar items, materials, or processes; interpretative direction and techniques; and any other type of guidance information that may help the Government or its contractors in the design, construction, selection, management, support, or operation of systems, products, processes, or services.

This NASA Technical Handbook applicable to NASA Headquarters and NASA Centers, including Component Facilities and Technical and Service Support Centers. It may also apply to the Jet Propulsion Laboratory (a Federally Funded Research and Development Center), other contractors, recipients of grants, cooperative agreements, or other agreements only to the extent specified or referenced in applicable contracts, grants, or agreements.

This NASA Technical Handbook establishes a common framework for consistent practices across NASA programs. Its contents are equally applicable to any spacecraft. It was developed to address the concerns associated with the in-flight buildup of charge on internal spacecraft components and on external surfaces related to space plasmas and high-energy electrons and the consequences of that charge buildup. This NASA Technical Handbook is not a substitute for engineering expertise but is instead meant to serve as a guide. Simply applying guidelines in this NASA Technical Handbook for a specific mission does not make good requirements. Tailoring the guidelines for a specific mission by an ESD expert is essential for good requirements. Failure to properly take into account spacecraft charging concerns has been found to significantly contribute to the loss of spacecraft functions and indeed loss of the entire vehicle.

Requests for information should be submitted via “Feedback” at https://standards.nasa.gov. Requests for changes to this NASA Technical Handbook should be submitted via MSFC Form 4657, Change Request for a NASA Engineering Standard.

Original Signed by Adam West for — **June 7, 2022**

Ralph R. Roe, Jr.
NASA Chief Engineer

Approval Date

TABLE OF CONTENTS

SECTION		PAGE
DOCUMENT HISTORY LOG		**2**
FOREWORD		**3**
TABLE OF CONTENTS		**4**
LIST OF APPENDICES		**6**
LIST OF FIGURES		**6**
LIST OF TABLES		**8**
1.	**SCOPE**	**10**
1.1	Purpose	14
1.2	Applicability	14
2.	**APPLICABLE DOCUMENTS**	**15**
3.	**ACRONYMS, ABBREVIATIONS, SYMBOLS, AND DEFINITIONS**	**15**
3.1	Acronyms, Abbreviations, and Symbols	15
3.2	Definitions	23
4.	**INTRODUCTION TO PHYSICS OF CHARGING AND DISCHARGING**	**26**
4.1	Physical Concepts	26
4.1.1	Plasma	26
4.1.2	Penetration	28
4.1.3	Charge Deposition	30
4.1.4	Conductivity	31
4.1.5	Breakdown Voltage	32
4.1.6	Dielectric Constant	33
4.1.7	Electron Fluxes (Fluences) at Breakdown	34
4.2	Electron Environment	36
4.2.1	Units	37
4.2.2	Substorm Environment Specifications	38
4.3	Modeling Spacecraft Charging	39
4.3.1	The Physics of Surface Charging	39
4.3.2	The Physics of Dielectric Charging	41
4.4	Discharge Characteristics	42
4.4.1	Dielectric Surface Breakdowns	43
4.4.2	Buried (Internal) Charge Breakdowns	45

TABLE OF CONTENTS (Continued)

SECTION		PAGE
4.4.3	Spacecraft-to-Space Breakdowns	45
4.5	Coupling Models	45
4.5.1	Lumped-Element Modeling (LEM)	46
4.5.2	Electromagnetic Coupling Models	46
4.5.3	Coupling onto Wires into Internal Electronics	46
5.	**SPACECRAFT DESIGN GUIDELINES**	**47**
5.1	Processes	48
5.1.1	Introduction	48
5.1.2	Design	50
5.1.3	Analysis	50
5.1.4	Test and Measurement	50
5.1.5	Inspection	51
5.2	Design Guidelines	51
5.2.1	General ESD Design Guidelines for Space Charging	52
5.2.2	Surface ESD Design Guidelines, Excluding Solar Arrays	64
5.2.3	Internal ESD Design Guidelines	66
5.2.4	Solar Array ESD Design Guidelines	69
5.2.5	Special Situations ESD Design Guidelines	78
6.	**SPACECRAFT TEST TECHNIQUES**	**85**
6.1	Test Philosophy	85
6.2	Simulation of Parameters	87
6.3	General Test Methods	88
6.3.1	ESD-Generating Equipment	88
6.3.2	Methods of ESD Application	92
7.	**CONTROL AND MONITORING TECHNIQUES**	**101**
7.1	Active Spacecraft Charge Control	101
7.2	Environmental and Event Monitors	102
8.	**MATERIAL NOTES AND TABLES**	**103**
8.1	Dielectric Material List	103
8.2	Conductor Material List	106

LIST OF APPENDICES

APPENDIX		PAGE
A	The Space Environment	108
B	Environment, Electron Transport, and Spacecraft Charging Computer Codes	136
C	Internal Charging Analyses	147
D	Test Methods	153
E	Voyager SEMCAP Analysis	167
F	Simple Approximations: Spacecraft Surface Charging Equations	168
G	Derivation of Rule Limiting Open Circuit Board Area	171
H	Expanded Worst-Case Geosynchronous Earth Environments Descriptions	174
I	References	176
J	Index	201

LIST OF FIGURES

FIGURE		PAGE
1	Earth Regimes of Concern for On-Orbit Surface Charging Hazards for Spacecraft Passing Through Indicated Latitude and Altitude Based on DMSP and Freja Observations, et al	12
2	Earth Regimes of Concern for On-Orbit Internal Charging Hazards for Spacecraft with Circular Orbits, the Charging Flux under 30 mil Al Shielding is Plotted	12
3	Illustration of a Simple Plasma	28
4	Plasma Interactions with Spacecraft Surfaces, Refer to Section 4.3.1 for Terminologies	28
5	Electron/Proton Continuous-Slowing-Down Approximation (CSDA) Ranges in Aluminum	29
6	Internal Charging, Illustrated	30
7	Example of Lichtenberg Figure by ESD	31
8	(a) IESD Hazard Levels versus Electron Flux (Various Units) and (b) Point Form of Ohm's Law in Eq. 3	35
9	Suggested Worst-Case Geostationary Integral Electron Flux Environment	37
10	Permissible Area versus Depth to Ground or Ground-Referenced Plane. Two lines corresponding to dielectric strengths of 10^6 V/m and 10^7 V/m are shown.	69
11	Examples of Solar Array Failure	71
12	Measured Gallium Arsenide (GaAs) Coupon I/V Failure Threshold.	72

LIST OF FIGURES (Continued)

FIGURE		PAGE
13	Measured Silicon (Si) Coupon I/V Failure Threshold	72
14	An Intercell Gap	74
15	Grouting Barrier to Stop Arcs	74
16	GaAs Coupon with RTV Barrier Installed	74
17	Si Coupon with RTV Barrier Installed	74
18	NASA Lewis Research Center (LeRC) (now Glenn Research Center [GRC]) Solar Array Space Charging and ESD Test Setup	78
19	Electron Trajectories for Galileo	83
20	MIL-STD-1541A Arc Source	90
21	Typical RF-Radiated Fields from MIL-STD-1541A Arc Sources	93
22	Paths for ESD Currents Through Structure	94
23	Examples of System-Level ESD Test Waveforms; (a) Direct Measurement with Very Short Leads on Its Output and (b) Measurement during a System-Level Test with 9 Meters of Attachment Wiring (Two 4.5 m Lengths)	98
24	Dielectric Time Constant Based on Resistivity and Dielectric Constant	106
25	Occurrence Frequencies of Geosynchronous Plasma Parameters (NASA-TP-2361)	120
26	Suggested Time History for Simulating a Substorm (NASA-TP-2361)	120
27	(a) Average Flux at Geosynchronous Orbit for E >2 MeV Electrons as Measured by the GOES Spacecraft over ~One Solar-Cycle (1986-1995) and (b) Average Differential Flux for 1.8–3.5 MeV Electrons Measured by LANL between 1989 and 2018 (Reeves, 2020)	122
28	Observed Smoothed Sunspot Numbers for (a) 1986–1995 and (b) 1989-2018 (Reeves, 2020)	122
29	L-Shell Values (Units of Earth Radii) Around Earth's Equator (0° Latitude) versus East Longitude	123
30	AE8 >0.5 MeV Daily Electron Fluence and CRRESRAD Annual Dose Caused by >1 MeV Electrons Plotted as Functions of Satellite East Longitude at 6.6 Re for the AE8 (>0.5 MeV) and CRRESRAD (>1 MeV) Models	123
31	Cumulative Probability of Occurrence of GOES-7 E >2 MeV Electron Fluxes for Several Different Assumptions	124
32	Schematic of Earth's Radiation Belts as Estimated by the AE8 and AP8 Models; Contours are for E >1 MeV Electrons and E >10 MeV Protons for 0° Longitude	127
33	Example of Nascap-2k Input Aurora Environment, DMSP Aurora Charging Case is Shown	129

LIST OF FIGURES (Continued)

FIGURE		PAGE
34	Solar Wind Parameters for a CME and a High-Speed Stream versus Time as Measured by the Ulysses Spacecraft	131
35	1-Hour Averaged Solar Wind Particle Spectra Based on Measurements Made by the Ulysses Spacecraft for Environments of Various Probability	131
36	1 MeV Electron Omnidirectional Flux Contours for Earth, Jupiter, and Saturn	135
37	Simple Charging Example	150
38	Typical Electron Beam Test Facility Setup	154
39	Testing for Breakdown Voltage	156
40	Testing for Volume Resistivity	157
41	Electron Beam Test for Resistivity	159
42	Non-Contacting Voltage Decay Resistivity Test	160
43	RC Time Constant	161
44	Determining Material Time Constant	162
45	V_{zap} Test Configuration	163
46	Typical Results for V_{zap} Test Showing Lines of Minimum Damage Threshold for Given Parameters (the Resistances of R2 in Figure 45)	164
47	MIL-STD-1541A Pulse Source for Transient Testing	165
48	Permissible Open Area of a Circuit Board Material versus Depth to a Ground Plane or Power Plane (Preferred) or Other Circuit Traces When Threshold Energy is 1 µJ and the Dielectric Constant is 4.7	173

LIST OF TABLES

TABLE		PAGE
1	90^{th} Percentile Geosynchronous Plasma Environment	39
2	Examples of Different Magnitudes of Surface ESD Event Parameters	45
3	Examples of Surface Coatings and Materials Acceptable for Spacecraft Use	58
4	Surface Coatings and Materials to be Avoided for Spacecraft Use	59
5	Examples of Estimated Space-Generated ESD Spark Parameters	88
6	Examples of Several ESD Sources	89
7	Dielectric Material Characteristics for Internal Charging Studies	105
8	Conductor Characteristics for Charging Studies (Approximate)	106

LIST OF TABLES (Continued)

TABLE		PAGE
9	Average Parameters from Referenced Spacecraft	118
10	Standard Deviations	119
11	Characteristics of the Solar Wind at 1 AU in the Ecliptic Plane	130
12	Nominal Solar Wind Plasma Environments	132
13	The Magnetospheres of Earth, Jupiter, and Saturn	132
14	Representative Charging Levels (Volts) at Earth, Jupiter, and Saturn Based on a Simple Charging Design Tool	134
15	Properties of the Major Transport Codes	144
16	Worst-Case Geosynchronous Environments	175

MITIGATING IN-SPACE CHARGING EFFECTS—A GUIDELINE

1. SCOPE

Spacecraft charging is known to be a potential source of serious damage to spacecraft systems and has even been blamed for total spacecraft loss. This NASA Technical Handbook is intended to describe conditions under which spacecraft charging might be an issue, generally explain why the problem exists, list typical design solutions, and provide an introduction to the process by which design specifics should be resolved.

This NASA Technical Handbook is also intended to be an engineering tool and is written at the graduate engineering level for use by aerospace engineers, system designers, program managers, and others concerned with space environment effects on spacecraft. Much of the environmental data and material response information has been adapted from published and unpublished scientific literature for use in this NASA Technical Handbook. As it is not possible to place all the necessary knowledge into one document, this NASA Technical Handbook should be used as a preliminary reference and/or checklist only. Its primary intent is to identify if spacecraft charging is an issue for a particular mission and suggest steps to mitigate its effects.

Spacecraft charging, defined as the buildup of charge in and on spacecraft materials, is a significant phenomenon for spacecraft in certain Earth and other planetary environments. Design for control and mitigation of surface charging, the buildup of charge on the exterior surfaces of a spacecraft related to space plasmas, was treated in detail in NASA-TP-2361, Design Guidelines for Assessing and Controlling Spacecraft Charging Effects (1984). Design for control and mitigation of internal charging, the buildup of charge on the interior parts of a spacecraft from higher energy particles, was treated in detail in the original version of NASA-HDBK-4002, Avoiding Problems Caused by Spacecraft On-Orbit Internal Charging Effects (1999). NASA-HDBK-4002 was written as a companion document to NASA-TP-2361. In 2011, the previous version of this NASA Technical Handbook, NASA-HDBK-4002A, combined NASA-STD-4002 and NASA-TP-2361 with some further improvements. This NASA Technical Handbook is a companion document to NASA-STD-4005, Low Earth Orbit Spacecraft Charging Design Standard.

Since the previous version, NASA-HDBK-4002A, there have been developments in the understanding of spacecraft charging issues and mitigation solutions, as well as advanced technologies needing new mitigation solutions. Those new developments were the motivation for this revision. Also, there have been many inputs and questions from the readers on the previous version. To address those, the typographical errors and errors in equations and tables are corrected, many figures are updated, and the statistical details for the environmental descriptions are improved. As in the heritage documents, the story still has unfinished business; and the proper way to address design issues for a specific spacecraft is to have skilled, ESD-knowledgeable engineers as part of the design team for those programs and missions where space charging is an issue.

This NASA Technical Handbook documents engineering guidelines and design practices to be used by NASA and other spacecraft designers to minimize the detrimental effects of spacecraft surface and internal charging in certain space environments. Section 4 contains space charging/ESD background and orientation; section 5 contains design guidelines; and section 6 contains spacecraft test techniques. The appendices are a collection of useful material intended to support the main body of the document, including a set of generic design requirements. Rather than an all-encompassing guideline or research report, this NASA Technical Handbook is a narrowly focused snapshot of existing technology and does not include some related technologies or activities as further clarified in what follows.

In-space charging effects are caused by interactions between the in-flight plasma and high-energy particle environments and spacecraft materials and electronic subsystems. Possible detrimental effects of spacecraft charging include disruption of or damage to subsystems (power, navigation, communications, instrumentation, etc.) because of charge buildup and ESD as a result of the spacecraft's passage through the space plasma and high-energy particle environments. Charged surfaces can also attract contaminants, affecting thermal properties, optical instruments, and solar arrays and can change particle trajectories, thus affecting plasma-measuring instruments. NASA-RP-1375, Failures and Anomalies Attributed to Spacecraft Charging, lists and describes examples of spaceflight failures caused by inadequate designs.

Figure 1, Earth Regimes of Concern for On-Orbit Surface Charging Hazards for Spacecraft Passing Through Indicated Latitude and Altitude Based on Defense Meteorological Satellite Program (DMSP) and Freja Observations, and Figure 2, Earth Regimes of Concern for On-Orbit Internal Charging Hazards for Spacecraft with Circular Orbits, the Charging Flux under 30 mil (1 mil=0.001 in) Al Shielding is Plotted, illustrate the approximate regions of concern for charging as defined in this NASA Technical Handbook. Figure 1 is to be interpreted as the worst-case surface charging that may occur in the near-Earth environment. The north/south (N/S) latitudinal asymmetry assumes the magnetic North Pole is tilted as much as possible for this view. Potentials are calculated for an aluminum sphere spacecraft in shadow. The low Earth orbit (LEO) aurora environment used in the Figure 1 calculation is detailed in Appendix A.3.4. Note that at altitudes above 400 km, spacecraft charging can exceed 400-500 V, which has the possibility of generating discharges. The DMSP, the Freja, and other satellites have reported significant charging in the LEO auroral zones many times (as high as -3000 V), and one satellite (ADEOS-II) at an altitude of 800 km experienced total failure due to spacecraft charging (Cooke [1998]; Kawakita and others [2004]; Maejima and others [2004]).

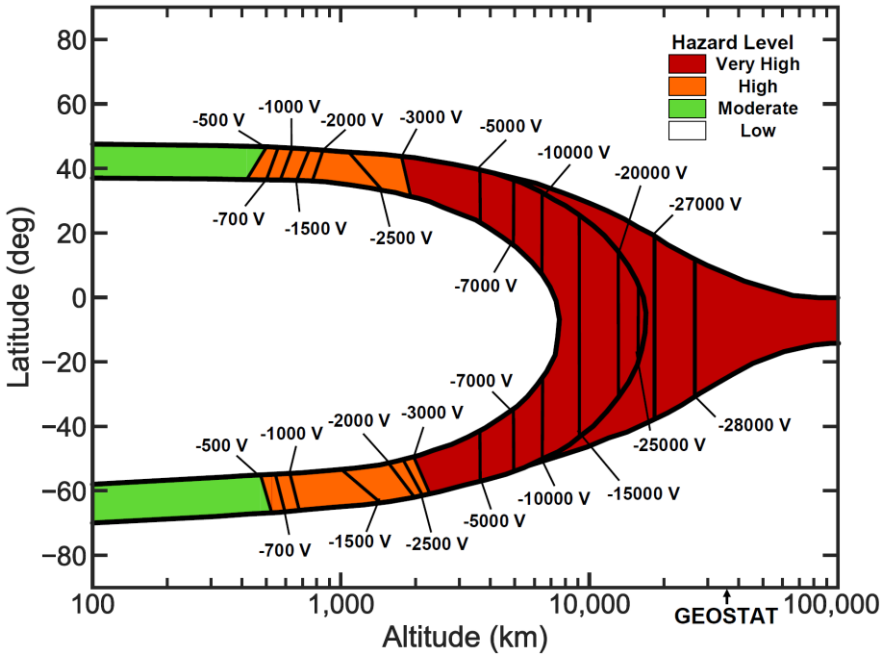

Figure 1—Earth Regimes of Concern for On-Orbit Surface Charging Hazards for Spacecraft Passing Through Indicated Latitude and Altitude Based on DMSP and Freja Observations, et al.

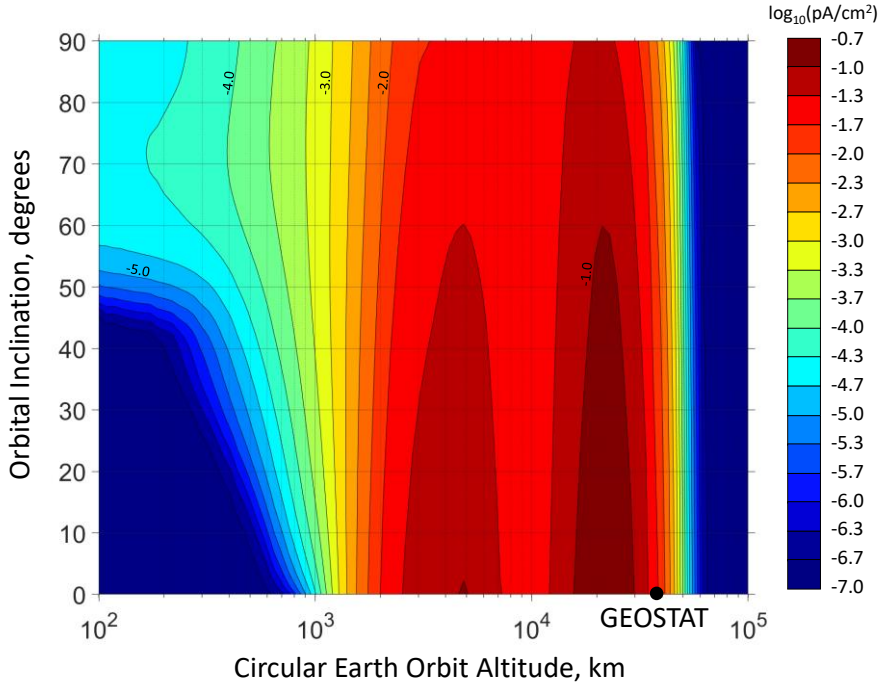

Figure 2—Earth Regimes of Concern for On-Orbit Internal Charging Hazards for Spacecraft with Circular Orbits, the Charging Flux under 30 mil Al Shielding is Plotted

Figure 2, which illustrates Earth's internal charging threat regions, is estimated assuming averages over several orbits since the internal charging threat usually has a longer time scale. The plot reflects the approximate internal charging threat for satellites with the indicated orbital parameters. The average charging flux of a dielectric material (30 mil polyimide was used for the simulations) under 30 mil aluminum spherical shield is plotted. It is intended to illustrate the approximate regions of concern for internal electrostatic discharge (IESD). For actual assessment, the actual shielding, dielectric configuration, and time duration should be considered.

Geosynchronous orbit (GEO), a circular orbit in the equatorial plane of Earth at ~35,786 km altitude, is perhaps the most common example of a region where spacecraft are affected by spacecraft charging; but the spacecraft charging can occur at lower Earth altitudes, Earth polar orbits, Jupiter, and other places where spacecraft can fly.

In this NASA Technical Handbook, the distinction between surface charging and internal charging is defined as follows. Surface charging is a phenomenon which determines the potentials of the spacecraft surfaces directly exposed to space (areas that can be seen and touched on the outside of a spacecraft) through interactions with space plasmas and sunlight. Internal charging is a charging phenomenon which governs all the other potentials due to charge deposition: (1) the potential of the conductors shadowed by the surface layers which are not electrically connected to the surface-exposed conductors and (2) the internal potentials of (surface) exposed dielectrics, and the internal and surface potentials of internal dielectrics. Typically, the time scale of the surface charging (frame potential of spacecraft with respect to plasma) is less than one second (though differential potentials between surfaces can take hours to be established) and that of the internal charging is longer than one hour. The corresponding electron energy range for surface charging is low energy plasma up to a few tens of keV (~50 keV) and that of the internal charging is ~10 keV and higher (the electron below ~10 keV does not contribute much to the internal charging because of its secondary electron emission). (The electrons with energies from 10 keV to a few tens of keV may contribute both to surface and internal chargings, but usually the contributions are not critical.) Surface discharges occur on or near the outer surface of a spacecraft and discharges often have to be coupled to an interior affected site rather than directly to the victim. In that case, energy from surface arcs is attenuated by the coupling factors necessary to get to victims (most often inside the spacecraft) and, therefore, is less of a direct threat to electronics. External wiring, connectors, and antenna feeds, of course, are susceptible to this threat. Internal charging, by contrast, may be caused by energetic particles that can penetrate and deposit charge very close to a victim site, and cause a discharge directly to a victim pin or wire with very little attenuation. As such, internal charging represents a potentially more severe threat to the spacecraft systems.

Internal charging is sometimes called deep dielectric charging or buried charging. Use of the word dielectric can be misleading, since ungrounded (floating) conductors can also present an IESD threat to spacecraft. This NASA Technical Handbook details the methods and designs necessary to mitigate both in-flight surface and internal charging concerns. The physics and design solutions for both are often similar.

1.1 Purpose

The purpose of this NASA Technical Handbook is multifold. First, it serves as a single reference source that contains suggested detailed spacecraft design requirements and procedures to minimize the effects of spacecraft charging and to limit the effects of the resulting ESD. Second, it contains supplementary material and references to aid in understanding and assessing the magnitude of the phenomenon. References to trademarked products and products from specific companies do not constitute endorsement by NASA.

1.2 Applicability

This NASA Technical Handbook applies to Earth-orbiting spacecraft that pass through the hazardous regions identified in Figures 1 and 2 (medium Earth orbit [MEO], LEO, and GEO, with less focus on Polar Earth Orbit [PEO]), as well as spacecraft in other energetic plasma environments such as those at Jupiter and Saturn, and interplanetary solar wind charging environments. Designs for spacecraft with orbits in these regions should be evaluated for the threat of external (surface) and/or internal charging as noted. NASA-RP-1354, Spacecraft Environments Interactions: Protecting Against the Effects of Spacecraft Charging, describes environment interactions mitigation design techniques at an introductory level.

Specifically, this NASA Technical Handbook does not address LEO Spacecraft Charging at orbital inclinations such that the auroral zones are seldom encountered. That region is the purview of NASA-STD-4005 and NASA-HDBK-4006, Low Earth Orbit Spacecraft Charging Design Handbook. This NASA Technical Handbook applies to other regions, including LEO orbits where auroral transits are expected. Additionally, this NASA Technical Handbook does not address design for the control and mitigation of Paschen breakdown, corona discharge, or multipactor phenomena as those topics are the purview of NASA-HDBK-4007, Spacecraft High-Voltage Paschen and Corona Design Handbook. This NASA Technical Handbook is intended to be complementary to NASA-STD-4005, NASA-HDBK-4006, and NASA-HDBK-4007. Note that mitigation techniques for low inclination LEO orbits may differ from those that apply to regions covered by this NASA Technical Handbook. Spacecraft in orbits, such as GEO transfer orbits, that spend time in both regimes, should use mitigation techniques that apply to both regimes. It also does not include such topics as landed assets (lunar or Martian landers) and their electrostatic dust charging, spacecraft sources of charging, such as various types of electric propulsion or plasma sources, International Space Station (ISS)-specific design considerations (these encompass substantially different design concerns that are unique to ISS), solar array-driven charging (see references), magnetic field interactions relating to spacecraft charging (refer to tether and ISS sources for information), Mars-, Venus-, asteroid-, or Moon-specific charging environments, including surface charging environments, plasma contactors in detail (see ISS references), and Extra Vehicular Activity (EVA) needs (see ISS references). Lightning effects are also not included (reference NASA-STD-4010, NASA Standard for Lightning Launch Commit Criteria for Space Flight). This NASA Technical Handbook does not provide specific design advice for pending or future projects. Finally, it does not discuss highly elliptical (Molniya) orbits.

This NASA Technical Handbook is approved for use by NASA Headquarters and NASA Centers, including Component Facilities and Technical and Service Support Centers. It may also apply to the Jet Propulsion Laboratory (JPL) (a Federally Funded Research and Development Center), other contractors, recipients of grants, cooperative agreements, or other agreements only to the extent specified or referenced in their applicable contracts, grants, or agreements.

This NASA Technical Handbook, or portions thereof, may be referenced in contract, program, and other Agency documents for guidance.

This NASA Technical Handbook recommends engineering practices for NASA and other space programs and projects. The major focus is on known energetic space plasma regions (Earth and Jupiter usually), but the principles could be extended for design against triboelectric charging as experienced during a launch, descent through a low-pressure atmosphere, and charging caused by wind-driven dust particles. This NASA Technical Handbook, however, does not include such extensions.

KNOWLEDGE CHECK

1.1 What is the stated purpose of this document, and does it match your purpose?
1.2 What is a definition of spacecraft charging?
1.3 Will this document teach you what you need to be a spacecraft charging expert? Why/why not?
1.4 What are some spacecraft orbits needing ESD controls during design?
1.5 In what sense are Figures 1 and 2 “worst-case” charging environments?
1.6 Is surface charging or internal charging more of an ESD threat?

2. APPLICABLE DOCUMENTS

None.

Appendix I contains all the document references as well as other literature known to the authors as containing useful information.

3. ACRONYMS, ABBREVIATIONS, SYMBOLS, AND DEFINIgTIONS

3.1 Acronyms, Abbreviations, and Symbols

~	approximately
°	degree
>	greater than
<	less than
±	plus or minus
%	percent
λ_D	characteristic distance

Π	Pi
1D	one dimensional
2D	two dimensional
3D	three dimensional
A	ampere (unit of current)
ac	alternating current
ACE	Advanced Composition Explorer
ACR	Anomalous Cosmic Ray
ADEOS-II	Japanese satellite (802.92 km, 98.62°, 101 min), Dec 2002-Oct 2003
AE8	NASA Space Radiation Model for Trapped Electrons
AF	Air Force
AFGL	Air Force Geophysics Laboratory
AFRL	Air Force Research Laboratory
AIAA	American Institute of Aeronautics and Astronautics
Al	aluminum
ALT	altitude
AP8	NASA Space Radiation Model for Trapped Protons
ASTM	formerly meant American Society for Testing Materials. It is not an acronym anymore. Now it is ASTM International.
ATS	Applications Technology Satellite (-5 and -6) geostationary satellites
AU	Astronomical Unit (Earth to Sun distance, ~ 150,000,000 km)
BDD	Burst Detector Dosimeter
bs	backscattered
C	coulomb
CAD	Computer-aided Design
CEASE	Compact Environmental Anomaly Sensor
CGS	centimeter-gram-second
cm	centimeter
CME	Coronal Mass Ejection
CMOS	Complementary Metal-Oxide-Semiconductor
CNES	Centre National d'Etudes Spatiales, the French space agency
CPA	Charged Particle Analyzer
CPE	Charged Particle Environment
CPH	photoelectron current
CREME96	Cosmic Ray Effects on MicroElectronics 1996
CRRES	Combined Release and Radiation Effects Satellite
CRRESELE	CRRES electron flux energy spectrum environmental code
CRRESPRO	CRRES proton flux energy spectrum environmental code
CRRESRAD	CRRES dose versus depth environmental code
CSDA	Continuous Slowing Down Approximation
CTS	Communications Technology Satellite
CXD	Combined X-ray and Dosimeter

d	day
dB	decibel
dc	direct current (zero frequency)
DDD	Displacement Damage Dose
dE/E	Energy channel width (dE) expressed as fraction of nominal median energy (E) for channel
deg	degree
DERA	Defense Evaluation and Research Agency
DESP	Space Environment Department (France)
DICTAT	DERA Internal Charging Threat Analysis Tool
div	division
DMSP	Defense Meteorological Satellite Program (800 km, 99°, 110 min)
DoD	Department of Defense
DUT	Device Under Test
DynaPAC	Dynamic Plasma Analysis Code
E	electric field, energy, East
e	electron (charge = 1.6022×10^{-19} coulomb)
ε	total permittivity $\varepsilon = \varepsilon_0 \times \varepsilon_r$
ε_0	free space permittivity (= 8.85×10^{-12} F/m)
ε_r	relative permittivity or dielectric constant
ECSS	European Cooperation on Space Standardization
EGS	Monte Carlo transport code
EMC	Electromagnetic Compatibility
EMI	Electromagnetic Interference
EMP	Electromagnetic Pulse
EPAM	Electron, Proton, and Alpha Monitor
Eq.	equation
ESA	European Space Agency
ESD	Electrostatic Discharge
EURECA	European Retrievable Carrier
EUV	Extreme UltraViolet
eV	electron volt
EVA	Extra Vehicular Activity
EWB	Environmental WorkBench, no longer supported
F	farad (measure of electrical capacitance)
FEP	fluorinated ethylene propylene
FFRDC	Federally Funded Research and Development Center
FLUMIC	Flux Model for Internal Charging
FR4	flame retardant 4, common printed circuit board material
ft	foot
g	gram
GaAs	gallium arsenide

Galileo	European plan for a GPS-like system of satellites; 23,222 km altitude, 56° inclination
	A NASA spacecraft sent to Jupiter
GCR	Galactic Cosmic Ray
Ge	germanium
Geant4	a particle transport code, the European counterpart to MCNP6
GEO	Geosynchronous Earth Orbit (about 35,786 km/22,236 mi altitude, 24-hr period)
GEOSTA	geostationary
GHz	gigahertz
GIRE	Galileo Interim Radiation Electron environment model for Jupiter
GOES	Geosynchronous Operational Environmental Satellite
GPS	Global Positioning Satellite (constellation, 20,100 km, 55°, 718 min)
GRC	Glenn Research Center (formerly Lewis Research Center)
GSE	Ground Support Equipment (or SE)
GSFC	Goddard Space Flight Center
GUI	Graphical User Interface
H	magnetic field (or B in free space)
	hydrogen
H^+	hydrogen ion
h, hr	hour
H field	Magnetic field (common usage)
HBM	Human Body Model
HDBK	handbook
HEO	Highly Elliptical Orbit, used synonymously for Molniya orbit
HIC	Heavy Ion Counter
HOPE	Helium, Oxygen, Proton, and Electron
Hz	hertz, unit of frequency (1 cycle per second)
I	current (A)
i	differential angular intensity (or flux); (example: ions/(m^2 s sr keV))
I	integral angular intensity (or flux); (example: electrons/(m^2 s sr))
I/V	current versus voltage
IC	Integrated Circuit
IDM	Internal Discharge Monitor (flown on CRRES)
IEEE	Institute of Electrical and Electronics Engineers
IESD	Internal Electrostatic Discharge
in	inch
INTELSAT	International Telecommunications Satellite organization
IR	infrared
IRI	International Reference Ionosphere
ISO	International Standards Organization

ISPICE	A computer transient circuit analysis program; first commercial version of SPICE
ISS	International Space Station (~390 km altitude (varies), 51.6°, 92 min)
ITAR	International Traffic-in-Arms Regulations (restricted access to some information)
ITO	indium tin oxide
ITS	Integrated TIGER Series
J	Joule (unit of energy)
	current per unit area (A/cm^2)
j	omnidirectional differential flux; (example: electrons/(cm^2 s MeV))
J	omnidirectional integral flux; (example: electrons/(cm^2 s))
JAXA	Japanese Space Agency
JPL	Jet Propulsion Laboratory
K	Kelvin
keV	kiloelectron volt (10^3 eV)
kg	kilogram
km	kilometer
kohm	kilohm (10^3 ohm)
kV	kilovolt (10^3 V)
l	length
LANL	Los Alamos National Laboratory
LAT	latitude
LED	Light-Emitting Diode
LEM	Lumped-Element Model
LEO	Low Earth Orbit (about 200-2,000 km altitude; e.g., 657 km, 1.5 hr period)
LeRC	Lewis Research Center (now Glenn Research Center)
LET	Linear Energy Transfer
LNA	Low Noise Amplifier
m	meter, mass, milli
M	mega, million
mA	milliampere (10^{-3} A)
MAG	Magnetic Field Vectors
MagEIS	Magnetic Electron Ion Spectrometer
MCNP	Monte Carlo N-Particle transport code
MCNP6	The current version of MCNP
MCNPX	Monte Carlo N-Particle eXtended
MEO	Medium Earth Orbit (about 2,000-25,000 km altitude, ~6 hr period)
MeV	megaelectron volt
mho	a unit of electrical conductance, the reciprocal of resistance in ohm
MHz	megahertz (frequency, 10^6 Hz)
mil	one one-thousandth of an inch = 0.001 in = 0.0254 mm. Note: although mil is not an SI unit of measure, it is a standard unit of measure

	(unconverted to SI units) often used in this discipline to describe material thickness.
MIL	military
min	minute
mJ	millijoule (10^{-3} J)
MKS	meter-kilogram-second; a physical system of measurement that uses the meter, kilogram, and second as base units, forming the base of the International System of Units
MLI	MultiLayer Insulation (thermal blanket)
mm	millimeter
mohm	milliohm (10^{-3} ohm)
Mohm	megohm (10^{6} ohm)
Molniya	an elliptical orbit (apogee ~39,300 km, perigee 538 km, 11.8 hr period, ~63.2° inclination), HEO is also used synonymously.
MPA	Magnetospheric Plasma Analyzer
MSFC	Marshall Space Flight Center
MUSCAT	Multi Utility Spacecraft Charging Analysis Tool
mV	millivolt
N/S	north/south
nA	nanoampere (10^{-9} A)
NASA	National Aeronautics and Space Administration
NASCAP	NASA/Air Force Spacecraft Charging Analyzer Program, historic and generic
NASCAP/GEO	NASA/Air Force Spacecraft Charging Analyzer Program for Geosynchronous Orbit (replaced by Nascap-2k)
NASCAP/LEO	NASA/Air Force Spacecraft Charging Analyzer Program for Low Earth Orbit
Nascap-2k	latest version of NASCAP (as of 2010)
nC	Nanocoulomb (10^{-9} C)
N_E	electron number density
nF	nanofarad (10^{-9} F)
NGST	Northrop-Grumman Space Technology
N_I	ion number density
nm	nanometer
NMOD	The JPL Neptune Radiation Model
NOAA	National Oceanic and Atmospheric Administration
NOVICE	A charged-particle radiation transport code
ns	nanosecond (10^{-9} s)
NSSDC	National Space Science Data Center
nT	nanotesla (10^{-9} tesla), magnetic field unit
NUMIT	numerical model for estimating internal charging in dielectrics
O	Atomic oxygen
ohm	unit of electrical resistance

ONERA	Office National d'Etudes et Recherches Aérospatiales, the French national aerospace research center
OSR	Optical Solar Reflector
p	proton
pA	picoampere (10^{-12} A)
PC	Printed Circuit
PCU	Plasma Contactor Unit
PEO	Polar Earth Orbit (~80° or higher inclination, 700-1000 km altitude, ~100 min period)
PET	Proton/Electron Telescope
pF	picofarad (10^{-12} F)
photo	photon–emitted particles, e.g., photoelectrons
PIC	Particle In Cell
PIX, PIX-II	Plasma Interactions Experiment
POES	Polar Operational Environmental Satellite (~80° or higher inclination, 700-1000 km altitude)
POLAR	Potential of Large Objects in the Auroral Region
PT	Particle Tracking
PTFE	polytetrafluoroethylene (Teflon®)
Q	charge, coulombs
QA	Quality Assurance
R	resistance (ohm)
rad	a unit of absorbed radiation dose, defined as 1 rad = 0.01 Gy = 0.01 J/kg
RC	resistor-capacitor
R_e	distance compared to Earth's radius (1 R_e ~ 6378.136 km)
R_E	density of electron plasma environment
REPT	Relativistic Electron-Proton Telescope
RF	Radio Frequency
ρ	rho (volume resistivity) (ohm m or ohm cm)
ρ_s	rho-sub s (surface resistivity) (SI unit: ohm; more commonly, "ohm per square")
R_I	density of ion plasma environment
RIC	Radiation-Induced Conductivity
R_j	distance compared to Jupiter's radius (1 R_j ~7.1492 x 10^4 km)
RP	Reference Publication
R_s	distance compared to Saturn's radius (1 R_s ~6.0268 x 10^4 km)
RSICC	Radiation Shielding Information Computational Center
RTV	Room Temperature Vulcanizing
s	second
S	siemens (reciprocal of resistance) (1/R)
σ	sigma (conductivity; units: $(\text{ohm cm})^{-1}$)
s/d	seconds per day (86400)

s/h	seconds per hour (3600)
SAIC	Science Applications International Corporation
SAMPEX	Solar, Anomalous, and Magnetospheric Particle Explorer
SAMPIE	Solar Array Module Plasma Interactions Experiment
SAS	Solar Array Simulator
SATRAD	SATurn RADiation model
SCATHA	Spacecraft Charging at High Altitudes (satellite) (1979-1986, 28,000-42,000 km, 8.3° inclination)
SCMD	Spacecraft Charging Materials Database
SCR	Silicon-Controlled Rectifier
SCTC	Spacecraft Charging Technology Conference
SE	Support Equipment (nonflight hardware) (or GSE)
Sec	secondary emission
SEE	Single Event Effect
	(NASA) Space Environment Effects program
SEISS	Space Environment in Situ Suite
SEMCAP	Specification and Electromagnetic Compatibility Program
SEP	Solar Energetic Particle (or Proton) event
SEU	Single Event Upset
SHIELDOSE	charged-particle radiation transport code
Si	silicon
SI	Système Internationale or metric system of measurement
SOHO	SOlar and Heliospheric Observatory
SOPA	Synchronous Orbit Particle Analyzer (Los Alamos)
SPE	Solar Proton Event
SPENVIS	Space Environment Information System
SPICE	Simulation Program for Integrated Circuit Emphasis, a computer transient circuit analysis program
SPINE	Spacecraft Plasma Interactive Network
SPIS	Spacecraft Plasma Interactive System
sqrt	square root
sr	steradian
SSO	Semi-Synchronous Orbit, ~20,000 km, 12 hr period
STD	standard
SWEPAM	Solar Wind Electron, Proton, and Alpha Monitor
SWPC	Space Weather Prediction Center
t	time, thickness
T	temperature
T_E	temperature for electron plasma environment
T_I	temperature for ion plasma environment
TID	Total Ionizing Dose
TP	Technical Publication

TRACE	Transition Region and Coronal Explorer
TRIM	radiation transport code
TRW	TRW Incorporated (now Northrop Grumman)
TSS-1R	Tethered Satellite System – first re-flight
µ	micro, representing a factor of $x10^{-6}$
µC	microcoulomb (10^{-6} C)
UCSD	University of California at San Diego
µF	microfarad (10^{-6} F)
µJ	microJoule (10^{-6} J)
µm	micrometer (10^{-6} m)
UMOD	The JPL Uranus Radiation Model
µs	microsecond (10^{-6} s)
USA	United States of America
USAF	United States Air Force
UV	ultraviolet
µW	microWatt
v	velocity
V	volt, voltage
V_b	voltage breakdown
V_c	co-rotation velocity of specified region
VDA	Vacuum Deposited Aluminum
W	Watt, West
WDC	World Data Center (NOAA)
yr	year
ZOT	zinc orthotitanate paint

3.2 Definitions

Arrhenius Behavior: An Arrhenius plot displays the logarithm of a reaction rate constant versus the reciprocal of temperature (1/T); adherence to or deviation from a straight line describes an Arrhenius behavior.

Auroral Zone: Geomagnetic latitudes between ~60°-70° north/south (N/S), where auroras are present.

Blow-off: The effect of an ESD when material and charge are expelled by an ESD.

Bonding: The process of providing good electrical connection across faying surface mechanical interfaces to minimize electrical potential differences between equipment and individual parts of structure.

Bulk Resistivity (or Volume Resistivity): A fundamental material property which measures how strongly it resists electric current. It has a unit of ohm m.

Buried Charging: Refers to charging internal to a spacecraft, often meaning within dielectrics, but possibly in floating conductors. The authors prefer the term internal charging.

Conductor: For the purpose of this spacecraft charging document, a conductor is a material that is used for carrying current or is similarly conductive and acting as part of a shield or ground plane structure. Copper and aluminum are typical conductors. See Insulator, Dielectric, and Static-conductive.

Dark Conductivity: The direct current conductivity of a component under no radiation nor light illumination. Reciprocal of volume resistivity.

Debye Length (Debye Radius): Characteristic measure of distance (λ_D) in a plasma for which charge carriers have interaction or significant influence. Over one Debye length, the charges are screened and the electric potential decreases in magnitude by 1/e.

Deep Dielectric Charging: Charging internal to dielectrics caused by energetic electrons. (See the term Buried Charging.) The authors prefer the term internal charging, unless specifically referring to dielectrics.

Dielectric: For the purpose of spacecraft charging, a dielectric is a resistive material that may be synonymous with Insulator. This document suggests dielectrics have a bulk resistivity of $>10^9$ ohm cm or a surface resistivity of $>10^{10}$ ohm/square. See Conductor and Static-conductive.

Faraday Cage: An enclosure used to block electromagnetic fields. Faraday cage may be formed by a continuous covering of conductive material, or by a mesh of conductive materials with the holes smaller than the characteristic dimension of electromagnetic field. In this NASA Technical Handbook, a Faraday cage mostly refers to a continuously covered Faraday shield.

Floating: A conductor is floating if it is ungrounded or has no defined reference to spacecraft ground. (See the term Ground Referenced.)

Geosynchronous/Geostationary Orbit: A circular orbit in the equatorial plane of Earth at ~35,768 km altitude.

Ground Referenced: Not floating, meaning that there is a defined path to structure ground, even if the referenced item is not at zero-volt. For example, the +28-V power line is not grounded, but it is electrically connected to structure ground, and thus it is not floating. It cannot accumulate stray charges.

Grounding: Bonding to a zero-volt reference point (structure ground), often the chassis.

Internal Charging: A charging phenomenon which governs all the potentials due to charge deposition other than surface charging potential: (1) the potential of the conductors shadowed by the surface layers which are not electrically connected to the surface-exposed

conductors and (2) the internal potentials of (surface) exposed dielectrics, and the internal and surface potentials of internal dielectrics.

Isotropic: Having a physical property of uniformity in all orientations/directions.

L1-L5: Unique Lagrange/Libration Points where spacecraft sent there tend to stay put with respect to two massive astronomical objects. At Lagrange points, the gravitational pull of two large masses precisely equals the centripetal force required for a small object to move with them.

Lichtenberg Figure: A branching tree-like feature that appears on the surface or interior of insulating materials that results from electric discharge.

Molniya: An elliptical orbit with an apogee of ~39,300 km, perigee of 538 km, an 11.8 hr period, and a ~63.2° inclination.

Ohm per Square: A unit of surface resistivity. The resistance of a flat, relatively thin sheet of the material, measured from one edge of a square section to the opposite edge. Proper unit is ohm.

Omnidirectional Flux: The flux over all directions not considering the directional distribution of the particles which can be non-isotropic. For isotropic environment, the omnidirectional flux is 4 times the flux to a flat surface. The integration over solid angle is 4π.

Permittivity: The ability of a substance to store electrical energy in an electrical field.

Plasma Ground: A conceptual term for the ambient space plasma that is assumed to be charge neutral. This volume exists outside the local plasma at a distance equal to or larger than the Debye length. This reference volume is considered to be the “space plasma ground” against which the spacecraft absolute potential is measured.

Plasma Sheath: The layer around the spacecraft where plasma’s quasi-neutrality is broken. The thickness of the plasma sheath is several Debye lengths.

Spacecraft Charging: The buildup of charge in and on spacecraft materials; a significant phenomenon for spacecraft in certain Earth and other planetary environments.

Static-Conductive: For the purpose of spacecraft charging, a static-conductive material is one that is adequately conductive to conduct any space plasma charges to ground so that the charging effects have minimal or no impact on spacecraft operations. These are partially resistive materials that are neither conductors nor insulators. There is not an official definition in this document because the proper range is dependent on charging flux and configuration of a static-conductive material, but an approximate range of resistivity for static-conductive materials is less than 10^{10} ohm/square for thin materials and 10^{9} ohm cm for bulk materials. And it has to be

properly grounded to be useful for mitigation of spacecraft charging. See Dielectric and Conductor.

Surface Charging: A phenomenon which determines the potentials of the spacecraft surfaces directly exposed to space through interactions with space plasmas and sunlight.

Triple Junction Point: In this NASA Technical Handbook, refers to a place where a dielectric, a conductor, and space all meet at one point. Intense electric fields may exist and cause ESDs at triple junction points.

Victim: Any part, component, subsystem, or element of a spacecraft that can be adversely affected by an arc discharge (or field effects, in the case of some science instruments).

KNOWLEDGE CHECK

3.1 Are these definitions compatible with your understanding of the needs of this NASA Technical Handbook? If not, please suggest alternatives. Similarly, please send the office of primary responsibility designee acronyms, etc., that you believe should be added (with definition).

4. INTRODUCTION TO PHYSICS OF CHARGING AND DISCHARGING

The fundamental physical concepts that account for space charging are described in this section. Appendix A describes this further with equations and examples. For design guidelines only, see section 5.

4.1 Physical Concepts

Spacecraft charging occurs when charged particles from the surrounding plasma and energetic particle environment stop on the spacecraft, either on the surface, on interior parts, in dielectrics, or in conductors. Other factors affecting charging include biased solar arrays or plasma emitters. Charging can also occur when photoemission occurs; that is, solar photons cause surfaces to emit photoelectrons and when secondary electrons are generated. The variations in potential that occur after that determine whether the charging will cause problems or not.

4.1.1 Plasma

A plasma is a partially ionized gas in which some of the atoms and molecules that make up the gas have some or all of their electrons stripped off leaving a mixture of ions and electrons that can develop a sheath that can extend over several Debye lengths. Except for LEO, where oxygen^{+} (O^{+}) is the most abundant species, the simplest ion, a proton (corresponding to ionized hydrogen, H^{+}) is generally the most abundant ion in the environments considered here. The energy of the plasma, its electrons and ions, is often described in units of electron volts (eV). This is the kinetic energy that is given to the electron or ion if it is accelerated by an electric potential of that many volts. While

temperature (T) is generally used to describe the disordered microscopic motion of a group of particles, plasma physicists also use it as another unit of measure to describe the kinetic energy of the plasma. (Strictly speaking, temperature is only well defined when the plasma can be described by a Boltzmann distribution.) For electrons, numerically T(K) equals T(eV) x 11,604, e.g., 4,300 eV is equivalent to 50 million Kelvin (K).

The kinetic energy of a non-relativistic particle is given by the following equation:

$$\boldsymbol{E = \frac{1}{2} m v^2} \qquad \text{(Eq. 1)}$$

where:

E = kinetic energy (J, 1 J = 6.242 x 10^{18} eV)
m = mass of the particle (kg)
v = velocity of the particle (m/s).

Considering that protons are 1,836 times more massive than electrons, electrons in a plasma in thermal equilibrium generally have a velocity ~43 times that of protons. This translates into a net instantaneous flux or current of electrons onto a spacecraft that is much higher than that of the ions (typically near nA/cm^2 for electrons versus pA/cm^2 for protons at geosynchronous orbit). This difference in flux is one reason for the observed charging effects (a surplus of negative charges on affected regions). For electrons, numerically the velocity (v_e) equals sqrt(E) x 593 km/s and for protons the velocity (v_p) equals sqrt(E) x 13.8 km/s, when E is in eV. For electron with an energy larger than ~100 keV, the relativistic equation instead of Eq. 1 should be used.

Although a plasma may be described by its average energy, there is actually a distribution of energies. The rate of charging in the interior of the spacecraft (e.g., after propagation through shielding) is a function of the flux versus energy, or spectrum, of the plasma at energies well in excess of the mean plasma energies (for GEO, the plasma mean energy may reach a few 10s of keV). While surface charging is usually correlated with electrons in the 0 to ~50 keV energy range, significant internal charging is associated with the high-energy electrons (10 keV and higher) (refer to the definitions of surface charging and internal charging in section 1).

A simple plasma and its interactions with a surface are illustrated in Figure 3, Illustration of a Simple Plasma, and Figure 4, Plasma Interactions with Spacecraft Surfaces, Refer to Section 4.3.1 for Terminologies. The electrons (e^-) and ions (represented by H^+ in Figure 3) are moving in random directions (isotropic) and with different speeds (a spectrum of energies). Figure 4 illustrates surface charging on exterior surfaces. To estimate surface charging, both the electron and ion spectra should be known from 0 to 50 keV. Although fluxes may be directional, omnidirectional fluxes are assumed in this NASA Technical Handbook because
(1) spacecraft orientation relative to the plasma is often not well defined and (2) the pitch angles of "beaming" electrons traveling along magnetic field lines vary over a wide range, even such "beaming" electrons may appear to be quasi-isotropic.

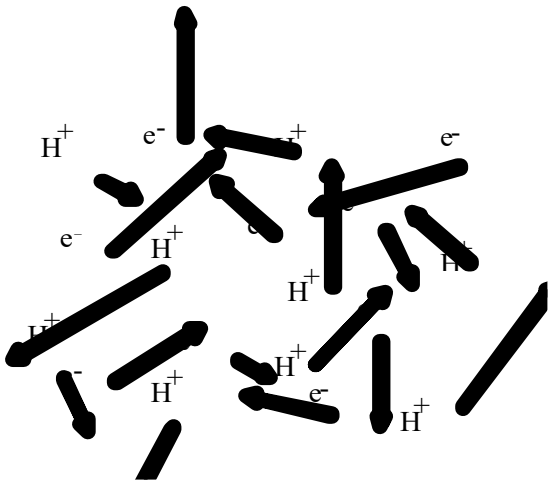

Figure 3—Illustration of a Simple Plasma

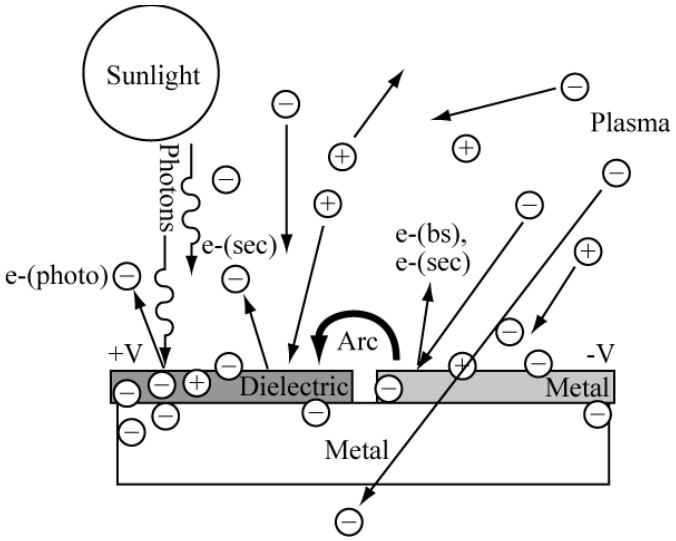

Figure 4—Plasma Interactions with Spacecraft Surfaces, Refer to Section 4.3.1 for Terminologies

4.1.2 Penetration

Electrons and ions will penetrate matter. The depth of penetration of a given species (electron, proton, or other ion) depends on its energy, its atomic mass, and the composition of the target material. Figure 5, Electron/Proton Continuous-Slowing-Down Approximation (CSDA) Ranges in Aluminum, shows the penetration range (through CSDA) versus energy of electrons and protons into aluminum and represents the approximate maximum penetration depth into a slab of aluminum. To first order, only particles with an energy corresponding to a range greater than the spacecraft shield thickness can penetrate into the spacecraft interior. If the material is not aluminum, an equivalent penetration depth is roughly the same number of grams per square centimeter (g/cm^2, also called areal density) of the material's thickness. For a given electron energy, however, the penetration depth of high-Z material is slightly smaller than the penetration depth of low-Z material, which means that high-Z materials (such as tantalum and tungsten) are more effective electron shield material than low-Z materials (such as aluminum).

This NASA Technical Handbook uses the terms surface charging and internal charging. The literature also uses the terms buried dielectric charge or deep dielectric charge for internal charging. These terms are misleading because they give the impression that only dielectrics can accumulate charge. Although dielectrics can accumulate charge and discharge to cause damage, floating conductors can also accumulate charge and also have to be considered an internal charging threat. In fact, the charges in conductors can rapidly be redistributed so that floating conductors can discharge with a higher peak current and a higher rate of change of current than a dielectric and can be a greater threat.

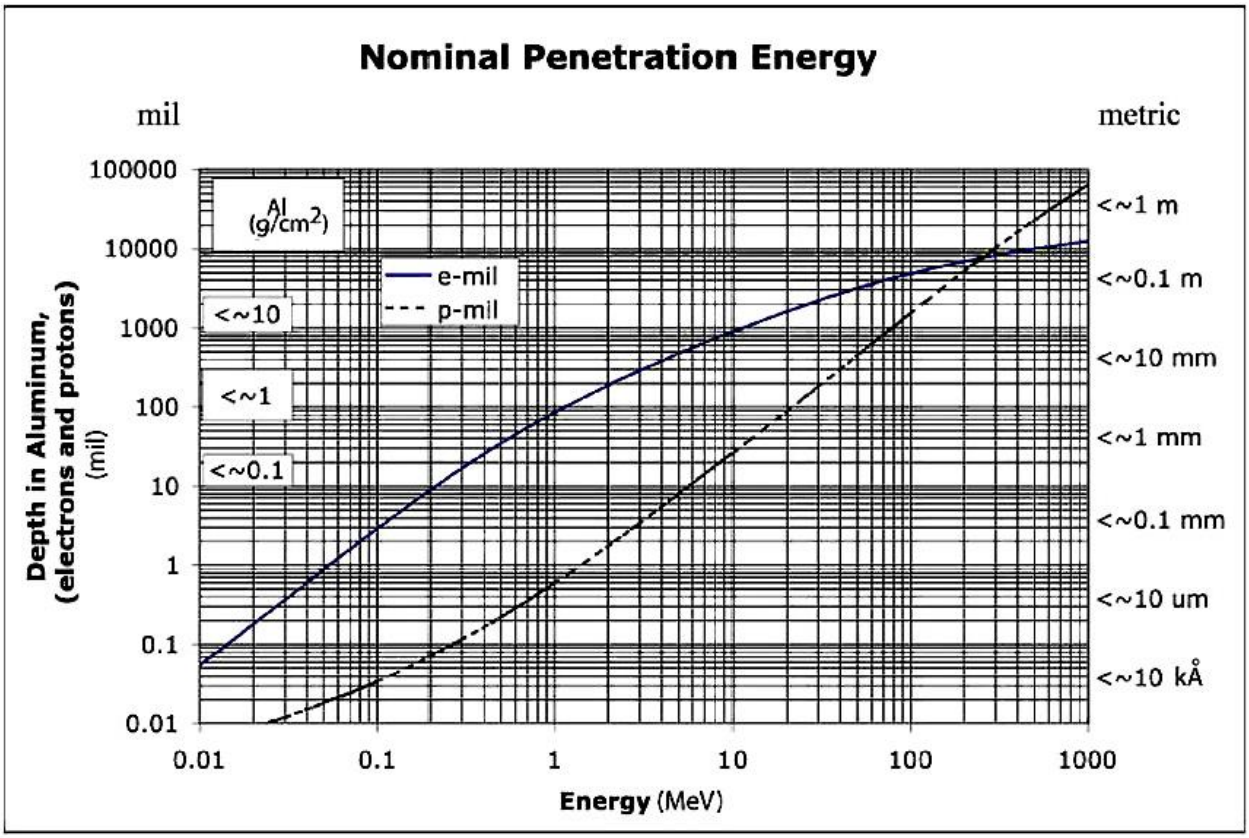

Figure 5—Electron/Proton Continuous-Slowing-Down Approximation (CSDA) Ranges in Aluminum

Notes:

1. Protons stop close to the CSDA range shown, while electrons are deposited in a larger range below the CSDA range.
2. Surface charging: 0 – 50 keV electrons.
3. Overlap between surface and internal chargings: 10 – 50 keV electrons.
4. Internal charging: 10 keV and higher electrons.
5. For GEO orbits, the practical range of interest for internal charging is 100 keV to 1.5 MeV (reference Figure 9), (~3 to 130 mil of aluminum thickness).
6. Data for chart from ESTAR and PSTAR, at https://physics.nist.gov/PhysRefData/Star/Text/ESTAR.html and https://physics.nist.gov/PhysRefData/Star/Text/PSTAR.html.
7. http://mpg.physics.usu.edu/range/, Utah State Electron Range Approximation Tool.

Protons are often not considered for spacecraft charging because the greater impinging flux of electrons at the same energy and (for internal charging) the lesser penetration of protons reduces the internal flux to a negligible amount. Higher atomic mass particles are even less of a threat because of their much lower fluxes.

Because electrons may stop at a depth less than their maximum penetration depth and because the electron spectrum is continuous, the penetration-depth/charging-region will be continuous, ranging

from the charges deposited on the exterior surface to those deposited deep in the interior. Internal charging may happen even "inside the Faraday Cage." For a spacecraft that is built with a Faraday Cage thickness of 30 or more mils of aluminum equivalent, this would mean that internal effects deal with the portion of the electron spectrum above 500 keV and the proton spectrum above 10 MeV. At GEO orbits, the practical range of energy for internal charging is 100 keV to ~1.5 MeV, bounded on the lower end by the fact that most spacecraft have at least 3 mil of shielding (when there is less shielding such as coverglass, lower energy from 10 keV should also be considered) and on the upper end by the fact that, as will be shown later (reference Figure 9), common GEO environments above 1.5 MeV do not have enough particle flux to cause internal charging problems.

Figure 6, Internal Charging, Illustrated, illustrates the concept that energetic electrons will penetrate into interior portions of a spacecraft. Having penetrated, the electrons may be stopped in dielectrics or on floating conductors. If too many electrons accumulate, the resultant high electric fields inside the spacecraft may cause an ESD to a nearby victim circuit. Note that the internal ESD resembles surface ESD with the exception that circuits are rarely exposed victims on the exterior surface of a spacecraft; and with the condition that charging rates are slower, internal ESD results in a greater direct threat to circuits.

The term "ESD" in this document is general, including surface and internal discharges, or may refer only to surface discharges. The term IESD refers to ESDs due to internal charging as defined in Chapter 1.

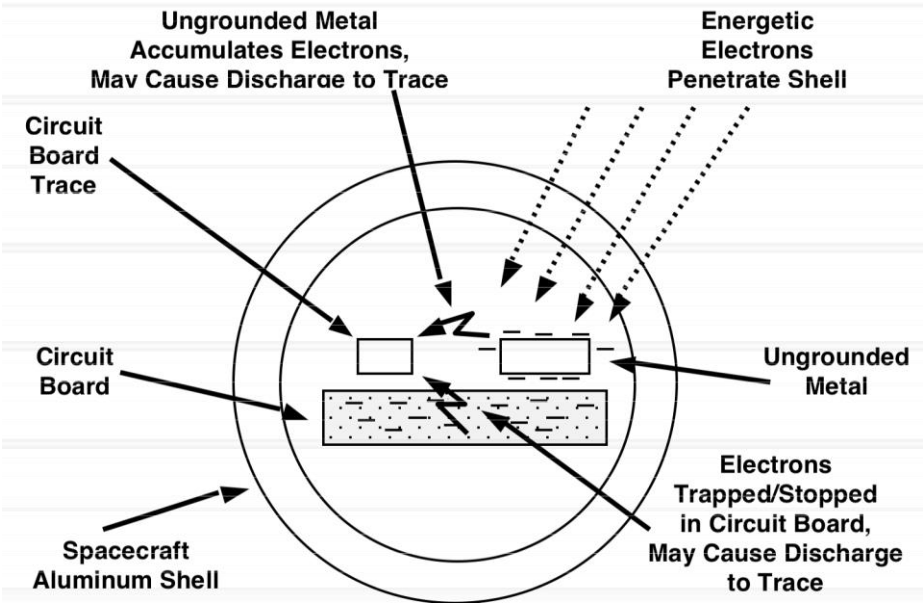

Figure 6—Internal Charging, Illustrated

4.1.3 Charge Deposition

The key step in analyzing a design for the internal charging threat is to determine the charge deposition inside the spacecraft. It is important to know the amount of charge deposited in or on a

given material as well as the deposition rate, as these determine the distribution of the charge and hence the local electric fields. A breakdown (discharge) will eventually occur when the local electric field exceeds the breakdown threshold field of the material or between dissimilar surfaces with a critical potential difference. (Figure 7, Example of Lichtenberg Figure by ESD, shows an example of how discharge swept an entire acrylic glass block.) The actual breakdown can be triggered by a variety of mechanisms, including the material defect sites and the plasma cloud associated with a micrometeoroid or space debris impact. The amplitude and duration of the resulting pulse are dependent on the deposited charge. These values in turn determine how much damage may be done to spacecraft circuitry.

Figure 7—Example of Lichtenberg Figure by ESD

Charge deposition is not only a function of the spacecraft configuration but also of the external electron spectrum. Given an electron spectrum and an estimate of the exterior shielding, the penetration depth versus the energy chart (reference Figure 5) permits an estimate of electron deposition as a function of depth for any given equivalent thickness of aluminum, from which the likelihood of a discharge can be predicted. Because of complexities, including hardware geometries, it is normally better to run a Monte Carlo electron transport code to more accurately determine the charge deposited at a given material element within a spacecraft. Appendix B lists examples of environment and transport codes.

4.1.4 Conductivity

Material conductivity plays an important role in determining the likelihood of a breakdown. The actual threat posed by internal charging depends on accumulating charge until the resultant electric field stress causes an ESD. Charge accumulation depends on retaining the charge after deposition. Since internal charging fluxes at GEO are on the order of 1 pA/cm^2 (1 pA = 10^{-12} A), resistivities on the order of 10^{12} ohm cm will conduct charge away (see Eq. 3), if grounded, so that high local

electric field stress (10^7 to 10^8 V/m) conditions cannot occur and initiate an arc. Unfortunately, modern spacecraft dielectric materials such as Teflon® (polytetrafluoroethylene) and Kapton® (polyimide), flame retardant 4 (FR4, glass-reinforced epoxy laminate material) circuit boards, and conformal coatings often have high enough resistivities to cause problems (reference section 8.1 in this NASA Technical Handbook). If the internal charge deposition rate exceeds the leakage rate, these dielectrics can accumulate charge to the point that discharge to nearby conductors are possible. If that conductor leads to or is close to a sensitive victim, there could be disruption or damage to the victim circuitry.

Note that the conductivity of a dielectric may vary significantly with temperature, dose, and dose rate. The temperature dependence is often not simple as in some cases it follows Arrhenius behavior while in others it may depend on $\exp\left[-\frac{A}{T^{1/4}}\right]$ (A: a constant, T: temperature, reference Gillespie, 2013). The total ionizing dose (TID) can change the charge trap density and therefore the conductivity. Incident radiation may excite charges into conduction states that are not thermally available. This radiation-induced conductivity (RIC)—which also can change with temperature, dose, and dose rate—may significantly increase conductivity in some materials subjected to radiation (reference Gillespie, 2013). Based on these uncertainties and the difficulty in making RIC measurements, it is often easier to err on the conservative side and not consider beneficial RIC effects in ESD protection analyses. Conductivity test methods are discussed in Appendix D.4 – D.7.

Metals, although conductive, may be a problem if they are electrically isolated by more than 10^8 ohm (the actual threshold resistance depends on the metal area and charging flux, reference Eq. 11-1). Examples of metals that may be isolated (undesirable) are radiation spot shields, structures that are deliberately insulated, capacitor cans, integrated circuit (IC) and hybrid cans, transformer cores, relay coil cans, wires, radio frequency (RF) circuits with direct current (dc) isolated conductors, and capacitively coupled striplines in RF couplers and filters that may be isolated by design or by switches, etc. Each and every one of these isolated items could be an internal charging threat and should be scrutinized for its contribution to the internal charging hazards.

4.1.5 Breakdown Voltage

The breakdown voltage is typically defined as the voltage at which the dielectric strength of a particular sample (or air gap) cannot sustain the voltage stress and a breakdown (arc) is likely to occur. Be aware that published breakdown voltages mean different things depending on the source such as the average breakdown voltage, the Weibull 63.2% likelihood breakdown voltage, or the breakdown inception voltage (reference Appendix D.3). Often, it is not explicitly stated which of these was used. For spacecraft charging applications, the most relevant measure to conservatively judge if discharges can happen is the breakdown inception field, i.e., the minimum electric field at which breakdown may occur in a material. See Appendix D for details and recommended test methods.

The breakdown threshold field (V/m), often called dielectric strength, is the relevant physical quantity for the intrinsic breakdown strength of a dielectric. Even though the dielectric strength should be material constant, the thicker materials usually are reported to have smaller dielectric

strength. Extrinsic factors such as manufacturing blemishes or handling damage can all contribute to the variations in breakdown threshold field that is observed in practice.

Despite the fact that dc breakdown has been studied for decades, there is not yet a generally accepted physics-based theoretical model. The extensive structural disorder of most dielectrics together with underlying quantum mechanical effects preclude theoretical calculations of breakdown with exact solutions. Approximate physical models such as those proposed by Crine, et al. (1989, 2016) or Andersen, et al. (2015) can be used to estimate the time to breakdown at fields above breakdown inception field. Statistical models such as Weibull distributions together with confidence intervals are frequently used to quantify distributions of breakdown likelihood (reference Dissado and Fothergill [1992]).

As a rule of thumb, if the dielectric strength, especially the breakdown inception field, is not known, most common good quality spacecraft dielectrics may break down when their internal electric fields exceed 2 x 10^7 V/m (508 V/mil). As a practical matter, because of sharp corners, interfaces, and vias that are inevitably present in printed circuit (PC) boards, the nominal breakdown field may be less. The extreme lower bound on electric fields capable of producing ESD is calculated to be on the order of 1 x 10^6 V/m (25.4 V/mil) (reference Andersen, et al. [2017]). Below this minimum field, breakdown is exceedingly unlikely regardless of the material in question. Lowest breakdown field limits, either theoretical limits or anecdotal rules of thumb, can be conservative since breakdown threshold fields in practice may range between 10^6 - 10^8 V/m depending on the individual material and environment.

Note that the same material and even an individual sample discharges at a range of electric fields. To conservatively judge if discharges can happen, the lowest breakdown threshold field (breakdown inception field) should be used. On the other hand, when the effect of the discharge is conservatively assessed, the largest electric field the material can hold before a discharge happens should be considered. When an electric field is relatively low (10^6 - 10^7 V/m), discharges may happen depending on materials; but the discharge magnitude will be smaller because the stored charge per volume at given electric fields is relatively small and a single discharge cannot sweep a large volume.

4.1.6 Dielectric Constant

The dielectric constant of a material, or its relative permittivity, is a measure of the electric field inside the material compared to the electric field in a vacuum. The permittivity of a material (ε) is the product of the permittivity of free space (ε_0 = 8.85 x 10^{-12} F/m) and the dielectric constant (ε_r, a dimensionless quantity) of the material in question ($\varepsilon = \varepsilon_0 \times \varepsilon_r$). Dielectric constants of insulating materials used in spacecraft construction generally range from 2.1 to as high as 10. Assuming a dielectric constant of 2.7 (between Teflon® and Kapton®) is an adequate approximation if the exact dielectric constant is not known. Appendix D.8 in this NASA Technical Handbook provides examples of the use of the dielectric constant for calculating time constants.

4.1.7 Electron Fluxes (Fluences) at Breakdown

For IESD, the electron flux for a given time interval (or fluence) at a location is a critical quantity. Figure 8, (a) IESD Hazard Levels versus Electron Flux (Various Units), and (b) Point Form of Ohm's Law in Eq. 3, compares spacecraft disruptions as functions of environmental flux at the victim location. Experience and observations from the Combined Release and Radiation Effects Satellite (CRRES) and other satellites have shown that if the incident internal flux is less than 0.1 pA/cm^2, there have been few, if any, internal charging problems (2 x 10^{10} e/cm^2 in 10 hr appears to be the threshold). Bodeau, et al. (2005; 2010) report problems with sensitive circuits at even lower levels on some newer spacecraft. For geostationary orbits, the flux above 1.5 MeV is usually less than 0.1 pA/cm^2 (see Figure 9), and a generally suitable level of protection can be provided by 130 mil of aluminum equivalent including all shielding (see Figure 5). Modern spacecraft are being built with thinner walls or only thermal blankets (less mass), so the simple solution to the internal charging problem (adding shielding everywhere) cannot be implemented. However, adding non-floating metallic spot shield near sensitive regions can help in many cases.

Figure 8 (reference Frederickson, et al. [1992]) also allows a direct comparison between common units as used in the literature and other places in this document (i.e., 10^6 e/cm^2 s is about 0.2 pA/cm^2). Appendix A.1.2.5 contains additional information about IESD studies on CRRES.

The approximation of 0.1 pA/cm^2 noted as a nominal threshold for internal charging difficulties is experientially based, not physics based, and thus has limits. This is loosely based on CRRES data (though verified by other researchers) for "typically used materials" and at or near room temperature. If highly resistive materials are used in cold situations, a long-term charge accumulation, typically 10 hours to as long as a few months, is possible so that threshold flux can be smaller than 0.1 pA/cm^2. Likewise, for shorter duration exposure, ground tests show higher flux limits. For those cases, further test or analysis should be done.

The threshold deposited fluence is related to the breakdown threshold field as shown in Eq. 2.

$$\begin{aligned} Q &= C\,V \\ Q &= (\varepsilon \cdot A / d)\,V \\ Q/A &= \varepsilon \cdot (V / d) = \varepsilon E \end{aligned} \qquad \text{(Eq. 2)}$$

where:

Q	=	total deposited charge (C)
Q/A	=	total deposited charge per unit area, the deposited fluence (C/m^2)
C	=	capacitance (F)
ε	=	permittivity of the material = $\varepsilon_o \cdot \varepsilon_r$ (F/m)
ε_o	=	permittivity of free space = 8.85 x 10^{-12} F/m
ε_r	=	dielectric constant of the material, usually between 2 and 4 (unitless)
A	=	area of the sample = length x width (m^2)
d	=	thickness, top to bottom (m)
V	=	voltage (V)
E	=	Electric field (V/m).

For example, when dielectric constant is 2 and the breakdown threshold field is 2 x 10^7 V/m, the threshold deposited fluence is ~2 x 10^{11} e/cm^2.

Also, if the charging duration is determined by the material properties (resistor-capacitor [RC]) time constant, Appendix D.8) and not by any flux variation due to the trajectory or space weather, the threshold flux can be related to the effective resistivity (reciprocal of total conductivity) and breakdown threshold field by Eq. 3.

$$Q/A = J_{th}\, t = J_{th} \cdot (\varepsilon \rho) = \varepsilon E_{th}$$
$$J_{th} = E_{th} / \rho = E_{th}\, \sigma \qquad \text{(Eq. 3)}$$

where:

J_{th} = threshold deposited flux (A/m^2)
t = material's RC time constant
ρ = resistivity corresponding to total conductivity (ohm m)
σ = total conductivity including dark conductivity, radiation-induced conductivity, and other components (ohm m)$^{-1}$

For example, when resistivity is 2 x 10^{16} ohm m and the breakdown threshold field is 2 x 10^7 V/m, the threshold deposited flux is 0.1 pA/cm^2. The corresponding charging constant in this case is ~100 hours. A practical equilibrium can be reached after ~300 hours, three time constants.

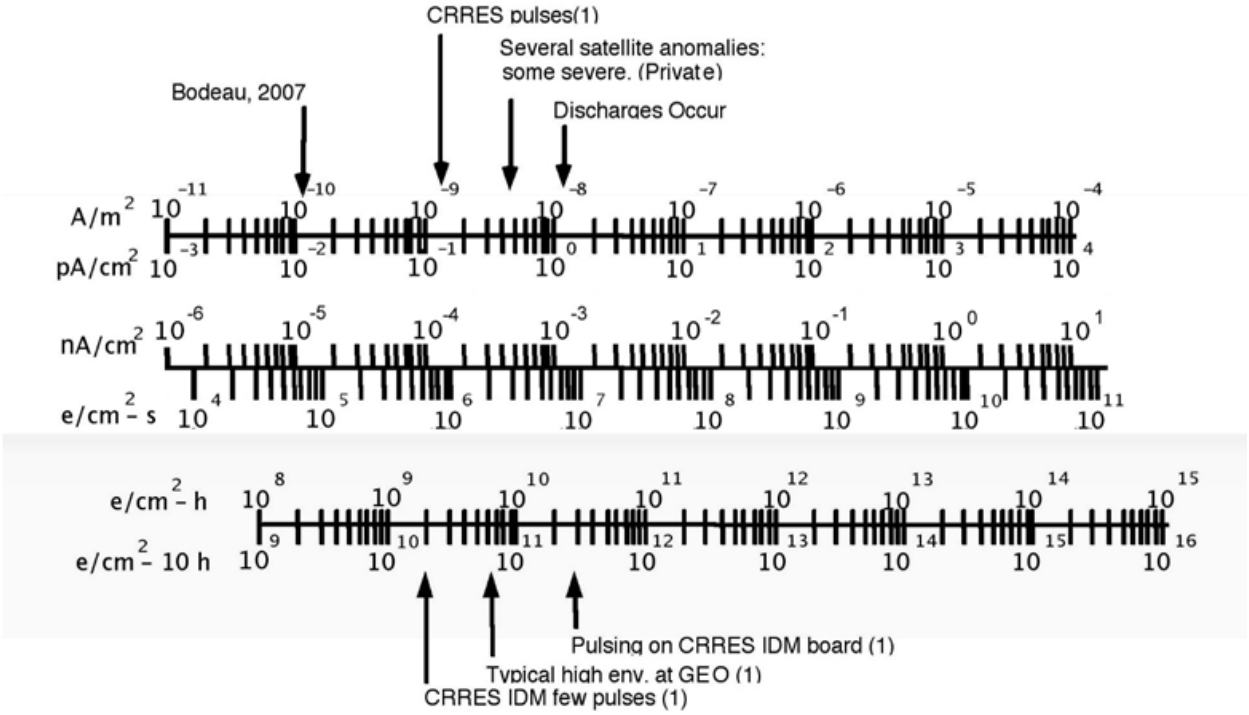

(a)

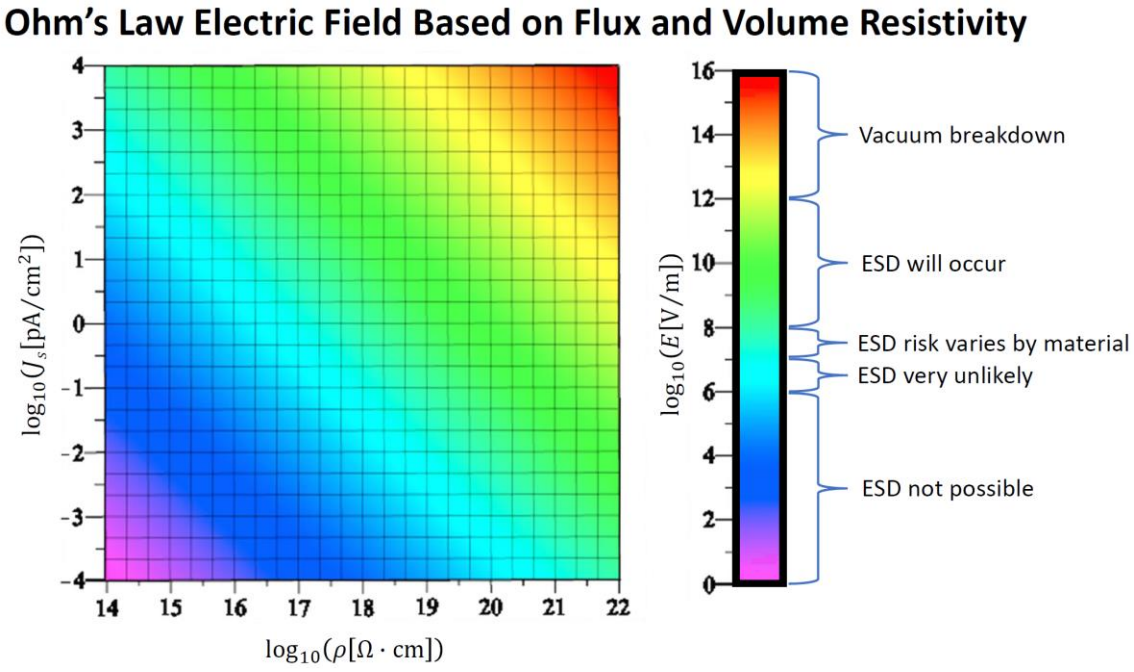

(b)

Figure 8—(a) IESD Hazard Levels versus Electron Flux (Various Units) [(1)]Frederickson (1992) **and (b) Point Form of Ohm's Law in Eq. 3**

4.2 Electron Environment

To assess the magnitude of the IESD concern for a given orbit, it is necessary to know the electron charging environment along that orbit (as noted before, the protons generally do not have enough penetrating flux to cause a significant internal charge). The electron orbital environments of primary interest (in terms of number of affected spacecraft) are GEOs, MEOs, and PEOs. Other orbital regimes that are also known to be of interest are Molniya orbits and Jupiter and Saturn (see Appendix A.3 and A.4). For a spacecraft that uses electric orbit raising to move the spacecraft to a final orbit, the electron environments and passage durations through different regions in the orbit raising path should be considered.

The 11-year variation between the most severe electron environments and the least severe can vary over a 100:1 range and shows correlation with the solar cycle (see Appendix A.2.2.1, Figures 27 and 28). A project manager might consider "tuning" the radiation protection to the anticipated service period; but even in quiet years, the worst flux sometimes will be as high as the worst flux of noisy years. As a result, the environment presented in this NASA Technical Handbook represents a conservative, worst-case level for GEO for any phase of the solar cycle.

Figure 9, Suggested Worst-Case Geostationary Integral Electron Flux Environment, shows a worst-case GEO internal charging spectrum generated by selecting dates when the Geosynchronous Operational Environmental Satellite (GOES) E >2 MeV electron data values were elevated to extremely high levels and then using worst-case electron spectrum data from the geosynchronous Synchronous Orbit Particle Analyzer (SOPA) instrument for the same days. It is a worst-case,

approximately a 99.9th percentile event (happened for 1 day in 3 years of observation) charging environment which lasted a few to tens of hours depending on the energy. (Appendix A.1.2.3 and A.1.2.4 contain descriptions of the GOES satellite and SOPA instrument.) This suggested worst-case environment is almost the same as the 99.99th percentile, 1-day averaged flux simulated by IRENE version 1.55.002 (see Appendix B.1.2). For a one-year mission, the probability of not having a flux higher than this 99.99th percentile environment is 96% ($0.9999^{365} = 0.96$). The GEO integral electron spectrum varies with time in both shape and amplitude. Figure 9 also plots the corresponding long-term nominal electron spectrum as estimated by the NASA AE8min code (Vette, et al. [1979] and Vette [1991]) for the same energy range. The large difference between the nominal time-averaged (AE8) and shorter-term worst-case conditions is characteristic of the radiation environment at Earth. While higher environments are less frequent, they do occur.

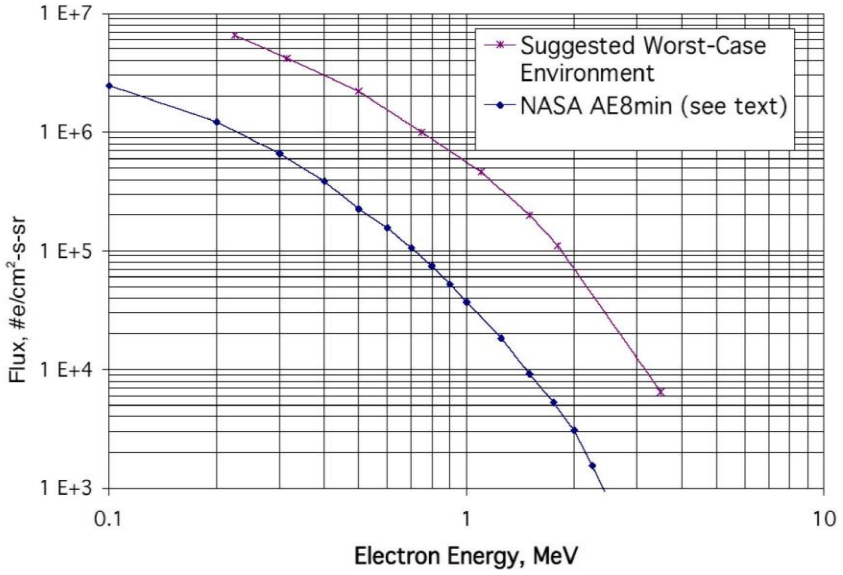

Energy	WC Flux
MeV	e/cm^2 s sr
0.225	6.5 x 10^6
0.315	4.2 x 10^6
0.5	2.2 x 10^6
0.75	9.9 x 10^5
1.1	4.6 x 10^5
1.5	2.0 x 10^5
1.8	1.1 x 10^5
3.5	6.5 x 10^3

Upper: Worst-case short-term GEO environment (May 11, 1992, 197° East longitude peak environment lasting about one day, with no added margin).

Lower: NASA AE8min long-term average environment (200° East longitude).

Figure 9—Suggested Worst-Case Geostationary Integral Electron Flux Environment
(Note: Integral flux is for the total flux greater than specified energy.)

4.2.1 Units

The primary units that describe the electron environment are flux and fluence. In this NASA Technical Handbook, flux corresponds to the rate at which electrons pass through or into a surface element. Although the units of omnidirectional flux (J) are often in terms of electrons per square centimeter per second ($J = 4\pi I$), units here will generally be the number of electrons per square centimeter per steradian per second (I). The unit of the flux on a flat surface (J_s) can be the same as the omnidirectional flux, but the value of it differs from the omnidirectional flux by the factor of 4

for isotropic distribution ($J_s = \pi I$). The time unit (per day or per second, for example) should be explicitly present. Some reports present fluence (flux integrated over time) but additionally describe the accumulation period (a day or 10 hours, for example) which then can be converted to an average flux. Electron fluxes may also be expressed as amperes (A) or picoamperes (pA) per unit area (often per cm^2). Figure 8 interrelates various flux and fluence units.

The flux can be described as an integral over energy (electrons with energy exceeding a specified value as shown in Figure 9) or differential (flux in a unit of energy). ESD damage potential is related to the stored energy which is related to fluence (again, time x flux).

4.2.2 Substorm Environment Specifications

Worst-case plasma environments should be used in predicting surface potentials on spacecraft. The ambient space plasma and the photoelectrons generated by solar extreme ultraviolet (EUV) are the major sources of spacecraft surface charging currents in the natural environment. The ambient space plasma consists of electrons, protons, and other ions, the energies of which are described by the temperature of the plasma as discussed in section 4.1.1 of this NASA Technical Handbook. The net current to a surface is the sum of currents caused by ambient electrons and ions, secondary electrons, photoelectrons, and other sources, e.g., ion engines, plasma contactors, and the spacecraft velocity relative to the plasma. The spacecraft velocity relative to the plasma can contribute to surface currents in LEO, where ram and wake effects may be present. A spacecraft in the environment accumulates surface charges until current equilibrium is reached, at which time the net current is zero. The EUV-created photoelectron emissions usually dominate in GEO and typically prevent the sunlit spacecraft surfaces and the structure (ground) from reaching large negative potentials. Shadowed surfaces will reach large negative potentials relative to space, to structure ground and to nearby sunlit surfaces.

The density of the plasma also affects spacecraft charging. A tenuous plasma of less than 1 particle/cm^3 will charge the spacecraft and its surfaces more slowly than a dense plasma of thousands of particles/cm^3.

Although the photoelectron current associated with solar EUV dominates over most of the magnetosphere in and near GEO during geomagnetic substorms, the ambient substorm electron current can often control and dominate the charging process. Unfortunately, the ambient plasma environment at GEO is very difficult to describe as it can be very anisotropic along the magnetic field lines and can be dominated by highly variable substorms. Detailed particle spectra (flux versus energy) are available from several missions such as the Applications Technology Satellites (ATS-5, ATS 6), Spacecraft Charging at High Altitudes (SCATHA), and the SOPA instruments; but these are often not easily incorporated into charging models. Rather, for simplicity, only the isotropic currents and Maxwellian temperatures are usually used by modelers; and these only for the electrons and protons. Even so, useful answers can be obtained with this simple representation. For a worst-case electrostatic charging analysis, the single Maxwellian isotropic environmental characterization given in Table 1, 90^{th} Percentile Geosynchronous Plasma Environment, is recommended. (Tables 9 and 10 in Appendix A.2.1 and Appendix H show alternative representations of the GEO worst-case environments, including anisotropies.)

Table 1 lists a 90th percentile single-Maxwellian representation of the GEO environment (which is expected to last about one day and happens one day per every ten days on average). Appendix A.1.1 describes the spacecraft charging equations and methods by which these values can be used to predict spacecraft charging effects. If the worst-case analysis shows that spacecraft surface differential potentials are less than 100 V, there should be no ESD problem. If the worst-case analysis shows a possible problem, use of more realistic plasma representations and spacecraft charging models should be considered.

A more comprehensive discussion of plasma parameters is given in Appendix A.1.1. Alternate descriptions of plasma parameters are presented in Appendix A.2.1, Tables 9 and 10, Figure 25, and Appendix H and include fluxes and energies that might be used for material charging testing.

Table 1—90th Percentile Geosynchronous Plasma Environment

ITEM	UNIT	VALUE	DESCRIPTION
N_E	cm^{-3}	1.12	electron number density
T_E	eV	1.2×10^4	electron temperature
N_I	cm^{-3}	0.236	ion number density
T_I	eV	2.95×10^4	ion temperature

Several actual worst-case data sets for the ATS-5 and -6 satellites, and the SCATHA satellite with average values, standard deviations, and worst-case values are presented in the appendices. Additionally, percentages of yearly occurrences are given, and finally, a time history of a model substorm has been provided. All of these different descriptions of plasma parameters can be used to help analyze special or extreme spacecraft charging situations.

Garrett (1979), Hastings and Garrett (1996), Roederer (1970), Garrett (1999), and other texts on space physics contain more detailed explanations of the radiation and plasma environment.

4.3 Modeling Spacecraft Charging

Analytical modeling techniques should be used to predict charging effects. In this section, approaches to predicting spacecraft potentials resulting from encounters with plasma environments (see section 4.3.1) or high-energy particle events (see section 4.3.2) are discussed to set the context for the charging analysis process described in the subsequent sections. The descriptions are intended to provide an overview only with the details specifically left to the appendices. Even the simple methods described, however, can be used to identify possible discharge conditions (reference section 4.4) and, based on coupling models (see section 4.5), to establish the spacecraft and component-level test requirements. Again, details are intentionally left to the appendices for the interested reader.

4.3.1 The Physics of Surface Charging

Although the physics behind the spacecraft charging process is quite complex, the formulation at GEO at least can be expressed in straightforward terms. The fundamental physical process for all spacecraft charging is that of current balance: at equilibrium (typically achieved in milliseconds for

the overall spacecraft, seconds to minutes on isolated surfaces relative to vehicle ground, and up to hours between surfaces), all currents sum to zero. The potential at which equilibrium is achieved for the spacecraft is the potential of the surface with respect to the space plasma ground; similarly, each surface will achieve a separate equilibrium relative to space plasma and the surrounding surfaces. In terms of the ambient plasma current (reference Garrett [1981]), the basic equation expressing this current balance for a uniformly conducting spacecraft at equilibrium is (see Appendix F for details):

$$I_E(V) - [I_I(V) + I_{PH}(V) + I_{Secondary}(V)] = I_T \qquad \text{(Eq. 4)}$$

where:

V	=	spacecraft surface potential relative to the space plasma (volt, V)
I_E	=	incident electron current to the spacecraft surface (ampere, A)
I_I	=	incident ion current to the spacecraft surface (A)
$I_{Secondary}$	=	additional electron currents from secondaries, backscatter, and any man-made sources (A); see Appendix F for details
I_{PH}	=	photoelectron current (A)
I_T	=	total current to spacecraft (at equilibrium, $I_T = 0$) (A).

As a simple illustration of the solution of Eq. 4, assume that the spacecraft is a conducting sphere, it is in eclipse ($I_{PH} = 0$), the secondary currents are ~0, and the plasmas are single Maxwell-Boltzmann distributions. As discussed in Appendix F, the first-order currents for the electrons and ions are given by the following simple current versus voltage (I/V) curves (assuming a negative potential on the spacecraft):

Electrons

$$I_E = I_{E0} \exp(qV/kT_E) \quad V<0 \text{ repelled} \qquad \text{(Eq. 5)}$$

Ions

$$I_I = I_{I0} [1 - (qV/kT_I)] \quad V<0 \text{ attracted} \qquad \text{(Eq. 6)}$$

where:

$$I_{E0} = A_E (qN_E/2) (2kT_E/\pi m_E)^{1/2} \qquad \text{(Eq. 7)}$$

$$I_{I0} = A_I (qN_I/2) (2kT_I/\pi m_I)^{1/2} \qquad \text{(Eq. 8)}$$

and:

A_E	=	electron collection area (m^2)
A_I	=	ion collection area (m^2)
N_E	=	density of electrons in ambient plasma (m^{-3})
N_I	=	density of ions in ambient plasma (m^{-3})
m_E	=	mass of electrons (9.109×10^{-31} kg)
m_I	=	mass of ions (proton: 1.673×10^{-27} kg)
q	=	magnitude of the electronic charge (1.602×10^{-19} coulombs)

T_E = plasma electron temperature in eV
T_I = plasma ion temperature in eV.

To solve the equation and find the equilibrium potential of the spacecraft relative to the space plasma, V is varied until $I_T = 0$. As a crude example, for GEO during a geomagnetic storm, the potential is usually on the order of 5-10 kV whereas T_I is typically ~20-30 keV implying that $|qV/T_I|<1$ so $I_I \sim I_{I0}$. Ignoring secondary currents, these approximations lead to a simple proportionality between the spacecraft potential and the ambient currents and temperatures:

$$V \sim -T_E \ln(I_{E0}/I_{I0}) \quad \text{(Eq. 9)}$$

That is, to first order in eclipse (see, however, Appendix F), the spacecraft potential in eV is roughly proportional to the plasma temperature expressed in eVs and the natural log of the ratio of the electron and ion currents—a simple but useful result for estimating the order of the potential on a spacecraft at geosynchronous orbit.

To summarize, surface charge modeling is a process of computing current balance for (1) the overall vehicle, (2) next, isolated surfaces relative to spacecraft ground, and (3) ultimately, the current flow between surfaces. An I/V relationship is determined for each surface configuration and the adjacent surfaces, and then, given the plasma environment, the potential(s) at which current balance is achieved are computed. Clearly, this can become a complicated time-dependent process as each electrically isolated surface on a spacecraft approaches a unique equilibrium leading to differential charging (the cause of most surface charging generated spacecraft anomalies). Fortunately, computer codes like Nascap-2k (see Appendix B.3.2) have been developed that can readily handle very complex spacecraft configurations.

4.3.2 The Physics of Dielectric Charging

The computations involved in estimating dielectric charging resemble surface charging calculations with the inclusion of space charge. That is, the basic problem is the calculation of the electric field and charge density in a self-consistent fashion over the three-dimensional (3D) space of interest—typically a dielectric volume. Gauss's law has to be solved subject to the continuity equation and Ohm's law. As detailed in Appendix C.1, for a simple one-dimensional (1D) planar approximation, these equations (for electrons) can be reduced to a single equation where the charge buildup in a dielectric at a position x in the dielectric at time t can be described by:

$$\frac{\partial(\varepsilon(x)E(x,t))}{\partial t} + \sigma(x,t)E(x,t) = -J_R(x,t) \quad \text{(Eq. 10)}$$

where:

E = electric field (V/m) at x for time t
σ = conductivity in (ohm m)$^{-1}$ = $\sigma_o + \sigma_r$
σ_o = dark conductivity in (ohm m)$^{-1}$
σ_r = radiation-induced conductivity in (ohm m)$^{-1}$
ε = $\varepsilon_o \varepsilon_r$ (material permittivity, F/m)

ε_o = free-space permittivity = 8.8542 x 10^{-12} F/m

ε_r = dielectric constant (dimensionless)

J_R = incident particle flux (current density in A/m^2) where $-\partial J_R/\partial x$ is charge deposition rate at x

Note in particular that the total current consists of the incident current J_R (primary and secondary particles) and a conduction current σE driven by the electric field developed in the dielectric (the ohmic term). Integrating Eq. 10 in x across the dielectric layer then gives the variation of electric field in the dielectric at a given time. The results are stepped forward in time and the process repeated to give the changing electric field and charge density in the dielectric. As in the case of surface charging, computer codes such as NUMIT (see Appendix B.3.4) and DICTAT (see Appendix B.3.6) have been developed to carry out these computations and predict the buildup of electric field in the dielectric—when that field E exceeds the breakdown potential of the material, an arc discharge is possible. Also, a 3-dimensional version of NUMIT (called 3D NUMIT, Appendix B.3.5) has been developed and is being used.

4.4 Discharge Characteristics

Charged spacecraft surfaces, environmentally caused or deliberately biased, can discharge; and the resulting transients can couple into electrical systems. A spacecraft in space may be considered to be a capacitor relative to the space plasma potential. The spacecraft, in turn, is divided into numerous other capacitors by the dielectric surfaces used for thermal control and for power generation. This system of capacitors can be charged at different rates depending upon incident fluxes, time constants, and spacecraft configuration effects.

The system of capacitors floats electrically with respect to the space plasma potential. This can give rise to unstable conditions in which charge can be lost from the spacecraft to space. While the exact conditions required for such breakdowns are not known, what is known is that breakdowns do occur and that the conditions that lead to breakdowns can be bounded.

Breakdowns, or discharges, occur because charge builds up in spacecraft dielectric surfaces or between various surfaces on the spacecraft. Whenever this charge buildup generates an electric field that exceeds a breakdown threshold, charge may be released from the spacecraft to space or to an adjacent surface with a different potential. This charge release will continue until the electric field can no longer sustain an arc. Hence, the amount of charge released will be limited to the total charge stored in or on the dielectric of the floating conductor at the discharge site. Charge loss or current to space or another surface causes the dielectric surface voltage (at least locally) to relax toward zero. Since the dielectric is coupled capacitively to the structure, the charge loss will also cause the structure potential to become less negative. In fact, the structure could become positive with respect to the space plasma potential. The exposed conductive surfaces of the spacecraft will then collect electrons from the environment (or attract back the emitted ones) to reestablish the structure potential required by the ambient conditions. The whole process for a conducting body to charge relative to space can take only a few milliseconds while, in contrast, differential charging between the surfaces may take from a few seconds to hours to reach equilibrium. Multiple

discharges can be produced if intensities remain high long enough to reestablish the conditions necessary for a discharge.

It is well known in the spacecraft solar array community that there can be a charge loss over an extended area of the dielectric (reference NASA-TP-2361, Design Guidelines for Assessing and Controlling Spacecraft Charging Effects). This phenomenon is produced by the plasma cloud from a discharge sweeping over dielectric surfaces where the underlying conductor is electrically connected to the arc site. Charge loss from inverted gradient (solar array charged positively) solar array arcs has been seen for distances of 2 meters and more from the arc site and can involve capacitances of several 100s of picofarads (pF) in the discharge depending on configuration. This phenomenon can produce area-dependent charge losses capable of generating currents of 4-5 amperes. Normal gradient (solar array charged negatively) arcs can be much larger. The differential voltages necessary to produce this large charge-clean-off type of discharge may be as low as 1,000 V on solar arrays dependent on the specific type of array, geometric configuration, or environment. In modeling the charged surfaces swept free of charge by an arc, one should assume that all areas with substrates directly electrically connected to the arc site and with a line-of-sight to the arc site will be discharged and calculate the arc energy accordingly (reference Amorim, et al. [2005]).

Because sunlight tends to charge all illuminated surfaces a few volts positive relative to the ambient plasma and shaded dielectric surfaces may charge strongly negatively, differential charging is likely to occur between shadowed surfaces and sunlit surfaces or the underlying spacecraft structure ground. Since breakdowns are believed to be related to differential charging, they can occur during sunlit charging events. Entering and exiting eclipse, in contrast, result in a change in absolute charging for all surfaces except those weakly capacitively coupled to the structure (capacitance to structure less than that of spacecraft to space, normally $<2 \times 10^{-10}$ F). Differential charging in eclipse develops slowly and depends upon differences in secondary yield. In the following paragraphs, each of the identified breakdown mechanisms is summarized.

4.4.1 Dielectric Surface Breakdowns

If either of the following criteria is exceeded, discharges can occur:

a. If electric fields reach a magnitude that exceeds the breakdown threshold field of the surrounding “empty” space, a discharge may occur (see for example, Naidu and Kamaraju [2009]). A published rule of thumb (reference Coakley [1987]) is that if the dielectric surface voltages resulting from spacecraft surface charging are greater than ~500 V positive relative to an adjacent exposed conductor, a breakdown may occur. In this NASA Technical Handbook, a more conservative 400-V differential voltage threshold of concern has been adopted for ESD breakdown. This is not true for induced potentials such as from solar arrays or Langmuir probes; these should be analyzed separately. The physics of electric field breakdown in gases has been explained by Townsend (see, for example, Naidu and Kamaraju [2009]).

b. If the interface between a visible surface dielectric and an exposed grounded conductor has an electric field greater than 2×10^{7} V/m, a discharge may occur (reference NASA-TP-2361).

Note that edges, points, gaps, seams, and imperfections in surface materials can increase electric fields and promote the probability of discharges. These items are not usually modeled and have to be found by close inspection of the exterior surface specifications. In some cases, a plasma cloud generated by a micrometeoroid/debris impact at the site or gas release such as by a thruster firing could trigger the breakdown (reference Garrett and Close [2013]).

The first criterion can be exceeded by solar arrays in which the high secondary yield of the coverglass can result in surface voltages that are positive with respect to the metalized interconnects. This criterion can also apply to metalized dielectrics in which the metalized film (such as silver-Teflon® film), either by accident or design, is isolated from structure ground by a large or non-existent resistance (essentially only capacitively coupled). In the latter case, the dielectric can be charged to large negative voltages (when shaded), and the metal film will become more negative than the surrounding surfaces and act as a cathode or electron emitter.

In both of these conditions, stored charge is initially ejected to space in the discharge process. This loss produces a transient that can couple into the spacecraft structure and possibly into the electronic systems. Current returns from space to the exposed conductive areas of the spacecraft. Transient currents flow in the structure depending on the electrical characteristics. It is assumed that the discharge process will continue until the voltage gradient or electric field that began the process decreases below threshold. The currents flowing in the structure will oscillate according to structure capacitances and inductances and damp out according to its resistive and radiative losses.

The computation of charge lost in any discharge is highly speculative at this time. Basically, charge loss can be considered to result from the depletion of two capacitors; namely, that stored in the spacecraft, which is charged to a specified voltage relative to space, and that stored in a limited region of the dielectric at the discharge site. The prediction of charge loss requires not only the calculation of voltages on the spacecraft, but also a careful review by an experienced analyst as well.

As a guide, the following charge loss categories are useful (as adapted from NASA-TP-2361):

$0 < Q_{lost} < 0.5$ μC—minor discharge
$0.5 < Q_{lost} < 2$ μC—moderate discharge
$2 < Q_{lost} < 10$ μC—severe discharge

Energy, voltage, or discharge considerations can also be quantified as a means to characterize the severity of a dielectric discharge (or discharge from an isolated conductor). Assuming a dielectric constant of 2, dielectric strength of 2×10^7 V/m, and dielectric thickness of 10 mil (254 μm), (corresponding voltage of 5.08 kV) and using the Q_{lost} criteria above in standard equations yields the following data shown in Table 2, Examples of Different Magnitudes of Surface ESD Event Parameters:

Table 2— Examples of Different Magnitudes of Surface ESD Event Parameters

SIZE	**Q** (C)	**Area** (cm^2)	**C** (F)	**E**(J)
Minor, up to	500 nC	14.1 cm^2	98 pF	1.3 mJ
Moderate, up to	2 µC	56.6 cm^2	394 pF	5.1 mJ
Severe	10 µC	282.5 cm^2	1969 pF	25.4 mJ

Note that the values in the table vary depending on dielectric constant, dielectric strength, and thickness of the dielectrics. For example, if the dielectric thickness is 5 mil, the voltage will be decreased to 2.54 kV and the capacitance and energy for 500 nC case will be changed to 197 pF and 635 µJ, respectively (reference Eq. 2 and Eq. 57).

4.4.2 Buried (Internal) Charge Breakdowns

This section refers to the situation in which charges have sufficient energy to penetrate to bulk of a dielectric and are trapped. If the dielectric surface is maintained near zero potential because of photoelectron, secondary electron emission, or use of a dissipative surface coating, strong electric fields may exist between the buried charge and the surface of the material which can lead to breakdowns to the dielectric surface. (Even without the condition of near zero potential on the surface, the electric field between the buried charge layer and underlying structure ground can be large which can also lead to discharges.) Breakdown can occur whenever the internal electric field exceeds the dielectric strength (2×10^7 V/m for typical dielectric). Table 7, section 8.2, lists the typical dielectric strength of common dielectric materials.

A layer of charge with 2.2×10^{11} e/cm^2 will create a 2×10^7 V/m electric field in a material with a dielectric constant of 2. (The E-field is proportional to charge and inversely proportional to the dielectric constant.)

4.4.3 Spacecraft-to-Space Breakdowns

Spacecraft-to-space breakdowns are generally similar to dielectric surface breakdowns but involve only small discharges. It is assumed that a strong electric field exists on the spacecraft surfaces—usually because of a geometric interfacing of metals and dielectrics. This arrangement periodically triggers a breakdown of the spacecraft capacitor. Since this spacecraft-to-space capacitance tends to be of the order of 2×10^{-10} F, these breakdown transients should be small and rapid. Based on an assumption of 2 kV breakdown, the resulting stored energy is minor, in accordance with Table 2.

4.5 Coupling Models

Coupling model analyses have to be used to determine the hazard to electronic systems from exterior discharge transients. In this section, techniques for computing the influence of exterior discharge transients on interior spacecraft systems are discussed. Benchmarks of LEM and SEMCAP predictions with tests show poor agreement (errors of 20 dB or more, discussed in Appendix E). Both approaches are particularly poor at modeling coupling of external discharges to

harnesses inside spacecraft structures. Nevertheless, models are useful for qualitative risk assessments that can guide designs and focus (but not replace) qualification testing.

4.5.1 Lumped-Element Modeling (LEM)

LEMs have been used to define the surface charging response to environmental fluxes (reference Robinson and Holman [1977]; Inouye [1976]; Massaro, et al. [1977]; Massaro and Ling [1979]) and are currently used to predict structural currents resulting from surface discharges and coupling into the external and internal cables. The basic philosophy of a LEM is that spacecraft surfaces and structures can be treated as electrical circuit elements—resistance, inductance, and capacitance. The geometry of the spacecraft is considered only to group or lump areas into nodes within the electrical circuit in much the same way as surfaces are treated as nodes in thermal modeling. These models can be made as simple or as complex as is considered necessary for the circumstances.

The LEMs for discharges assume that the structure current transient is generated by capacitive coupling to the discharge site and is transmitted in the structure by conduction only. An analog circuit network is constructed by taking into consideration the structure properties and the geometry. This network has to consider the principal current flow paths from the discharge site to exposed conductor areas—the return path to space plasma ground. Discharge transients are initiated at regions in this network selected as being probable discharge sites by surface charging predictions or other means. Choosing values of resistance, capacitance, and inductance to space can control transient characteristics. Network computer transient circuit analysis programs such as ISPICE, the first commercial version of SPICE (Simulation Program with Integrated Circuit Emphasis), and any variants of SPICE can solve the resulting transients within the network.

LEMs developed to predict surface charging rely on the use of current input terms applied independently to surfaces. Since there are no terms relating the influence of charging by one area on the incoming flux to other areas, the predictions usually result in larger negative voltages than actually observed. Other modeling techniques that take these 3D effects into account, such as is done in Nascap-2k (see Appendix B.3.2), predict surface voltages closer to those measured. Here, Nascap-2k is the currently recommended analysis technique for surface charging.

4.5.2 Electromagnetic Coupling Models

Numerous programs have been developed to study the effects of electromagnetic coupling on circuits. Such programs have been used to compute the effects of an electromagnetic pulse (EMP) and that of an arc discharge. One program, the Specification and Electromagnetic Compatibility Program (SEMCAP) developed by TRW Incorporated (now Northrop-Grumman Space Technology or NGST) (reference Heidebrecht [1975]) has successfully analyzed the effects of arc discharges on an actual spacecraft, the Voyager spacecraft. See Appendix E for more discussions.

4.5.3 Coupling onto Wires into Internal Electronics

Discharges from surface charging or internal charging can arc to a ground referenced conductor (point of conductor referenced to spacecraft ground). The point of a ground referenced conductor can be a wire conductor that carries the discharge threat to internal electronics. The discharge can

be modeled as a voltage source or a current source coupling to the internal electronics. The discharge threat and the victim electronics can be modeled as an electrical circuit and solved by software such as SPICE and any of its variants.

Another discharge coupling mechanism is radiative coupling. Surface or internal ESD can produce an e-field that can couple onto wire conductors directly or through antenna elements. Field coupling analysis can be performed by various Electromagnetic Compatibility (EMC) field coupling software to predict the current flow in the wire. The wire type, geometry including length, layout including routing and distance above ground plane and circuit impedance on both ends can be used to predict the coupled current onto the victim part. Then, the vulnerability of the victim can be solved by circuit modeling using circuit analysis code such as the variants of SPICE.

KNOWLEDGE CHECK

4.1 What are the orbital parameters and temporal parameters that constitute a severe charging environment?
4.2 Why is "grounding" or "ground referencing" of conductive elements useful in helping reduce spacecraft charging?
4.3 Why is the breakdown field of a material pertinent in estimating the threat from spacecraft charging? How accurate is the rule of thumb of 2×10^7 V/m? How would you report the risk due to using the default (rule of thumb)? Is it conservative (leading to over-protection) or otherwise (leading to a weaker design)?
4.4a How does the material dielectric constant affect charging results?
4.4b Calculate energy stored in a dielectric slab, as if it were a capacitor, to get some ideas. Describe.
4.5 Deduce the electron flux that leads to dielectric breakdown, based on the electrons stored (stopped in) the dielectric as compared to the material's dielectric strength.
4.6 Would you use the Figure 9 "Suggested Worst-Case" or the "NASA AE8min" environment to analyze the environmental ESD threat to a spacecraft? Why?
4.7a Verify by a dimensional analysis that Equations 5 to 10 are internally consistent.
4.7b Compute the results of Equations 1 to 9 using centimeter-gram-second (CGS) input parameters.
4.7c Compute the results of Equations 1 to 9 by changing all CGS input parameters to SI meter-kilogram-second (MKS) and providing answers also in SI. Convert answer to CGS to see if it matches Knowledge Check 4.7b.
4.8 Prove the "proportionality relationship" between spacecraft potential and ambient currents and temperatures as shown in Equation 9.
4.9 Prove the claim shown in the last paragraph of section 4.4.2 and that it does not depend on the thickness of the material.

5. SPACECRAFT DESIGN GUIDELINES

Section 5.1 describes processes *involved* in immunizing a spacecraft against spacecraft charging problems. Section 5.2 lists design guidelines.

If the reader wishes to make a requirements document, the basic requirements include:

a. Determine whether or not the mission passes through or stays in regions with a charging threat. (Do not overlook even transient environment since significant differential surface charging can occur over minutes.)

b. If in a charging threat region, determine the threat that is applicable to that environmental exposure involving energy spectrum, flux, fluence, and duration in that environment.

c. Implement measures to mitigate the threat to an acceptable level.

As a reminder, this total document contains no design requirements although its guidelines are quite often copied as requirements for projects. Many of these are captured and listed as ‘rules of thumb’ in the INDEX in the final pages of this NASA Technical Handbook. We have noted before and emphasize again that this NASA Technical Handbook will sensitize readers to a background to spacecraft charging difficulties, with many specific numbers and equations as examples only. However, any design requirements intended to support a specific project should be written by a person experienced in the spacecraft charging community. At this time, no certification process exists to validate the knowledge of such persons; so project owners should determine as best they can the qualifications of persons involved to immunize their space project from adverse consequences of spacecraft charging.

Sections 5.2.1 (General ESD Design Guidelines for Space Charging), 5.2.2 (Surface ESD Design Guidelines, Excluding Solar Arrays), 5.2.3 (Internal ESD Design Guidelines), 5.2.4 (Solar Array ESD Design Guidelines), and 5.2.5 (Special Situations ESD Design Guidelines) in this NASA Technical Handbook can be used as aids.

5.1 Processes

The system developer should demonstrate through design practices, test, and analysis that spacecraft charging effects will not cause a failure to meet mission objectives. This section briefly discusses those processes.

5.1.1 Introduction

The classic approach to avoiding or eliminating electromagnetic problems is to look at the source of the problem, the victim, and the coupling between them. In the case of spacecraft charging, excess electrons deposit on surface or external spacecraft areas or penetrate directly to victim circuit areas, the charge being buried in a circuit board immediately adjacent to the victim. As a result, the three elements (source, coupling, and victim) are not always clearly distinguishable. For that reason, this NASA Technical Handbook has disregarded these categories; however, this approach may sometimes be fruitful and is described below for completeness.

5.1.1.1 Source

The basic source of in-space charging problems is the charged particle environment (CPE). If that environment cannot be avoided, the next sources of ESD threats are items that can store and accumulate charge and/or energy, especially for internal charging. Floating (ungrounded/unreferenced/isolated) conductors are hazardous because they can accumulate charge and energy. Excellent dielectrics can accumulate charge and electrostatic energy as well. Limiting the charge storing material or charging capacity is a useful method for reducing the internal charging threat. This can be accomplished by providing a bleed path for conductors or by having only small quantities of charge-storing materials.

5.1.1.2 Coupling

Coupling energy from a source via a spark (ESD) is very configuration-dependent and a function of the radiated and directly coupled signals. An ESD can occur in a variety of ways, such as from metal-to-metal, metal-to-space, metal-to-dielectric, dielectric-to-dielectric, dielectric breakdown, etc. The configuration of the charges determines the type of breakdown and hence the form of coupling. An isolated conductor can discharge directly into an IC lead causing serious physical damage at the site, or the arc can induce an attenuated signal into a nearby wire causing little damage but inducing a spurious signal. As these examples illustrate, the coupling has to be estimated uniquely for each situation. Eliminating coupling paths from a spark source to a victim will significantly lower the ESD threat. Coupling paths can be eliminated by separation, shielding, or filtering.

5.1.1.3 Victim

A victim is any part, component, subsystem, or element of a spacecraft that can be adversely affected by an arc discharge (or field effects, in the case of some science instruments). Given the different effects of ESDs, the types and forms of victims can be highly variable. ESD and EMC-induced parts failures, while major problems, are not the only ones. Effects can range from the so-called soft errors, e.g., a memory element may be reset, to actual mechanical damage where an arc physically destroys material. Thus, the victims can range from individual parts to whole systems, from electronic components to optical parts. Discharging in glass has long been known to cause fracturing and damage to optical windows or dielectrics, but empirical data suggest optical lenses have apparently had a largely successful usage in space. The major victims and design sources will be either individual electronic components or cables that can couple the transient discharge into a subsystem. Shielding or filtering at the victim or replacing the victim with an ESD-tolerant alternative can limit the adverse effects of ESDs. In the case of field effects on science instruments, placing grounded conductive material around an opening or re-orienting the field of view has proven effective in limiting adverse effects.

5.1.2 Design

The designer should be aware of design guidelines to avoid surface and internal charging problems (see sections 5.2.2 and 5.2.3). **All guidelines should be considered in the spacecraft design and applied appropriately to the given mission.**

5.1.3 Analysis

Analysis should be used to evaluate a design for charging in the specified orbital environment. Two major approaches to such analysis are: a simple analysis ignoring design complexities or a detailed analysis considering the actual spacecraft design, perhaps with a computer code. A very simple analysis of internal electrostatic charging is illustrated in Appendix C. An example of a simple surface charging analysis is described in Appendix F. Several appropriate computer codes for more detailed analyses are listed in Appendix B.3.

5.1.4 Test and Measurement

Testing usually ranks high among the choices to estimate the likelihood and magnitude of discharges and to verify and validate the survivability of spacecraft hardware in a given environment. To simulate the spacecraft charging environment, it is difficult to replicate the actual plasma environment and total threat in all respects. The real electron environment can envelop the whole of the spacecraft and has a spectrum of energies. No test facility exists that can replicate all the features of that environment. As a consequence, verification and validation of charging protection are done with lower level hardware tests and with less realistic test environments. This does not reduce the value of the tests, but additional analyses have to be done to provide design validation where testing alone is inadequate. Several tests that can be performed to validate different aspects of charging are briefly described below.

5.1.4.1 Material Testing

Material electrical properties should be known before they are used in a design. The key material properties needed are the ability to accumulate charge, i.e., resistivity or conductivity and dielectric strength, and the pulse threat, e.g., stored charge, electrostatic energy. Secondary but important parameters include how properties such as resistivity can change with time in space, temperature (cold is more resistive), radiation dose, and atomic oxygen erosion, and, to a lesser extent, radiation-induced and E-field-induced conductivity. Other properties are secondary electron emission, backscatter emission, and photoelectron emission properties. Surface contamination of materials that occurs over time in space also changes their charging behavior, so the charging response at beginning of mission and end of mission may be very different.

Information about these parameters can be obtained from reference texts or by electron beam tests or conventional electrical tests. (Section 8.1 in this NASA Technical Handbook contains a sample dielectric materials list.) Analyses or tests can be used to determine the threat for particular sizes and shapes of these materials. Some test methods are described in Appendix D. Note that the

material's electrical properties can be changed significantly depending on the test conditions such as vacuum and temperature.

5.1.4.2 Circuit/Component Testing

The susceptibility threshold of components (transistors, ICs, etc.) is useful in understanding the threat from ESD events. The susceptibility can be a disruption threshold or a damage threshold. A V_{zap} test (see Appendix D.9) can be used to determine a component's capability to withstand the effects of an electrical transient pulse. When a damage threshold is determined, the number of pulses applied at a given voltage level should be carefully considered.

5.1.4.3 Assembly Testing

Potentially susceptible assemblies should be tested for sensitivity to ESD. The assembly to be tested is to be mounted on a baseplate and tested while operating. Pulses are generated by a pulse injection device or by an electron exposure of actual discharge-source material. Pulses are to be injected through the box of the assembly or injected into the pins of the connector while the performance of the assembly is monitored for upsets. The pulses used are to cover the expected range of current amplitudes, voltages, and pulse durations. It is very important that the pulse injection device be isolated electrically from the assembly being tested and the monitoring equipment. It is also important to ensure the transient does not disturb the support equipment.

5.1.4.4 System Testing

System-level testing can be the final proof that a system can survive a given environment. (The possibility of latent damage always has to be considered when flight hardware is tested.) For IESD environments, system testing is not feasible. Materials, circuit, and assembly testing, together with analysis, have to provide the system-level verification for internal charging concerns.

5.1.5 Inspection

Inspection is an important means for recognizing and minimizing the possibility of spacecraft charging discharge-induced anomalies. This inspection should be conducted as the spacecraft is being assembled by a person experienced in recognizing likely areas of concern from environmentally induced interactions. A list of acceptable values of resistance for joints and connections within the spacecraft should be generated ahead of the inspection, but the inspection should take a broader view and look for other possible areas of concern. Also, the existence of extra dielectrics, floating conductors, and shadowed region not shown in the design should be inspected.

5.2 Design Guidelines

This section contains general guidelines and quantitative recommendations on design guidelines/techniques that should be followed in hardening spacecraft systems to spacecraft charging effects. This section contains design guidelines divided into sections for General (see section 5.2.1), Surface Charging (see section 5.2.2), Internal Charging (see section 5.2.3), Solar

Arrays (see section 5.2.4), and Special Situations (see section 5.2.5) in this NASA Technical Handbook.

All guidelines depend on the specific mission environment. Tailoring the guidelines for a specific mission by an ESD expert is essential for good requirements. If one does not have access to an ESD expert, consult with the NESC "Space Environments" Technical Discipline Team.

5.2.1 General ESD Design Guidelines for Space Charging

5.2.1.1 Orbit Avoidance

If possible, avoid orbits and altitudes where charging is an issue. Usually, this is not an option. (Figures 1 and 2 show hazardous environments near Earth.) Spacecraft using electric propulsion to thrust the spacecraft to GEO orbit will need to make trades between additional design and mission life cost. Consideration needs to be given to accumulated radiation dose and charging hazard versus the savings in spacecraft fuel. The transfer orbit plan should be optimized for a specific mission (reference Wong and Kim [2016]).

5.2.1.2 Shielding

Shield all electronic elements with sufficient thickness so that the internal charging rate is benign. Shielding of electrons is a complex subject because electrons scatter as they pass through matter. The shielding geometry is very important. Experience has shown that for GEO orbits and today's hardware, an adequate shielding level has been on the order of 110 mil of aluminum-equivalent shielding, but 130 mil is more conservative and may be necessary for certain situations (see sections 4.1.7 and 5.2.3.2.2). This is the total shielding accounting for geometry, including spacecraft structure. A more accurate determination can be done by a Monte Carlo simulation capable of handling detailed geometric and spacecraft material descriptions and comparing results to the sensitivity of possible victims.

Shield all electronic elements using a Faraday Cage construction. The primary spacecraft structure, electronic component enclosures, and electrical cable shields should provide a physically and electrically continuous shielded surface around all electronics and wiring (Faraday Cage). The primary spacecraft structure should be designed as an electromagnetic-interference- (EMI-) tight shielding enclosure (Faraday Cage). The purposes of the shielding are to decrease entry of charged particles into the spacecraft interior and to shield the interior electronics from the radiated and conducted noise of an electrical discharge on the exterior of the spacecraft. All shielding should provide at least 40 dB attenuation of radiated electromagnetic fields associated with surface discharges. Few mils thickness of aluminum or magnesium will easily provide the desired attenuation, if made electromagnetically tight. This enclosure should be as free from holes and penetrations as possible. Many penetrations can be closed by use of well-grounded metallic meshes and plates. All openings, apertures, and slits should be eliminated to maintain the integrity of the Faraday Cage. (For example, reference Bogorad, et al. [2008].)

The vacuum deposited aluminum (VDA) metallization on multilayer insulation (MLI) thermal blankets is insufficient to provide adequate electromagnetic shielding for both EMC and external ESD (at frequencies of ESD pulses (100 kHz to 10 MHz)). Nor does it provide sufficient mass to reduce the external flux to levels that prevent internal charging. Layers of aluminum foil mounted to the interior surface and properly grounded can be used to increase the shielding effectiveness of blankets or films. Aluminum honeycomb structures and aluminum face sheets can also provide significant attenuation. Electronic enclosures and electrical cables exterior to the main Faraday Cage region should also be shielded to extend the coverage of the shielded region to 100% of the electronics. Unless all seams, penetrations, gaps, etc., are shielded with a totally connected conductive skin, the Faraday Cage implementation is incomplete and cannot be counted as proper protection to the interior electronics. For example, a viewing aperture of a star tracker is a penetration. Other examples include “mouse holes” for cable penetrations and vent holes. All have to be given careful attention as to their effects on the violation of the Faraday Cage principle.

Cable shields exterior to the Faraday Cage are used to maintain and extend the cage region from their exit/entrance of the main body of the spacecraft. Cable shields should be fabricated from metallic foil, sheet, or tape. Standard coaxial braid shielding or metalized plastic tape wraps on wires do not provide adequate shielding protection for internal charging protection and should not be used alone. Shields should be terminated when they enter the spacecraft structure from the outside and carefully grounded at the entry point with a 360-degree manner around the connector at each end of the cable. This technique can be found in any standard EMC textbook and is used by all spacecraft cabling fabrication departments. Braid shields on wires should be soldered to any overall shield wrap and grounded at the entrances to the spacecraft. Conventional shield grounding through a connector pin to a spacecraft interior location cannot be used without violating the total shielding integrity.

Electrical terminators, connectors, feedthroughs, and externally mounted components (diodes, etc.) should be electrically shielded, and all shielded connector covers have to be bonded to the common structural ground of the space vehicle.

5.2.1.3 Bonding

Bond all structural elements. Identify isolated conducting elements and provide bonding to chassis for those areas. Make a separate bond strap for conductive items mounted at the end of dielectric booms. Every conductive internal part should be connected by a deliberate or leakage impedance to chassis of 10^8 ohm or less in a vacuum at the operation temperature. Conductive fittings on dielectric structural parts should also comply.

All conducting elements, surface and interior, should be bonded to a common electrical ground reference, either directly, through a charge bleed-off resistor, or via a controlled voltage on the conductor as in electrical/electronic circuitry (nothing electrically floating).

All structural and mechanical parts, electronics boxes, enclosures, etc., of the spacecraft should be electrically bonded to each other. All principal structural elements should be bonded by methods that assure a dc resistance of less than 2.5 mohm at each joint if required for EMC or electrical

ground referencing reasons (see NASA-STD-4003A); otherwise, a high value bleed resistance is permissible.

The collection of electrically bonded structural elements is referred to as structure or structure ground. The objective is to provide a low-impedance path for any ESD-caused currents that may occur and to provide an excellent ground for all other parts of the spacecraft needing grounding. If structure ground reference has to be carried across an articulating joint or hinge, a ground strap, as short as possible, should carry the ground across the joint. Relying on bearings for a ground path is unacceptable. If structural ground has to be carried across slip rings on a rotating joint, at least two (preferably more) slip rings should be dedicated to the structural ground path, some at each end of the slip ring set. The bond to structure should be achieved within 15 cm of the slip ring on each end of the rotating joint. Slip rings chosen for grounding should be remote from any slip rings carrying sensitive signals.

5.2.1.3.1 Surface Materials and Their Bonding

All spacecraft surface (visible, exterior) materials should be conductive in an ESD sense (see section 5.2.1.5). All such conductive surface materials should be electrically bonded (grounded) to the spacecraft structure. Because they are intended to drain currents directly from space environment, the bonding requirements are more stringent than those for internal materials. The dc impedance to structure has to remain less than 10^7 ohm over the service life of the bond in vacuum, under temperature, under mechanical stress, etc.

5.2.1.3.2 Wiring and Cable Shields and Their Bonding

All wiring and cabling entering or exiting the shielded Faraday Cage portion of the spacecraft (reference section 5.2.1.2) has to be shielded. Those cable shields and any other cable shields used for ESD purposes have to be bonded (grounded) to the Faraday Cage at the entry to the shielded region as follows:

a. The shield has to be terminated 360 deg around a metal shielded backshell, which in turn has to be terminated to the chassis 360 deg around the cabling.

b. The shield bond (ground) should not be terminated by using a connector pin that penetrates the Faraday Cage and receives its ground inside the shielded region.

c. A mechanism should be devised that automatically bonds the shield to the enclosure/structure ground at the connector location such as a backshell that captures the shield and is grounded directly to structure at the interconnect panel. A ground lug that uses the shortest possible ground wire could be provided for the shield if a grounded backshell cannot be used, and procedures that verify that the shield is grounded at each connector mating should be established. Even a short length of wire from a ground lug to structure will introduce an inductance that degrades the effectiveness of the shield, so bonding of the shield through a well-grounded backshell is preferred.

d. The other end of the cable shield should be terminated in the same manner. The goal is to maintain shielding integrity even when some electronics units have to be located outside the basic shielded region of the spacecraft. (Even when there is no readily available nearby "ground" (for example, for temperature sensors, heaters, or deployment switches), designers should attempt to ground the cable shield and sensor shield; if not possible, verify that there is enough shielding not to have discharges at all or the resulting discharges are not strong enough to damage or disturb the sensor electronics.)

Note that a braided shield can be a good EMI/EMC shield but is not a good ESD shield. To minimize the discharge magnitude, a conductive tape with 100% visual coverage with a minimal gap is needed (see section 5.2.1.12, Kim, et al. [2010]).

5.2.1.3.3 Electrical and Electronic Grounds

Signal returns and power grounds (zero-volt reference points) require special attention in the way they are connected to the spacecraft structure ground. NASA-HDBK-4001, Electrical Grounding Architecture for Unmanned Spacecraft, is a good reference. For ESD purposes, a direct wiring of electrical/electronic units to structure is most desirable. In particular, do not use separate ground wires daisy-chained from unit to unit or from each unit to a distant single point (star ground) on the structure.

5.2.1.4 Conductive Path

Have a conductive path to the structure for all circuitry. A simple and direct ground path is preferred without outside wiring to the ground point. Note areas where circuits or wires may be isolated for any reason. Place bleed resistors on all circuit elements that may become unreferenced (floating) during mission events, such as switching or connector de-mating. Use NASA-HDBK-4001 as a guide to eliminate ground loops if necessary.

5.2.1.5 Material Selection

Limit usage of excellent dielectrics. Metals are conductive, and protecting them from internal charging is a relatively simple matter of ensuring a charge leakage path. The materials of concern in controlling internal charging are dielectrics. Prominent dielectrics in modern spacecraft include, but are not limited to, Teflon®, Kapton®, polyetheretherketone (PEEK), ULTEM® (polyetherimide), G10 (fiberglass epoxy laminate sheet), the resins of carbon composites, and most circuit board materials, including FR4. These are excellent charge-storing materials. Their use should be minimized or avoided if possible, especially in large blocks. Usages such as wire insulation or thin films (5 mil, for example) seem to contribute less or no problems on the interior of spacecraft. Circuit board materials may be a problem, but densely populated boards with a ground plane are less of a problem; short paths through the dielectric to nearby circuit traces permit easy electron bleed-off. Validate material performances with electron beam tests in accordance with Appendix D.2. Brunson and Dennison (2007) and Gillespie (2013) have measured dielectric resistivity at lower temperatures and quantified the known increase in resistivity with decreasing temperature.

To the extent possible, make all interior dielectrics electrically leaky. Internal dielectrics should be static-dissipative or leaky. This applies specifically to circuit boards but would be desirable for all dielectrics, including cable wiring and conformal coatings. The degree of leakiness or conductivity does not need to be great enough to interfere with circuit performance. It can be on the order of 10^4 to 10^{11} ohm cm or of 10^5 to 10^{12} ohm/square (see Appendix D.4 for a discussion of ohm/square) and still provide a bleed path to electrons for internal charging purposes. Verify that the conductivity and resistivity remain adequate over the mission life. Meeting this guideline and also providing the other necessary properties (mechanical, workable, etc.) may be a challenge because carbon doping, a typical method to make a dielectric leaky, may alter dielectric's mechanical properties.

Make all spacecraft exterior surfaces at least partially conductive. The best way to avoid differential charging of spacecraft surfaces is to make all surfaces conductive and bonded to the spacecraft structure. Typical spacecraft surface materials often include insulating materials such as Mylar® **(**biaxially-oriented polyethylene terephthalate), Kapton®, Teflon®, PEEK, ULTEM®, G10, fiberglass, glass, quartz, or other excellent dielectrics. It should be recognized in the design phase that there may be areas for which use of dielectric surfaces is particularly crucial, such as areas adjacent to receivers/antennas, sensitive detectors (Sun and Earth detectors, plasma wave detector, etc.), areas where wires connected to sensitive electronics are running nearby, or areas where material contamination or thermal control are critical. For these applications, use of (grounded) dissipative coatings, such as indium tin oxide (ITO) or germanium (Ge) is recommended.

Composite materials comprised of small conducting particles distributed in a dielectric material such as some paints or carbon-loaded polymers are often attractive options creating non-metallic but still conducting spacecraft components or surfaces. Be aware that common conductivity measurement techniques may significantly overestimate the conductivity of these materials (see Appendix D.5). Ensure materials retain the desired conduction properties for a mission's thermal and radiation environment (reference Green, et al. [2019]). When a sufficiently conductive composite material is used for RF devices, the increased RF insertion loss is to be considered.

This section first defines the conductivity guidelines for spacecraft surface materials. Materials that are typically used are then evaluated and their usage is discussed. Analysis is suggested to estimate the effects of any dielectric surfaces that may remain on the spacecraft. At the conclusion of this section, use of materials with a high secondary electron yield is discussed.

5.2.1.5.1 Surface Materials Selection Advice

By the proper choice of available materials, the differential charging of spacecraft surfaces can be minimized. At present, the only proven way to eliminate spacecraft potential variations is by making all surfaces conductive or charge-dissipative and connecting them to a common ground.

Surface coatings in use for this purpose include conductive conversion coatings on metals, conductive paints, and transparent, partially metallic vacuum-deposited films, such as ITO. Table 3, Examples of Surface Coatings and Materials Acceptable for Spacecraft Use, describes some of the more common acceptable surface coatings and materials with a successful use history. Table 4,

Surface Coatings and Materials to be Avoided for Spacecraft Use, describes other common surface coatings and materials that should be avoided if possible.

The following materials have been used to provide conducting surfaces on the spacecraft (remember, these conductive surfaces have to be grounded or at least not floating):

a. Vacuum-metalized dielectric materials in the form of sheets, strips, or tiles. The metal-on-substrate combinations include aluminum, gold, silver, and Inconel® alloys on Kapton®, Teflon®, Mylar®, and fused silica.

b. Thin, conductive front-surface coatings, Ge and Stamet coatings and ITO on fused silica, Kapton®, Teflon®, or dielectric stacks. Cracking and flaking of the conductive coating should be examined.

c. Conductive paints, fog (thin paint coating), carbon-filled Teflon®, carbon-filled polyester on Kapton®, or black Kapton®. Conductivity at the expected minimum temperature should be verified.

d. Conductive adhesives.

e. Exposed conductive facesheet materials (graphite/epoxy - abraded with fine sandpaper to remove dielectric epoxy from the surface (reference Green and Dawson [2015] and Likar, et al. [2015a]), or a conductive coating/paint is needed). Make sure that there is no charging threat after the mitigation (such as abrasion or adding conductive or charge-dissipative coating). Because each graphite/epoxy facesheet can be constructed differently, it needs to be tested after surface mitigation.

f. Etched metal grids or bonded (or heat embedded) metal meshes on nonconductive substrates. From the ESD viewpoint, this is generally NOT a good conductive surface, similar to a braid shield of a cable. The ESD compatibility needs to be verified by test.

g. Aluminum foil or metalized plastic film tapes. Make sure that the metal layer is grounded.

Because of the variety in the configuration and properties of these materials, there is a corresponding variety in the applicable bonding techniques and specific concerns that have to be addressed to ensure reliable in-flight performance.

The following practices have been found useful for grounding/bonding surface materials:

a. Conductive adhesives should be used to bond fused silica, Kapton®, and Teflon® second-surface mirrors (especially metallic mirror layer) to conductive substrates that are grounded to structure. If the substrate is not conductive, metal foil or wire ground links should be laminated in the adhesive and bolted to structure. Only optical solar reflectors (OSRs) with conductive back surfaces (example: Inconel®) should be used.

Table 3—Examples of Surface Coatings and Materials Acceptable for Spacecraft Use

Note: Have to be grounded to chassis

MATERIAL	COMMENTS
Paint (carbon black)	Work with manufacturer to obtain paint that satisfies ESD conductivity guidelines of section 5.2.2 of this NASA Technical Handbook and thermal, adhesion, radiation tolerance, and other needs.
GSFC NS43 paint (yellow)	Has been used in some applications where surface potentials are not a problem; apparently will not discharge.
ITO (250 nm)	Can be used where some degree of transparency is needed; has to be properly grounded. For use on solar cells, optical solar reflectors, and Kapton® film, use sputtered method for application and not vapor deposited.
Zinc orthotitanate paint (white ZOT)	Possibly the most conductive white paint; adhesion difficult without careful attention to application procedures, and then difficult to remove.
Alodine® or Chemfilm	Conductive conversion coatings for magnesium, aluminum, etc., are acceptable.
DuPont Kapton® XC family	Carbon-filled polyimide films; 100XC with nominal resistivity of 2.5 x 10^4 ohm cm (5 x 10^6 ohm/square), 160XC (370 ohm/square), and 275XC (260 ohm/square); not good in atomic oxygen environment without protective layer (ITO, for example). (100CB is not a conductive black Kapton®.)
Deposited conductors	Examples: aluminum, gold, silver, Inconel® alloy on Kapton®, Teflon®, Mylar®, and fused silica.
Conductive paints (such as Z93C55, Z307, BR-127 NC/ESD)	Over dielectric surfaces, with some means to assure charge bleed-off. Ensure conductivity at all operating temperatures.
Carbon (or carbon nanotube)-filled Teflon® or Kapton®	Carbon filler helps make the material conductive. Ensure that fillers are evenly distributed and that there is sufficient conductivity in relevant environment.
Conductive adhesives	Especially if needed for bridging between a conductor and ground.
Conductive surface materials	Graphite epoxy (abraded to remove outer dielectric epoxy) or metal.
Etched metal grids	Etched or bonded to dielectric surfaces, frequent enough to have surface appear to be grounded. NOT good from ESD viewpoint.
Aluminum foil or metalized plastic film tapes	If they can be tolerated for other reasons such as thermal behavior.

b. When conductive adhesives are used, the long-term stability of the materials system has to be verified, particularly conductivity in vacuum after thermal cycling, compatibility of the materials (especially for epoxy adhesive) in differential thermal expansion, and long-term resistance to galvanic corrosion.

c. Metalized Teflon® is particularly susceptible to ESD degradation, even when grounded. Avoid using it. If there is no substitute for a specific application, the effects of EMI, contamination, and optical and mechanical degradation especially due to radiation dose have to be evaluated.

d. Paints (ESD-conductive/leaky) should be applied to grounded, conductive substrates; the primer has to be conductive, too. If painting over a grounded surface is not possible, paint coverage should be extended to overlap grounded conductors around the paint's perimeter.

e. Ground tabs have to be provided for free-standing (not bonded down) dielectric films with conductive surfaces.

Table 4—Surface Coatings and Materials to be Avoided for Spacecraft Use

MATERIAL	COMMENTS
Anodize	Anodizing produces a high-resistivity surface to be avoided for ESD applications. The coating can be made quite thin and might be acceptable if measurement shows good enough conductivity.
Fiberglass material	Resistivity is too high and is worse at low temperatures.
Paint (white)	In general, unless a white paint is measured to be acceptable, it is unacceptable. (Examples of typical non-conductive white paints: S13G/LO and Z306)
Mylar® (uncoated)	Resistivity is too high.
Teflon® (uncoated)	Resistivity is too high. Teflon® has demonstrated long-time charge storage ability and causes catastrophic discharges.
Kapton® (uncoated)	Generally unacceptable because of high resistivity; however, in continuous sunlight applications if less than 0.13 mm (5 mil) thick, Kapton® is sufficiently photoconductive for use.
Silica cloth	Has been used for antenna radomes. It is a dielectric; but because of numerous fibers or if used with embedded conductive materials, ESD sparks may be individually small. It has particulate issues, however.
Quartz and glass surfaces	It is recognized that solar cell coverglasses and second-surface mirrors have no substitutes that are ESD acceptable; they can be ITO coated with minor performance degradation, and the ITO has to be grounded or ground referenced. Their use has to be analyzed and ESD tests performed to determine their effect on neighboring electronics. Be aware that low temperatures significantly increase the resistivity of glasses (reference Hoeber, et al. [1998]). It should be carefully evaluated before usage.

f. Several techniques for bonding thin, conductive front-surface coatings such as ITO exist. At least one commercial manufacturer has found the added cost of a reliable ITO coating and bonding/grounding/referencing method on OSRs and coverglasses has provided excellent in-orbit performance and is worth that cost. The methods include welding of ground wires to front-surface metal welding contacts, front-surface bonding of coiled ground wires (to allow for differential thermal expansion) by using a conductive adhesive, and chamfering the edges of OSRs before ITO coating to permit contact between the coating and the conductive adhesive used to bond the OSR to its substrate.

g. For MLI, extending the aluminum foil tab to the front surface is suitable.

5.2.1.5.2 Nonconductive Surfaces

It is best to coat all non-conductive dielectric surfaces with a conductive or charge dissipative coating (and ground it). Because the spacecraft surface cannot be made 100% conductive, an analysis has to be performed to show that the design is acceptable from an ESD standpoint. Note that not all dielectric materials have the same charging or ESD characteristics. The choice of dielectric materials can affect surface potential profiles significantly. For example, it has been shown (reference Hoeber, et al. [1998] and Bever and Staskus [1981]) that different coverglass materials have differing resistivities and that all are affected by temperature. Cover slide material without ITO coating can noticeably affect spacecraft charging.

An adequate analysis preceding the selection of materials has to include a spacecraft charging analysis to determine surface potentials and voltage gradients, spark discharge parameters (amplitude, duration, frequency content), and EMI coupling. The cost and mass involved in providing adequate protection (by shielding and electrical redesign) could tilt the balance of the trade-off to favor the selection of, for example, less optically transmissive coverglasses that are more reliable from spacecraft charging, discharging, and EMI points of view.

The proven materials have their own cost, mass, availability, variability, and fabrication effects. In addition, uncertainties relating to spacecraft charging effects have to be given adequate consideration. Flight data have shown apparent optical degradation of standard, stable thermal control materials, e.g., OSRs and Teflon® second-surface mirrors, that is in excess of ground test predictions, part of which could be the result of charge-enhanced attraction of charged contaminants. In addition, certain spacecraft anomalies and failures may have been reduced or avoided by using charge control materials.

When the spacecraft design is completed, the remaining dielectric materials on the surface of the spacecraft have to be evaluated for their ESD hazard due to their differential charging. Potential stored energy, nearby potential victims, and possible paths to victims have to be evaluated to see if a spacecraft threat exists. Each dielectric region has to be assessed for its breakdown voltage, its ability to store energy, and the effects it can have on neighboring electronics (disruption or damage) and surfaces (erosion or contamination).

5.2.1.5.3 Surface Secondary Emission Ratios

Other means to reduce surface charging exist but are not well developed and are not in common usage. One suggestion for metallic surfaces is an oxide coating with a high secondary electron yield. This concept, in a 3D surface charging simulation, reduced charging of a spacecraft dramatically and reduced differential charging of shaded Kapton® slightly. Any selected materials should be carefully analyzed (for example using NASCAP-2k) to ensure they do not create

problems of their own and will function as required over their intended lives and degrees of surface contamination.

5.2.1.6 Radiation Spot (Local) Shields and Other Floating Metals

It is essential for ESD protection to ground-reference radiation spot shields. Bodeau (2005; 2010) in particular emphasizes this rule. ESD ground-referencing can be done in a number of ways. If a partially conductive urethane or other conformal coating has appropriate resistivity (on the order of 10^{10} or less ohm cm), a separate ground path is unnecessary. However, continuity of conformal coats over large edges (spot shields, relay and other components) needs to be verified by inspection, as the coatings flow after application and before curing. Also, it has to be determined that any solution, such as partially conductive urethane, will not degrade (increase resistivity) in the expected radiation, thermal, and long-term vacuum environments. (This relatively large resistivity, $<10^{10}$ ohm cm, is generally acceptable for interior dielectrics since charging fluxes are lower on the interior of a spacecraft. Check actual charging fluxes if uncertain about a particular application.)

5.2.1.7 Filter Circuits with Lumped Elements or Circuit Choices

Use low pass filters or suppression diodes on interface circuits to suppress the incoming ESDs. Use low-speed, noise-immune logic, if possible. Use Complementary Metal-Oxide-Semiconductor (CMOS) circuits that have higher interface noise immunity. Beware of the latch-up sensitivity of CMOS. For ESD purposes, the filter or protection network has to be applied so that it is physically at the unit interfaces. Note: RF systems typically employ high pass or bandpass filters that use series capacitance and shunt inductance. If the cut-on frequency is high enough (e.g., GHz range), it will prevent passing of most of the ESD spectrum to the down-stream circuits. The low-frequency blocking action of the capacitors will dc isolate the center conductor of the RF coax, potentially creating a floating metal hazard (which should be avoided). The breakdown voltage of the blocking cap is significantly lower than the coax cable itself and determines when breakdowns will occur (and not the internal electric field across the dielectric on the coax). Also, the filter must be qualified (tested) to demonstrate that it survives the ESD pulses at its input.

Electrical filtering should be used to protect circuits from discharge-induced upsets. All circuits routed into the Faraday Cage region, even though their wiring is in shielded cabling, run a higher risk of having ESD-caused transient currents on them. Initial design planning should include ESD protection for these circuits. It is recommended that filtering be applied to these circuits unless analysis shows that it cannot be used or is not needed.

The usual criterion suggested for filtering is to eliminate noise shorter than a specific time duration, i.e., above a specific frequency. On the Communications Technology Spacecraft (CTS), in-line transmitters and receivers effectively eliminated noise pulses of less than 5-us duration, which were suitable to its circuitry. Similar filtering concepts might include a voltage threshold or energy threshold. Filtering is believed to be an effective means of preventing circuit disruption and should be included in system designs. Any chosen filtering method should have analyses and tests to validate the selected criteria. Filters should be rated to withstand the peak transient voltages and currents over the mission life. Today’s circuitry with smaller feature sizes and lower operating

voltages may need even more stringent filtering for ESD protection. High-speed interfaces will need cable shielding to minimize the threats since they cannot be filtered.

5.2.1.8 Isolate Transformer Primary-to-Secondary Windings

Isolate the primary and secondary windings of all transformers. Reduce primary-to-secondary winding capacitance to reduce common mode noise coupling. This is an EMC solution to reduce coupling of ESD-induced noise.

5.2.1.9 Bleed Paths for Forgotten Floating Conductors

Provide a conductive bleed path for all conductors (including structural elements) (unless it is proven to have no ESD threat), including, but not limited to, the following items:

a. Signal and power transformer cores and inductor cores.

b. Capacitor cans.

c. Metallic IC and hybrid device cases and lids (cans, housings).

d. Unused connector pins and unused wires in cables, including those isolated by switching.

e. Relay cans.

f. Unused circuits in multi-packs.

g. Circuit board interdigitated RF filter elements.

h. Thin film conductive optics layer.

i. Metalized films, especially on thermal radiators and blankets.

j. Heat sinks

These items may be protected by stray leakage, by deliberate resistors to ground, through their (not-too-resistive) conformal coating, normal bleed paths, or small charge/energy storage areas. Ensure that the presumed bleed path really works or that the floating items are not an ESD threat before depending on stray leakage for ESD protection. Alternatively, if tested in an electron beam facility and no problems are noted, then additional ESD grounding may not be necessary.

5.2.1.10 Interior Paints and Conformal Coatings

Most paints and conformal coatings are dielectrics and can be charged by energetic particles. This has to be considered in evaluating the likelihood of interior charging of a design. If conductive coatings are used, these have to be grounded to the structure to allow charge to bleed off and the

conductivity has to be checked at the operating condition (temperature, vacuum, radiation dose, etc.).

5.2.1.11 Cable Harness Layout

Route cable harnesses away from apertures as much as possible. Care should be taken in the layout of the electrical harnesses inside the Faraday cage to minimize exposure to the environment's energetic particles. The harness should not be close to the edges of apertures. This guidance is not always met since harnesses are often routed along the edges of panels and then to the unit connectors on the tops or sides of the unit chasses to avoid having to make blind connector mates to the units. Gaps between panels, and cutouts ("mouseholes") are often located here and provide leakage of external ESD fields into the spacecraft interior. Closing the gaps in the faraday cage can significantly reduce external ESD coupling to the harnesses inside.

5.2.1.12 External Wiring

Provide additional protection for external cabling. Cables external to the spacecraft structure should be given adequate protection. The dielectric insulators, jackets, and heat shrink tubing can charge to a point where discharge can occur. At present, there are no simple design rules for the degree of shielding needed. It is recommended to minimize discharge magnitude that cables be tightly wrapped by a conductive tape with 100% visual coverage to minimize gaps where discharges can propagate. The conductive layer of wrapped tape (when there is a non-conductive layer in the tape) should make a direct contact between turns. A tight wrapping with a conductive tape with a conductive adhesive will work well.

5.2.1.13 Slip Ring Grounding Paths

Carry bonds and grounds across all articulated and rotating joints. For a rotating joint with slip rings, the chassis or frame ground (bond) has to be carried through the slip ring also and then grounded. Note that for the case of the solar array and other situations that may be involved in transfer of ESD current, a series resistance in the path from spacecraft frame to solar array frame will be required to limit the amount of current that can carry this ESD current into the spacecraft (see section 5.2.4.3.t).

5.2.1.14 Wire Separation

Segregate cabling from outside the spacecraft after it enters the Faraday Cage. Wires coming from outside the spacecraft should be filtered, preferably at the entry point but certainly before being routed with other interior cabling. This is based on an assumption of external ESD noises and is to prevent coupling to the interior. It is a poor design practice to route the filtered and unfiltered wires together in the same bundle because noise can be coupled between them.

5.2.1.15 ESD-Sensitive Circuits/Parts

Pay special attention to ESD-sensitive circuits and parts especially when discharges are expected to occur in the vicinity. Discharge can damage parts as well as induce upset on circuitry. In the parts

list, flag all parts that are less than Human Body Model (HBM) Class 2 ESD-sensitive in accordance with MIL-STD-883-3, Test Method Standard, Electrical Tests (Digital) for Microcircuits (Method 3015.9, Electrostatic Discharge Sensitivity Classification [Human Body Model]). Note that the voltage used for HBM classification is the voltage at the capacitor rather than the actual transient pulse voltage at the parts (see Appendix D.9). Do a charging analysis after completion of the spacecraft design. Evaluate the charging rates with respect to section 5.2.2 of this NASA Technical Handbook parameters. Perform an assessment of discharge rate and magnitude. Discharge rate and magnitude can also be estimated by testing of the material in the design configuration. Conducted discharge current waveform can be measured. An E-field probe can also be used to capture the radiated RF field from the discharge. The RF radiated field as shown in section 6.3.2.1 of this NASA Technical Handbook can be used as reference. Protect the parts if they might be damaged by an expected threat (discharge magnitude and total number of expected discharges during mission) and protect the circuit from upset due to the coupled transient. The project level margin on voltage, current and/or RF field should be used in the design.

5.2.1.16 Procedures

Institute proper handling, assembly, inspection, and test procedures to ensure the electrical continuity of the space vehicle grounding system. The continuity of the space vehicle electrical grounding and bonding system is of great importance to the overall design susceptibility to spacecraft charging effects. In addition, it will strongly affect the integrity of the space vehicle EMC design. Proper handling and assembly procedures have to be followed during fabrication of the electrical grounding system. All ground ties should be carefully inspected, and dc resistance levels should be tested during fabrication and again before delivery of the space vehicle. A final check of the ground system continuity during preparation for space vehicle launch is desirable.

A related reference is NASA-HDBK-4001 which describes how to establish an electrical grounding architecture system for power and signals. This NASA Technical Design Handbook is complementary to the ESD effort.

5.2.2 Surface ESD Design Guidelines, Excluding Solar Arrays

5.2.2.1 Qualitative Surface ESD Guidelines

Refer to General ESD Design Guidelines, section 5.2.1, in this NASA Technical Handbook.

5.2.2.2 Quantitative Surface ESD Guidelines

These detailed surface conductivity design guidelines are equation-based to assist designers in accounting for differing geometries and material conductivities. Since these are general, projects should formulate their own rules. The following guidelines are presented to achieve less than 10 V differential charging, assuming 5 nA/cm^2 charging flux.

To discharge surfaces that are being charged by space plasmas, a high resistivity to ground can be tolerated because the plasma charging currents are small. The following guidelines are suggested:

a. Conductive materials, e.g., metals, have to be grounded to structure with resistance, expressed in ohm:

$$R < 2 \times 10^9/A \quad \text{(Eq. 11)}$$
$$R < V/J_sA \quad \text{(Eq. 11-1)}$$

where:
- V = differential potential (V), 10 V is used here
- J_s = charging flux (A/cm^2), 5 x 10^{-9} A/cm^2 is used here
- R = resistance (ohm)
- A = exposed surface area of the conductor in square centimeters (cm^2).

b. Partially conductive surfaces, e.g., paints, applied over a grounded conductive surface have to have a resistivity-thickness product, expressed in ohm cm^2

$$\rho t < 2 \times 10^9 \quad \text{(Eq. 12)}$$
$$\rho t < V/J_s \quad \text{(Eq. 12-1)}$$

where:
- ρ = material resistivity in ohm cm
- t = material thickness in cm.

c. Partially conductive surfaces applied over a dielectric and grounded at the edges have to meet the following inequality, expressed in ohm cm^2, such that

$$\rho h^2/t < 4 \times 10^9 \quad \text{(Eq. 13)}$$
$$\rho h^2/t < 2V/J_s \quad \text{(Eq. 13-1)}$$

where:
- ρ = material resistivity in ohm cm
- t = material thickness in cm
- h = greatest distance on a surface to a ground point in cm.

In all cases, the usage or application process has to be verified by measuring resistance from any point on the material surface to structure. Problems can occur. For example, one case was observed in which a non-conductive primer was applied underneath a conductive paint; the paint's conductivity was useless over the insulating primer.

All bonding methods have to be demonstrated to be acceptable over the service life of the spacecraft. It is recommended that all joint resistances and surface resistivities be measured to verify compliance with these guidelines. Test voltages to measure resistivity of dielectric samples should be at least 500 V. See Appendix D.5 in this NASA Technical Handbook for measurement examples.

Bonding methods have to be able to handle current bleed-off from ESD events, vacuum exposure, thermal expansion and contraction, etc. As an example, painting around a zero-radius edge or at a seam between two dissimilar materials could lead to cracking and a loss of electrical continuity at that location.

5.2.3 Internal ESD Design Guidelines

Guidelines for internal hardware are often the same as for the guidelines for surfaces.

5.2.3.1 Qualitative Internal ESD Guidelines

Refer to General ESD Design Guidelines, section 5.2.1, in this NASA Technical Handbook. Internal regions also have surfaces, and surface rules apply.

5.2.3.2 Quantitative Internal ESD Guidelines

Quantitative guidelines are recommended in the following sections.

5.2.3.2.1 Bonding/Grounding Conductive Elements

Unused spacecraft cables and conductive elements on spacecraft surface greater than 3 cm^2 in surface area (significantly smaller area for conductive elements on circuit boards) or longer than 25 cm in length have to be ground referenced (reference Leung, et al. [1983]). It does not mean floating conductors smaller than 3 cm^2 and shorter than 25 cm can be used freely for all circumstances. All floating conductors should be assessed before use; be sure to provide a deliberate or known bleed path for all radiation spot shields and IC lids. For other wires and metal, being in a circuit is usually adequate. It is best not to have any deliberate floating metals, including unused connector pins as an example. Exceptions are allowed in situations in which one of the following conditions is true:

a. Discharges will not occur in the expected charging environment.

b. The discharges expected to occur will not damage or disrupt the most sensitive circuits in the vicinity nor cause EMI that exceeds the EMC requirements, assuming separate EMC requirements exist.

These historic quantitative guidelines may need reconsideration for newer spacecraft. For example, ECSS-E-ST-20-06C, Space Engineering, Spacecraft Charging Standard, recommends a maximum of 1 cm^2 ungrounded metal on the surface of a spacecraft.

5.2.3.2.2 Shielding to Limit Internal Electron Fluxes

Determine electron fluxes at all part locations using a worst-case electron spectrum (see Figure 9 for GEO) and shield all electronic circuitry to the following levels (see Figure 8 basis with no margin; projects may wish to consider margins):

GEO orbit approximate rule of thumb to limit IESD: If there are 130 mils of aluminum-equivalent shielding, it was previously stated (4.1.7) that there is no need to shield further; and there is no need to do an electron transport analysis unless there is a desire to save mass (GEO orbit approximate rule only). Bodeau's (2005; 2010) recommendations for lower flux limits have the effect of raising this further in Earth GEO orbits.

If the computed flux at the location of the dielectric is less than 0.1 pA/cm^2, the circuit needs no additional shielding (any electron environment). (Basis: less than 2 x 10^{10} e/cm^2 deposited in 10 hr—using only the incident fluence is more conservative.) Note, however, that Bodeau (2005; 2010) and Balcewicz, et al. (1998) recommend one-tenth of this (0.01 pA/cm^2) based on studies of in-orbit anomalies, which begins to present difficulties in implementation. Note also that this recommendation based on 10 hours of charging duration depends on the assumed room temperature bulk resistivities of commonly used dielectric materials. For applications which are constantly at cryogenic temperatures, the flux limit has to be adjusted downward to account for the increased cryogenic bulk material resistivities (see in particular Bodeau [2010]). Also note that ECSS-E-ST-20-06C and Bodeau (2010) recommend longer flux integration times to account for dielectric materials with time constants greater than 10 hours (see Eq. 3 for the relation between the threshold flux and the material time constant). For spacecraft that use electric propulsion for transfer orbit to GEO, the peak charging duration and magnitude is determined by the rate and path the spacecraft transits through the heart of the electron belt (reference Wong [2016] and Likar, et el. [2015b]).

5.2.3.2.3 Filter Circuits

For wiring shielded to less than the levels of section 5.2.3.2.2 of this NASA Technical Handbook, attached circuits can be protected by filtering (in frequency domain and/or in time domain). For example, to protect an interior circuit from a discharge on external sources such as temperature transducers that are located outside the main box of the spacecraft, an RC filter or diode protection can be used to suppress any ESD effects. Typically, 2X of the estimated threat (in magnitude and in number of expected discharges during mission life) is used as the source for the filter assembly design.

5.2.3.2.4 Voltage Stress

Keep the electric field stress in dielectrics below the dielectric strength of the material (see section 4.1.5 of this NASA Technical Handbook). When designing high-voltage systems, keep the electric field well below the dielectric strength of the material or gap. This voltage stress could be in circuit board dielectrics being charged by the incident electron flux while the adjacent metals remain at a low voltage. Other sites of concern are floating metal radiation shields on insulating surfaces charged by the electron flux while the adjacent surfaces remain at low voltages or insulated surfaces being charged while internal wires remain at low voltage. Destructive sustaining arcs can be triggered in power circuits and supplies by otherwise non-destructive discharges, so power wiring should never be bare (exposed). All such possible sources have to be eliminated where possible.

5.2.3.2.5 Coat Circuit Boards with Leaky Dielectric

Use leaky/conductive conformal coating on circuit boards. Leung and Mikkelson (2007) use a 10^{10} ohm cm clear coating, resulting in an automatic bleed path of resistance (R), such that 10^9 ohm $< R < 10^{13}$ ohm (the upper limit depends on the mission environment and shielding). This shunt leakage will not affect circuit operation but can help bleed off internal charging. The coating has been space qualified (temperature cycle, vacuum, etc.). It has demonstrated dramatic reduction in discharge voltages on its victims in laboratory tests and does not involve circuit or board layout changes. At present, the specific formulation is a proprietary product, but the concept could be adapted.

5.2.3.2.6 Fill Circuit Board Material with Grounded/Referenced Metal

When shielding is less than the levels of section 5.2.3.2.2 of this NASA Technical Handbook, limit the regions where charge can accumulate. Place grounded (best) or ground referenced traces in open (unused) areas. This idea was adopted from the previous version of this NASA Technical Handbook (Revision A) to minimize the size of any ESD arc inside of a circuit board by reducing the dielectric volume that might contain a discrete lump of ESD energy. For most electronics parts, it is safe if the ESD energy can be limited below 1 µJ (see Figure 45). It was not developed in response to a specifically identified failure in space *and has not been validated*. The derivation is shown in Appendix G.

Circuit boards and flex circuits should be designed so that any metal area greater than 0.3 cm^2 should also have a bleed path with the same ESD grounding limits of 0 to 10 Mohm resistance to ground. They should be designed so that there will be no open (unused) surface areas greater than 0.3 cm^2. Otherwise, place a metal land that is ESD grounded with 0 to 10 Mohm resistance to ground in the unused dielectric area. (Note that 0.3 cm^2 condition is derived with the assumption of 1×10^6 V/m dielectric strength and other parameters specified in Appendix G. This guideline should be tailored for a given mission with the appropriate parameters.)

This effect is shown in Figure 10, Permissible Area versus Depth to Ground or Ground-Referenced Plane, which also proposes a guideline for circuit board exposed dielectric areas. (The term “ground-referenced” in the figure means (a) not floating or (b) referenced within the circuit (see section 3.2 of this NASA Technical Handbook).) The design guideline assumes a standard FR4 circuit board material with the dielectric constant of 4.7. The term “depth to ground or ground-referenced plane” means the distance from any dielectric to a ground or ground-referenced plane. For example, if the board is 60 mil thick with a ground plane on one external surface, the depth to ground plane is 60 mil; if both exterior surfaces are ground (or power) planes, the depth to ground plane is 30 mil.

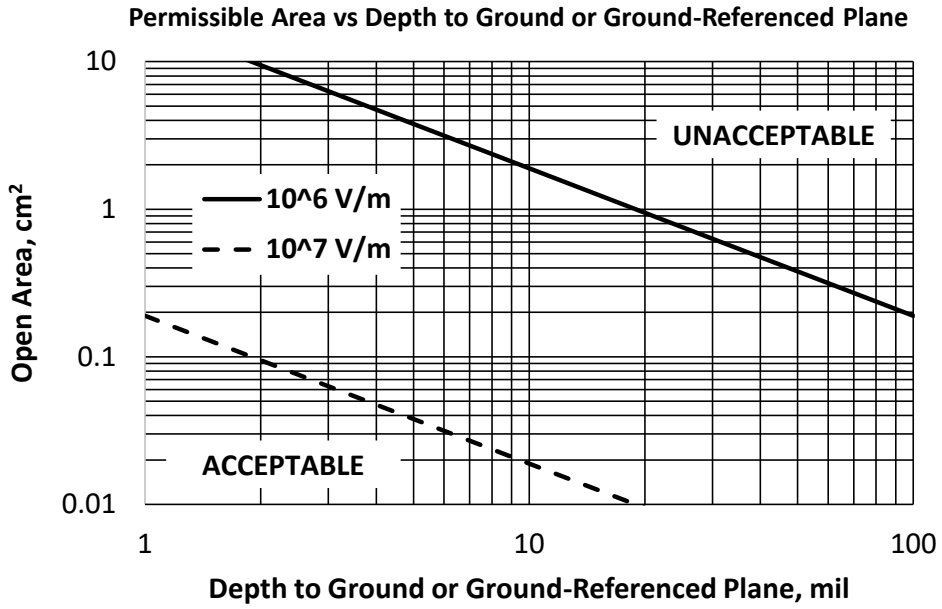

Figure 10—Permissible Area versus Depth to Ground or Ground-Referenced Plane. Two lines corresponding to dielectric strengths of 10^6 V/m and 10^7 V/m are shown.

5.2.4 Solar Array ESD Design Guidelines

This section contains guidelines to protect solar arrays from ESD charging problems.

5.2.4.1 Solar Array Possible ESD Problem Areas

Solar arrays, with their possibly high operating voltages and their available power, can cause the following spacecraft charging effects:

a. Arcing with loss of power and permanent damage to the solar arrays if the arcing is sustained by power from the array itself or by power from the spacecraft internal stored energy.

b. Arcing with momentary loss of power and degradation of solar arrays (similar to that listed in section 5.2.4.1.a of this NASA Technical Handbook, but without sustained arc).

c. Charging of spacecraft structures with respect to the plasma and resultant problems (contamination by attraction of charged surfaces and/or possible erosion of surfaces (sputtering) as species are attracted to the surface). This is very noticeable in LEO environments (see NASA-STD-4005).

d. Disruption of science (electric fields from the surface potentials of solar arrays will alter the path of electrons and ions so that plasma measuring instruments will not record the proper directionality of electrons and ions entering their field of view).

e. Loss of power related to current leakage at exposed conductors in the array. A dramatic rise in power loss can occur at string potentials of ~200 to 1000 V positive with respect to plasma potential related to the phenomenon of snap-over. At a geometry- and material-dependent voltage, the current in the array's I/V curve makes a dramatic change to increasingly larger currents because of enhanced secondary emission and greater plasma contact area.

5.2.4.2 Background

The following are basic rules to avoid spacecraft charging issues related to solar arrays that can cause surface damage, upset science instruments on the spacecraft, or may result in power loss to the space plasma and resultant ESDs and damage. The rules are gleaned from several sources. Good references for this subject include Ferguson and Hillard (2004); NASA-STD-4005; NASA-HDBK-4006, Low Earth Orbit Spacecraft Charging Design Handbook; Katz, et al. (1998); Hoeber, et al. (1998); and references therein.

There are many satellite solar arrays that operate at or above 28 V. Maxar's 1300 series satellites operating at 100 V have the most flight history for high voltage arrays. Boeing, Lockheed Martin, and other satellite manufacturers, including those from Japan and Europe, also have flight history for medium to high voltage arrays. The ISS uses voltage >100 V, and the array is massive. The ISS charging has been investigated in several papers, including those by Mikatarian, et al. (2002), Mandell, et al. (2003), Wright, et al. (2008), and Minow, et al. (2010 and 2018). There has been considerable focus in the community on solar array charging and mitigation, for example the Spacecraft Charging Technology Conferences. Designers should consider the guidelines stated in section 5.2.4.3 of this NASA Technical Handbook. All designs need to be tested in the anticipated environment.

It is not necessary to use all the design ideas listed herein because that would cause excess mass, cost, reduced efficiency, etc. Trade-offs are needed to achieve an adequate design. The point is that after the design has been optimized by engineering and analysis, the final design has to be verified by test with as realistic test conditions as possible. The test considerations are described in the following material which includes a shopping list of design features.

To illustrate the severity of the problem, Figure 11, Examples of Solar Array Failure, shows the type of damage that may occur to solar arrays if the design is inadequate in a space plasma environment.

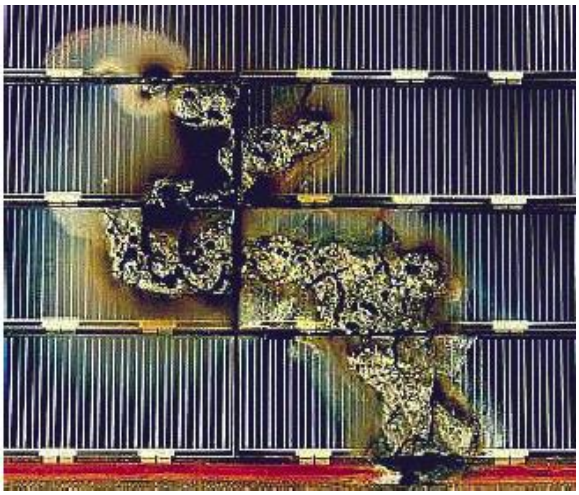

(a) Failure caused by in-flight ESD arcing

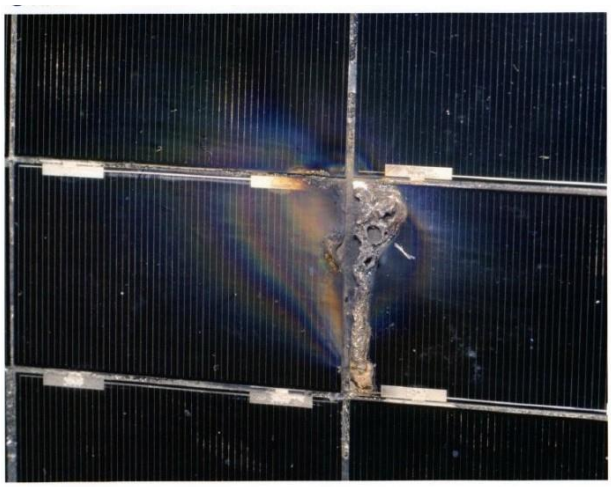

(b) Failure caused by ground ESD arcing

Figure 11—Examples of Solar Array Failure

Figure 11(a) is a photograph of a solar array recovered from the European Space Agency (ESA) European Retrievable Carrier **(**EURECA) mission, by the Space Shuttle as presented in NASA-HDBK-4006. As space failures typically are not retrieved, ground tests have to be performed for failure analysis. These do not represent an actual product that failed in space as Figure 11(a) reports. As an example of the corresponding ground simulation, Figure 11(b) shows a solar array that failed in a plasma environment during ground test (reference Ferguson [1998] and Davis, et al. [1999]).

5.2.4.3 Solar Array Design Guidelines to Protect Against Space Charging and ESDs

a. Build solar arrays (including the backside components, such as diode boards, harness, connectors) so they do not arc. This is a difficult guideline with the present trend toward higher power solar arrays with higher voltages (to minimize wiring size and mass).

b. Test any new design in a representative plasma and energetic particle environment; test with a voltage margin on the solar array to assure that the design is adequate.

c. Arrays with 40 V or less maximum cell-to-cell potential difference are assumed not to be a hazard with margin. This has been measured to be a reasonable guideline. Potentials on the order of 80 V cell-to-cell potential difference can, however, initiate arcs on unprotected solar array designs. Note that string voltages may be ~20 percent higher than nominal if they are not carrying current/open-circuited. Voltages are significantly higher post-eclipse due to the low temperatures reached in eclipse. And the eclipse transition period has been observed to be high risk for external discharges.

d. Place blocking diodes in series with each string so that an arc on a single string (or any other fault) will not be sustained by energy/current from the other strings on the array or the main bus stored energy. Available currents on the order of 2 A can sustain an arc with unprotected solar array designs. Size the diodes to tolerate the maximum anticipated ESD arc or short circuits to

chassis. Based on the short-circuit current limits of current generation solar cells, sustained arcs on arrays with a blocking diode per string are not possible, unless illumination greater than 1-sun (due to extra reflection) is present.

Figures 12, Measured Gallium Arsenide (GaAs) Coupon I/V Failure Threshold, and 13, Measured Silicon (Si) Coupon I/V Failure Threshold, from Hoeber, et al. (1998) illustrate rules in sections 5.2.4.3.c and 5.2.4.3.d in this NASA Technical Handbook. (Also, see Bodeau [2012 and 2014].)

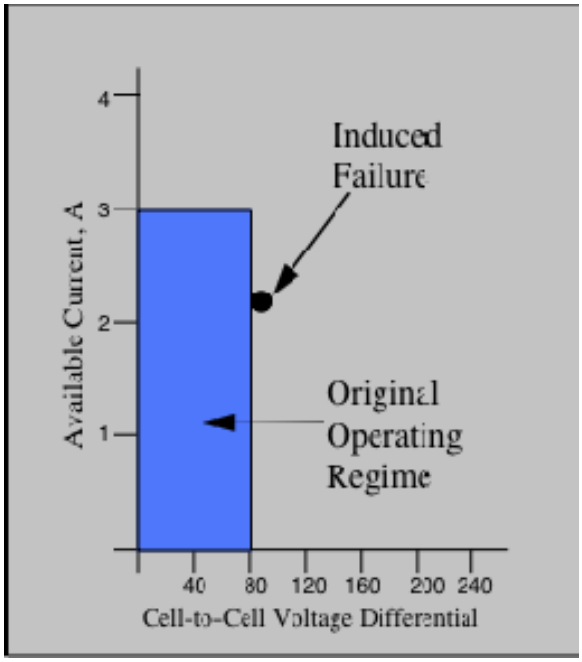

Figure 12—Measured Gallium Arsenide (GaAs) Coupon I/V Failure Threshold

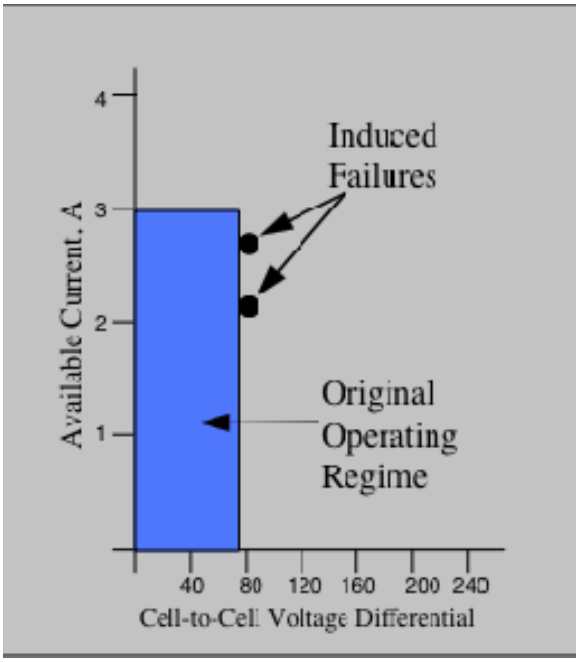

Figure 13—Measured Silicon (Si) Coupon I/V Failure Threshold

e. Especially for LEO, consider building arrays so that they are not negatively grounded to the spacecraft frame/chassis ground. A “floating array,” if the power converter can provide isolation, is one option. With this design, the array voltage with respect to the plasma will adjust to minimize power loss currents from the array through the plasma potential (assuming a conventionally built array, with exposed cell potentials on the edges). This results in a (soft) virtual ground such that about 5% of the array area is higher than the plasma potential, and 95% of the array is lower than the plasma potential. The authors generally oppose any totally floating conductor system.

An alternate option to floating that addresses the same issue is to ground the solar array at the positive end. This has less effect on the overall spacecraft potential and less current/energy losses to space. The best fixed grounding solution to keep the spacecraft frame at plasma potential is to ground the solar array strings to frame at about 5 to 10% of the distance (potential) from the positive end of the solar array. The objectives are to reduce the power loss of leakage current through the plasma and to reduce the voltage of any one part of the array with respect to local plasma below potentials that could trigger an arc. The two objectives do not have the same solution,

so a compromise may be necessary. Analyses of the applicable charging currents, power loss, and resulting voltage balance should be done before adopting this design approach (see NASA-HDBK-4006). The reason that this design might be more useful at LEO is that the greater plasma density has a greater impact on the space charging concerns listed in these paragraphs. A similar situation may exist if an electric thruster effluent impacts the solar array or if some other higher density plasma surrounds the arrays.

f. Design the solar arrays to avoid excessive power loss, e.g., keep the positive voltage with respect to frame less than ~100 V. The remedy here if high voltages have to be used is to insulate the high-voltage metal regions (interconnects and wiring) with insulating grout (space-qualified room temperature vulcanized [RTV] silicone). Avoid any air pockets/voids in the grouting. This latter instruction is very important because entrained air can assist in creating a Paschen discharge, meaning that it takes less voltage to trigger an arc. The fabrication processes have to be well thought out, the assembly personnel have to be well-trained, and fabrication inspections (quality assurance [QA]) have to be part of the process. (See NASA-HDBK-4007.)

g. Do not vent any gas onto or in the vicinity of exposed solar array potentials. A discharge can be triggered at lower voltages in the presence of the resultant partial pressure regimes. Most typically, the gas would be attitude control gas venting but could also be cryogenic cooler gas venting (again, a possible Paschen discharge). (See NASA-HDBK-4007.)

h. Insulate the solar arrays so that there is no potential-carrying conductor exposed to space. The simplest concept is to grout all the spaces between solar cells as in section 5.2.4.3f in this NASA Technical Handbook. Figures 14, An Intercell Gap, and 15, Grouting Barrier to Stop Arcs, from Hoeber, et al. (1998) illustrate the configuration being discussed. Figure 15 illustrates a shortcut that may be permissible if testing demonstrates its adequacy. The figure assumes that cells 1 and 3 are connected in a string and that the potential between them is small, so no grouting is placed between them. Cells 1 and 2 and 3 and 4, by contrast, are adjacent strings with different potentials and need insulation the full distance of their shared edge. At the regions labeled RTV Barrier, the RTV is extended out a bit at the corner as an extra insulation where higher electric fields may be present. In Figure 15, b grout width; in Figure 14, b, r, g, and x are variables used in equations in Hoeber, et al. (1998). A full RTV barrier would be the most robust design.

Figures 16, GaAs Coupon with RTV Barrier Installed, and 17, Si Coupon with RTV Barrier Installed, based on Hoeber, et al. (1998), when compared to the original operating regime illustrated in Figures 12 and 13, show the improvement when grouting is used**.**

i. Use slightly conductive coverglasses to limit electric fields at potential arc sites.

j. Use coverglasses with large overhang to limit electric fields in the plasma region.

k. Limit the differential potential between adjacent cells in the array to reduce arc likelihood. As a limit, 40 V is suggested; but test the array design.

l. Make the cell inter-gap spacing wide enough so that there will be no arcing. Testing in plasma has to be performed for the chosen candidate designs. This design solution is less likely, because it reduces cell density and thus results in less power density (W/m^2 and/or W/kg).

m. Verify that solar array materials will not outgas in space or decay at high temperatures.

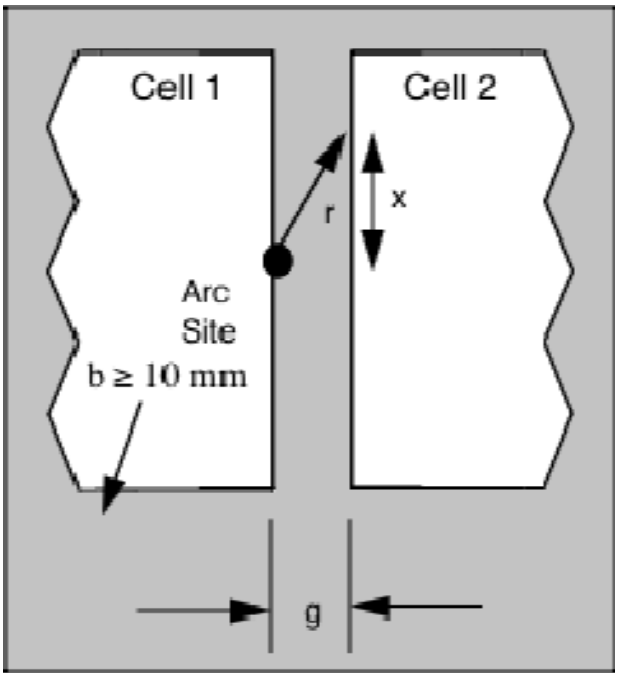

Figure 14—An Intercell Gap

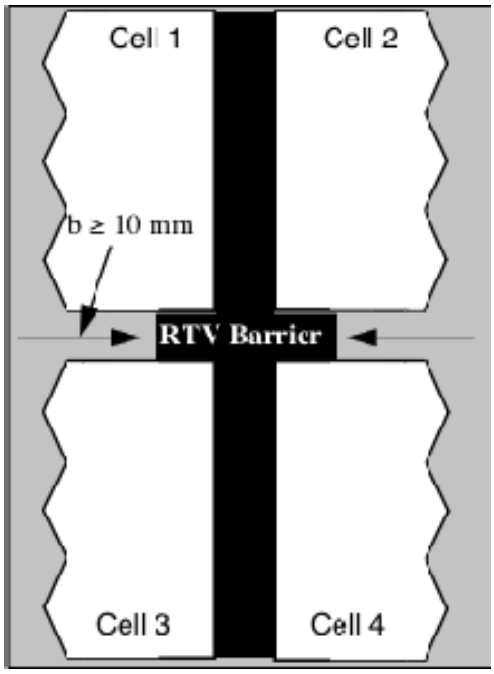

Figure 15—Grouting Barrier to Stop Arcs

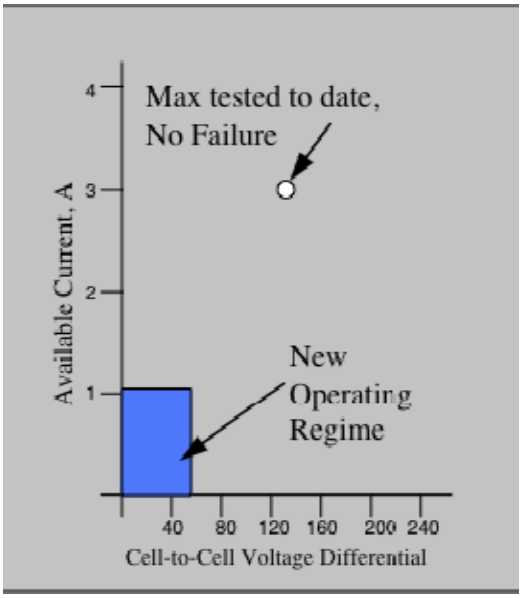

Figure 16—GaAs Coupon with RTV Barrier Installed

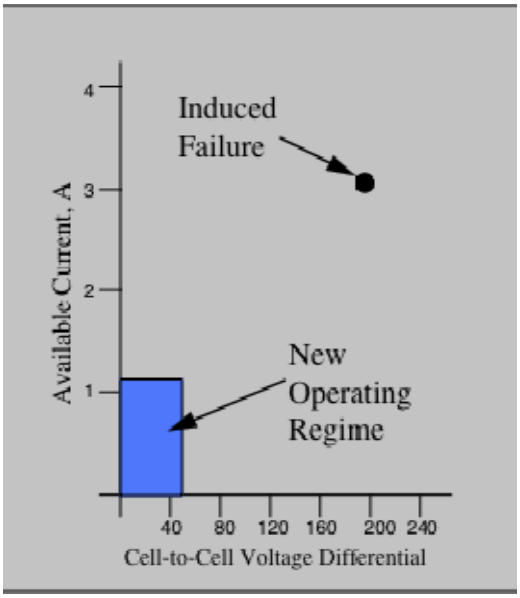

Figure 17—Si Coupon with RTV Barrier Installed

n. For polar LEO missions, make all insulating materials thick enough to withstand the anticipated electric fields so that they are below the breakdown inception electric field of that material. Do not make the materials so thick that they accumulate charge to the degree that they cause (internal charging) problems. Make this part of the ESD analysis/test process.

o. Use a plasma contactor (neutral plasma beam) on the spacecraft as a means to keep the spacecraft at plasma potential. This is useful in LEO or for performing low-energy plasma measurements or to reduce erosion of surfaces caused by impact of attracted charged particles. Any such active device carries reliability concerns in addition to mass, complexity, power consumption, and consumables; but the ISS contactors are working well.

p. Use thin dielectrics (when the dielectric is on direct contact with non-floating conductor) with lower resistivities such that a charge will not build up in the anticipated environment. Examples include wire insulation, substrates, and structures. The idea is to make the resistivity-thickness product so that charge can bleed off through the material to ground faster than hazardous potentials can arise on the material surface or in its volume.

q. Do not put ESD-sensitive electronics near where a solar array discharge may occur. An example would be a thermistor or its wiring placed near the solar cells so that ESD energy can be carried back to an ESD-sensitive telemetry data multiplexing unit.

r. Filter solar array wiring, preferably at the entry to the spacecraft Faraday Cage, but definitely before it enters the power supply. If solar array wiring is not filtered at the entry point to the Faraday Cage, shield the wiring from that point to the power supply.

s. Filter temperature sensors and other data signals from the solar array as they enter the spacecraft or at least at the entry point into their electronic sensing box.

t. Isolate the solar array substrate ground from spacecraft chassis ground. Place a ~2 to 250 kohm isolation resistance between the solar array substrate/frame and spacecraft chassis. This will limit currents from the solar array to its substrate and returning through the spacecraft structure. The resistance should be calculated for all the parameters of the solar array and environment. This is a different rule compared to NASA-TP-2361, which recommended that the solar array structure be carefully grounded to the spacecraft structure. Extra mechanical complexity will be required to provide the necessary insulation between the main spacecraft and the solar array structure. Special attention must be given to conductive structural components, signal line shields and connector backshells, and other conductors that may inadvertently provide a low resistance shunt path to ground bypassing the intended panel substrate resistive isolation. The array ground to spacecraft ground isolation must be verified after installation of the array and before launch. See Bogus, et al. (1985), for example.

The resistor lower bound size should be a value that limits any fault currents to a small value that will interrupt any holding currents caused by a triggering ESD event from the array to the structure. Assuming 1 mA as a maximum permissible sustained fault current (very conservative) on a 100 V

array, the calculation would be 100 V/1 mA or 100 kohm as the minimum solar array structure isolation from the spacecraft chassis.

The resistor upper bound sizing relates to controlling the differential potential of the array with respect to chassis. For example, if space plasma charging currents are expected to be 1 nA/cm^2 (GEO), the maximum value of collected current would be calculated as array area times 1 nA/cm^2. If we assume that the maximum array support structure potential with respect to the spacecraft bus is desired to be less than ~10 V and the array area is 4 m^2, this gives 250 kohm as the maximum solar array isolation from the spacecraft chassis.

u. Consider all possible scenarios. For example, in LEO regimes, the plasma can initiate an arc for 75 V arrays, and the arc can be sustained by the power of the solar array. At GEO and other locations, the arc initiator could be charging the dielectric surfaces (this environment requires perhaps as much as a 400-V differential to the array wiring) in the vicinity of a conductor with the same result. The design should accommodate any situation that occurs, with focus on the anticipated environment, if known. Extreme temperatures, solar illumination, cell-to-cell potentials, and plasma density and temperatures are some of the environmental parameters.

v. Consider Si-based solar cells versus GaAs-based solar cells. However, to date, no clear evidence has shown that Si or GaAs cells are inherently less likely to have ESDs. The ESDs from solar cell assemblies depend primarily on the coverglass used rather than the type of solar cell.

w. Insulate the solar array connector power (+) wires leading into the spacecraft as much as possible. Separate power (+) wires from return (-) wires and low voltage signal lines in the harness and in connectors. Solar array drive assembly details include isolating wiper arms and slip ring spacer insulator height (reference Inguimbert, et al. [2007]).

x. Consider use of the Stretched Lens Array as advocated by Brandhorst (2007). This is a concentrator technology that may eliminate many space charging problems with solar arrays and has been space qualified.

5.2.4.4 Solar Array Testing Rules for Space Charging Characterization

Figure 18, NASA Lewis Research Center (LeRC) (now Glenn Research Center [GRC]) Solar Array Space Charging and ESD Test Setup (reference Hoeber, et al. [1998]), shows the typical elements of a solar array ESD charging threat test. This figure is intended to provide a simple introduction to test needs. Also, consider the ESD test method described in ISO 11221 (2011), Space Systems – Space Solar Panels – Spacecraft Charging Induced Electrostatic Discharge Test Methods. Many solar array test plans become increasingly complex with attempts to add better simulation of reality but in a limited test space and with sample coupons rather than the real full-size article. The test layout in Figure 18 may be modified to reflect a more specific knowledge of solar array equivalent schematics or changed if newer applicable requirements documents become available. Additional details involve capacitances to simulate stored energy in the capacitance of the cells that can cause an initial high current pulse, inductances in wiring that can cause ringing and resonances, and a grounded substrate that may provide a ground return for an arc. A well-thought-out test has a number of details needed to simulate the space situation as closely as possible.

Test parameters that add to the complexity include:

a. Actual spacing and construction of the solar array.

b. Simulation of the plasma environment.

c. Simulation of the higher energy electron environment.

d. Simulation of the Sun.

e. Temperature of the array/coverglass, including occultation (no solar simulation).

f. Energy storage of a string (capacitance to ground if a partial array is used).

g. Simulation of the solar array dynamics, including transient voltage slew rate and capacitance to ground.

h. Simulation of the wiring (capacitance and inductance effects).

i. Presence of grounded or isolated cell substrate.

j. Backside array components. (There were anomalies due to sustained arc on backside components. (Reference Bodeau [2015].)

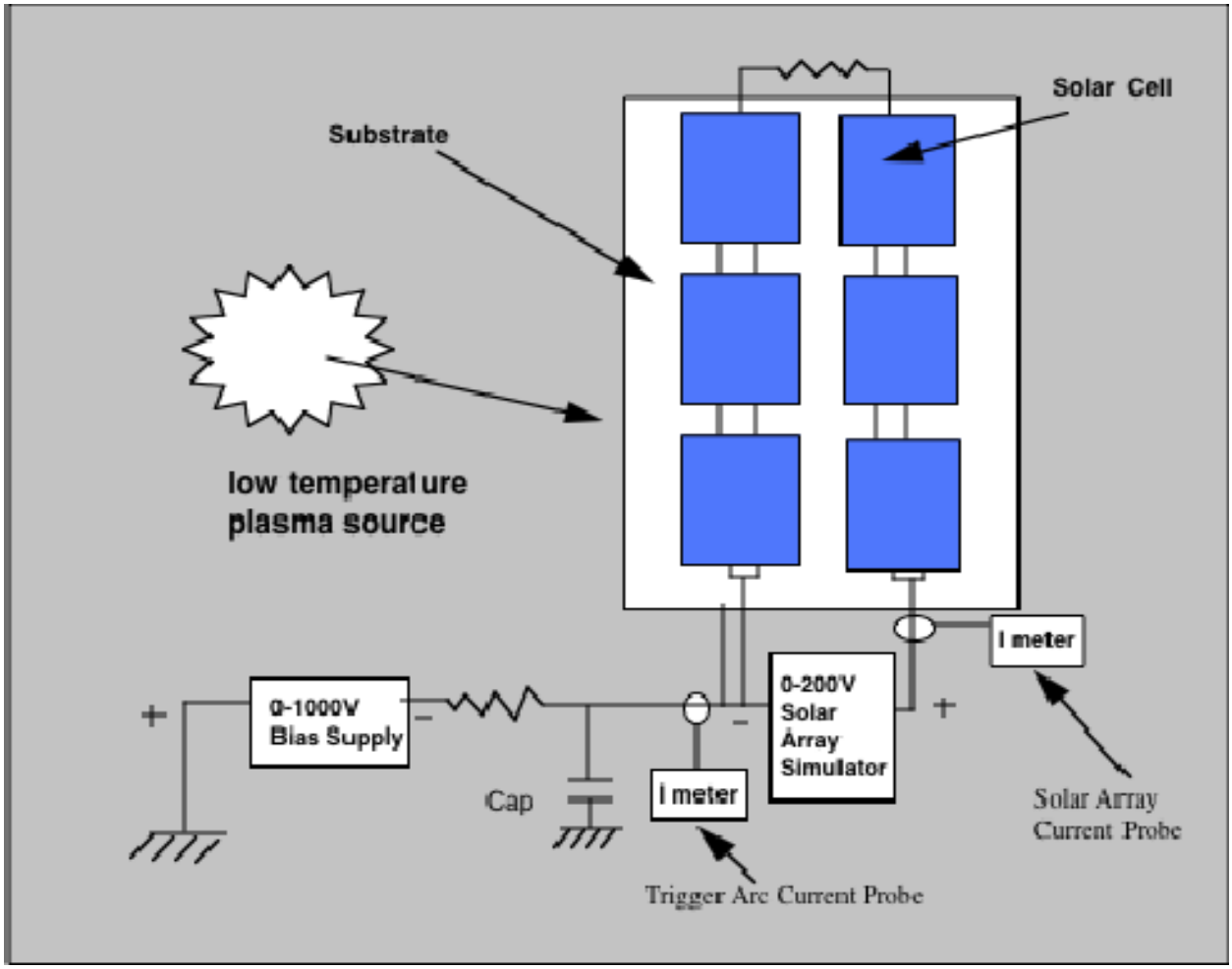

Figure 18—NASA Lewis Research Center (LeRC) (now Glenn Research Center [GRC]) Solar Array Space Charging and ESD Test Setup

Amorim, et al. (2005) is an excellent paper showing solar array arcing current as measured in the laboratory with discussion and interpretations for space needs.

5.2.5 Special Situations ESD Design Guidelines

The guidelines in this section are special situations that are easier to treat separately. General ESD design guidelines are provided in section 5.2.1 of this NASA Technical Handbook.

5.2.5.1 Thermal Blankets

All conductive layers in MLI blankets have to be electrically grounded or ground referenced to the structure. The conductive multilayer surfaces in each separate blanket should be electrically connected to each other by ground tabs at the blanket edges. Each tab should be made from a 2.5 cm-wide strip of 50 μm-thick aluminum foil. The strip should be accordion folded and interleaved between the blanket layers to give a 2.5- by 2.5-cm contact area with all metalized surfaces and the blanket front and back surfaces. Non-conductive spacer or mesh material has to be

removed from the vicinity of the interleaved tab; or it has to be verified that all conductive layers are grounded if spacer/mesh material is not removed. The assembly should be held in place with a metallic nut and bolt that penetrates all blanket layers and captures 2.0 cm-diameter metallic washers positioned on the blanket front and back surfaces and centered in the 2.5- by 2.5-cm tab area. The washers may have different diameters, with the inner surface of the smaller washer recessed to ensure maximum peripheral contact area between the interleaved foil strip and each metalized blanket surface. The tab should be grounded to structure by a proven a technique such as a wire that is as short as possible (15 cm maximum) or conductive Velcro®.

Redundant bonding tabs on all blankets should be implemented as a minimum. Tabs should be located on blanket edges and spaced to minimize the maximum distance (typically 1 m) from any point on the blanket to the nearest tab. Extra tabs may be needed on odd-shaped blankets to meet the condition that any point on a blanket should be within 1 m of a ground tab.

The following practices should be observed during blanket design, fabrication, handling, installation, and inspection:

a. Verify layer-to-layer blanket bonding during fabrication with an ohmmeter.

b. After installation, verify less than 10 ohm dc resistance between blanket and structure with an ohmmeter. (See Verification details in test procedures.) (The resistance can be higher depending on the size of blanket and charging environment.)

c. Close blanket edges (cover, fold in, or tape) to prevent direct irradiation of inner layers.

d. Do not use crinkled, wrinkled, or creased metalized film material.

e. Handle blankets carefully to avoid creasing of the film or possible degradation of the ground tabs.

f. If the blanket exterior is conductive (paint, ITO, Ge, Stamet, fog), make sure that it is grounded. Verify with an ohmmeter.

g. Usage of a conductive exterior is recommended but, when not used for a LEO mission, exterior material should be a dielectric material with very high dielectric strength such as Kapton®.

5.2.5.2 Thermal Control Louvers

Bond/ground the thermal control louver blades and axles. The easiest way to bond the blades to chassis is to have the bimetal spring electrically bonded at both the blade/axle and the spacecraft structure. Alternatively, place a thin wiper wire from spacecraft chassis to the axle.

5.2.5.3 Antenna Grounding

Antenna elements usually should be electrically grounded to the structure. Implementation of antenna grounding will require careful consideration in the initial design phase. All metal surfaces, booms, covers, and feeds, should be grounded to the structure by wires and metallic screws. (Antenna design with floating metals should be avoided.) All waveguide elements should be electrically bonded together with spot-welded connectors and grounded to the spacecraft structure. These elements have to be grounded to the Faraday Cage at their entry points. Conductive epoxy can be used where necessary, but dc resistance of about 1 ohm should be verified by measurements.

5.2.5.4 Antenna Apertures

Spacecraft RF antenna aperture covers usually should be ESD conductive and grounded. Charging and arcing of dielectric antenna dish surfaces and radomes can be prevented by coating them with grounded ESD-conductive material. Antenna performance should be verified with the ESD coating installed.

For a dielectric radome, problems of damage to nearby electronics have been encountered. Sometimes the radome may be spaced very near low noise amplifiers (LNAs). If the radome surface charges, electrostatic attraction may draw its surface near the LNAs, and a spark could destroy them; this is a suspected culprit for some on-orbit failures. In such a case, the radome has to be spaced far enough away that it cannot damage any LNA or similar nearby electronic devices.

A similar problem exists if there are metal antenna elements in a dielectric matrix, all exposed on the surface. An ESD arc from the dielectric to the antenna element, carried down a coaxial cable to the receiver front end (or transmitter output), can do the same sort of damage. Situations such as this (ESD events caused by surface metals near dielectrics that are carried down to delicate electronics) have to be handled with care; filtering or diode protection has to be applied to protect the electronics from damage.

Coverings on antenna feeds and parabolas should be considered. Isolated dielectric materials on an antenna system, especially near feed lines, can store excess charge or energy. For example, if there is an isolated dielectric mounted on top of a fiberglass separator that is adjacent to the feed electrical path, there can be discharges directly into the receiver. These dielectrics are special problems because they are on the outside of the spacecraft and have less shielding. Engineering model charging/discharging tests may be required to assess the hazards posed by the radome/antenna/feed discharges to the receiver or LNA.

5.2.5.5 Antenna Reflector Surfaces Visible to Space

Grounded, conductive spacecraft charge control materials should be used on antenna reflector rear surfaces visible to space. Appropriate surface covering techniques have to be selected when the surface is not sufficiently conductive. Such methods include conductive paints, or ESD conductive (charge bleeding) paints overlapping grounded conductors. Properly constructed thermal blankets may also accomplish this need to prevent surface charging.

Ungrounded array elements, such as for special antenna surfaces, may include ungrounded conductors as a necessary part of their design, e.g., tuned reflector array elements. These may be left ungrounded if test or analysis shows that the stored energy available from space charging will not affect any possible victims without adequate self-protection on all leads.

5.2.5.6 Transmitters and Receivers

Spacecraft transmitters and receivers should be immune to transients produced by ESDs, including those from dielectrics in the antenna and feed system. Transmitter and receiver electrical design has to be compatible with the results of spacecraft charging effects. The EMI environment produced by spacecraft ESD should be addressed early in the design phase to permit effective electrical design for immunity to this environment. The transmitter, receiver, and antenna system should be tested for immunity to ESDs near the antenna feed, and from the antenna and cables connected to the transmitters and receivers. Consider the possibility of an arc from a dielectric that sparks to the center conductor of a coaxial cable to a delicate receiver or transmitter device at the other end of that coaxial cable. Change the design if necessary. Verification tests should be established by an experienced ESD engineer and verified by the RF designers.

5.2.5.7 Attitude Control Packages

Attitude control electronics packages should be made insensitive to ESD transients. Attitude control systems often require sensors that are remote from electronics packages in Faraday Cage shielding. This presents the risk that ESD transients will be picked up and conducted into electronics, especially via the cabling if shielded inadequately. Particular care has to be taken to ensure immunity of interface circuits to ESD upset in such cases.

5.2.5.8 Deployed Packages

Deployed packages should be grounded by using a flat ground strap extending the length of the boom to the vehicle structure. Several spacecraft designs incorporate dielectric booms to deploy payloads. The payload electrical system may still require a common ground reference or the experiment may require a link to some electric potential reference. In these cases, it is recommended that a flat ground strap be used to carry this ground tie to the vehicle structure. Electrical wiring extending from the deployed payload to the spacecraft interior has to be carried inside or along the dielectric booms. This wiring should be shielded and the shield grounded at the package end and at the Faraday Cage entrance.

5.2.5.9 Ungrounded Materials

Specific items that cannot be grounded because of system requirements should undergo analysis to assure specified performance in the charging environment. Certain space vehicles may contain specific items or materials that cannot be grounded. For example, a particular experiment may have

a metallic grid or conducting plate that has to be left floating. If small, these items may present no unusual spacecraft charging problems; however, this should be verified through analysis or test.

5.2.5.10 Honeycomb Structures

Honeycomb structures need special bonding methods. Be aware that the aluminum honeycomb interior may be isolated from conductive and grounded face sheets by felt prepreg adhesive-impregnated material. A small ground wire running across the aluminum honeycomb and pressed against the edge can provide a bonding. The conductive face sheets may lose their grounding when they are butted against each other. Develop processes that assure all metal parts of the honeycomb structure and face sheets will be grounded. After assembly, the inner parts cannot be checked to see if they are grounded.

5.2.5.11 Deliberate or Known Surface Potentials

If a surface on the spacecraft has to be charged (e.g., detectors on a science instrument), it should be recessed or shielded so that the perturbation in the surface electrostatic potential is less than 10 V. Scientific instruments that have exposed surface voltages for measurement purposes such as Faraday cups require special attention to ensure that the electrostatic fields they create will not disrupt adjacent surface potentials or cause discharges by their operation. They can be recessed so that their fields at the spacecraft surface are minimal or shielded with grounded grids. These detector apertures should have a conductive grounded surface around them and in their field of view. An analysis may be necessary to ensure that their presence is acceptable from a charging standpoint and that surrounding surfaces do not affect the measurements.

Figure 19, Electron Trajectories for Galileo (reference Harel [1982]), presents an analytic result showing the disturbances in electron paths in the presence of electric fields from spacecraft surface charging, in this case from dielectric surfaces charged by space plasma. Figure 19 shows a calculation of particle trajectories traced backwards from the sensor as distorted by electric fields on parts of the Galileo spacecraft. The 10 curves represent paths of 1- to 50-eV electrons, with lines at logarithmically equally spaced energies. The distorted paths of the lower energy electrons show clearly in this simulation. The design as a result was changed to permit undistorted science measurements.

5.2.5.12 Spacecraft-Generated Plasma Environment

The total plasma environment includes plasma generated by spacecraft electric propulsion (arcjets, Hall thrusters, and Ion thrusters) and possibly other sources. This was shown to be a critical consideration because when thrusters are fired, they can surround GEO spacecraft with LEO-type plasma. That plasma can have a major impact on, as a minimum, GEO solar array designs. It is especially important if thrusters are fired during the time a spacecraft is negatively charged by GEO plasma. It can result in unexpected synergistic effects that can lead to ESD events and damage to solar arrays (see Likar, et al. [2006]).

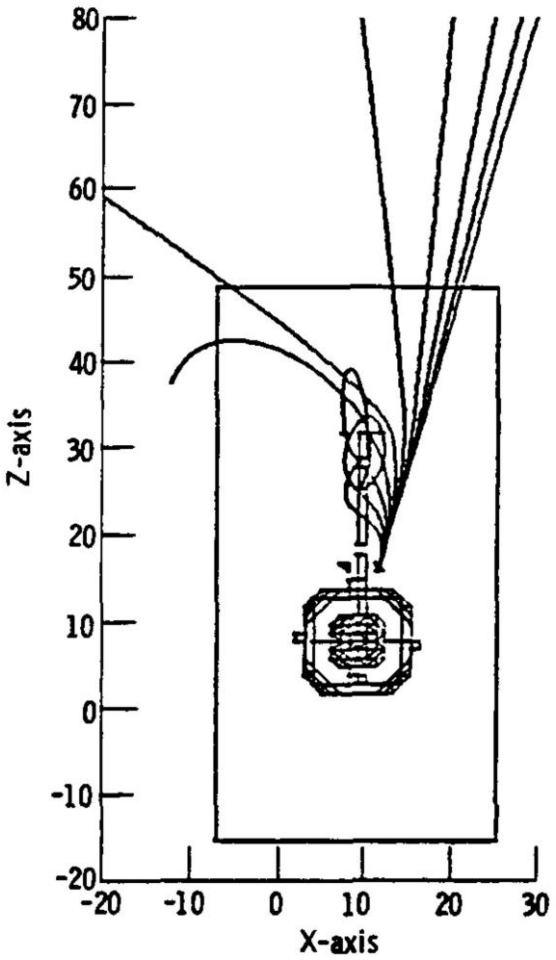

Figure 19—Electron Trajectories for Galileo

KNOWLEDGE CHECK

5.1 What are the three elements that must be present for an ESD to cause problems?
5.2 What is the most efficient way to approach solving an ESD problem?
5.3 How can an overall design approach be applied to mitigation of spacecraft charging? What is different about the design approach for spacecraft charging and any other environmental threats?
5.4 Name three analytic approaches/codes to assess the spacecraft charging threat to a spacecraft.
5.5 Obtain reference data sources for material properties that relate to spacecraft charging, circuit/component ESD sensitivity to disruption or damage.
5.6 What spacecraft hardware/assembly levels might have spacecraft charging (ESD/electric fields) tests before the final assembly?
5.7 How might a complete spacecraft test be implemented?
5.8 What are the merits of a design walk-through, both in the design stage by reviewing assembly documents, and later on complete assemblies and/or the complete spacecraft?
5.9 Make a checklist that could be used for design assessment.

5.10 How likely is the ability to change orbital parameters to avoid spacecraft charging threat situations?

5.10 Why and when can excellent dielectrics be used on outer surfaces of a spacecraft in a spacecraft charging environment?

5.11 Prove that an earlier simplified guideline, "isolated conductors have to be grounded with less than 10^6 ohm to structure" can be derived from Eq. 11 when the conductor area is 2 x 10^3 cm^2. When is the earlier guideline less conservative than Eq. 11?

5.12 Prove that an earlier simplified guideline, "materials applied over a conductive substrate have to have bulk resistivities of less than 10^{11} ohm cm" can be derived from Eq. 12 when the material thickness is 0.2 mm. When is the earlier guideline less conservative than Eq. 12?

5.13 Prove that an earlier simplified guideline, "materials applied over a dielectric area have to be grounded at the edges and have a resistivity less than 10^9 ohm per square" can be derived from Eq. 13 when the greatest distance to a ground is 2 cm. When is the earlier guideline less conservative than Eq. 13?

5.14 Prove that 10-hour fluence of 0.1 pA/cm^2 is 2.25 x 10^{10} e/cm^2 and the corresponding electric field in a dielectric with dielectric constant of 2 between parallel plate is 2.0 x 10^6 V/m.

5.15 Why is mechanical (conductive shielding; e.g., a Faraday Cage construction) not always the best solution?

5.16 In what situations will a Faraday Cage not be feasible to mitigate spacecraft charging effects?

5.17 In what respects are Electromagnetic Compatibility (EMC or E3) environmental mitigations compatible with and supportive of spacecraft charging mitigations?

5.18 In what respects are particle radiation environmental mitigations compatible with and supportive of spacecraft charging mitigations?

5.19 In what respects or conditions are thermal environmental mitigation requirements compatible with spacecraft charging mitigations?

5.20 In what respects (under what circumstances) are spacecraft charging mitigations not compatible with EMC requirements; with particle radiation mitigation requirements; with thermal control requirements?

5.21 Why is electrical "bonding" important in control of spacecraft charging (and EMC)?

5.22 Why is there a separate section of design guidelines for solar arrays?

5.23 What are possible consequences of ESD events on solar arrays that make them important with respect to spacecraft charging?

5.24 Review and note suggested useful changes, clarifications, additions, subtractions, etc., as felt applicable.

5.25 Why do thin dielectrics contribute less to IESD problems than thicker ones?

5.26 Why must temperatures be considered for dielectrics, especially at cold temperatures of the dark side surface of a spacecraft?

5.27 What manufacturers provide partially dielectric materials that are suitable both as insulation to limit leakage current and as a bleed path to prevent storage of energy that could damage hardware if an ESD spark initiates from those materials?

5.28 Find the size of a radiation spot shield on your hardware if used. Determine the electron spectrum arriving at the spot shield based on your flight orbit, in a normal (perpendicular) direction. Calculate the number of electrons stopped and stored in a floating spot shield of

that size in that environment. Calculate the stored energy, assuming a 1-mil layer of dielectric adhesive that bonds the spot shield to its protected IC's ground point. Find the ESD energy threshold for IC damage. Compare the two and make an assessment for your hardware's survivability.

5.29 When can the listed (and unlisted) items in section 5.2.1.9 be left floating on your spacecraft?

5.30 The equations and other recommendations shown in section 5.2.2.2 are based on some roughly standard values. Work the equations backward to see if you can find the nominal/standard used values assumed for these equations for the various parameters of:

- electron beam flux and energy spectrum
- assumed accumulation time (fluence)
- breakdown voltage limits of dielectrics
- electric field limits of concern near dielectric surfaces
- damage energy limits of solid-state devices.

5.31 Derive the equation and parameters that created Figure 10.

5.32 Name 3 problems that can occur due to solar array charging.

5.33 Why would grounding the solar array at a point not at the extreme + or – ends of a solar array possibly be of value in plasma environments?

5.34 Search for papers, standards, national requirements, or others that provide standard test protocols to determine ESD design adequacy of a specific solar array.

5.35 If you work in an organization that has experienced ESDs or possibly ESD-caused anomalies on solar arrays, have these design suggestions been violated? List them.

6. SPACECRAFT TEST TECHNIQUES

Spacecraft and systems should be subjected to transient upset tests to verify immunity. It is the philosophy in this NASA Technical Handbook that testing is an essential ingredient in a sound spacecraft charging protection program. In this section, we review the philosophy and methods of testing spacecraft and spacecraft systems. NASA-HDBK-4002A was largely unchanged from the analogous section in NASA-TP-2361. However, the current version has a number of substantive changes from the previous version, NASA-HDBK-4002A.

6.1 Test Philosophy

The philosophy of an ESD test is identical to that of other environmental qualification tests:

a. Subject the spacecraft to an environment representative of that expected.

b. Make the environment applied to the spacecraft more severe than expected with a safety margin to give confidence that the flight spacecraft will survive the real environment. Make the safety margin consistent with the estimated accuracy of the test environment.

c. Have a design qualification (prototype) test sequence that is extensive and includes the following:

(1) Test of all units of hardware.
(2) Use of long test durations.
(3) Incorporation of as many equipment operating modes as possible.
(4) Application of the environment to all surfaces of the test unit.

d. Have a flight hardware test sequence of more modest scope: delete some units from test if qualification tests show sufficient design margins; use shorter test durations; use only key equipment operating modes; and/or only apply the environment to a limited number of surfaces.

Ideally, both prototype and flight spacecraft should be tested in a charging simulation facility. They should be electrically isolated from ground and exposed to electron, ion, and EUV radiation levels corresponding to worst-case charging environment conditions. Systems should operate without upset throughout this test. Generally, there is a reluctance to subject flight hardware to this kind of test. One important reason is the possibility of latent damage, i.e., internal physical damage to circuitry that apparently still functions but that has weakened it and may lead to later failure. For that reason, flight hardware is ESD tested less frequently than developmental hardware. For the same reason, flight hardware might be subjected to lower test amplitudes as a precaution to demonstrate survivability but without margin or lesser margins than the prototype.

Because of the difficulty of simulating the actual environment (space vacuum and plasma parameters, including species such as ions, electrons, and heavier ions; mean energy; energy spectrum; and direction), spacecraft charging tests often take the form of assessing unit immunity to electrical discharge transients. The best way to estimate the expected discharge parameters is testing the discharge source such as dielectric or floating conductor using an electron beam mimicking the appropriate space condition. However, analyses are often used for discharge parameter estimations.

Tests at room ambient temperature using radiated and injected transients are more convenient. These ground tests, however, cannot simulate all the effects of the real environment because the transient source may not be in the same location as a region that may discharge and because a spark in air has a slower risetime than a vacuum arc. The sparking device’s location and pulse shape have to be analyzed to provide the best possible simulation of coupling to electronic circuits. To account for the difference in risetime, the peak voltage might be increased to substitute for the slower dV/dt (time rate of change of the voltage) parameter of a vacuum arc. Alternatively, the voltage induced during a reduced amplitude test could be measured and the in-flight noise extrapolated from the measured data and compared to the response threshold of the hardware in question. As with all ideas, there is often a negative; in this case adding additional wiring attached to external non-flight measurement hardware can affect the coupled amplitude.

There are no simple rules to be followed in determining whether or how much to test. General guidance dictates that an engineering version of the hardware be tested in lieu of the flight hardware and that this testing has margins that are more severe than the expected environment. The trade-offs are common to other types of environmental testing; the main difference is that the ESD- and IESD-specific threats are more difficult to replicate in practical tests than for other environmental disciplines.

The dangers in not testing are that serious problems related to surface or internal charging will go undetected and that these problems will later affect the survivability of the spacecraft. The best that can be done in the absence of testing is good design supplemented by analysis. Good IESD and surface charging design techniques are always appropriate, no matter what the overt environmental threat is and should be followed as a necessary precaution in all cases.

A proper risk assessment involves a well-planned test, predictions of voltage stress levels at key spacecraft components, verification of these predictions during test, checkout of the spacecraft after test, and collaboration with all project elements to coordinate and assess the risk factors.

6.2 Simulation of Parameters

Because ESD test techniques are not well established, it is important to understand the various parameters that have to be simulated, at a minimum, to perform an adequate test. On the basis of their possibility of interference to the spacecraft, the following items should be considered in designing tests:

a. Spark location.
b. Radiated fields or structure currents.
c. Area, thickness, and dielectric strength of the material.
d. Total charge involved in the event.
e. Breakdown voltage.
f. Current waveform (risetime, width, falltime, and rate of rise [in ampere per second]).
g. Voltage waveform (risetime, width, falltime, and rate of rise [in volt per second]).

Table 5, Examples of Estimated Space-Generated ESD Spark Parameters, shows typical values calculated for representative spacecraft to guide preparation of a similar threat table for your spacecraft. The values listed in this table were compiled from a variety of sources, mostly associated with the Voyager and Galileo spacecraft for the environment at Jupiter. The values for each item, e.g., those for the dielectric plate, have been assembled from the best available information and made into a more or less self-consistent set of numbers. The process is described in the footnotes to Table 5. Leung, et al. (1983) and Whittlesey (1978) contain further description and discussion. Because they were difficult to determine, various sources were used; as a result, the numbers on any single row may not be self-consistent. For example, the available charge (Coulombs) may be calculated by the capacitance times the discharge voltage (adjusting units as needed, for example converting all to SI). The integral of the discharge current vs. time (coulombs) should give a similar value.

Table 5—Examples of Estimated Space-Generated ESD Spark Parameters

EXAMPLE OF ESD SOURCE	C (nF) (1)	V_b (kV) (2)	E (mJ) (3)	I_{pk} (A) (4)	T_R (ns) (5)	T_P (ns) (6)
Dielectric plate to conductive substrate	20	1	10	2 (7)	3	10
Exposed connector dielectric	0.150	5	1.9	36	10	15
Paint on high-gain antenna	300	1	150	150	5	2400
Conversion coating on metal plate (anodize)	4.5	1	2.25	16	20	285
Paint on optics hood	550	0.360	35.6	18	5	600

Notes:
1. Capacitance computed from surface area, dielectric thickness, and dielectric constant.
2. Breakdown voltage computed from dielectric thickness and material dielectric strength.
3. Energy computed from $E = 1/2\ CV^2$.
4. Peak current estimated based on measured data; extrapolation based on square root of area.
5. Discharge current risetime measured and deduced from test data.
6. Discharge current pulse width to balance total charge on capacitor.
7. Replacement current in longer ground wire; charge is not balanced.

You should not copy these parameters because they were tuned to specific hardware located on the listed spacecraft under our cognizance. You need to make and establish your own threat list with expected environmental parameters. You may even need further columns for additional parameters that may be significant to your project.

6.3 General Test Methods

This section contains representative types of ESD test equipment and ESD application methods.

6.3.1 ESD-Generating Equipment

Several representative types of test equipment are tabulated in Table 6, Examples of Several ESD Sources, and described later. Where possible, typical parameters for that type of test are listed.

Table 6 shows examples of different test sources that might be used as surrogates for the values determined in Table 5. The technology of ESD test sources has changed over time, and currently commercial ESD testers can be purchased from various vendors. The threat parameters that you have established all need to be scrutinized and used in a manner so that you use the best approximations to the environmental parameters of Table 5.

Table 6—Examples of Several ESD Sources

ESD GENERATOR TEST SIMULATION	**C** (nF)	$\mathbf{V_b}$ (kV)	**E** (mJ)	$\mathbf{I_{pk}}$ (A)	$\mathbf{T_R}$ (ns)	$\mathbf{T_P}$ (ns)
MIL-STD-1541A (auto coil) (1)	0.035	19	6.3	80	5	20
Flat plate 20 cm x 20 cm at 5 kV, 0.075 mm (3 mil) Mylar® insulation	14	5	180	80	35	880
Flat plate with lumped-element capacitor	550	0.450	56	15	15	(2)
Capacitor direct injection	1.1	0.32	0.056	1	3-10	20
Capacitor arc discharge	60	1.4	59	1000	(3)	80
Commercial ESD tester	0.15	20	30	130	5	22

Notes:
1. Parameters were measured on one unit similar to the MIL-STD-1541A, Electromagnetic Compatibility Requirements for Space Systems, design.
2. RC time constant decay can be adjusted with an external resistor in the circuit.
3. Value uncertain.

6.3.1.1 MIL-STD-1541A Arc Source

The schematic and usage instructions for the MIL-STD-1541A arc source are presented in Figure 20, MIL-STD-1541A Arc Source. The arc source can be manufactured relatively easily and can provide the parameters necessary to simulate a space-caused ESD event. The only adjustable parameter for the MIL-STD-1541A arc source is the discharge voltage achieved by adjusting the discharge gap and, if necessary, the adjustable dc supply to the discharge capacitor. As a result, peak current and energy vary with the discharge voltages. Since the risetime, pulse width, and falltime are more or less constant, the voltage and current rates of rise and fall are not independent parameters. This permits some degree of flexibility in planning tests but not enough to cover all circumstances. MIL-STD-1541A was cancelled in 2017, but the replacement documents no longer reference this test method.

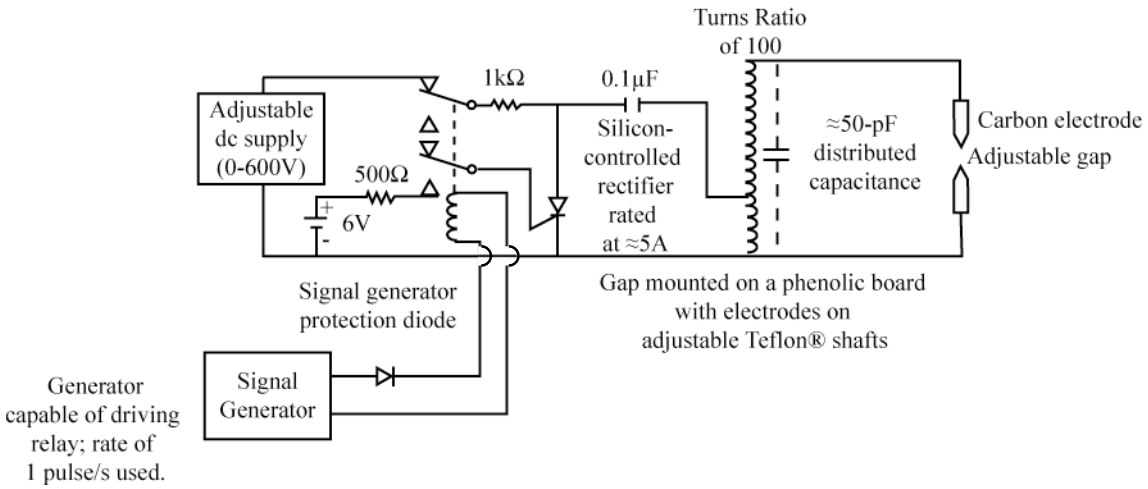

Typical Gap-Spacing and Voltage Breakdown (V_b) Level

Gap (mm)	V_b (kV)	Approximate Energy Dissipated (μW)
1	1.5	56.5
2.5	3.5	305
5	6	900
7.5	9	2000

Figure 20—MIL-STD-1541A Arc Source

6.3.1.2 Flat-Plate Capacitor

A flat-plate capacitor made of aluminum foil over an insulator can be used in several circumstances. Examples of spacecraft areas that can be simulated by a flat-plate capacitor are thermal blanket areas, dielectric areas such as calibration targets, and dielectric areas such as non-conductive paints. The chief value of a flat-plate capacitor is to permit a widespread discharge to simulate the physical path of current flow. This can be of significance where cabling or circuitry is near the area in question. Also, the larger size of the capacitor plates allows them to act as an antenna during discharge, producing significant radiated fields.

Table 6 shows one example of the use of a flat-plate capacitor. Several parameters can be varied, chiefly the area and the dielectric thickness; both of these affect the capacitance, the discharge current, and the energy. The discharge voltage of the flat plate can be controlled by using a needle-point discharge gap at its edge that is calibrated to break down before the dielectric. This gap also affects discharge energy. In this manner, several mechanical parameters can be designed to yield discharge parameters more closely tailored to those expected in space.

The difficulties of this method include the following:

a. The test capacitor is usually not as close to the interior cabling as the area it is intended to simulate, e.g., it cannot be placed as close as the paint thickness.

b. The capacitance of the test capacitor may be less than that of the area it is intended to simulate. To avoid uncontrolled dielectric breakdown in the test capacitor, its dielectric may have to be thicker than the region it simulates. If so, the capacitance will be reduced. The area of the test capacitance can be increased to compensate, but then the size and shape will be less realistic.

6.3.1.3 Lumped-Element Capacitors

Use of lumped-element capacitors (off-the-shelf, manufactured capacitors) can overcome some of the objections raised about flat-plate capacitors. They can have large capacitances in smaller areas and thus supplement a flat-plate capacitor if it alone is not adequate. The deficiencies of lumped-element capacitors are as follows:

a. They generally do not have the higher breakdown voltages (greater than 5 kV) needed for ESD tests.

b. Some have a high internal resistance and cannot provide the fast risetimes and peak currents needed to simulate ESD events.

Generally, the lumped–element capacitor discharge would be used most often in lower voltage applications to simulate painted or anodized surface breakdown voltages and in conjunction with the flat-plate capacitors.

6.3.1.4 Commercial Human Body Model ESD Tester

A commercial human body discharge source (Schaeffner or Haefely, among others, supplies one such test device) can be used for simulated HBM-type discharges. These sources can be battery operated and also provide a capacitive discharge pulse. The charging voltage is variable so that the amplitude can be controlled. Transients from this source are fast (about 150 ns) and the signal is very clean.

6.3.1.5 Other Source Equipment

Wilkenfeld, et al. (1982) describes several other similar types of ESD simulators. It is a useful document if further descriptions of ESD testing are desired.

6.3.1.6 Switches

A wide variety of switches can be used to initiate the arc discharge. At low voltages, semiconductor switches can be used. The MIL-STD-1541A arc source uses a Silicon-Controlled Rectifier (SCR) to initiate the spark activity on the primary of a step-up transformer; the high voltage occurs at an air spark gap on the transformer’s secondary. Also, at low voltages, mechanical switches can be used, e.g., to discharge modest-voltage capacitors. The problem with mechanical switches is their bounce in the early milliseconds. Mercury-wetted switches can alleviate this problem to a degree.

For high-voltage switching in air, a gap made of two pointed electrodes can be used as the discharge switch. Place the tips pointing toward each other and adjust the distance between them to about 1 mm/kV of discharge voltage. The gap has to be tested and adjusted before the test, and it has to be verified that breakdown occurred at the desired voltage. For tests that involve varying the amplitude, a safety gap connected in parallel is suggested. The second gap should be securely set at the maximum permissible test voltage. The primary gap can be adjusted during the test from zero to the maximum voltage desired without fear of inadvertent overtesting. Do the test by charging the capacitor (or triggering the spark coil) and relying on the spark gap to discharge at the proper voltage.

The arc source's power supply has to be isolated sufficiently from the discharge so that the discharge is a transient and not a continuing arc discharge. A convenient test rate is one spark per second. To accomplish this rate, it is convenient to choose the capacitor and isolation resistor's resistance-capacitance time constant to be about 0.5 s and to make the high-voltage power supply output somewhat higher than the desired discharge voltage.

For tests that involve a fixed discharge voltage, gas discharge tubes are available with fixed breakdown voltages. The advantage of the gas discharge tube over needle points in air is its faster risetime and its very repeatable discharge voltage. The gas discharge tube's dimensions (5 to 7 cm or longer) can cause more RF radiation than a smaller set of needle-point air gaps.

Another type of gas discharge tube is the triggered gas discharge tube. This tube can be triggered electronically, much as the gate turns on an SCR. This method has the added complexity of the trigger circuitry. Additionally, the trigger circuitry has to be properly isolated so that discharge currents are not diverted by the trigger circuits.

6.3.2 Methods of ESD Application

The ESD energy can range from very small to large (as much as 1 J but usually millijoules). The methods of application can range from indirect (radiated) to direct (applying the spark directly to a piece part). In general, the method of application should simulate the expected ESD source as much as possible. Several typical methods are described here.

6.3.2.1 Radiated Field Tests

The sparking device can be operated in air at some distance from the component. This technique can be used to check for RF interference to communications or surveillance receivers as coupled into their antennas. It can also be used to check the susceptibility of scientific instruments that may be measuring plasma or natural radio waves. One measured RF-radiated test spectrum is shown in Figure 21, Typical RF-Radiated Fields from MIL-STD-1541A Arc Sources, as measured at one meter from the arcing source.

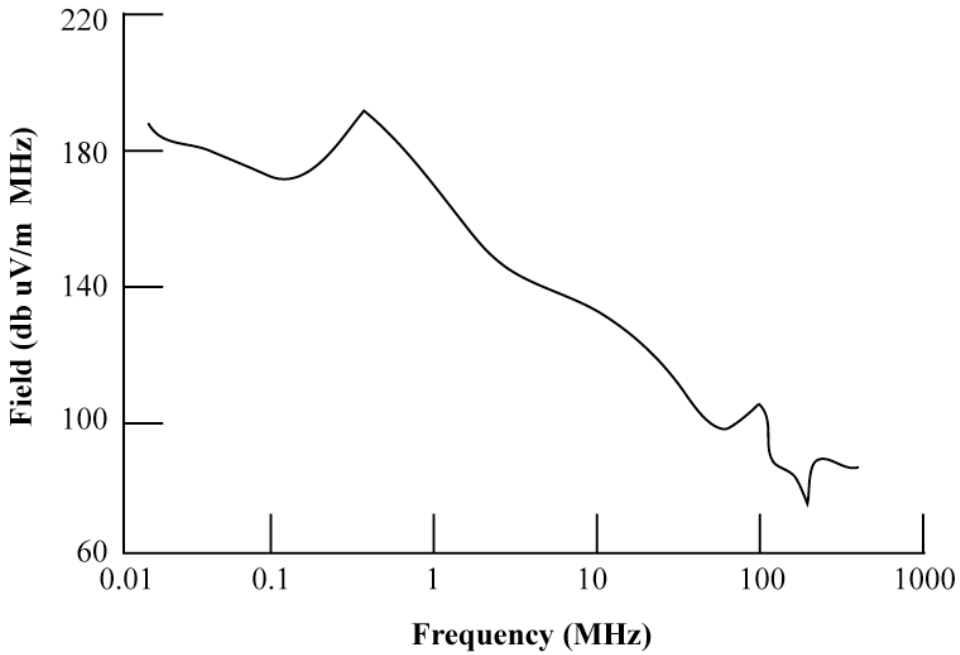

Figure 21—Typical RF-Radiated Fields from MIL-STD-1541A Arc Sources

6.3.2.2 Single-Point Discharge Tests

Discharging an arc onto the spacecraft surface or a temporary protective metallic fitting with the arc current return wire in close proximity can represent the discharge and local flowing of arc currents. This test is more severe than the radiated test since it is performed immediately adjacent to the spacecraft rather than some distance away.

This test simulates only local discharge currents; it does not simulate blow-off of charges which cause currents to be distributed through the entire structure of the spacecraft.

6.3.2.3 Structure Current Tests

The objective of structure current testing is to simulate blow-off of charges from a spacecraft surface. If a surface charges and a resultant ESD occurs, the spark may vaporize and mechanically remove material and charges without local charge equalization. In such a case, the remaining charge on the spacecraft will redistribute itself and cause structural currents.

Defining the actual blow-off currents and the paths they take is difficult. Nevertheless, it is appropriate to do a structure current test to determine the spacecraft susceptibility, using test currents and test locations supported by analysis as illustrated in section 6.2 and Table 5 of this NASA Technical Handbook. Typically, such a test would be accomplished by using one or more of the current paths shown in Figure 22, Paths for ESD Currents through Structure:

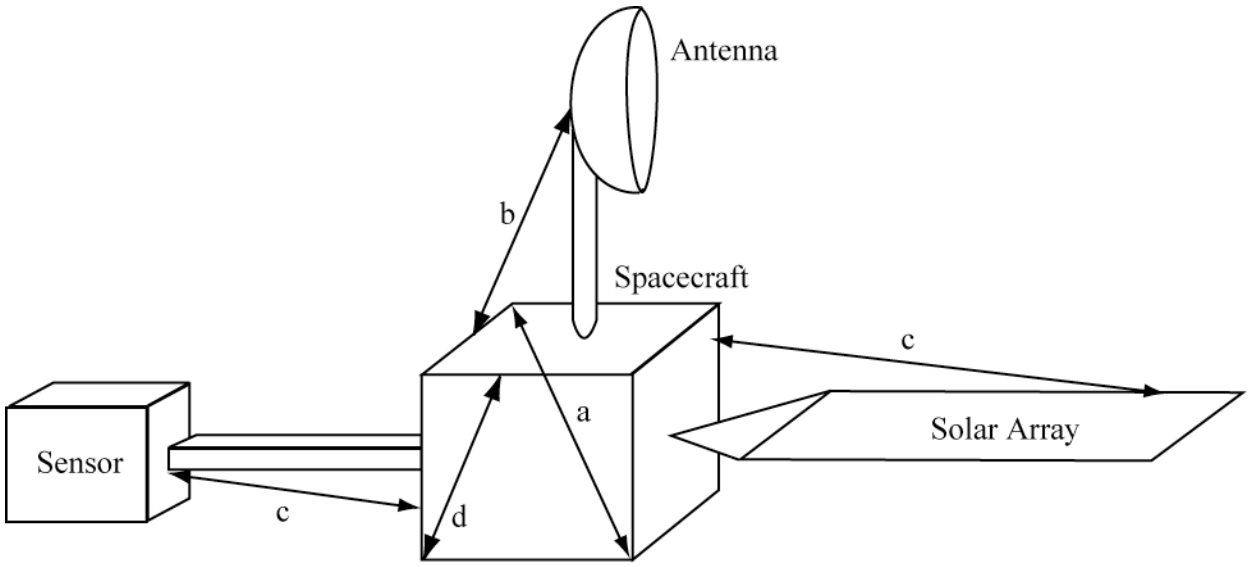

Figure 22—Paths for ESD Currents through Structure

a. Diametrically opposed locations (through the spacecraft).

b. Protuberances (from landing foot to top, from antenna to body, and from thruster jets to opposite side of body).

c. Extensions or booms (from end of sensor boom to spacecraft chassis and from end of solar panel to spacecraft chassis).

d. From launch attachment point to other side of spacecraft.

The tests using current paths “a” and “d” are of a general nature. Tests using current paths “b” and “c” simulate probable arc locations on at least one end of the current path. These test points include thrusters, whose operation can trigger an incipient discharge, and also landing feet and the attachment points, especially if used in a docking maneuver, when they could initiate a spark to the mating spacecraft.

Test “c” is an especially useful test. Solar panels often have glass (non-conductive) coverglasses, and sensors may have optics (non-conductive) that can cause an arc discharge. In both cases, any blow-off charge would be replaced by a current in the supporting boom structure that could couple into cabling in the boom. This phenomenon is possibly the worst-case event that could occur on the spacecraft because the common length of the signal or power cable near the arc current is the longest on the spacecraft.

6.3.2.4 Part Testing

Many electronic devices are tested and characterized for their susceptibility to an electrical transient that simulates fabrication handling. It follows the MIL-STD-883-3, Method 3015.9, HBM (see

Appendix D.9). If the discharges (especially the pulse duration of the discharges) to electronic devices is expected to be similar to the HBM transient, or in other words, the characteristic pulse duration is closer to 150 ns, the HBM class of the electronic device can be used for the assessment. If the transient parameters are far from the HBM transient, the immunity of the electronic device against the expected discharges needs to be separately tested. The immunity of the electronic devices can also be used in SPICE-type simulation when the discharge sources are not in the vicinity of the electronic device.

6.3.2.5 Unit Testing

Unit ESD testing serves the same purpose as it serves in standard environmental testing, i.e., it identifies design deficiencies at a stage when the design is more easily changed. It is, however, very difficult to provide a realistic determination of the unit's environment as caused by an ESD on the spacecraft.

6.3.2.5.1 General

A unit testing program could specify a single ESD test for all units or could provide several general categories of test requirements. The following test categories are provided as a guide:

a. Internal units (general) have to survive, without damage or disruption, the MIL-STD-1541A arc source test (discharges to the unit but no arc currents through the unit's chassis).

b. External units mounted outside the Faraday Cage (usually exterior sensors) have to survive the MIL-STD-1541A arc source at a 5-kV level with discharge currents passing from one corner to the diagonally opposite corner (four pairs of locations).

c. For units near a known ESD source (e.g., Kapton® thermal blankets), the spark voltage and other parameters have to be tailored to be similar to the expected spark from that dielectric surface.

d. Degradation of solar cells to solar array discharges are assessed via methods of AIAA S-111A, Qualification and Quality Requirements for Space Solar Cells, and AIAA S-112A, Qualification and Quality Requirements for Electrical Components on Space Solar Panels. For arrays operating at voltages >30V and string or circuit current levels >1A (Bodeau [2012 and 2014]), solar array coupons should be tested to demonstrate immunity to sustained vacuum arcs using methods outlined in ISO 11221. Array backside hardware (e.g., diode boards terminal boards, connectors and power harness) should also be tested using adaptations of ISO 11221 methods, such as described in Bodeau (2013).

6.3.2.5.2 Unit Test Configuration

ESD tests of the unit (subsystem) can be performed with the subsystem configured as it would be for a standard EMC-radiated susceptibility test. The unit is placed on and electrically bonded to a grounded copper-topped bench. The unit is cabled to its support equipment which is in an adjacent

room. The unit and cabling should be of flight construction with all shields, access ports, etc., in flight condition. All spare cables should be removed. Any monitoring of device responses to the ESD should be done via spacecraft wiring and circuitry (not added measurement wiring) so that the ESD test visibility is the same as will be seen in flight.

6.3.2.5.3 Unit Test Operating Modes

The unit should be operated in all modes appropriate to the ESD arcing situation. Additionally, the unit should be placed in its most sensitive operating condition (amplifiers in highest gain state, receivers with a very weak input signal) so that the likelihood of observing interference from the spark is maximized. The unit should also be exercised through its operating modes to assure that mode change commands are possible in the presence of arcing.

6.3.2.6 Spacecraft Testing

A good system-level test will provide the most reliable determination of the expected performance of a space vehicle in the charging environment. Such a test should be conducted on a representative spacecraft before exposing the flight spacecraft to ensure that there will be no inadvertent overstressing of flight units.

A detailed test plan has to be developed that defines test procedures, instrumentation, test levels, and parameters to be investigated. Test techniques will probably involve current flow in the spacecraft structure. Tests can be conducted in ambient environments, but screen rooms with electromagnetic dampers are recommended. MIL-STD-1541A system test requirements and radiated EMI testing are considered to be a minimal sequence of tests.

The spacecraft should be isolated from ground. Instrumentation has to be electrically screened from the discharge test environment and be carefully chosen so that instrument response is not confused with spacecraft response. The spacecraft and instrumentation should be on battery power. Complete spacecraft telemetry should be monitored. Voltage probes, current probes, E and H field current monitors, and other sensors should be installed at critical locations. Sensor data should be transmitted with fiber optic data links for best results. Oscilloscopes and other monitoring instruments should be capable of resolving the expected fast response to the discharges (use instrumentation that can measure your best estimate of frequency content).

The test levels should be determined from analysis of discharging behavior in the worst-case environment expected (for example, the substorm environment for GEO missions). It is recommended that full level testing, with test margins, be applied to structural, engineering, or qualification models of spacecraft with only reduced levels applied to flight units. The test measurements, e.g., structural currents, harness transients, and upsets, are the key system responses that are to be used to validate predicted behavior.

6.3.2.6.1 General

Spacecraft testing is generally performed in the same fashion as unit testing. A test plan of the following sort is typical (see Figure 22):

a. The MIL-STD-1541A radiated test is applied around the entire spacecraft.

b. Spark currents from the MIL-STD-1541A arc source are applied through the spacecraft structure from launch vehicle attachment points to diagonally opposite corners.

c. ESD currents are passed down the length of booms with cabling routed along them, e.g., sensor booms or power booms. Noise pickup into cabling and circuit disruption are monitored.

d. Special tests are devised for special situations. For example, dielectric regions, such as quartz second-surface mirrors, Kapton® thermal blankets, and optical viewing windows should have ESD tests applied on the basis of their predicted ESD characteristics.

Examples of system level ESD current injection test results are shown in Figure 23, Examples of System Level ESD Test Waveforms; (a) Direct Measurement with Very Short Leads on Its Output and (b) Measurement during a System-Level Test with 9 meters of Attachment Wiring (Two 4.5 m Lengths). The MIL-STD-1541A ESD waveform generator was measured directly with very short leads on its output, with nothing else attached. The peak current is about 66 A, risetime about 5.2 ns, and a time base of 20 ns/div. The waveform was later measured during a system-level test. The current was applied via 9 meters of attachment wiring (two 4.5-m lengths) from the same MIL-STD-1541A sparker to the top of a spacecraft, with the current return at the solar array drive on the body of the spacecraft. Because of inductance in the long leads, the risetime has increased to 40 ns, the peak current is now 15 A, and the time base is 200 ns/div. (Scale factors in these historic pictures are different in each picture and include attenuations and probe factors.)

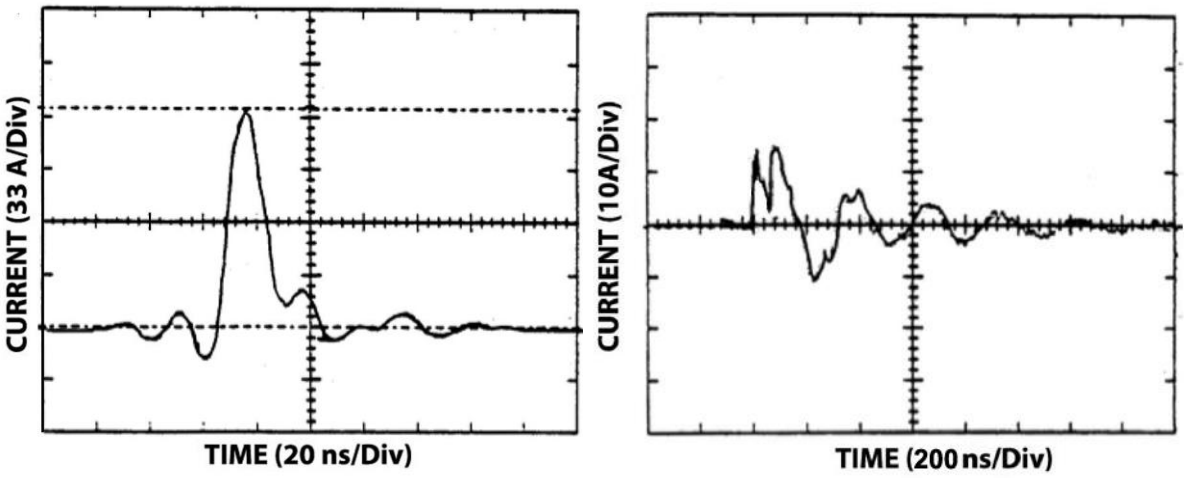

Figure 23— Examples of System-Level ESD Test Waveforms; (a) Direct Measurement with Very Short Leads on Its Output and (b) Measurement during a System-Level Test with 9 Meters of Attachment Wiring (Two 4.5-m Lengths)

6.3.2.6.2 Spacecraft Test Configuration

The spacecraft ESD testing configuration ideally simulates a 100% flight-like condition. This may be difficult because of the following considerations:

a. Desire for ESD diagnostics in the spacecraft.
Note that it is best not to have extra non-flight wiring in the test setup.

b. Non-realistic power system (no solar array).
It is rare to have a solar array simulator (SAS) that mimics the output impedance of the actual solar array, but try or try to account for the differences.

c. Local rules about grounding the spacecraft to facility ground.
One way to comply with local rules for "grounding" the spacecraft structure is to have a resistive ground reference of some value (we have used a 250 kohm resistor) during this test.

d. Cost and schedules to completely assemble the spacecraft for the test and later disassemble it if failures or anomalies occur.

e. The possible large capacitance to ground of the spacecraft in its test fixture.
Lift the spacecraft off the ground to achieve the estimated spacecraft capacitance to space, often on the order of 200 pF (using a spherical estimate of spacecraft dimensions).

f. ESD coupling onto non-flight test cabling.
Use minimal non-flight test cabling.

g. Risk of immediate or latent damage to the spacecraft.
Have all organizations review and understand the test and concur with the test procedure.

h. Plasma source

6.3.2.6.3 Test Diagnostics

To obtain more information about circuit response than can be obtained by telemetry, it is common to use an oscilloscope to measure induced voltages related to the ESD test sparks at key circuits. If improperly implemented, the very wires that access the circuits and exit the spacecraft to test equipment, e.g., oscilloscopes, will act as antennas and show noise that never would be present without those wires.

Two approaches have been used with some success. The first is using conventional oscilloscope probes with great care. Long oscilloscope probes (3 m) were procured from Tektronix. For the circuits being monitored, a small tee breakout connector was fabricated and inserted at the connector nearest the circuit. Two oscilloscope probes were attached to each circuit's active and return wires, and the probe tips were grounded to spacecraft structure in the immediate vicinity of the breakout tee. The probe grounds were less than 15 cm from the probe tip. The signal was measured on a differential input of the oscilloscope. Before installation, the probes were capacitively compensated to their respective oscilloscope preamplifiers, and it was verified that their common-mode voltage rejection was adequate (normal good practice). The two probe leads were twisted together and routed along metal structure inside the spacecraft until they could be routed out of the main chassis enclosure. They were then routed (still under thermal blankets) along the structure to a location as remote as possible from any ESD test location and finally routed to the oscilloscope. The oscilloscopes were isolated from building ground by isolation transformers, and ground referenced to the spacecraft chassis near the exit point of the test probes. Clearly, this method permits monitoring only a few circuits (reference Whittlesey [1978]).

A second method of monitoring ESD-induced voltage waveforms on internal circuits is the use of battery-powered devices that convert voltages to light-emitting diode (LED) signals. LED signals can be transmitted by fiber optics to exterior receiving devices, where the voltage waveform is reconstructed. As with the oscilloscope probes, the monitoring device has to be attached to the wires carefully with minimal disturbance to circuit wiring. The fiber optics cable has to be routed out of the spacecraft with minimal disturbance. The deficiency of such a monitoring scheme is that the sending device has to be battery powered, turned on, and installed in the spacecraft before spacecraft buildup; and it has to operate for the duration of the test. The need for batteries and the relatively high-power consumption of LED interface circuits severely restrict this method.

Another proposed way to obtain circuit response information is to place peak-hold circuitry (tattle-tales) at key circuit locations, installed as described above. This method is not very useful because the only datum presented is that a certain peak voltage occurred. There is no evidence that the ESD test caused it, and there is no way to correlate that voltage with any one of the test sequences. For analysis purposes, such information is worthless.

6.3.2.6.4 Use of External (Non-Flight) Power Supplies

Spacecraft using solar cells or nuclear power supplies often have to use support equipment (SE) power supplies for ground test activities and are not totally isolated from ground. In such cases, the best work-around is to use an isolated and balanced output power supply with its wires routed to the spacecraft at a height above ground to avoid stray capacitance to ground. The power wires should be shielded to avoid picking up stray radiated ESD noise; the shields should be grounded at the SE end of the cable only.

6.3.2.6.5 Facility Grounding

To simulate flight, the spacecraft should be isolated from ground. Normal test practice dictates an excellent connection to facility ground. For the purpose of the ESD test, a temporary ground of 0.2 to 2 Mohm or more will isolate the spacecraft. Generally, 0.2 to 2 Mohm is sufficient grounding for special test circumstances of limited duration and can be tolerated by the safety or QA organization for the ESD test.

6.3.2.6.6 Cost and Schedules to Assemble and Disassemble Spacecraft

Often testing is done in the most compact form possible, attempting to interleave several tasks at one time or to perform tasks in parallel. This practice is incompatible with the needs of ESD testing and has to be avoided. A thermal vacuum test, for example, is configured like the ESD test but has numerous (non-flight) thermocouple leads penetrating from the interior to the exterior of the spacecraft. These leads can act as antennas and bring ESD-caused noise into spacecraft circuitry where it never would have been. Dynamic (shake table) test configurations have the same problem with the accelerometers.

6.3.2.6.7 Spacecraft Capacitance to Ground during Test

If stray capacitance to facility ground is present during the ESD test, it will modify the flow of ESD currents. For a better test, the spacecraft should be physically isolated from facility ground. It can be shown that raising a 1.5-m-diameter spherical spacecraft 0.5 m off the test flooring reduces the stray capacitance nearly to that of an isolated spacecraft in free space. A dielectric, e.g., wood, support structure can be fabricated for the ESD test and will provide the necessary capacitive isolation.

6.3.2.6.8 ESD Coupling onto Non-Flight Test Cabling

One method of reducing ESD coupling to and from the spacecraft on non-flight test wiring is the use of ferrite beads on all such wiring. The most realistic approach is to have no non-flight cabling, leaving only information that would be visible while in flight, at the expense of extra diagnostic information.

KNOWLEDGE CHECK

6.1 Generate a Table 5 replica with various dielectrics on the outer surfaces of a spacecraft at your facility.
6.2 If you have an ESD spark simulator in your facility (EMC) lab, write down its ESD test parameters per Table 6. Bonus question: Find two ESD spark test simulators; write down and compare the ESD test parameters per Table 6.

7. CONTROL AND MONITORING TECHNIQUES

7.1 Active Spacecraft Charge Control

Charge control devices are a means of controlling spacecraft potential. Various active charged-particle emitters have been and are being developed and show promise of controlling spacecraft potential in the space plasma environment. At this time, only neutral plasma devices (both ion and electron emitters) have demonstrated the ability to control spacecraft potential in geomagnetic substorms. These devices are sometimes recommended for charge control purposes (reference Purvis and Bartlett [1980] and Olsen and Whipple [1977]). Plasma contactors are currently the most widely used charge control devices.

When the ISS decided to use high-voltage (+160 V) solar arrays, it was predicted that the ISS would experience significant spacecraft charging. If an astronaut conducting EVA is exposed to the potential difference, a possible electrical shock hazard arises. To limit the ISS chassis charging due to solar array electron current collection, plasma contactor units (PCUs) were used as a “ground strap” to the local plasma. The PCUs move the excess charge accumulated on the ISS chassis back into the ionosphere, thereby minimizing any spacecraft charging. The PCUs were rated to continuously emit as much as 10 amps of accumulated charge back into the ionosphere and respond to changes in the ISS current collection in a fraction of a second. The PCUs were designed and verified such that ISS chassis potential would never go more negative than -40 V when the PCUs were operating (reference Carruth, Jr., et al. [2001] and Hernandez-Pellerano, et al. [2014]).

Emitted particles constitute an additional term in the current balance of a spacecraft. Because the ambient current densities at geosynchronous altitude are quite small, emitting small currents from a spacecraft can have a strong effect on its potential, as has been demonstrated on the ATS-5 and ATS-6, SCATHA, and other spacecraft. However, devices that emit particles of only one electric charge, e.g., electrons, are not suitable for active potential control applications unless all spacecraft surfaces are conducting. Activation of such a device will result in a rapid change of spacecraft potential. Differential charging of any insulating surfaces will occur, however, and cause potential barrier formation near the emitter. Emission of low-energy particles can then be suppressed. Higher energy particles can escape, but their emission could result in the buildup of large differential potentials. On the other hand, devices that emit neutral plasmas or neutralized beams, e.g., hollow cathode plasma sources or ion engines, can maintain spacecraft potentials near plasma ground and suppress differential charging. These are a possible type of charge control devices at the cost of reliability and complexity.

7.2 Environmental and Event Monitors

The occurrence of environmentally induced discharge effects in spacecraft systems is usually difficult to verify. Often the only thing known about an anomaly is that it occurred at some spacecraft time. Since most spacecraft are not well instrumented for environmental effects, the state of the environment at the time of the anomaly typically has to be inferred from the environmental data from the other spacecraft or ground observation. Investigations also have to include spacecraft state. This has to include possible switching events that occurred at the time and may be the cause of the observation. Unfortunately, environmental data are not necessarily representative of the environment at the spacecraft location and, in fact, generally show a poor correlation.

This problem could be addressed if spacecraft carried a set of environmental monitors, e.g., a simple monitor set designed to measure the characteristic energy and current flux as well as to monitor transients on harness positions within the spacecraft (reference Sturman [1981]. This situation is changing as more organizations become aware of the ability to construct compact sensors for environmental monitoring and anomaly attribution. The largest organization to recognize this at this time is the U.S. Air Force, which through a memorandum issued by the Secretary of the Air Force is requiring environmental sensors on future spacecraft that it is acquiring (reference Gruss [2015]. The Air Force Research Laboratory has developed the Compact Environmental Anomaly Sensor (CEASE) (reference Lindstrom, et al. [2018] to address this, and the Aerospace Corporation has built a less-well-instrumented design called ECP-Lite for smaller spacecraft). ESA has also developed similar sensors with its standard radiation monitor (reference Mohammadzadeh, et al. [2003]). (A radiation environment, thus measured, can then be converted to an electron charging environment. See Appendix C.4.1, Dose to Fluence Approximation, in this NASA Technical Handbook.)

Spacecraft charging effect monitors require data analysis support to produce the desired results. Transient monitors capable of measuring the pulse characteristics have also been used (reference Koons [1981]). If they were carried on a number of operational satellites, the technology community would be able to obtain a statistical base relating charging to induced transients. Satellite operators, on the other hand, would be able to tell when charging is of concern, to establish operational procedures to minimize detrimental effects, and to separate system malfunctions from environmentally induced effects.

It is recommended that monitor packages be carried on all spacecraft. These packages should consist of a dosimeter, energetic plasma environment detector, surface potential monitor, and transient voltage pulse detector.

KNOWLEDGE CHECK

7.1 What value can an active charge control system provide to a project in an engineering sense? What value can an active charge control system provide to scientific investigatory instruments on the spacecraft?

7.2 Who would you lobby in your organization at the beginning of a project to place an environmental monitor on your spacecraft to enable ESD problem identification and/or

measure the plasma environment with a modest degree of accuracy? Or who would you see to be an advocate to management to implement this?

7.3 Compare the costs of an environmental monitor to that of an anomaly investigation board that does not have sufficient information to rule out spacecraft charging or radiation damage.

8. MATERIAL NOTES AND TABLES

This section has been included to place examples of material resistivity, RIC, density, and dielectric strength properties in one convenient place for ESD analysts. These lists contain spacecraft materials that might often be considered when doing penetrating electron charging analyses, charge accumulation analyses, and breakdown estimates.

Caveat emptor! While the lists are generally representative, the reader should re-check the parameters, especially the resistivity, RIC, and dielectric strength parameters for any detailed work. As shown in Table 7, Dielectric Material Characteristics for Internal Charging Studies, these materials properties may vary significantly—in some cases by many orders of magnitude—with temperature, electrical stress, radiation, contamination, etc. (reference Dennison [2015]). One should also note that two samples of nominally the same material may exhibit different charging properties based on subtle differences in manufacturing or aging history (reference Saiki, et al. [2015]). What is more troubling is that some common materials such as circuit boards are manufactured to specifications that may be met using a variety of different materials or processes. It has also been observed that a single trade name covers several variants of a material (e.g., ULTEM® or Kapton®). And a close inspection of circuit board specifications (e.g., FR4 or Arlon 85-N (polyimide laminate and prepreg system)) reveals there are multiple compliant layups or indeed materials for the core, ground plane, and prepreg layers. This results in different materials with the same trade name and same functions that may have different charging properties.

For nano-particle loaded dielectrics percent fill and the uniformity of the distribution of nano-particles can result in significant variations in charge transport properties. When testing composite materials, great care should be taken to ensure that the test method will result in an answer that is representative of the application. See Appendix D.

8.1 Dielectric Material List

The partial list of basic dielectric material properties in Table 7 is provided for illustration and reader convenience only. Data were taken from Westman (1968), Shugg (1995), and various other sources, including manufacturer data sheets. For sensitive ESD applications, designers should ensure materials properties come from a source that is shown to be relevant to their mission environment or test the materials properties themselves in a representative way. See Appendix D.

At the time of writing this edition, NASA has begun the process of creating the Spacecraft Charging Materials Database (SCMD), https://maptis.ndc.nasa.gov/scmd. In its initial release, the database is very limited; it is anticipated that it will become the primary reference for spacecraft materials properties as the database grows—at least in part through user-submitted materials

properties contributions. SCMD will be publicly available via a free registration. Some of the data may only be specified minimum or maximum limits and not typical values; actual resistivity values may differ by many orders of magnitude, e.g., FR4. Note that in practice dielectric strength should be specified as a function of thickness and may be extrapolated to other thicknesses roughly as the inverse square root of the thickness. Each project has to be responsible for compiling its own list based on the most current and relevant data. Frederickson, et al. (1986) contains lists of dielectric properties for materials not included here.

Other often-significant effects not tabulated here include temperature, radiation-induced conductivity, and electric field-induced conductivity.

Figure 24, Dielectric Time Constant Based on Resistivity and Dielectric Constant, shows how resistivity and dielectric constant together combine to determine material time constants (see Appendix D.8) and indicate relative desirability for ESD-sensitive applications. “Safe” time constants will vary depending on mission, shielding, and temperature. As an example, “safe” (difficult to accumulate charge) has time constants less than 3 hours, “dangerous” (too resistive and likely to cause on-orbit ESD issues in space plasma environments) has time constants greater than 30 hours. An uncertain/marginal region falls in between these limits. From this chart, it can be seen that materials with resistivities on the order of 10^{18} ohm cm or more such as Kapton® or Teflon® are undesirable from an ESD standpoint. Table 8, Conductor Characteristics for Charging Studies (Approximate), shows resistivity and density information for some conductors. References are the same as Table 7 (from mixed sources for illustration only).

These tables are shown as illustrations of the bookkeeping that should be done during an ESD mitigation program for your particular spacecraft.

Table 7—Dielectric Material Characteristics for Internal Charging Studies[1]

PARAMETER/ MATERIAL (units)	DIELECTRIC CONSTANT[2]	DIELECTRIC STRENGTH[3, 7] (V/mil @ mil)	DC VOLUME RESISTIVITY[4] (ohm cm)	DENSITY (g/cm^3)/ density in relation to aluminum	TIME CONSTANT[5] (as noted)	RIC CONSTANT[8] (s/rad ohm cm)
DIELECTRICS						
Ceramic (Al_2O_3)	7.1 – 10.1	200-380 @ 197 340 @ 125 635-760 @ 11.8	10^{15} - >10^{18}	3.37-3.99 /0.68-0.8	10 min - >10 d	10^{-18} – 10^{-14}
Delrin®	3.1 – 4.4	380 @ 125 813 @ 39.4	10^{13} - >10^{15}	1.33-1.61 /0.49-0.6	2.7 s - >6.5 min	
FR4	4.7	2000 @ 20 420 @ 62	>10^9 >4 x 10^{14}	1.78/0.66	>141 s	
Kapton® HN	3.4 – 3.5	3800 @ 1	> 10^{18}	1.4/0.51	3.5 d	10^{-18} – 10^{-14}
Kapton®	--	580 @ 125	> 10^{18}	1.4/0.51	3.5 d	
Mylar®	3	7000 @ 1	10^{18}	1.4/0.51	3.1 d	10^{-21} – 10^{-17}
Polystyrene	2.5	5000 @ 1	10^{16}	1.05/0.39	37 min	10^{-24} – 10^{-15}
Quartz, fused	3.78	410 @ 250 500 @ 3	>10^{19}	>2.6	>38 d	10^{-16} – 10^{-15}
Teflon® (generic)[6]	2.1	2-5k @ 1	> 10^{18}	2.1/0.78	2.1 d	
Teflon® (generic)[6]	--	500 @ 125	> 10^{18}	2.1/0.78	2.1 d	10^{-19} – 10^{-15}
(Blank lines below are for reader's notes and additions.)						

Notes:

1. If the numbers in the table are "greater than," the actual time constants could be greater than shown (calculated) in this table. The numbers in this table are for room temperature. At low temperatures, the resistivity values may become much greater and the time constants for charge bleed-off can be much greater.
2. Permittivity = relative permittivity (dielectric constant) x 8.85 x 10^{-12} F/m.
3. ~508 V/mil is the same as 2 x 10^7 V/m.
4. Resistivity (ohm m) = resistivity (ohm cm)/100.
5. Time constant (s) = permittivity (F/m) x resistivity (ohm m).
6. Generic numbers for Teflon®; polytetrafluoroethylene (PTFE) and fluorinated ethylene propylene (FEP) are common forms in use for spacecraft.
7. Value at power frequencies
8. RIC exponent is bounded by 0.5 and 1 and is often close to 1. Ranges given by those found in published literatures.

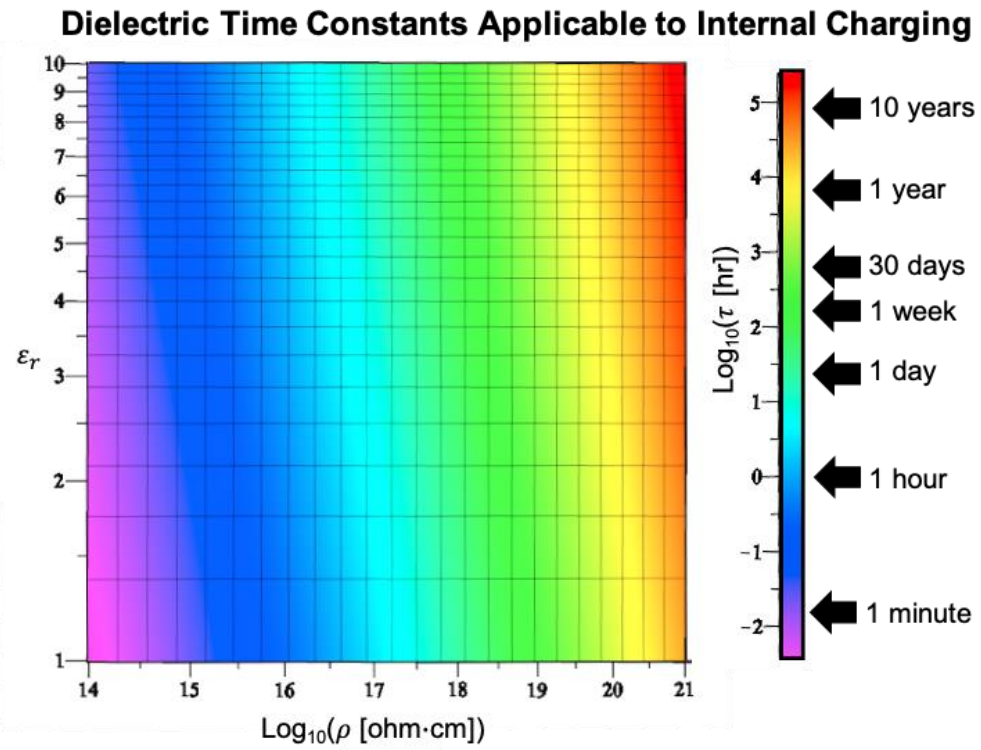

Figure 24—Dielectric Time Constant Based on Resistivity and Dielectric Constant

8.2 Conductor Material List

The partial list of basic conductor characteristics in Table 8 is provided for illustration and reader convenience only.

Table 8—Conductor Characteristics for Charging Studies (Approximate)

PARAMETER/ MATERIAL UNITS	DC VOLUME RESISTIVITY (ohm cm (x10^{-6}))	DC VOLUME RESISTIVITY (re: aluminum)	DENSITY (g/cm^3)	DENSITY (re: aluminum)
Aluminum	2.62	1	2.7	1
Aluminum Honeycomb	Variable	Variable	~0.049	~0.02
Brass (70-30)	3.9	1.49	8.5	3.15
Carbon graphite	5-30	1.9-11.45	1.3-1.95	0.48-0.72
Copper	1.8	0.69	8.9	3.3
Graphite-epoxy:epoxy	Variable	Variable	1.5	0.56
Gold	2.44	0.93	19.3	7.15
Invar	81	30.9	8.1	3
Iron-steel	9-90	3.43-34.3	7.87	2.91
Lead	98	37.4	11.34	4.2
Kovar A	284	108.4	~7.8	~2.89
Nickel	7.8	2.98	8.9	3.3
Magnesium	4.46	1.7	1.74	0.64

PARAMETER/ MATERIAL UNITS	DC VOLUME RESISTIVITY (ohm cm ($x10^{-6}$))	DC VOLUME RESISTIVITY (re: aluminum)	DENSITY (g/cm^3)	DENSITY (re: aluminum)
Silver	1.6	0.61	10.5	3.89
Stainless Steel (SS304)	73	27.9	7.9	2.93
Tantalum	13.9	5.3	16.6	6.15
Titanium	48	18.3	4.51	1.67
Tungsten	5.6	2.14	18.8	6.96
(Blank lines below are for reader's notes and additions.)				

Notes:

1. See text for references and accuracies.
2. Densities from various sources match well; resistivities may vary.
3. Resistivity (ohm m) = resistivity (ohm cm)/100.

KNOWLEDGE CHECK

8.1. Make a list like Table 7 for dielectric materials that would need to have their parameters as needed for your project. Then populate the lines of the table with the appropriate materials identified as of ESD concern for your project.
8.2. Where would you obtain applicable parameters for your spacecraft?
8.3. Populate the table with those numeric technical parameters for your spacecraft.
8.4. Estimate the accuracy (error bars) for each of the numeric parameters, with the source of that estimate (and saying, "this is just a guess and placeholder till we get better answers" is permissible, and quite often appropriate to focus attention to obtain resources to measure them yourself in your materials test lab).
8.5. Look at Figure 24. Is it clear and understandable and easy to use?
8.6. Is Figure 24 correct and does it have zero size error bars?
8.7. Now, go back to Table 7 and answer the following questions.
8.8. What do you think are the materials presently in Table 7 that have big error bars?
8.9. Can you put some speculated error bars onto those material's technical parameters?
8.10. Would your answers affect your confidence in using Figure 24?
8.11. Research parameter numbers for one or two of the materials. Name your technical source for your answers (e.g., specific manufacturer data sheet; material properties sources; etc.)
8.12. Do you think that Table 7, as presently printed, is acceptable to use without thought?

APPENDIX A

THE SPACE ENVIRONMENT

A.1 PURPOSE

This Appendix provides an introduction to space environments and supplements the material presented section 4 of this NASA Technical Handbook. It presents many of the concepts introduced in section 4 in more detail for the interested reader.

A.1.1 Quantitative Representations of the Space Environment

Earth's plasma is properly described in terms of a so-called phase space density or distribution function. Space plasmas can be described most simply in terms of the Maxwell-Boltzmann distribution. As this representation lends itself to efficient manipulation when carrying out charging calculations, it is often the preferred way for describing plasmas. The Maxwell-Boltzmann distribution F_i is given by:

$$F_i(v)\, d^3v = [n_i\{m_i/(2\pi kT_i)\}^{3/2}] \exp\{-m_i v^2/(2kT_i)\}\, d^3v \qquad \text{(Eq. 14)}$$

where:

n_i = number density of species i (m^{-3})
m_i = mass of species i (kg)
k = Boltzmann constant (=1.38 x 10^{-23} J/K)
T_i = characteristic temperature of species i (K)
v = velocity (m/s)
F_i = distribution function of species i (s^3/m^6)
d^3v = $4\pi v^2 dv$ for isotropic environment (m^3/s^3)

Unfortunately, the space plasma environment is seldom a Maxwell-Boltzmann distribution. However, given the actual plasma distribution function, it is possible to define (irrespective of whether the plasma is Maxwell-Boltzmann or not) moments of the particle distribution that reveal characteristics of its shape. In most cases, these moments can then be used to determine an approximate Maxwell-Boltzmann distribution. We define the first four of these characteristic moments as:

$$\langle ND_i \rangle = 4\pi \int_0^\infty (v^0) F_i v^2 dv \qquad \text{(Eq. 15)}$$

$$\langle NF_i \rangle = \int_0^\infty (v^1) F_i v^2 dv \qquad \text{(Eq. 16)}$$

$$\langle ED_i \rangle = (4\pi m_i/2) \int_0^\infty (v^2) F_i v^2 dv \qquad \text{(Eq. 17)}$$

$$\langle EF_i \rangle = (m_i/2) \int_0^\infty (v^3) F_i v^2 dv \qquad \text{(Eq. 18)}$$

where:

$\langle ND_i \rangle$ = number density of species i
$\langle NF_i \rangle$ = number flux of species i per unit solid angle

$\langle ED_i \rangle$ = energy density of species i
$\langle EF_i \rangle$ = energy flux of species i per unit solid angle

For the Maxwell-Boltzmann distribution of Eq. 14, these assume the following values:

$$\langle ND_i \rangle = n_i \quad \text{(Eq. 19)}$$
$$\langle NF_i \rangle = (n_i/2\pi)(2kT_i/\pi m_i)^{1/2} \quad \text{(Eq. 20)}$$
$$\langle ED_i \rangle = (3/2)n_i kT_i \quad \text{(Eq. 21)}$$
$$\langle EF_i \rangle = (m_i n_i/2)(2kT_i/\pi m_i)^{3/2} \quad \text{(Eq. 22)}$$

It is often easier to measure the moments, e.g., number flux, of the plasma distribution function than the actual distribution function in terms of energy or the temperature. This is particularly true for space plasmas where the temperature is not well defined. As an illustration, from the first four moments, two definitions of the plasma temperature consistent with a Maxwell-Boltzmann distribution are possible as follows:

$$kT_{av} = 2\langle ED \rangle/3\langle ND \rangle \quad \text{(Eq. 23)}$$
$$kT_{rms} = \langle EF \rangle/2\langle NF \rangle \quad \text{(Eq. 24)}$$

For a true Maxwell-Boltzmann plasma, these quantities would be equal; for actual plasmas, T_{rms} is usually greater than T_{av}. Even so, experience has shown that a representation in terms of two Maxwell-Boltzmann distributions is, in fact, a better mathematical representation of the space plasma than a single Maxwellian. That is, the plasma distribution for a single species can be represented by:

$$F2(v) = \{m/(2\pi k)\}^{3/2} [\{n_1/(T_1)^{3/2}\}\exp(-mv^2/2kT_1) + \{n_2/(T_2)^{3/2}\}\exp(-mv^2/2kT_2)] \quad \text{(Eq. 25)}$$

where:
n_1 = number density for population 1
T_1 = temperature for population 1
n_2 = number density for population 2
T_2 = temperature for population 2

In most cases, this representation fits the data quite adequately over the energy range of importance to spacecraft surface charging, namely, ~1 eV to 100 keV. Further, it is very simple to derive n_1, T_1, n_2, and T_2 directly from the four moments so that a consistent mathematical representation of the plasma can be established that incorporates the simplicity of the Maxwell-Boltzmann representation while maintaining a physically reasonable picture of the plasma. The distinction between T_{av}, T_{rms}, T_1, and T_2 has to be kept in mind whenever reference is made to a Maxwell-Boltzmann distribution, as this is only an approximation at best to the actual plasma environment.

Although the Maxwell-Boltzmann distribution can be used for representing the high-energy electron environment for internal charging, it is typically not as useful. More typically, the electron environment above ~100 keV approaches a functional form represented by a power law or the more complex Kappa distribution which better represents the non-thermal tail in the electron distribution

at higher energies. For example, if a power law distribution $A_o E^{-x}$ is assumed for *i(E)*, the differential intensity (also often called "flux"), the integral intensity *I*(E) would give:

$$I(E) = -\int_E^{\infty} i(E')\, dE' = -(A_o E^{1-X})/(1-X) \qquad \text{(Eq. 26)}$$

where:

i(E) = $-dI(E)/dE$ = differential angular intensity (or flux) = particles per unit time per unit area per unit energy per unit of solid angle at energy *E* (example: n#/(cm^2 s sr MeV))

I(E) = integral (over energy) angular intensity (or flux) = particles per unit time per unit area per unit of solid angle from energy *E* to infinity (example: n#/(cm^2 s sr))

E = energy of particle

A_o,X = Constants

The omnidirectional fluxes are then given by

$$j(E) = \int_o^{\pi} d\alpha \int_o^{2\pi} i(E) \sin(\alpha) d\phi \qquad \text{(Eq. 27)}$$

$$J(E) = \int_o^{\pi} d\alpha \int_o^{2\pi} I(E) \sin(\alpha) d\phi \qquad \text{(Eq. 28)}$$

where:

j(E) = omnidirectional differential flux = particles per unit time per unit area per unit energy integrated over 4π steradians at energy *E* (example: n#/(cm^2 s MeV))

J(E) = omnidirectional integral flux = particles per unit time per unit area over 4π steradians from energy *E* to infinity (example: n#/(cm^2 s))

α = particle pitch angle (radians) for particles in a magnetic field or, in the absence of a magnetic field, the angle relative to the normal to a surface

Some publications, including NASA's AE8/AP8 family of radiation models, use the term omnidirectional integral flux as defined above, which implies an isotropic (uniform in all directions) particle flux. This is our *J* or the omnidirectional integral flux. Other publications report intensity (flux) per steradian (or our *I* with units of #/cm^2 s sr). Assuming an isotropic plasma (a common simplifying assumption), the two are related by:

$$J = 4\,\pi\, I \qquad \text{(Eq. 29)}$$

Similarly, after integrating *I* from E = 0 to ∞ and converting from charge/s to amperes, the net current per unit area, J_s, to a flat surface for an isotropic flux, when integrated over angle relative to the surface normal (Eq. 28), can be shown to be:

$$J_s = \pi\, q\, I \qquad \text{units: A/cm}^2 \qquad \text{(Eq. 30)}$$

where:

q = charge per particle 1.6 x 10^{-19} Coulomb per particle

The reduction of 1/4 is due to two factors. The first 1/2 is because the current to a surface only comes from one side of the surface. The second 1/2 is the average value of current due to the integral over angle for non-normal incidence. If the flux is not isotropic, these simple calculations have to be redone for the actual angular distribution. [Note: To avoid confusion, in the rest of this

NASA Technical Handbook, the total current to a spacecraft will be defined as "I_t" where $I_t = J_s$ x (collection area).]

The preceding is true for the fluxes and currents impacting the surface. For penetration calculations, the geometry of the shielding has to be carefully considered in estimating the fluxes in a material or inside the shielding. For example, the non-normally incident electrons cannot penetrate as deep as normally incident electrons because of the longer path length through the shielding to a given point. The difference depends on the depth and on the spectrum of the electrons; accurate calculations require specialized codes which will be discussed later in the appendices.

A.1.2 Data Sources

The following subsections briefly list some satellites and sources from which environmental data can be obtained. This is not intended to be a complete list. The data sources chosen here are notable for accessible data and/or their historical importance to the spacecraft charging community. Note that there are problems in attempting to obtain calibrated particle data from space. Energetic electron detector data are, as an example, sometimes affected by the presence of energetic protons that generate secondary electrons during their passage through the detector. Detectors may degrade and become less efficient over time or may not even be initially calibrated over all energy ranges. View factors and orientation relative to the magnetic field also contribute to uncertainties in the count rate to flux conversion. Despite these concerns, the errors are usually small enough to permit the data to be used in estimating charging, at least for engineering purposes.

A.1.2.1 Advanced Composition Explorer (ACE) Spacecraft

The ACE spacecraft was launched in 1997 to the L1 liberation point 1.5 million km in front of the Earth along the Earth-sun line (reference Stone [1998]). It provides data from nine instruments to characterize the solar wind and galactic cosmic ray environment. The National Oceanic Atmospheric Administration (NOAA) provides real-time data products from ACE detailing the solar wind conditions. Real-time solar wind data and charged particle data for identifying solar particle events are derived from four sensors: EPAM (Energetic Ions and Electrons), MAG (Magnetic Field Vectors), SIS (High Energy Particle Fluxes), and SWEPAM (Solar Wind Electron, Proton, and Alpha Monitor). EPAM provides data on energetic ions (H, He, CNO, and Fe) from 0.05- 5.0 MeV/nucleon and energetic electrons from 40-130 keV. MAG provides vector magnetic field data at the L1 point. SIS provides isotopic composition of energetic nuclei from He to Ni over energies of 10 to 100 MeV/nucleon. Finally, of most relevance to spacecraft charging is the SWEPAM instrument that provides measurements of the solar wind composition. It measures protons and alpha particles from 0.26-36 keV and electrons from 1 eV to 1.35 keV. The real-time data are available at NOAA's Space Weather Prediction Center (SWPC) located at https://www.swpc.noaa.gov/products/ace-real-time-solar-wind. Archived data and detailed instrument descriptions can be found at the ACE science center at

http://www.srl.caltech.edu/ACE/ASC/. It is anticipated that ACE will remain operational until 2024 at which point its station-keeping fuel will be exhausted.

A.1.2.2 ATS-5, ATS-6

A major source of data on the geosynchronous plasma environment has been the University of California at San Diego (UCSD) Low Energy Plasma Detectors on the NASA geosynchronous satellites ATS-5 and ATS-6. In particular, data were taken for electrons and ions (assumed to be protons) in 62 energy channels. For ATS-5, at a longitude of ~225° E, spectra were taken every 20 s in 112% (dE/E) energy intervals from 51 eV to 51 keV. For ATS-6, at a longitude of ~266° E, spectra were taken every 15 s in 113 percent dE/E intervals from 1 eV to 81 keV. The data are available from the National Space Science Data Center (NSSDC) in 10-min average bins for 50 days between 1969-1970 for ATS-5 and 10-min bins for 45 days between 1974-1976 for ATS-6. The data are in the form of observation time, spacecraft coordinates, and the four moments of the electron and ion distribution functions. These data were analyzed extensively in papers by Garrett and DeForest (1979) and Garrett, et al. (1981a,b). They, along with data from SCATHA, represented the primary source of statistical data on the geosynchronous orbit until recent studies of the Los Alamos National Laboratory (LANL) instruments (see section A.1.2.4). An additional 10 days of data from ATS-6 are also available for a unique period (September 14-25, 1976), during which the ATS-6 spacecraft passed by the LANL Charged Particle Analyzer (CPA) instrument on another geosynchronous spacecraft allowing careful cross-calibration of the particle instruments. Some descriptions of these data appear in Garrett, et al. (1980b). Jursa (1985) provides an excellent summary of Earth's space plasma environments that sets the context for these observations.

A.1.2.3 CRRES

Launched in 1990, the CRRES spacecraft provided the most accurate and detailed measurements of Earth's radiation belts in many decades. A landmark in internal charging (it carried the first experiment specifically designed to study internal charging), it provided extensive data on the location and occurrence of IESDs throughout the magnetosphere. CRRES was launched into an eccentric, 18° inclination orbit that took it from below the Van Allen belts out to geosynchronous orbit. It had an orbital period of 10 hours and measured from a few eV to 10 MeV electrons. The primary data are from July 25, 1990, to October 1991, and include extensive measurements of internal arcing rates in addition to the radiation data. These data and related software codes may be obtained via a Web search of AF-GEOSPACE; use link Fact Sheets: AF-GEOSPACE: AF-GEOSPACE; a software request form is provided. CRRES data from the MEA and HEEF instruments covering energetic electron energies from 0.1 to 7.0 MeV have been used as one of the data sources in the creation of the AE9 model. Data from the PROTEL instrument covering proton energies from 2-80 MeV were used as one of the data sources in the creation of the AP9 model described below.

A.1.2.4 DMSP

Since the mid-1960's until present, the Air Force has flown satellites in an 830 km, circular polar orbit for collection of terrestrial weather data. In addition, these satellites have included an

electrostatic analyzer that provides measurement of the electrons and ions. These instruments are oriented to look in the zenith direction to make measurements of precipitating particles as the satellites pass through the polar caps. The latest version called SSJ5 (flown since 2003) measures electrons and ions over an energy range from 30 eV to 30 keV in nineteen logarithmically spaced steps. Detailed information of SSJ5 and the archived data can be found at https://dmsp.bc.edu/html2/ssj5_inst.html and https://www.ngdc.noaa.gov/stp/satellite/dmsp/, respectively.

A.1.2.5 GOES

The most readily available data on the high-energy particle environments are those from the NOAA GOES series of spacecraft at geosynchronous orbit. The data of interest here consist primarily of E >2 MeV electron fluxes expressed in e cm^{-2} s^{-1} sr^{-1}. Starting with GOES 8, data are also available for the E > 800 keV electron environment. GOES-16 (December 2017) and beyond use a new instrument suite called Space Environment in Situ Suite (SEISS) to provide spectrally resolved data over a wide range of particle energies and species (reference Dichter, et al. [2015]). Of most interest to spacecraft charging is the MPS-LO instrument that provides measurements in 15 log spaced differential channels of electrons and protons from 0.03-30 keV. The instrument points anti-Earthward and its field of view which is 180º x 5º is broken up into twelve 15º x 5º segments. The MPS-HI instrument uses 5 electron telescopes (10 log spaced channels from 0.05-4 MeV) and 5 proton telescopes (11 log-spaced channels from 0.08-12 MeV) each with a 30º field of view that spans 170º in a fan centered on the anti-Earthward direction.

Data from at least early 1986 to the present are readily available. GOES satellites are generally positioned over the United States East and the West Coasts, but their exact positions have varied over the years. GOES 15 and earlier data are available at: https://www.ngdc.noaa.gov/stp/satellite/goes/dataaccess.html. GOES-16 and later data are available at https://www.ngdc.noaa.gov/stp/satellite/goes-r.html. For GOES space weather data from the last 7 days, go to https://www.swpc.noaa.gov/products/goes-electron-flux for electron flux and https://www.swpc.noaa.gov/products/goes-proton-flux for proton flux.

A.1.2.6 Los Alamos Detectors

Detectors on board various Department of Defense (DoD) geosynchronous spacecraft provided by the LANL have been in service since the 1970s. Higher energy channels are referred to as CPA or, currently, the SOPA experiments. The data cover a wide energy range, e.g., from E > 30 eV to E > 5 MeV for electrons and are available from 1976 through 2005. The data are well calibrated and provide a more detailed snapshot of the environment but have not been as readily available. Recent papers presenting the Los Alamos data are Boscher, et al. (2003) and Sicard-Piet, et al. (2008). SOPA data from multiple GEO satellites over the time period of 1989-2008 were used in the creation of the AE9 model described below.

In addition to SOPA, since 1989, LANL has been accumulating high-quality measurements of electron and proton energy flux spectra from 1 eV to 40 keV from Magnetospheric Plasma Analyzer (MPA) instruments aboard a series of geosynchronous spacecraft. These data not only

characterize the plasma but can also be used to infer the potential (relative to plasma) of the instrument ground and the presence of differential charging. From the raw data, spin-angle-averaged flux spectra, spacecraft potential, and various moments are computed. The density and temperature moments should be used cautiously with a full understanding of how they are computed (see Davis, et al. (2008) for details of the data analysis. Thomsen, et al. (2007) provides statistics on the electrons and ions over a full solar cycle along with detailed spectra.

Since 2017, LANL has publicly released charged particle data which have been collected from the Combined X-ray and Dosimeter (CXD) and Burst Detector Dosimeter for Block II-R (BDD-IIR) instruments on multiple Global Positioning Satellites (GPS) as described by Morley, et al. (2017). The CXD instrument provides energetic electron measurements from 0.12-5 MeV with 11 channels, and the BDD-IIR measures electrons from 0.077-5 MeV with 8 channels. CXD also measures protons with energies between 6 and 75 MeV, and BDD-IIR measures protons from 1.3 to 54 MeV. Because GPS operates at an altitude of 20200 km, these data are useful for internal charging studies in the MEO environment. Publicly available data from 2001-2017 can be found at https://www.ngdc.noaa.gov/stp/space-weather/satellite-data/satellite-systems/gps/.

A.1.2.7 Polar Orbiting Environmental Satellites (POES)

Since 1978, NOAA has flown space environment monitors on the POES satellites. These satellites are in a polar, sun-synchronous orbit at an altitude of 850 km. Current satellites carry the SEM-2 instrument used to study radiation belt dynamics and energetic electron precipitation (reference Peck, et al., 2015). The SEM-2 instruments provide energetic electron fluxes from 0.01 to 2.5 MeV and proton fluxes from 0.03 to 140 MeV. It should be noted that the sensors have been reported to have contamination issues, and there has been a revision in the processing of the data that occurred in 2013 to correct for this as detailed in the previous reference. Access to the data and further description of how NOAA processes the POES data can be found at https://www.ngdc.noaa.gov/stp/satellite/poes/index.html**.**

A.1.2.8 Solar, Anomalous, and Magnetospheric Particle Explorer (SAMPEX)

Launched in 1992, SAMPEX has returned a wealth of data on the low-altitude radiation environment up until reentry in November 2012. The satellite was in a high inclination (82°) polar orbit with an altitude of 520 by 670 km. Its orbit passed through many L-shells; and its data, although not from a high altitude, contain information from those L-shells. The SAMPEX Proton/Electron Telescope (PET) provides measurements on precipitating electrons from 0.4 to ~30 MeV over the polar regions. SAMPEX PET data from 1992 to 2004 have been used in the creation of the AE9 model. The SAMPEX Data Center is located at http://www.srl.caltech.edu/sampex/DataCenter/index.html**.**

A.1.2.9 SCATHA

Launched in 1979, the SCATHA satellite is another major source of spacecraft charging data. In addition to numerous experiments for measuring and controlling spacecraft charging, SCATHA measured the space environment between 5.5 and 7.7 R_e for a number of years. Of particular interest to environmental studies are the Air Force Geophysics Laboratory (AFGL) SC5 Rapid Scan

Particle Detector which measured the electron and ion environments at 1-s intervals over the range of 50 eV to 0.5 MeV and the UCSD SC9 Low Energy Plasma Detector which measured the electron and ion plasma every 0.25 s at energies of 1 eV to 81 keV (the instrument is a near-duplicate of the ATS-5 and ATS-6 instruments). As in the case of these two spacecraft, the data were extensively analyzed by Garrett and others (1981a,b), Mullen and Gussenhoven (1983), and Mullen, et al. (1986) to return similar statistical results that can be compared to the ATS-5 and ATS-6 findings. The data are available in the referenced documents and some through the NSSDC. SCATHA energetic electron data (0.25-4.5 MeV) from 1979 to 1991 have been used as a data source for the AE9 space environment model.

A.1.2.10 NASA Van Allen Probes (formerly Radiation Belt Storm Probes)

The most recent comprehensive scientific mission to study the Earth's radiation belts was the Van Allen Probes launched in 2012 and decommissioned in 2019 (reference Stratton, et al. [2013]). Two satellites operated in a highly elliptical orbit with an apogee altitude of 30,414 km and perigee of 21,887 km at a 10.2º inclination. The satellites were spun so that instruments could map out angular variations in in situ particle flux from their instruments. This mission contained a wide range of scientific instruments intended to study Earth's radiation belts. This included multiple charged particle detector suites, magnetometers, and electromagnetic field and waves measurements. Of these, the three instruments of most interest to the spacecraft charging community are the Helium, Oxygen, Proton, and Electron (HOPE) Mass Spectrometer, the Magnetic Electron Ion Spectrometer (MagEIS), and the Relativistic Electron-Proton Telescope (REPT). HOPE measures ions and electrons from 1 eV to 50 keV in 36 log-spaced steps in five different view directions to give full sky coverage (reference Funsten, et al. [2013]). MagEIS measures the angular distribution of energetic electrons from 20 keV to 4 MeV using four magnetic spectrometers (reference Blake, et al. [2013]). REPT uses a stack of silicon detectors in a sold-state particle telescope to measure energetic electrons from 1-10 MeV (reference Baker, et al [2013]). Data from these three sensors can be downloaded from the science and operations data center at https://rbsp-ect.lanl.gov/science/DataDirectories.php. The Van Allen Probe science gateway that has details on all the instruments is located at https://rbspgway.jhuapl.edu/. Data from MagEIS were used in the most recent version of AE9 (1.5), and REPT data have been used in AP9 (1.5 or later).

A.1.2.11 Other Sources

As mentioned in the introduction to this section, the data sets described here have typically been made available and/or are of historical significance to the spacecraft charging community. It is a far from complete list of available data about the space environment. In particular, some other missions that may be of interest are the NASA Polar satellite mission whose data can be found at https://pwg.gsfc.nasa.gov/polar/data_products.shtml and the NASA THEMIS missions which can be found at http://themis.ssl.berkeley.edu/index.shtml**.** The Japanese Space Agency (JAXA) also recently launched its Arase (previously called ERG) satellite that measures the energetic electron environment and has data available at https://ergsc.isee.nagoya-u.ac.jp/**.**

For anomaly investigations, it is desirable to determine quickly what the state of the electron environment was during the event. No appropriate plasma data may be available for either that time

period or for the particular spacecraft orbit. In that case, possible secondary sources are geomagnetic indices or environment and/or anomaly data from other spacecraft in orbit at the same time. These data are also of value as support material in carrying out anomaly investigations as they may allow identification of the actual cause such as surface charging or single event upsets (SEUs). NOAA's World Data Center (WDC) at Boulder, Colorado, provides a number of useful indices on a near real-time basis and maintains a spacecraft anomaly database. These materials can be addressed through the Web at https://www.ngdc.noaa.gov/stp/satellite/anomaly/satelliteanomaly.html.

As mentioned in section 7.2 of this NASA Technical Handbook, environment monitors on spacecraft as secondary payloads are becoming more common. If data from these environment monitors can be made publicly available, they can become very useful to those attempting to determine the correlation of the space environment with observed anomalies. It is recommended that more organizations fly these monitors and make the data publicly available for this purpose.

A.2 GEOSYNCHRONOUS ENVIRONMENT

A.2.1 Geosynchronous Plasma Environments

In this section, the geosynchronous plasma environment is described in terms of temperature and number density. This simple characterization of the environment assumes two species, electrons and protons, where the energy distribution of each species is described by the Maxwell-Boltzmann distribution (see Appendix A.1.1). This treatment is used because the Maxwell-Boltzmann function can be easily used in calculating spacecraft charging. If the Maxwell-Boltzmann distribution is not used, actual data should be curve fit digitally and integrated numerically at a much greater computational cost. If a single Maxwell-Boltzmann distribution is inadequate for a given circumstance, the measured data are often treated as the sum of two Maxwell-Boltzmann populations. Species such as oxygen and helium can be included as additional Maxwellian populations. Note: Other representations such as a Kappa distribution are also possible, but the Maxwell-Boltzmann distribution is adequate for most simple surface charging estimates.

The following text describes in greater detail the characterization of the geosynchronous plasma environment in terms of Maxwell-Boltzmann distribution and its moments. The interested reader is also referred to more recent studies of the charging environment using data from the LANL electron and ion spectrometers on a number of geosynchronous spacecraft. See, for example, Thomsen, et al. (2007) and Davis, et al. (2008) for the ~1 eV to ~45 keV/e electron and ion environments and Boscher, et al. (2003) for the corresponding 30 keV-2.5 MeV electron environment (the "POLE" model). Sicard-Piet, et al. (2008) have merged the LANL data with data from the Japanese Data Relay Test Satellite to cover the range from 1 keV to 5.2 MeV (the "IGE-2006" model).

An initial step in characterizing environments is to consider averages. Ten-min averages of approximately 45 days per spacecraft were estimated from the ATS-5, ATS-6, and SCATHA (experiment SC9) spacecraft. The corresponding averages (see Table 9, Average Parameters from Referenced Spacecraft) and standard deviations (see Table 10, Standard Deviations) for each spacecraft were then estimated. The ions were assumed to be protons in these tables. Note that, in

many cases, the standard deviation exceeded the average. This resulted from the great variability of the geosynchronous environment and illustrates the inherent difficulty of attempting to characterize the “average” plasma environment. (Another way of characterizing the data that avoids some of these problems is to assume that the data are statistically log-normally distributed.) These values are useful, however, in estimating the mean or pre-storm conditions that a spacecraft will experience, as the initial charge state of a spacecraft is important in determining how the vehicle will respond to a significant environmental change. Also, these averages give an approximate idea of how plasma conditions vary over a solar cycle since the ATS-5 data are for 1969-70, the ATS-6 data for 1974-76, and the SCATHA data for 1978.

A second way of considering environments is to look at worst-case situations. In addition to Table 9, several worst-case estimates of the parameters have been made for the geosynchronous environment (see Table 16, Appendix H). These values were derived from fits to actual plasma distributions observed during the several known worst-case ATS-6 and SCATHA charging events. The SCATHA spacecraft instrumentation allowed a breakout of the data into components parallel and perpendicular to the magnetic field and thus permitted a more realistic representation of the actual environment. These values are particularly useful in estimating the extremes in environment that a geosynchronous spacecraft is likely to encounter and are described in Appendix H.

Table 9—Average Parameters from Referenced Spacecraft

ELECTRON PARAMETERS			
PARAMETER	**ATS-5**	**ATS-6**	**SCATHA**
Number density (cm^{-3})	0.80	1.06	1.09
Current density (nA cm^{-2})	0.068	0.096	0.115
Energy density (eV cm^{-3})	1970	3590	3710
Energy flux (eV cm^{-2} s^{-1} sr^{-1})	0.98×10^{12}	2.17×10^{12}	1.99×10^{12}
Number density for population 1 (cm^{-3})	0.578	0.751	0.780
Temperature for population 1 (keV)	0.277	0.460	0.550
Number density for population 2 (cm^{-3})	0.215	0.273	0.310
Temperature for population 2 (keV)	7.04	9.67	8.68
Average temperature (keV)	1.85	2.55	2.49
Root-mean-square temperature (keV)	3.85	6.25	4.83
ION PARAMETERS (ASSUMED TO BE PRIMARILY H^+)			
PARAMETER	**ATS-5**	**ATS-6**	**SCATHA**
Number density (cm^{-3})	1.36	1.26	0.58
Current density (pA cm^{-2})	5.1	3.4	3.3
Energy density (eV cm^{-3})	13,000	12,000	9,440
Energy flux (eV cm^{-2} s^{-1} sr^{-1})	2.6×10^{11}	3.4×10^{11}	2.0×10^{11}
Number density for population 1 (cm^{-3})	0.75	0.93	0.19
Temperature for population 1 (keV)	0.30	0.27	0.80
Number density for population 2 (cm^{-3})	0.61	0.33	0.39
Temperature for population 2 (keV)	14.0	25.0	15.8
Average temperature (keV)	6.8	6.3	11.2
Root-mean-square temperature (keV)	12.0	23.0	14.5

Table 10—Standard Deviations

ELECTRON STANDARD DEVIATIONS			
PARAMETER STANDARD DEVIATION (±)	**ATS-5**	**ATS-6**	**SCATHA**
Number density (cm^{-3})	0.79	1.1	0.89
Current density (nA cm^{-2})	0.088	0.09	0.10
Energy density (eV cm^{-3})	3,100	3,700	3,400
Energy flux (eV cm^{-2} s^{-1} sr^{-1})	1.7×10^{12}	2.6×10^{12}	2.0×10^{12}
Number density for population 1 (cm^{-3})	0.55	0.82	0.70
Temperature for population 1 (keV)	0.17	0.85	0.32
Number density for population 2 (cm^{-3})	0.38	0.34	0.37
Temperature for population 2 (keV)	2.1	3.6	4.0
Average temperature (keV)	2.0	2.0	1.5
Root-mean-square temperature (keV)	3.3	3.5	2.9
ION STANDARD DEVIATIONS (ASSUMED TO BE PRIMARILY H^+)			
PARAMETER STANDARD DEVIATION (±)	**ATS-5**	**ATS-6**	**SCATHA**
Number density (cm^{-3})	0.69	1.7	0.35
Current density (pA cm^{-2})	2.7	1.8	2.1
Energy density (eV cm^{-3})	9,700	9,100	6,820
Energy flux (eV cm^{-2} s^{-1} sr^{-1})	3.5×10^{11}	3.6×10^{11}	1.7×10^{11}
Number density for population 1 (cm^{-3})	0.54	1.78	0.16
Temperature for population 1 (keV)	0.30	0.88	1.0
Number density for population 2 (cm^{-3})	0.33	0.16	0.26
Temperature for population 2 (keV)	5.0	8.5	5.0
Average temperature (keV)	3.6	8.4	4.6
Root-mean-square temperature (keV)	4.8	8.9	5.3

A third quantity of interest in estimating the effects of the space environment on charging is the yearly percentage of occurrence of the plasma parameters. The occurrence frequencies of the temperature and current (see Figure 25, Occurrence Frequencies of Geosynchronous Plasma Parameters [NASA-TP-2361]) were derived by fitting the observed distributions of electron and ion temperature for UCSD instruments on ATS-5, ATS-6, and SCATHA. The figures are useful in estimating the time during the year that a specified environment might be expected.

The fourth and a very important quantity of interest is how the plasma parameters vary with time during a charging event. The approaches determining this quantity range from detailed models simulating the magnetosphere to averages over many geomagnetic storms. For design purposes, we have adopted a simulation of the electron and proton current and temperature that approximates the natural variations in the potential as predicted by charging analysis codes. A time-history sequence suitable for modeling the worst effects of a geomagnetic storm is presented in Figure 26, Suggested Time History for Simulating a Substorm (NASA-TP-2361).

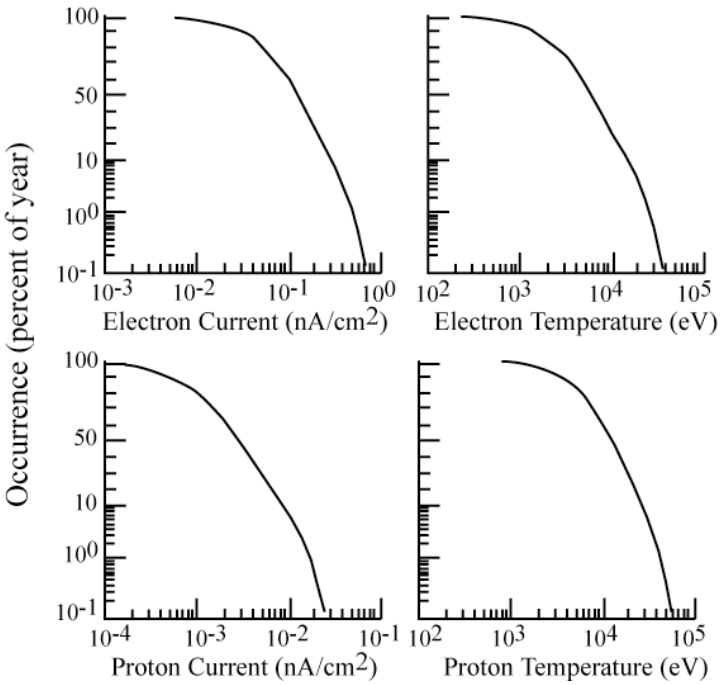

Figure 25—Occurrence Frequencies of Geosynchronous Plasma Parameters (NASA-TP-2361)

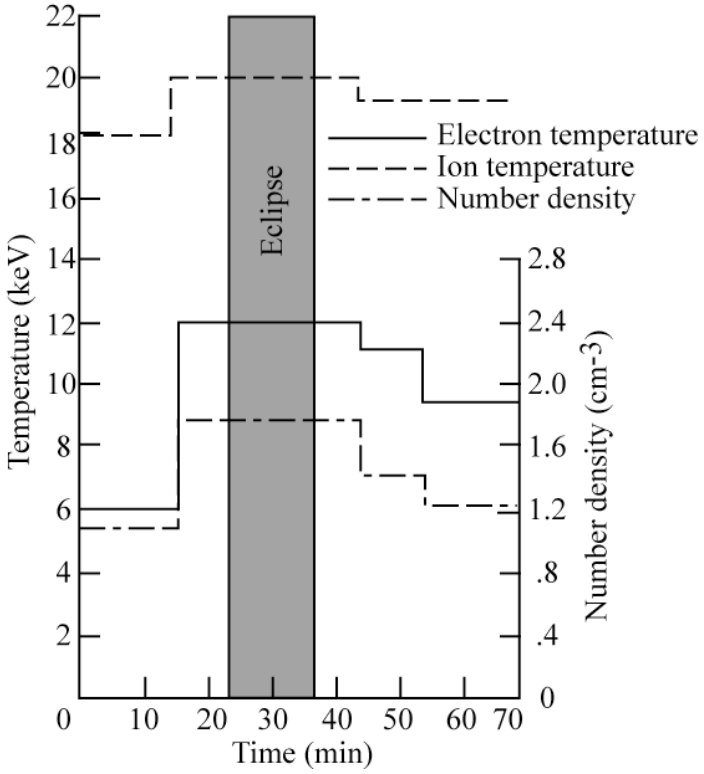

Figure 26—Suggested Time History for Simulating a Substorm (NASA-TP-2361)

A.2.2 Geosynchronous High-Energy Environments

Unlike the plasma environment, the high-energy electron geostationary environment (GEO) is perhaps the most well characterized of Earth orbits because of its importance for communications satellites. Quantitative data for GEO are more readily available than for other orbits. There are, however, a number of characteristics of the environment that need to be considered. These range from variations with longitude to rapid time-dependent variations in the high-energy electron spectra. Each of these is discussed below.

A.2.2.1 Variation with Solar Cycle

The high-energy electron population at GEO has a long-term variation with the solar or, more commonly, the sunspot cycle (about 11 years). The E >2 MeV electron population measured by the geosynchronous GOES-7 satellites and 1.8–3.5 MeV electron measured by LANL are loosely anti-correlated with the sunspot cycle—that is, when the solar sunspot number is low, the E >~2 MeV electron flux is high. This is shown in Figures 27, (a) Average Flux at Geosynchronous Orbit for E >2 MeV Electrons as Measured by the GOES Spacecraft over ~One Solar Cycle (1986-1995) and (b) Average Differential Flux for 1.8–3.5 MeV Electrons Measured by LANL between 1989 and 2018, and 28, Observed Smoothed Sunspot Numbers for (a) 1986-1995 and (b) 1989-2018 (reference Reeves [2020]).

Flying a mission at solar maximum would imply a relatively lower mission (>2 MeV) fluence/dose. Unfortunately, most GEO missions nowadays have durations much longer than 5 years; therefore, for projects with an unknown launch date, the satellite should be designed to withstand the worst of these periods. This can be a problem, as the range between the worst-case conditions and the least stressing is more than 100:1 in energetic electron flux. However, the Sun, which drives these environments, does not strictly obey averages; and even during times when the >2-MeV electron fluxes are usually supposed to be low, the energetic electron fluxes can be extremely high, which is more prominent for recent solar cycles. The project manager, knowing the mission schedule, may wish to assume some risk to save project resources; but the authors advise against such a strategy.

A.2.2.2 Variation with Longitude

The plasma/radiation environment is linked to Earth's magnetic field lines. Magnetic field lines are described in terms of L-values, the distance that a given magnetic field line crosses the magnetic equator in Earth radii (referenced to a dipole magnetic field model). Following a particular field line as it rotates around Earth traces out a surface called an L-shell. As charged particles (electrons, protons, etc.) are trapped to first order on a magnetic field line/L-shell, the radiation flux can be described in terms of the magnetic field strength at the observation point and the L-shell that passes through the point; this is the B-L coordinate system which is often used in modeling radiation belts. Because Earth's magnetic dipole is tilted and offset with respect to the Earth's rotational axis, real Earth B-L values vary in longitude around geosynchronous orbit (see Figure 29, L-Shell Values (Units of Earth Radii) Around Earth's Equator (0° Latitude) versus East Longitude (reference Stassinopoulos [1980]). Because the radiation environment is approximately constant on a particular L-shell at the magnetic equator, there is a change in the radiation environment at different

longitudes as different B-L values are encountered at GEO altitudes. The corresponding fluence and dose variations at GEO are shown in Figure 30, AE8 >0.5 MeV Daily Electron Fluence and CRRESRAD Annual Dose Caused by >1 MeV Electrons Plotted as Functions of Satellite East Longitude at 6.6 Re for the AE8 (>0.5 MeV) and CRRESRAD (>1 MeV) Models (reference Wrenn [1995]).

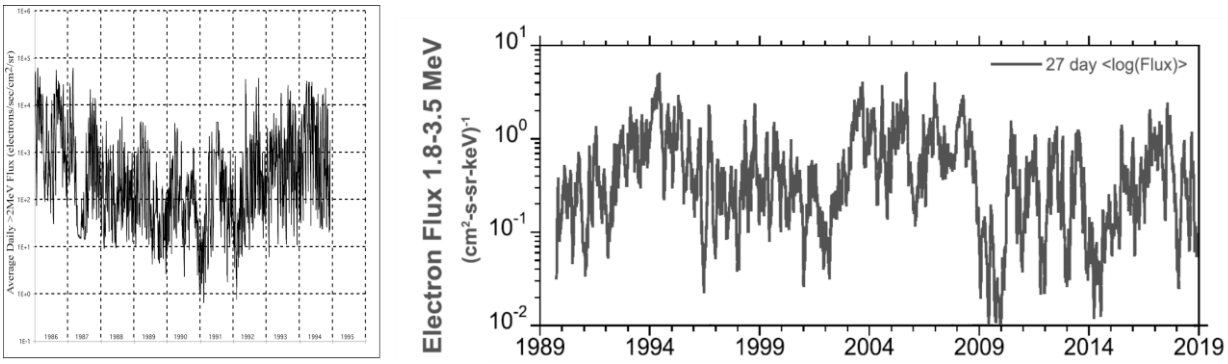

(a) (b)

Figure 27—(a) Average Flux at Geosynchronous Orbit for E >2 MeV Electrons as Measured by the GOES Spacecraft over ~One Solar Cycle (1986-1995) and (b) Average Differential Flux for 1.8–3.5 MeV Electrons Measured by LANL between 1989 and 2018 (Reeves, 2020)

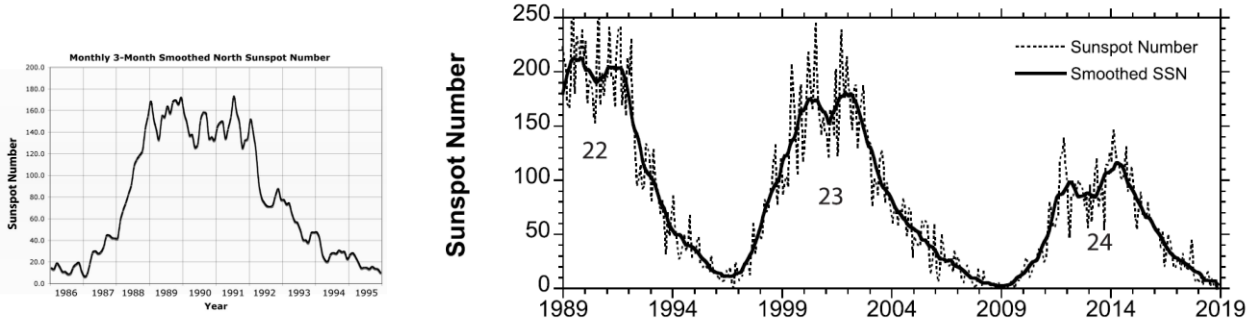

(a) (b)

Figure 28—Observed Smoothed Sunspot Numbers for (a) 1986-1995 and (b) 1989-2018 (Reeves, 2020)

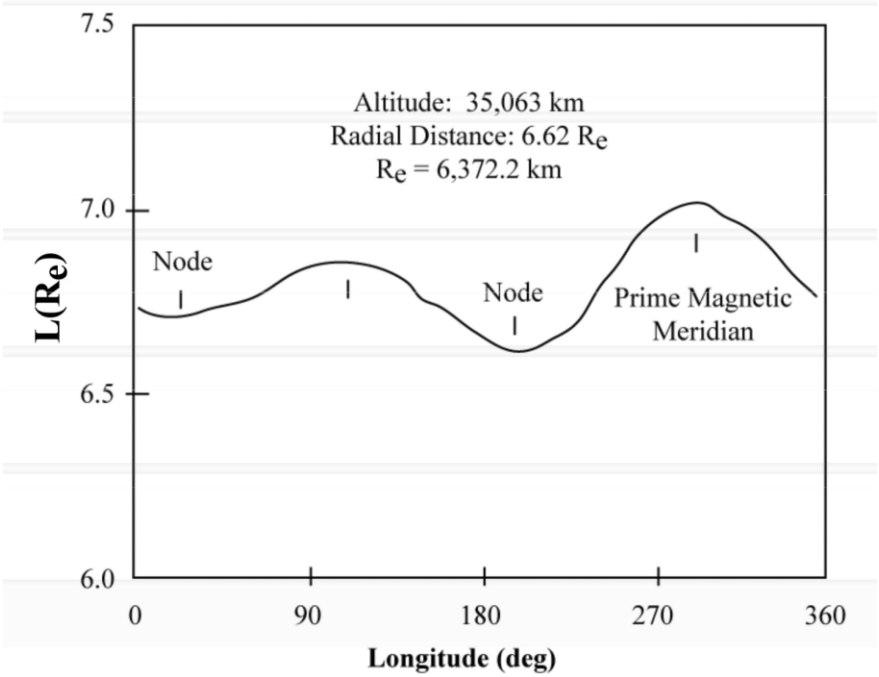

Figure 29—L-Shell Values (Units of Earth Radii) Around Earth's Equator (0° Latitude) versus East Longitude

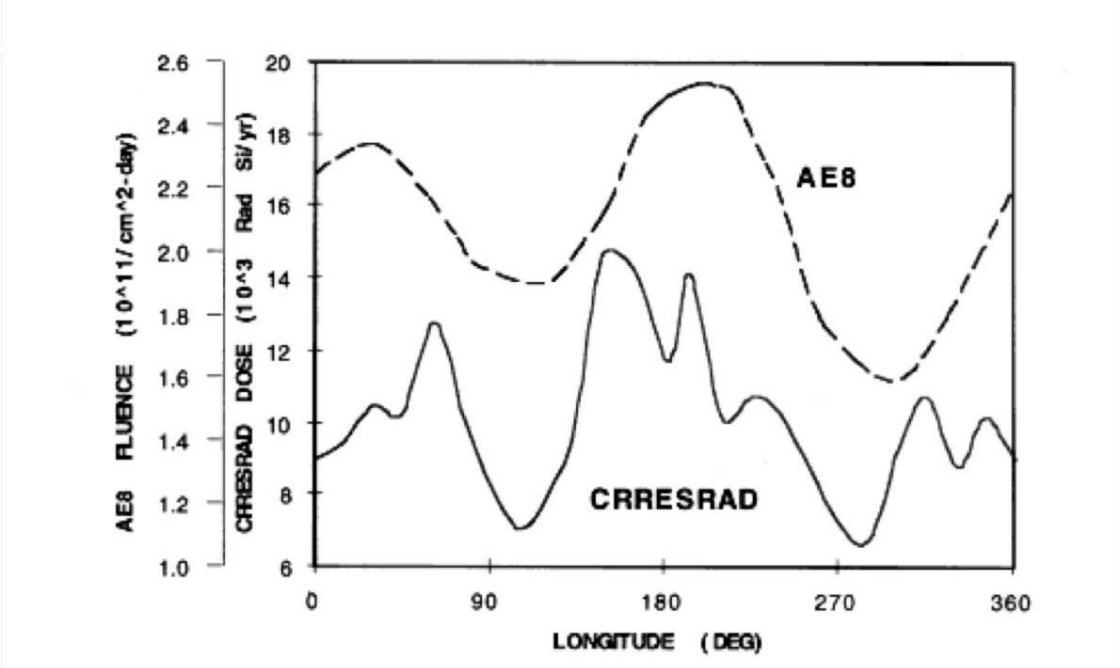

Figure 30—AE8 >0.5 MeV Daily Electron Fluence and CRRESRAD Annual Dose Caused by >1 MeV Electrons Plotted as Functions of Satellite East Longitude at 6.6 Re for the AE8 (>0.5 MeV) and CRRESRAD (>1 MeV) Models

The GEO electron fluences in Figure 30 are for the AE8 model and the dose from electrons for the CRRESRAD model. The figure is shown only to illustrate the average longitudinal variation. The

maximum electron environment should be used for all satellites, even if their longitudinal location is known. (Note that current IRENE/AE9 model does not show any longitude variation.)

A.2.2.3 Variation with Averaging Interval

In addition to long-term solar cycle variations, short-term temporal variations associated with geomagnetic activity and rapid changes in Earth's magnetosphere exist. As a consequence, the average high-energy electron flux varies with the time interval over which the averaging is carried out. This can be seen when a large data set, gathered with a high time resolution, is averaged over increasingly longer integration times. The GOES E >2 MeV electrons are returned with a 5-min resolution. The variation between the daily peak flux determined in a 5-min interval to the peak flux average in a 24-hour period is about 3 to 4 (the 24-hour average peak is, as would be expected, lower). This issue of averaging interval should be kept in mind when comparing different data sets. Analysis of Figure 27 data from Sauer (1996) gives a similar answer (see Figure 31, Cumulative Probability of Occurrence of GOES-7 E >2 MeV Electron Fluxes for Several Different Assumptions). Appropriate averaging time should be determined considering material's RC time constant and spacecraft trajectory (especially for highly elliptical orbit).

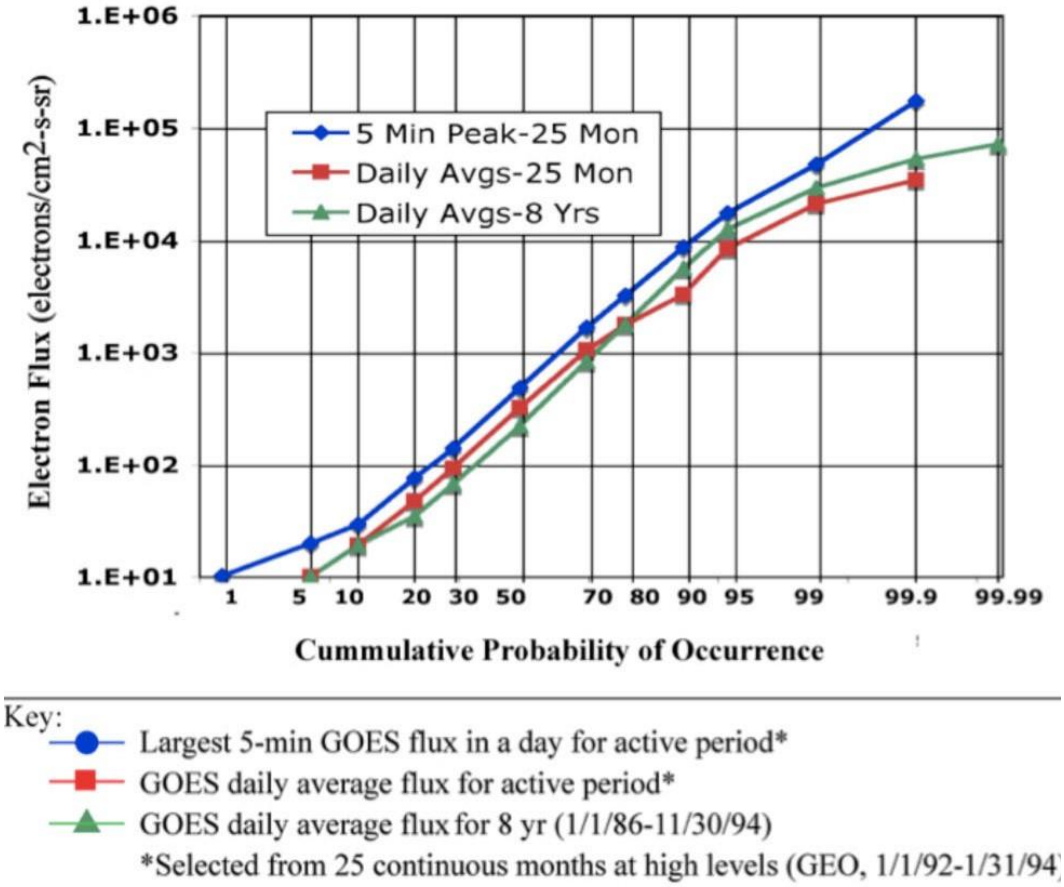

Figure 31—Cumulative Probability of Occurrence of GOES-7 E >2 MeV Electron Fluxes for Several Different Assumptions

A.2.2.4 Variation with Local Time

The high-energy electrons at a given geosynchronous longitude vary daily with local time. On active days, the flux variation is about 10:1 from local noon to local midnight, with the highest flux near local noon. (The NOAA web site, https://www.swpc.noaa.gov/products/goes-electron-flux, shows the current 5-min electron flux at GEO for the last 3-day interval). The normal 24-hour average of the GOES E >2 MeV electron flux (e cm^{-2} s^{-1} sr^{-1}) is about one-third of the peak daily flux (the highest flux in a 5-minute period) in these plots. This variation is less important for internal charging because (1) this variation is averaged out when charging time constant is much longer than 1 day, and (2) the day-by-day variation is larger than this variation when charging time constant is short.

A.2.2.5 Spectrum

The integral electron spectrum varies with time in both shape and amplitude. Figure 9 presents a worst-case high-amplitude energy spectrum from the LANL SOPA detectors averaged over a few hours compared with a spectrum predicted by the AE8 model, which is a long-term average. Data from the AE8 average show a different spectral shape as well as lower amplitudes. That is, the ratio of integral electron flux at 2 MeV to that at 600 keV is generally not the same from day to day. It can be seen that, whereas at low energies (E <100 keV), the curves approach each other, above 1 MeV the spectra rapidly diverge, with the worst-case spectrum approximately 2 orders of magnitude higher than the AE8 spectrum. This large difference between nominal, time-averaged, and short-term worst-case conditions is characteristic of the radiation environment at Earth. The AE8 model, because of its long-term averaging interval (~5 years), is inappropriate for internal charging calculations as the effects typically are on the order of days or less. The effects of radiation-induced conductivity have not been included in the statements above. Radiation-induced conductivity will reduce the internal electric field. The effect may become noticeable at ~2 MeV, but not enough material data are available to make use of that fact.

A.2.2.6 Amplitude Statistics

An excellent set of data for the statistical analysis of the long-term variations in the total electron flux at geosynchronous orbit is that from the NOAA GOES-7. The data are only available for electrons for E >2 MeV, but the measurements are from one detector and available for approximately one complete solar cycle (see Figure 27). Figure 31 plots the cumulative probability of occurrence of GOES-7 electron fluxes. The time span was an 8-year period encompassing the largest energetic fluxes in that solar cycle. Figure 31 shows amplitude statistics for three time intervals from that data set as follows:

a. For the worst 25 months, the day's highest 5-minute average flux.
b. For the worst 25 months, the daily average flux.
c. For the whole 8 years, the daily average flux.

The circles are the peak GOES electron flux data (largest amplitude 5-min value in the day) for times of higher flux (January 1, 1992, through January 31, 1994). The triangles correspond to the cumulative probability for the daily GOES average fluxes over the 8-year span from 1986 to 1994.

The squares correspond to the GOES data for all daily averages from January 1, 1992, through January 31, 1994. All data are from Sauer (1996). The key feature to be noted here is that a Gaussian probability distribution implied by a straight line fit from about 10% to about 95% does not explain the data above the 95th percentile. This makes it difficult to extrapolate with any confidence to a 99.99th percentile environment. The fall-off at the higher percentiles is real (reference Kennel and Petschek, 1966). Thus, the worst environments, although real, are less frequent than a simple Gaussian distribution would imply. The reader is cautioned about trying to use these probabilities for design purposes; use the worst-case energy spectrum of Figure 9.

A.3 OTHER EARTH ENVIRONMENTS

A.3.1 MEO

MEO ranges from roughly 2,000 to 25,000 km altitude with an electron flux peak at ~20,000 km altitude (the inner electron belt). For internal charging, it is the most stressing of the Earth environments. As the GPS, as well as some of the proposed multi-spacecraft communications systems, flies in this orbit, it is a major environment of concern in the study of internal charging phenomena. Figure 32, Schematic of Earth's Radiation Belts as Estimated by the AE8 and AP8 Models; Contours for E >1 MeV Electrons and E >10 MeV Protons for 0° Longitude (adapted from Daly [1988]), is a meridional schematic of Earth's radiation belts at 0° longitude showing the AE8 and AP8 predictions of the electron (E >1 MeV) and proton (E >10 MeV) fluxes. This plot clearly shows the two-belt structure of the electron belts and the horns that extend down to lower altitudes (the poles). It gives a clear picture of the MEO environment and how it is related to orbital characteristics. Each region has a unique spectrum associated with it, which would affect internal charging calculations. It should also be noted that a third electron belt can sometimes appear between the two main belts after severe geomagnetic storms. This belt can last for months before disappearing.

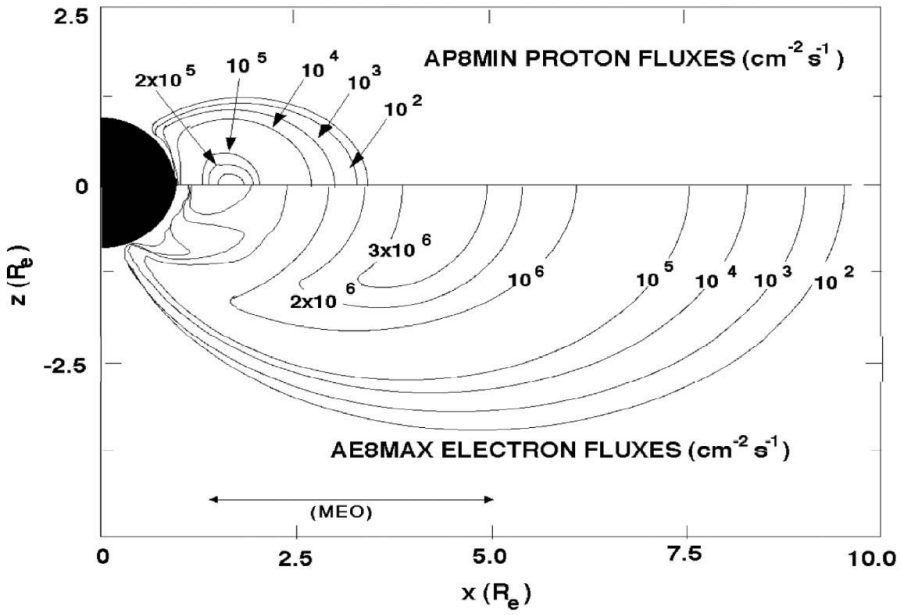

Figure 32—Schematic of Earth's Radiation Belts as Estimated by the AE8 and AP8 Models; Contours for E >1 MeV Electrons and E >10 MeV Protons for 0° Longitude

Note: Figure 32 shows both electron and proton fluxes as referenced to Earth's idealized dipole magnetic coordinates, combined onto one chart. The vertical axis is the magnetic pole axis with vertical units of Earth radii. The horizontal scale is magnetic equatorial distance from the axis in Earth radii. The upper half-chart represents protons; the southern hemisphere proton flux is a mirror image. The electrons (lower half-chart) also are symmetric above and below the magnetic equator in this coordinate system.

A.3.2 Polar Earth Orbit (PEO)

A second important orbital regime is that associated with highly inclined polar orbits. As seen in Figure 32, a polar orbit at low altitudes can pass through the horns of the electron belts and experience a significant, if short duration, flux of high-energy electrons. Many military spacecraft, most imaging spacecraft, and low-altitude communications fleets are in polar orbits. For low-altitude orbits (<1000 km), the risk of internal charging is present but generally much lower than at GEO or MEO. At higher altitudes, the interaction is dependent on the details of the orbit and can be minimized with a proper choice of eccentricity and inclination. Even so, any high-inclination orbit should be evaluated for potential internal charging issues early in the mission design.

PEO passes through aurora zones so that severe surface charging can happen (see Figure 1).

A.3.3 Molniya Orbit

Another common orbit for Russian spacecraft is the so-called Molniya orbit. A Molniya orbit follows an elliptical track with a perigee of 500 km and an apogee of 39,000 km. This orbit is

inclined at 63° and the period is on the order of 12 hr. As a spacecraft spends most of its time at apogee and at an apogee sub-satellite point of 63.4° north, this orbit provides good ground coverage for long periods of time at high latitudes over Russia. In this orbit, satellites traverse a full range of space environments from the higher density, low-energy plasma at LEO through the radiation belts to interplanetary environments. The orbit is also exposed to light and dark so that the satellite is subjected to all environmental variations. Again, the high-energy electron environment should be evaluated for possible internal charging issues for Molniya missions.

A.3.4 Low Earth Orbit (LEO) Aurora Environment used in Figure 1 Calculation

The potentials in Figure 1 are calculated for an aluminum sphere spacecraft in shadow using Nascap-2k following the same methodology used as the previous version of Figure 1 (reference Evans, et al. [1989]). The primary difference between the present version and previous version is the definition of the LEO auroral environment. In the present version of Figure 1, the high energy component (>50 eV) of the auroral environment used in the Nascap-2k simulations came from a Fontheim fit to the modified MIL-STD-1809, Space Environment for USAF Space Vehicles environment developed in Anderson's study (reference Anderson [2012]). To account for the low energy plasma depletion during aurora incidents, the low energy/thermal plasma environment used in the simulations is tuned at two separate altitudes (840 km and 1750 km) to match charging measurements from the DMSP and Freja spacecraft (-2000 V and -3000 V, respectively). The IRI2016 (see Appendix B.1.10) model is used to calculate the thermal plasma density below 2000 km. For the Nascap-2k simulations, the thermal plasma densities below 840 km and above 1750 km are scaled down from the international reference ionosphere (IRI) plasma densities by the factor of 20000 and 5000, respectively. Between 840 km and 1750 km, the two scaling factors are smoothed out using a Fermi function. Above 2000 km, the Chiu model (reference Chiu, et al. [1979]) is used to calculate the electron density and temperature. A separate scaling factor (16000) is used to smooth out the potentials produced by Nascap-2k between the IRI model and the Chiu model.

Figure 33, Example of Nascap-2k Input Aurora Environment, DMSP Aurora Charging Case is Shown, shows the Nasacp-2k input aurora environment for the DMSP altitude (840 km) as an example.

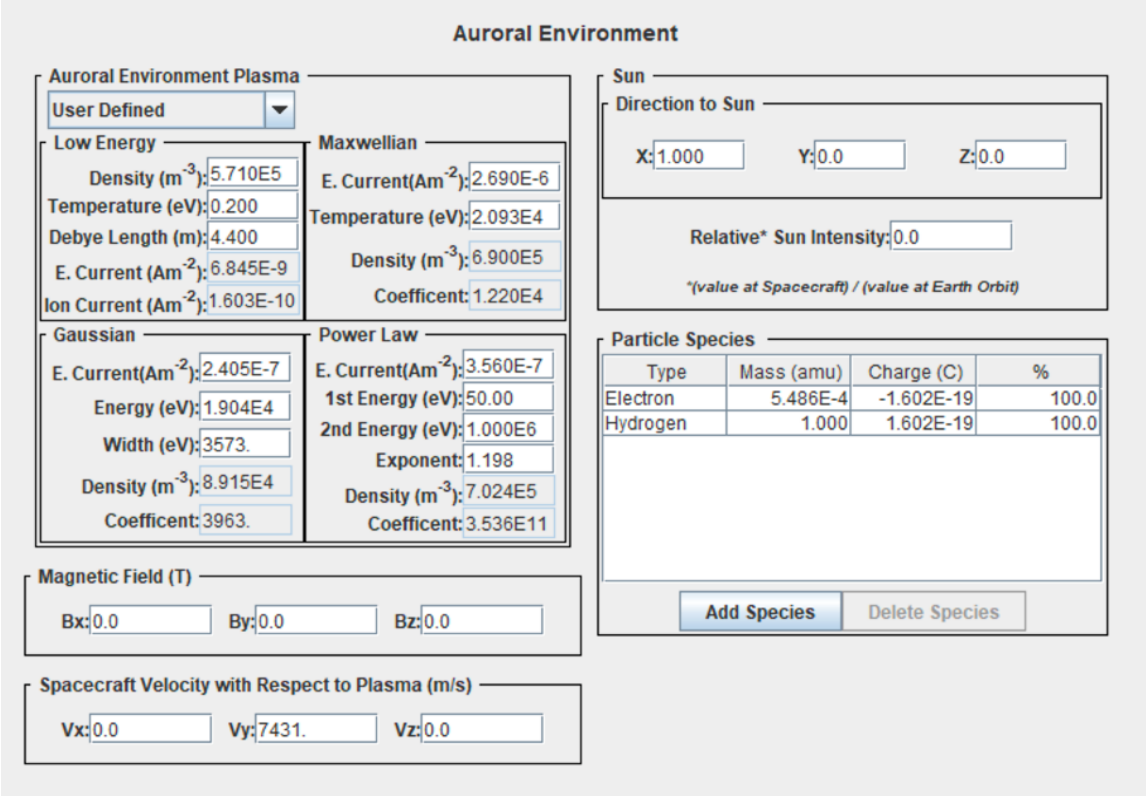

Figure 33—Example of Nascap-2k Input Aurora Environment, DMSP Aurora Charging Case is Shown

A.4 OTHER SPACE ENVIRONMENTS

A.4.1 Solar Wind

Aside from the energetic particle doses from sporadic solar proton events (SPEs) which are not particularly relevant to either surface or internal charging, the solar wind environment is relatively benign for most spacecraft charging applications. The solar wind is a fully ionized, electrically neutral, magnetized plasma that flows outward from the Sun. Table 11, Characteristics of the Solar Wind at 1 AU in the Ecliptic Plane, summarizes many of the characteristics of the solar wind in the ecliptic plane. Perhaps not clear from the table is that the solar wind is highly variable and is coupled to the 11-year solar cycle of activity. Recent years have seen the creation of an interplanetary system of solar wind weather stations designed to closely monitor both solar and solar wind activity, e.g., Ulysses, WIND, Solar and Heliospheric Observatory (SOHO), Yohkoh Observatory, ACE, and the Transition Region and Coronal Explorer (TRACE). One of these, Ulysses, has flown over the poles of the Sun and mapped the solar wind in three dimensions. These spacecraft have identified a variety of characteristic features associated with the solar wind plasma. Of particular interest are the so-called Coronal Mass Ejection (CME) events and the high-speed solar wind streams as these tend to dominate what might be termed extreme conditions. These are illustrated in Figure 34, Solar Wind Parameters for a CME and a High-Speed Stream versus Time as Measured by the Ulysses Spacecraft (reference Garrett and Minow [2007]) and demonstrate the

variability of the solar wind. It has, indeed, proven difficult, if not impossible, to define one or two worst-case solar wind charging environments, given the rich variety of plasma conditions and the potentially unique charging response of any given spacecraft design to those environments.

Table 11—Characteristics of the Solar Wind at 1 AU in the Ecliptic Plane

PROPERTY	MIN	MAX	AVG
Flux (#/cm^2 s)	10^8	10^{10}	2 to 3 x 10^8
Velocity (km/s)	200	2500	400 to 500
Density (#/cm^3)	0.4	80	5 to >10
Temperature (eV)	0.5	100	20
T_{max}/T_{avg}	1.0 (isotropic)	2.5	1.4
Helium Ratio (N_{He}/N_H)	0	0.25	0.05
Flow Direction	±15° from radial		~2° East
Alfven Speed (km/s)	30	150	60
B (nT)	0.25	40	6
B Vector	Polar Component Planar Component		Average in ecliptic plane Average in spiral angle ~45°

Minow, Parker, and their colleagues have carried out an in-depth review of the Ulysses and similar solar wind data. They have generated reference 1-hour averaged spectra for the solar wind electron and proton environments from the Ulysses data in terms of frequency of occurrence percentiles (see Figure 35, 1-Hour Averaged Solar Wind Particle Spectra Based on Measurements Made by the Ulysses Spacecraft for Environments of Various Probability, Minow, et al. [2005]). These spectra can be used to estimate surface and internal charging in the solar wind. As this level of detail is not needed in general for the surface charging studies, Maxwell-Boltzmann distributions can be assumed instead. Representative solar wind parameters under this assumption are tabulated for 1 AU and 0.5 AU in Table 12, Nominal Solar Wind Plasma Environments. (Note: For simplicity, only the core population for the solar wind electrons was considered, while the electron halo population was ignored.) Nominal solar wind properties for these two environments are listed in Table 12.

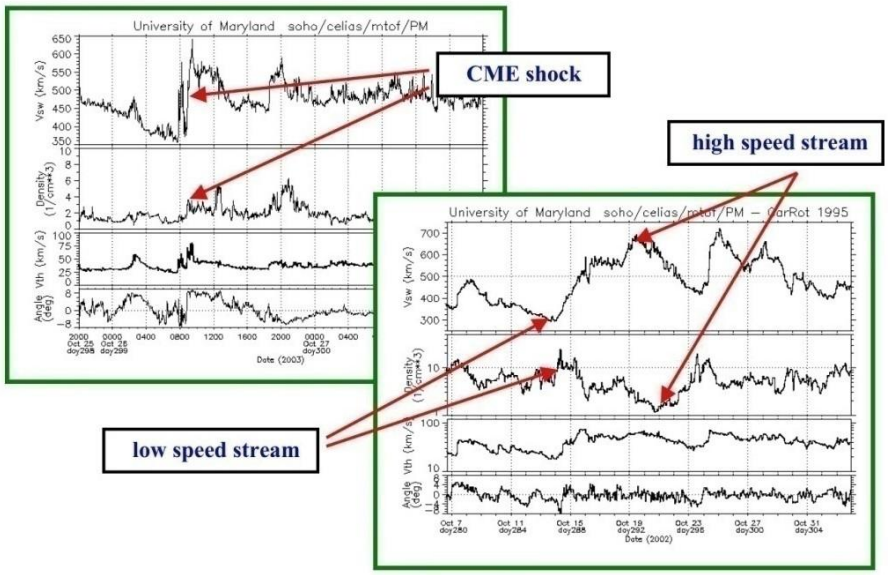

Figure 34—Solar Wind Parameters for a CME and a High-Speed Stream versus Time as Measured by the Ulysses Spacecraft

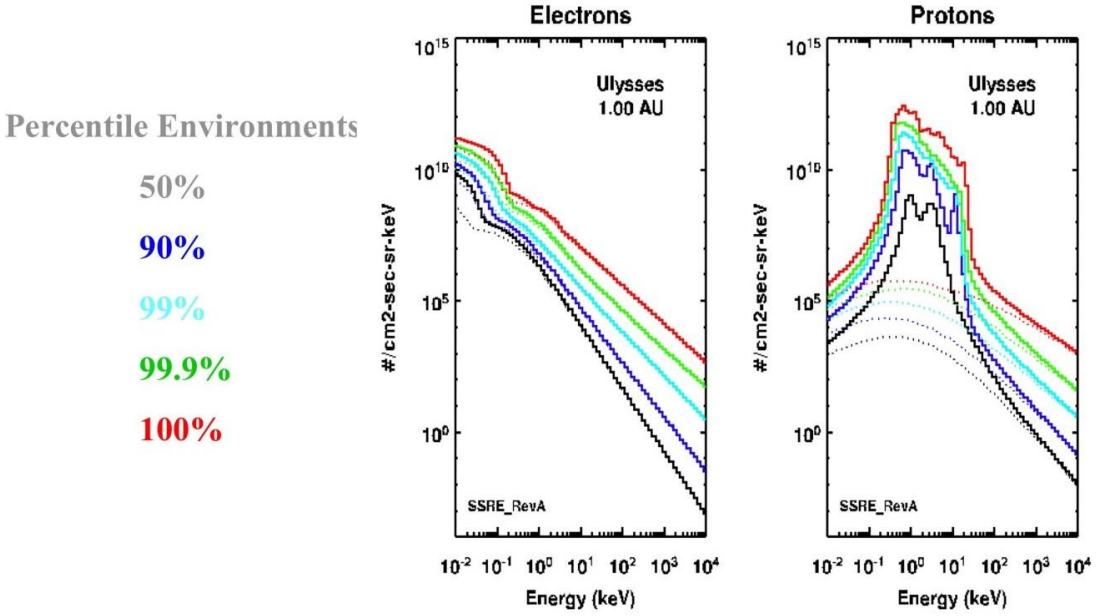

Figure 35— 1-Hour Averaged Solar Wind Particle Spectra Based on Measurements Made by the Ulysses Spacecraft for Environments of Various Probability

The solid lines represent flows from the Sun; dashed lines represent flows toward the Sun. From Minow, et al. (2005).

Table 12—Nominal Solar Wind Plasma Environments

PLASMA ENVIRONMENT	**0.5 AU**	**1.0 AU**
R_E (cm^{-3})	17	12.8
T_E (eV)	10.6	11.13
R_I (cm^{-3})	17	12.8
T_I (eV)	40	10
Photoelectron Current (C_{PH}) (nA/cm^2)	8	2
Spacecraft Velocity (km/s)	702	327
POTENTIALS (estimated)	**0.5 AU**	**1.0 AU**
Shadowed (insulator)	-22	-22.6
Sunlight (conductive)	11.7	7.5

R_E: density for electron plasma population
T_E: temperature for electron plasma population
R_I: density for ion plasma population
T_I: temperature for ion plasma population

A.4.2 Earth, Jupiter, and Saturn Magnetospheres Compared

Table 13, The Magnetospheres of Earth, Jupiter, and Saturn, lists the principal characteristics of the terrestrial, jovian, and saturnian magnetospheres. Jupiter and Saturn are roughly 10 times the size of Earth while their magnetic moments are, respectively, 2×10^4 times and 500 times larger. As the magnetic field at the equator is proportional to the magnetic moment divided by the cube of the radial distance, the terrestrial and saturnian magnetospheres scale similarly in terms of planetary radii. The jovian magnetic field, however, is 20 times proportionally larger. An additional consideration is that the photoelectron flux at 1 AU for the Earth is ~25 times that at Jupiter (~5 AU) and ~100 times that at Saturn (~10 AU).

Table 13—The Magnetospheres of Earth, Jupiter, and Saturn

	REGION/PARAMETER			
PLANET	**Equatorial Radius** (km)	**Magnetic Moment** ($G\ cm^3$)	**Rotation Period** (hr)	**Aphelion/Perihelion** (AU)
Earth	6.38×10^3	8.10×10^{25}	24.0	1.01/0.98
Jupiter	7.14×10^4	1.59×10^{30}	10.0	5.45/4.95
Saturn	6.00×10^4	4.30×10^{28}	10.23	10.06/9.01

The rotation rate is also an important factor. Both Jupiter and Saturn spin over twice as fast as Earth (~10 hr versus 24 hr). Given their strong magnetic fields, this means that the cold plasma trapped in these magnetospheres is forced to co-rotate at velocities much higher than a spacecraft's orbital velocity. This is opposite the situation at Earth where, at low altitudes, a spacecraft orbits at ~8 km/s faster than the ionospheric plasma. Co-rotation velocities can range from 30 to 40 km/s near Jupiter and Saturn to over 100 km/s in their outer magnetospheres. As the magnetosphere is the primary controlling factor for the local plasma environments, the charging environment differs considerably for each of these planets.

The magnetosphere of Jupiter is dominated by the following three factors:

a. The magnetic field tilt (11°) relative to its spin axis.
b. Its rapid rotation.
c. The jovian moon Io at 5 R_j.

Io generates a vast torus of gas. The rapid rotation of Jupiter's magnetic field forces the cold plasma associated with this torus to accelerate and expand by centrifugal force into a giant disc. The magnetic field tilt and rotation rate make this plasma disc move up and down so, at a given location, plasma parameters vary radically over a 10-hour period (or 5 hours in the plasma sheet). Jupiter's environment can be roughly divided into the following three populations:

a. The cold plasma associated with the Io torus and the plasma disc ($0 < E < 1$ keV).
b. The intermediate plasma and aurora (1 keV $< E <$ 100 keV).
c. The radiation environment ($E >$ 100 keV).

The cold plasma environment has high densities (~2000 cm^{-3}) and low energies (1 eV to 1 keV). This plasma consists of hydrogen, oxygen (singly and doubly ionized), sulfur (singly, doubly, and triply ionized), and sodium (singly ionized) ions. The intermediate plasma environment is made up of electrons (~1 keV) and protons (~30 keV) and assumed to vary exponentially from ~5 cm^{-3} for $r <$10 R_j to 0.001 cm^{-3} beyond 40 R_j. Co-rotation velocities vary from ~45 km/s at 4 R_j to ~250 km/s at 20 R_j.

Saturn is marked by a magnificent set of rings that are its most obvious feature and set it apart from all the other planets. Aside from the rings, Saturn’s magnetosphere resembles Jupiter’s—a cold inner plasma disk giving way to a lower density, slightly higher energy plasma disk at large distances. Although there is no Io-equivalent moon in the inner magnetosphere, there is still a fairly dense cold plasma sheet and, at ~20 R_s, Saturn's huge moon Titan contributes a large cloud of neutral gas in the outer magnetosphere. Unlike Jupiter, Saturn's magnetic field axis is apparently closely aligned with the spin axis so that the plasma ring around Saturn is relatively stable compared to that of Jupiter. Plasma co-rotation velocities are similar to those of Jupiter, though maximum velocities tend to peak a little above 100 km/s.

A simple design tool based on current balance and on Earth's, Jupiter's, and Saturn's cold and intermediate plasma environments (the latter also includes the aurora that have been observed at all three planets) has been used to estimate the spacecraft-to-space potentials for these planets. The results of this tool for a spherical spacecraft with aluminum surfaces are presented in Table 14, Representative Charging Levels (Volts) at Earth, Jupiter, and Saturn Based on a Simple Charging Design Tool, for several different plasma regions and situations. Based on this table, Earth clearly represents the worst threat to spacecraft. Negative potentials as high as 20,000 V are predicted near geosynchronous orbit in eclipse; and, indeed, potentials in excess of -20,000 V have apparently been observed. At Jupiter, potentials are more moderate. Large potentials are only observed if secondary emissions can be suppressed, unlikely but possible for some surface configurations. Conditions at Saturn are similar to those at Jupiter, though somewhat lower in general. Even so, spacecraft surface charging is still a concern for spacecraft survivability at these planets. Indeed, as

potentials of even a few tens of volts can seriously affect low-energy plasma measurements, spacecraft charging should be considered for scientific missions to these planets.

Table 14—Representative Charging Levels (Volts) at Earth, Jupiter, and Saturn Based on a Simple Charging Design Tool

REGION	Plasma Convection Velocity V_c (km/s)	POTENTIAL (in Sunlight)	POTENTIAL (no Sun/no secondaries)
Earth			
ionosphere	8	-0.7	-4.4
plasmasphere	3.7	-1.6	-3.8
auroral zone	8	-0.7	-500
geosynchronous	3	2.0	-20,000
Jupiter			
cold torus	44	-0.59	-1.2
hot torus	100	-60	-70
plasma sheet	150	-94	-130
outer magnetosphere	250	9.5	-2,500
Saturn			
inner plasma sheet	40	~5	-30
outer plasma sheet	80	~5	-500
hot outer magnetosphere	100	-100	-500

The high-energy electrons that are part of the radiation environment at each of the three planets are the source of internal charging. In Figure 36, 1 MeV Electron Omnidirectional Flux Contours for Earth, Jupiter, and Saturn, the 1 MeV electron flux contours for Earth (AE8Max model), Jupiter (Galileo Interim Radiation Electron [GIRE3] model, reference de Soria-Santacruz et al. [2016]; Garrett et al. [2017]), and Saturn (Saturn Radiation [SATRAD] model) are presented. In a number of studies (reference Leung, et al. [1986]; Frederickson, et al. [1992]), it has been demonstrated that fluences of 10^{10} electrons/cm^2 are roughly the level required for an IESD. The fluxes in the most intense regions in Figure 36 are on the order of 10^7, 10^8, and 10^6 electrons/cm^2 s for Earth, Jupiter, and Saturn, respectively. (Note: The inner radiation belt at Saturn is largely missing because of Saturn's ring system.) This implies internal charging times for 1 MeV electrons of ~10^3 s, ~10^2 s, and ~10^4 s. Flight experience has shown that the Earth poses moderate to severe IESD problems, Jupiter has severe IESD, and Saturn has not demonstrated any problems to date in agreement with these charging times.

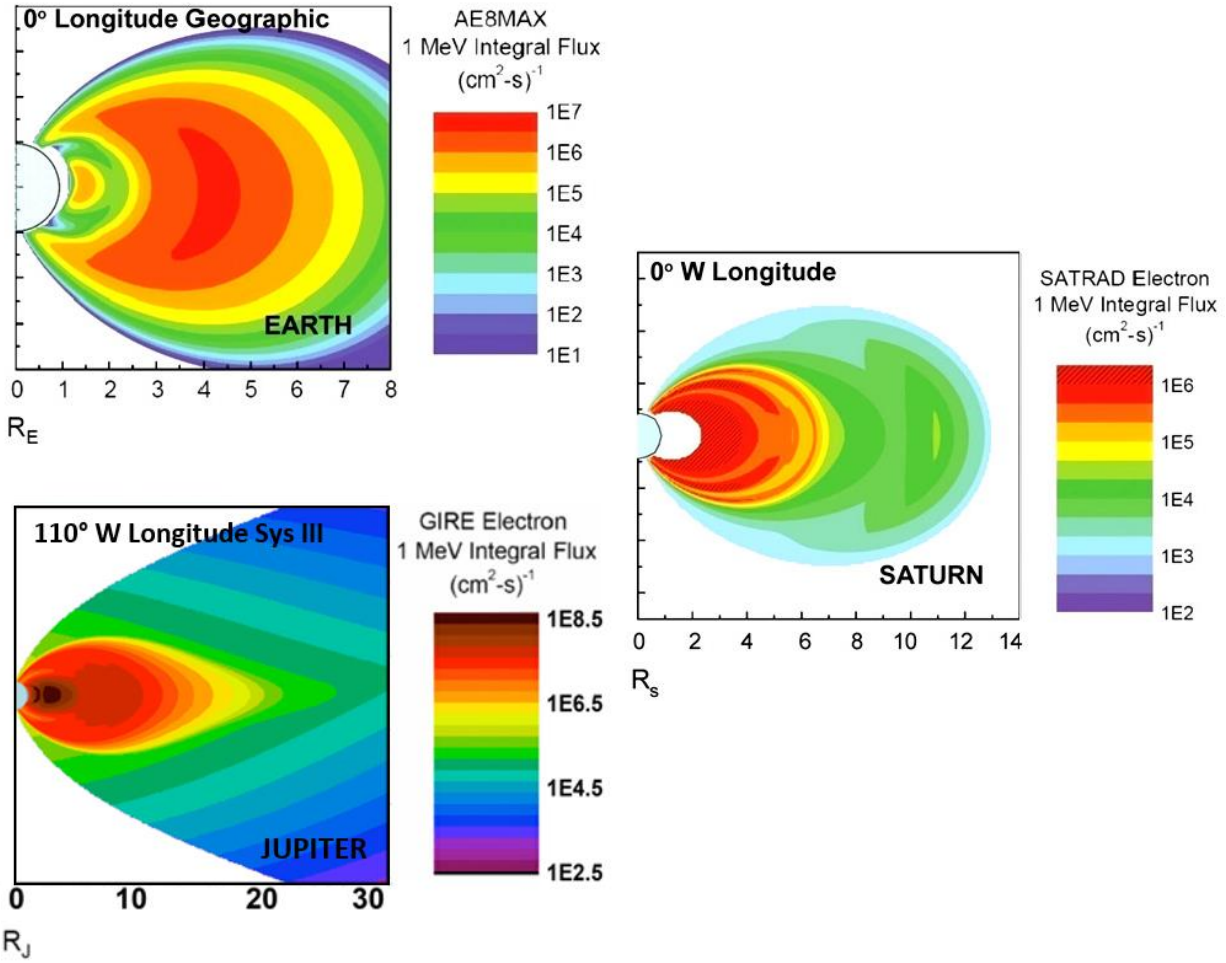

Figure 36—1 MeV Electron Omnidirectional Flux Contours for Earth, Jupiter, and Saturn
(models used: AE8Max, GIRE3, and SATRAD) (courtesy I. Jun, JPL)

APPENDIX B

ENVIRONMENT, ELECTRON TRANSPORT, AND SPACECRAFT CHARGING COMPUTER CODES

B.1 PURPOSE

This Appendix presents environment codes. Codes are listed below in alphabetical order. Note that some codes do both environments and transport but are listed in one place only.

B.1.1 AE8/AP8

The NASA AE8 (electrons) and AP8 (protons) radiation models are the traditional electron and proton models of Earth's radiation environment. The AE8 predictions for GEO are probably the most used estimates of the average environment. In these codes, the fluxes are long-term averages (~5 years or more). There are two versions of each model — AE8 solar minimum and AE8 solar maximum and AP8 solar minimum and AP8 solar maximum. They do not predict the peak electron fluxes that are necessary for the internal charging calculations recommended in this NASA Technical Handbook. Garrett (1999) reviews the output and problems with the AE8/AP8 models. Recently, AE8/AP8 model is getting replaced with IRENE (see section B.1.2 of this NASA Technical Handbook). However, the current version of this NASA Technical Handbook is mainly based on AE8/AP8 because IRENE still has a version-to-version variation and is not independently verified for LEO yet.

B.1.2 AE9/AP9/SPM (IRENE)

The AE9 (0.04-10 MeV e^-), AP9 (0.1 – 400 MeV H^+), and SPM (1 – 40 keV e^-, 1.15 – 164 keV H^+, 1.15 – 164 keV He^+, and 1.15-164 keV O^+) models were developed by the Air Force Research Laboratory and the Aerospace Research Corporation (reference Ginet, et al. [2013]). This model uses multiple datasets to create a statistical description (probability distributions) of the Earth's trapped radiation environment. This is intended to allow users to evaluate the variability in the environment. Users have several options when using this model as the more advanced use cases require significantly more computation time. A static mean (or percentile) run is based on the average (or percentile) of the probability distribution describing the measured data and provides a quick estimate. A perturbed mean (or percentile) run perturbs the distributions based on estimated errors in the measurement data (no time variability). This is done for a user-selectable number of runs that are then used to generate environment percentiles. This is intended for mission integrated quantities such as total ionizing dose, displacement damage, and fluence. SPM only supports this and the static modes of operation in the latest version (1.50.001). Because of this and the lack of local time variation, SPM is not intended to be used for surface charging (which is a transient effect) analysis. Finally, the full Monte Carlo version of the model accounts for both measurement errors and temporal variations in the radiation environment to recreate what may be seen across an ensemble of output runs. Statistics from these runs are intended to be used for transient quantities such as single-event effects and charge deposition for internal charging. It is important to aggregate

the runs correctly to get the desired statistic. Details on how to do this can be found in the AE9/AP9 Third Party Developer Guidance (reference O'Brien [2014]) and the Specification for Radiation Effects Kernels for Use with AE9/AP9 (reference O'Brien [2016]) that is available in the downloaded documentation with the model.

Unlike previous radiation models, it is designed to be an open architecture that allows new data to be ingested to update the model. Sixteen high energy electron data sets which include CRRES, SCATHA, SAMPEX, LANL-GPS, and LANL-GEO were used in version 1.0. These have been later augmented by the MagEIS instrument in version 1.5 of the model and later. Proton data for version 1.0 of the model came from CRRES, S3-3, POLAR, CEASE on TSX-5, and dosimeters on highly elliptical orbit (HEO) and ICO satellites. Proton data from the CEASE instrument on TACSAT-4 were incorporated in version 1.20 of the model and in version 1.50 REPT and RPS data from the Van Allen probes, ESA's Azur data, and the HiLET telescope on TWINS-2 were added.

The most recent publicly available version of the model is version 1.50.001 at the time of this writing while version 1.55.002 is available to U.S. government agencies and their contractors. Public access to the model is provided at: https://www.vdl.afrl.af.mil/programs/ae9ap9/. AE8/AP8 are also included with the download of AE9/AP9/SPM (IRENE).

B.1.3 CRRES

CRRES monitored Earth's radiation belts in an eccentric orbit for 14 months starting in July 1990. The data from the spacecraft are in the form of electron and proton flux and dose-depth curves as functions of time and altitude. Environment codes from CRRES include CRRESRAD (dose versus depth); CRRESPRO (proton flux energy spectrum); and CRRESELE (electron flux energy spectrum). They were available from the Air Force Research Laboratory (AFRL). The CRRES program is now incorporated into the AF-GEOSPACE program under the U.S. Defense Technical Information Center.

B.1.4 Flux Model for Internal Charging (FLUMIC)

FLUMIC, an environments model developed by ESA and part of the Defense Evaluation and Research Agency (DERA) Internal Charging Threat Analysis Tool (DICTAT), is a position-dependent worst-case model of electron fluxes in the outer radiation belt. The FLUMIC is explained in the DICTAT user's manual, http://www.spenvis.oma.be/help/models/dictat.html.

B.1.5 GIRE/SATRAD

The GIRE3, HIC, SATRAD, UMOD, and NMOD radiation environment models are used to estimate the radiation exposure to spacecraft in the out-of-plane radiation environments of Jupiter's, Saturn's, Uranus', and Neptune's magnetospheres, respectively. These models provide estimates of the high energy electron and ion fluxes at each planet. A time-versus-position trajectory is required as input into the codes. They were developed by NASA/JPL where they are maintained. Descriptions of the models are provided by the following documents:

GIRE3 (Galileo Radiation Model):	de Soria-Santacruz et al. [2016]; Garrett et al. [2017]
HIC (Galileo Heavy Ion Radiation Model):	https://trs.jpl.nasa.gov/handle/2014/41934
SATRAD (Saturn Radiation Model):	https://trs.jpl.nasa.gov/handle/2014/40618
UMOD (Uranus Radiation Model):	http://hdl.handle.net/2014/45462
NMOD (Neptune Radiation Model):	https://trs.jpl.nasa.gov/handle/2014/45708

The models can be accessed by contacting the authors of this document at JPL.

B.1.6 Handbook of Geophysics and the Space Environment

The Handbook of Geophysics and the Space Environment (reference Jursa [1985]) is an excellent and highly recommended reference for space environments, including plasma environments for Earth. Even though it was done in 1985, it has not been improved on as a single-source and consistent set of information on the Earth's environment, the solar wind, and the effects of these environments on space systems. It is available as a PDF online or through most library collections or as a used book.

B.1.7 L2 Charged Particle Environment (L2-CPE)

The L2-CPE model is an engineering tool that provides free field charged particle environments for the distant magnetotail, magnetosheath, and solar wind environments. L2-CPE is intended for use in assessing contributions from low-energy radiation environments (~0.1 keV to few MeV) to radiation dose in thin materials used in the construction of spacecraft to be placed in orbit about the Sun-Earth L2 point. Minow, et al. (2007) describes the status of the current version of the L2-CPE model, including the structure of the model used to organize plasma environments into solar wind, magnetosheath, and magnetotail environments, the algorithms used to estimate radiation fluence in sparsely sampled environments, the updated graphical user interface (GUI), and output options for flux and fluence environments. Information on the availability of the model can be obtained from the Natural Environments Branch, MSFC. Other references are Minow, et al. (2000, 2004a, 2005).

B.1.8 MIL-STD-1809, Space Environment for USAF Space Vehicles

Another source of particle estimates is MIL-STD-1809. This includes electron spectra that can be used in the electron transport codes for estimating IESD. It also has broader species information that supplements the focus on electron information in this NASA Technical Handbook. MIL-STD-1809 was published in 1991, and thus the information contained therein has been superseded by newer applicable ESD environment information. Additionally, it was written with a different approach to electron and proton environments: specifically, there are different sections for different Earth-bound mission locations, whereas this NASA Technical Handbook is focused on any satellites that NASA missions may encounter. For Earth-based missions, there are breakouts for various Earth missions based on altitude, orbital inclination, and includes variability ranges of the listed environment. This NASA Technical Handbook is focused on worst-case mission possibilities and basically mentions only ionized electrons and protons.

MIL-STD-1809 is still good as background to better understand fine-tuning if the missions and solar cycle are known in advance. This NASA Technical Handbook would contain only a few more severe environments and cannot achieve (perhaps) cost-saving ideas if a specific mission will not be in those worst-case environments.

Note that LEO Aurora environment used in Figure 1 calculation (A.3.4) is based on MIL-STD-1809.

B.1.9 Geosynchronous Plasma Model

The plasma environment below ~100 keV is required to estimate surface potentials at geosynchronous orbit. To provide this information, data from geosynchronous spacecraft are analyzed to generate models for analytically simulating the parameters necessary to characterize this plasma. As an early example, analytic fits to the electrons and protons was developed in terms of the daily Ap index and local time based on ATS-5 measurements (reference Garrett and DeForest [1979]). The simulation models the simultaneous variations in the warm plasma (50 eV to 50 keV) electron and ion populations during injection events. The model has been extended to include data from ATS-6 and the SCATHA spacecraft. Recently, an extensive data set based on magnetospheric plasma analyzer instruments on several Los Alamos National Laboratory geosynchronous satellites has become available (reference Denton, et al. [2015]). The 82 “satellite years” of data have been analyzed in terms of energy between ~1 eV to ~40 keV, local time, and the 3-hour K_p index. The resulting fits to the data are available in the form of a FORTRAN program from the authors. Such simulations can be employed in a variety of cases where knowledge of the general characteristics of the geosynchronous plasma is necessary.

B.1.10 International Reference Ionosphere (IRI)

The IRI is an empirical standard model of the ionosphere, updated yearly based on the following data sources: the worldwide network of ionosondes, the powerful incoherent scatter radars (Jicamarca, Arecibo, Millstone Hill, Malvern, St. Santin), the ISIS and Alouette topside sounders, and in situ instruments flown on many satellites and rockets. More information on the model and the model itself can be found at http://irimodel.org/.

B.1.11 Others

Alternate sources of space radiation data include Severn Communications Corporation, 1023 Benfield Boulevard, Millersville, MD, 21108 (including AP8 and AE8). Use their Web site to find various environmental papers published by their staff. As described in more detail in Appendix B.2.9 in this NASA Technical Handbook, the Space Environment Information System (SPENVIS) provides an on-line space environment “handbook” at http://www.spenvis.oma.be.

B.2 TRANSPORT CODES

Note that some codes do both environments and transport but are listed in one place only.

B.2.1 Cosmic Ray Effects on MicroElectronics 1996 (CREME96)

CREME96 is a web-based suite of tools hosted at https://creme.isde.vanderbilt.edu/. It includes models of the environment and allows simple transport/shielding calculations. It incorporates analysis capabilities for the following:

a. Creating numerical models of the ionizing radiation environment in near-Earth orbits for all the naturally occurring nuclei, from protons (atomic number Z = 1) to uranium (Z = 92):

(1) Galactic cosmic rays (GCRs).
(2) Anomalous cosmic rays (ACRs).
(3) Solar energetic particles (SEPs).
(4) Geomagnetically trapped particles.

b. Evaluating the resulting radiation effects on electronic systems in spacecraft and in high-altitude aircraft primarily for single-event effects (SEE):

(1) The software contains routines for calculating SEE rates as a function of spacecraft shielding and the external space radiation environment.
(2) Inputs include device characteristics and heavy-ion/proton ground test data.

c. Estimating the linear energy transfer (LET) radiation environment within manned spacecraft.

The TRANS module of the suite is limited to 1D and aluminum shielding.

Because CREME96 does not include electrons, it has limited applicability to spacecraft charging.

B.2.2 EGS

EGS is a Monte Carlo transport code. The suite is used primarily for electron beam experiment simulations. It is easy to use and incorporates validated physics models but is limited in geometry modeling and the space environments included. EGS is currently maintained as two versions, EGSnrc and EGS5. EGSnrc is maintained by the Ionizing Radiation Standards Group, Measurement Science and Standards, National Research Council of Canada at https://nrc.canada.ca/en/research-development/products-services/software-applications/egsnrc-software-tool-model-radiation-transport. EGS5 is maintained by KEK at http://rcwww.kek.jp/research/egs/egs5.html. Recent improvements may have added to its capabilities. Nelson, et al. (1985), Bielajew, et al. (1994), and Halbleib, et al. (1994) contain additional information.

B.2.3 Geant4

Geant4 is the European counterpart to Monte Carlo N-Particle (MCNP6). The Geant family of particle transport codes represents a unique international cooperative effort to model radiation

interactions. Many different groups and organizations have contributed specialized analytic components to the basic package. Geant4 is a collection of computer tools for the simulation of the passage of particles through matter. Its areas of application include high-energy, nuclear, and accelerator physics, as well as studies in medical and space science. The two main reference papers for Geant4 are published in Nuclear Instruments and Methods in Physics Research (reference Agostinelli, et al. [2003] and Allison, et al. [2016]); and Institute of Electrical and Electronics Engineers (IEEE) Transactions on Nuclear Science (reference Allison, et al. [2006]). The code and its derivatives make up probably the most sophisticated (and thus complex) modeling package currently available as it covers a much wider range of problems than space radiation effects. As such, it has a steep learning curve. There are special courses and seminars available for learning its many features. The homepage for Geant4 can be found at http://geant4.web.cern.ch/geant4/.

B.2.4 Integrated TIGER Series (ITS)

The ITS code provides electron flux and deposition and has been validated by experiment. It would be the first choice for the electron deposition calculations suggested in this NASA Technical Handbook. Some packages have been simplified to handle simple geometries such as cylinders and slabs. Contact: Radiation Shielding Information Computational Center (RSICC), Oak Ridge National Laboratory, Building 6025, MS 6362, P.O. Box 2008, Oak Ridge, TN 37831-6362 (ITS CCC-467). One Web page source is https://rsicc.ornl.gov/codes/ccc/ccc7/ccc-792.html. Another is http://prod-ng.sandia.gov/techlib-noauth/access-control.cgi/2008/083331.pdf.

ITS6.0 is a suite of four radiation transport codes which employs a Monte Carlo (mostly forward) technique. The four codes are as follows:

a. TIGER (1D)
b. CYLTRAN (2D)
c. ACCEPT (3D)
d. CAD (3D).

The codes handle electrons and photons.

B.2.5 MCNP

MCNP5 and MCNPX were unified into one package, MCNP6. MCNP6 is a three-dimensional general-purpose Monte Carlo N-Particle code that can model transport of many particle types. MCNP6 can be used to calculate electron flux, charge deposition rate, and energy deposition rate in complex geometries. MCNP6 has limited 3D geometry import (from computer-aided design [CAD]) capability; geometries are typically built by defining cells bounded by surfaces and combining those cells using Boolean operations.

The 3D capabilities of MCNP6 make it versatile and particularly useful for modeling complex geometries. The more detailed modeling capabilities allow for less conservative calculations than those made with 1D codes such as TIGER in ITS. The cost of using the more detailed software is increased problem set up and run time.

More information on MCNP can be found at: https://mcnp.lanl.gov/.

B.2.6 NOVICE

NOVICE is a neutral and charged-particle radiation transport code. It uses an adjoint Monte Carlo technique to model particle fluxes inside a user-specified 3D shield geometry in particular. NOVICE uses an inside-out particle tracking algorithm. The code handles electrons, photons, protons, neutrons, and heavy ions ($Z \geq 2$). It can handle fairly complex geometries and is fast as well as easier to use than full Monte Carlo simulation tools (MCNP6 and Geant4); however, it does not account for secondary particles due to nuclear interactions. This source may also have codes for electron deposition calculations, which needs to be verified with full Monte Carlo simulations such as ITS (1D), MCNP6 (3D), and Geant4 (3D). (See Jordan [1987-1998].)

B.2.7 FASTRAD

FASTRAD is an interactive 3D tool where a complex spacecraft model can be easily imported or built from basic geometries. Depending on the application, different modes can run to perform the radiation calculation through the specified materials and geometry. The options include ray-tracing, reverse Monte Carlo, and forward Monte Carlo methodologies. No nuclear interactions are included in the simulations (no high-Z); only the transport of protons and electrons is taken into account (reference Beutier, et al. [2003] and Pourrouquet, et al. [2016]). Recently, an internal charging simulation is being added.

B.2.8 SHIELDOSE

SHIELDOSE is a charged-particle radiation transport code that calculates the dose inside slab and spherical shield geometries. It also computes dose absorbed in small volumes of some detector materials under specified aluminum shield geometries. See Seltzer (1980) or Rodgers, et al. (2004). It is available as a part of SPENVIS. Using approximate dose-to-flux conversion factors, quick estimates of the corresponding electron flux inside the simple shield model can be obtained. See Appendix C.4.1 in this NASA Technical Handbook.

B.2.9 SPENVIS

This collection of computer models includes a number of environmental and interaction tools for estimating effects on spacecraft. Of particular interest is the DICTAT tool which is designed for spacecraft internal charging analysis and is available for use on the Web at https://www.spenvis.oma.be/ and https://www.spenvis.oma.be/help/background/charging/dictat/dictatman.html.

SPENVIS also has two surface charging calculation tools for simplified geometry, EQUIPOT and SOLARC. EQUIPOT calculates the equilibrium surface potential, which yields net zero current, for a simple geometry (a small isolated patch of material on a spherical spacecraft). SOLARC

simulates the current collection, voltage distribution, and material erosion on solar array for a simple solar array and spacecraft configuration.

SPENVIS includes tools designed for near-Earth and jovian analyses. It generates either a spacecraft trajectory or a coordinate matrix for input into the various tools. In addition to the DICTAT model (see Appendix B.3.6 in this NASA Technical Handbook), it incorporates analysis capabilities for the following:

a. Geomagnetic coordinates.
b. Trapped proton and electron fluxes and solar proton fluences.
c. Radiation doses (ionizing and non-ionizing) for simple geometries.
d. Sectoring analysis for dose calculations in more complex geometries.
e. Damage equivalent fluences for Si, GaAs, and multi-junction solar cells.
f. Geant4 Monte Carlo analysis for doses and pulse height rates in planar and spherical shields.
g. Ion LET and flux spectra and SEU rates.
h. Trapped proton flux anisotropy.
i. Atmospheric and ionospheric densities and temperatures.
j. Atomic oxygen erosion depths.
k. Spacecraft surface charging (EQUIPOT and SOLARC).
l. Meteoroid and debris environments.
m. A set of European Cooperation on Space Standardization (ECSS) space environment standard.
n. GIRE, the jovian radiation model.

B.2.10 TRIM

TRIM is a radiation transport code that employs a Monte Carlo (forward) technique. It is 1D and accommodates protons and heavy ions. It is used for proton and heavy ion beam simulation and covers the entire spectrum of heavy ion types. It is limited to 1D slab geometry, however, and only incorporates coulomb interactions. Also, because it does not include electrons, it has limited applicability to spacecraft charging.

B.2.11 Summary

The preceding transport codes are intended to be used in estimating internal charge deposition—a major step in estimating the probability of IESD. Table 15, Properties of the Major Transport Codes, provides a comparison of some IESD charging-specific parameters for the major analysis codes. Whereas codes like the TIGER, Geant4, and MCNP6 allow estimates of the flux (and fluence) with depth in the material, the DICTAT and NUMIT codes estimate the buildup of the fields in the material.

Table 15—Properties of the Major Transport Codes

CODE NAME	CALCULATES ELECTRON DEPOSITION?	USABLE FOR IESD?	RECOMMENDED FOR IESD CALCULATION?	CALCULATES E-FIELD?	USES RIC OR CONDUCTIVITY?
DICTAT	Y	Y	Y	Y	Y
EGS	Y	Y	N	N	N
Geant4	Y	Y	N	N	N
ITS	Y	Y	N	N	N
MCNP6	Y	Y	N	N	N
NUMIT	Y	Y	Y	Y	Y

B.3 CHARGING CODES

These codes generally calculate surface charging, potentials, E-fields, and other parameters that are of interest for an overall view of spacecraft charging. Look for one or more that best meet the needs of the project.

B.3.1 Multi-Utility Spacecraft Charging Analysis Tool (MUSCAT)

MUSCAT is a Japanese computer code that predicts potentials, with function similar to the NASA Charging Analyzer Program (NASCAP) (reference Muranaka, et al. [2008] and Hosoda, et al. [2008]). MUSCAT was developed for use for LEO, PEO, and GEO environments using parallelized commercial base workstations. MUSCAT has a GUI for spacecraft modeling and executing the calculation and visualization of the calculation results, thereby allowing spacecraft engineers to easily confirm the analysis result. The first operational version was released in 2009. To shorten the computation time, the computer code used with MUSCAT is a hybrid of the Particle-In-Cell (PIC) and Particle Tracking (PT) methods. MUSCAT Space Engineering Co., Ltd. (MUSE) (http://astro-muse.com) sells MUSCAT software and provides related support. Currently, services are domestically provided.

B.3.2 Nascap-2k and NASCAP Family of Charging Codes

Nascap-2k (reference Mandell, et al. [2006] and Davis, et al. [2003]) is a widely used interactive toolkit for studying plasma interactions with realistic spacecraft in three dimensions. It can model interactions that occur in tenuous (e.g., GEO orbit or interplanetary missions) and in dense (e.g., LEO orbit and the aurora) plasma environments. Capabilities include surface charging in geosynchronous and interplanetary orbits, sheath and wake structure and current collection in LEO, and auroral charging. External potential structure and particle trajectories are computed using a finite element method on a nested grid structure and may be visualized within the Nascap-2k interface. Space charge can be treated either analytically, self-consistently with particle trajectories, or consistent with imported plume densities. PIC capabilities are available to study dynamic plasma effects.

Material properties of surfaces are included in the surface charging computations. By locating severe surface voltage gradients in a particular design, it is possible to show where discharges could

occur. The effect of changes in the surface materials or coatings in those areas on minimizing voltage gradients can then be evaluated.

Nascap-2k is a successor code to NASCAP for Geosynchronous Orbit (NASCAP/GEO), NASCAP for Low-Earth Orbit (NASCAP/LEO), Potential of Large Objects in the Auroral Region (POLAR), and Dynamic Plasma Analysis Code (DynaPAC). NASCAP/GEO has been the standard 3D tool for the computation of spacecraft charging in tenuous plasmas since 1980. In the following two decades, the fully 3D computer codes NASCAP/LEO, POLAR, and DynaPAC were developed to address various other spacecraft-plasma interactions issues. Nascap-2k incorporates almost all the physical and numeric models of these earlier codes. Nascap-2k has been upgraded to work with (1) the extreme jovian environments (extreme magnetic field and extreme spacecraft velocity) and (2) environments including multiple Kappa distributions as well as Maxwell-Boltzmann distributions.

Nascap-2k is available on request to United States citizens only; a Web reference with access and other material is https://software.nasa.gov/software/MFS-32056-1.

B.3.3 Spacecraft Plasma Interaction System (SPIS)

SPIS, for Spacecraft Plasma Interaction Software, is a rich and advanced 3D modeling tool for the spacecraft-plasma interactions, able to model a large set of phenomena relative to spacecraft charging. SPIS includes an advanced 3D electrostatic plasma solver based on an unstructured mesh and able to dynamically model detailed sheath structures around complex and realistic geometries. There are versions for surface charging analysis (SPIS-SC) and internal charging analysis (SPIS-IC). SPIS became the de facto European reference tool for spacecraft charging analysis. Further information is available at: http://www.spis.org/software/spis.

B.3.4 NUMIT

NUMIT, originally developed by A. R. Frederickson, is a 1D computer code for estimating internal charging in dielectrics. It computes the full-time dependent current, voltages, and electric fields in the dielectric by iteratively solving a set of equations for mono-energetic electrons normally incident on one side of a dielectric. The current version, NUMIT 2.0 (reference Kim, et al. [2012]) has wider energy range (10 keV – 20 MeV) and now accepts time-varying spectrum of incident electrons.

B.3.5 3-Dimentional IESD Code, including 3D NUMIT

Few 3D internal charging tools have been developed or are being developed. 3D NUMIT is one of the well-established 3D IESD codes. 3D NUMIT is a technique for estimating internal charging in dielectrics in 3D. The original formulation of the technique used MCNP6 to calculate charge and energy deposition rates, and COMSOL finite element analysis software to model electric field development. In general, any radiation transport code that can calculate charge deposition rate can be used instead of MCNP6, and any finite element analysis tool that can accept charge deposition and dose rates as a function of position and solve for electric field can be used instead of COMSOL. See Kim, et al. [2017] for more detail.

B.3.6 DICTAT

DICTAT is a 1D internal charging computer code similar to NUMIT. DICTAT (reference Sorenson, et al. [2000]) calculates the electron current that passes through a conductive shield and becomes deposited inside a dielectric. From the deposited charge, the maximum electric field within the dielectric is calculated. This field is compared with the breakdown field for that dielectric to see if the material is at risk of an ESD. DICTAT is available through the SPENVIS Web site.

APPENDIX C

INTERNAL CHARGING ANALYSES

C.1 PURPOSE

This Appendix describes the physics and analysis of internal charging, whereas Appendix F addresses surface charging.

C.1.1 The Physics of Dielectric Charging

As stated earlier, the computations involved in estimating dielectric charging resemble surface charging calculations with the inclusion of space charge. That is, the basic problem is the calculation of the electric field and charge density in a self-consistent fashion over the volume of interest. In other words, Gauss's law is solved subject to the continuity equation. The relevant formulas are Gauss's law (in one dimension):

$$\frac{\partial(\varepsilon(x)E(x,t))}{\partial x} = \rho(x,t) \qquad \text{(Eq. 31)}$$

and the continuity equation (in one dimension):

$$\frac{\partial\rho(x,t)}{\partial t} = -\frac{\partial(J_c(x,t) + J_R(x,t))}{\partial x} \qquad \text{(Eq. 32)}$$

and Ohm's law (for electrons):

$$J_c(x,t) = \sigma(x,t)E(x,t) \qquad \text{(Eq. 33)}$$

These can be combined to give:

$$\frac{\partial(\varepsilon(x)E(x,t))}{\partial t} + \sigma(x,t)E(x,t) = -J_R(x,t) \qquad \text{(Eq. 34)}$$

where:

E = electric field at x for time t (V/m)
ρ = charge density at x for time t (C/m^3)
σ = conductivity in (ohm m)$^{-1}$ = σ_o + σ_r
σ_o = dark conductivity (ohm m)$^{-1}$
σ_r = radiation-induced conductivity (ohm m)$^{-1}$
ε = ε_o ε_r (F/m)
ε_o = free-space permittivity = 8.8542 x 10^{-12} F/m
ε_r = dielectric constant (unitless)

J_R = incident particle flux (current density in A/m^2) where $-\partial J_R/\partial x$ is charge deposition rate at x

J_c = particle flux (current density in A/m^2) due to conductivity at x

This equation follows from Gauss's law and current continuity with the total current consisting of the incident current J_R (primary and secondary particles) and a conduction current σE. It is solved at a given time t to give the charge variations in x in the dielectric. The results are then stepped forward in time to compute the time-varying charge density and electric field.

A simple solution for this equation assuming σ and J_R are independent of time for a dielectric between two metal plates with an initial imposed field is:

$$E = E_0 \exp\left(-\frac{\sigma t}{\varepsilon}\right) - \left(\frac{J_R}{\sigma}\right)\left[1 - \exp\left(-\frac{\sigma t}{\varepsilon}\right)\right] \quad \text{(Eq. 35)}$$

where:

E_o = imposed electric field at t=0 (V/m)

This is only a crude approximation to reality as geometrical effects, time variations in the conductivity and incident current, and other effects make numerical solution a necessity. It is, however, useful in understanding the time constants ($\tau = \varepsilon/\sigma$) involved in charging the dielectric—as time increases, the initial field E_o dies away tending toward the radiation-induced field given by J_R/σ with a time constant of τ and $\sigma = \sigma_o + \sigma_r$. Where the dose rate is high (enhancing the radiation-induced conductivity σ_r), the E field comes to equilibrium rapidly. In lightly irradiated regions where the time constant is long (the dark conductivity σ_o dominates), the field takes a long time to reach equilibrium.

The peak electric field (E_{max}) in the irradiated dielectric has been estimated by Frederickson, et al. (1986) for radiation with a broad energy distribution to be:

$$E_{max} = (A/k) / (1 + \sigma_o/k\dot{D}) \sim (A/k) \quad \text{(Eq. 36)}$$

where:

A = 3.84 x 10^{-8} s V/ohm rad m^2 (or C/rad m^2)

k = coefficient of radiation-induced conductivity in s/m ohm rad

$\dot{D}$ = average dose rate in rad/s

The second approximation follows for high flux conditions (reference Frederickson, et al. [1986]) when the radiation conductivity σ_r can be approximated by:

$$\sigma_r \sim k \dot{D}^{\Delta} \quad \text{(Eq. 37)}$$

where:

σ_r > σ_o for high fluxes
Δ ~ 1

The equation is in agreement with analytic solutions when they exist and, for some configurations, more complex numerical solutions. Typical values of k are $10^{-16} < k < 10^{-14}$ for polymers at ambient temperature (reference Frederickson, et al. [1986]). Inserting the range of values for k, E_{max} varies up to 10^6 to 10^8 V/m, respectively, the range where breakdowns are expected.

This simple analysis demonstrates several important concepts. First, by charging a dielectric surface and measuring how long it takes for the charge to bleed off (in the absence of RIC), one can estimate σ_o from $\sigma_o = \varepsilon/\tau$, where τ is measured by the experiment. In the presence of radiation, the foregoing demonstrates how the charge can be bled off by the RIC, σ_r. The equations imply that σ_r is proportional to dose rate. Ultimately, these equations can be used to estimate whether the potential will build up sufficiently in a dielectric to cause arcing—the key issue of concern here. Note, however, that both Δ and the k are temperature dependent, resulting in much lower σ_r at colder temperatures. Unfortunately, there are very little test data available in the literature to define those parameters (reference Gillespie, 2013). An analysis that demonstrates safety from arcing at ambient temperature does not guarantee safety at colder temperatures.

C.2 SIMPLE INTERNAL CHARGING ANALYSIS

The following example of a simple and conservative analysis (see Figure 37, Simple Charging Example) will be used to estimate the current flux deposited in a dielectric of a spacecraft at GEO. This method of analysis has matched a TIGER internal charging analysis to within 40% or better; it provides a good start to determine if there is a level of concern. If the simple analysis indicates that the flux is close to the design limit, then a complete analysis should be used to determine if the criteria is exceeded. In fact, if the simple analysis shows a level of concern, the region in question should probably have its design changed, if possible, or otherwise protected from internal charging. The example determines the flux of electrons into a 10-mil thick layer of Teflon® under a 10-mil thick sheet of aluminum. Figure 5 provides a mean penetration depth versus energy, and Figure 9 presents fluxes versus energy. Tables 7 and 8 list material densities.

In this example, the electron charge/flux entering and exiting each layer is calculated; the difference is the electron flux deposited in that layer. For dielectrics, if the deposited current in the layer is >0.2 pA/cm^2, that is considered as a potential concern and a more exact analysis should be done. The assumed electron environment is the worst-case GEO environment as shown in Figure 9. In Figure 5, 10 mil of aluminum require 250 keV energy electrons to penetrate the aluminum and enter the Teflon®. Teflon® density is 78% of aluminum (see Table 8); therefore, 10 mil of Teflon® is equivalent to 7.8 mil of aluminum. Electrons with greater than 300 keV can penetrate through the

17.8-mil aluminum equivalent and exit the sandwich. Referring to Figure 9, the worst-case flux entering the Teflon® is about 6 x 10^6 e/cm^2 s sr while the exiting flux is about 4.5 x 10^6 e/cm^2 s sr, leaving a net flux rate of accumulation of 1.5 x 10^6 e/cm^2 s sr in the Teflon®. Equivalent normally incident flux is one-fourth of the omnidirectional flux. For this simple example covered by 10 mil of aluminum, it is taken to be a factor of π times the flux per solid angle. Converting to current requires multiplying by 1.602 x 10^{-19} A s/e. The net (approximate) result is that the charging rate in the 10-mil layer of Teflon® is 0.75 pA/cm^2.

Electron Flux	Penetration Energy (Range)	Exiting Integral Flux
(1) Into 10 mil of aluminum	~250 keV	6 x 10^6 e/cm^2 s sr
(2) Through 10 mil of Teflon® (equivalent to 7.8 mil of aluminum, total 17.8 mil)	~300 keV	4.5 x 10^6 e/cm^2 s sr

(3) The net electron flux in the Teflon® is:

$$j1 = 6 - 4.5 \times 10^6 \text{ e/cm}^2 \text{ s sr} = 1.5 \times 10^6 \text{ e/cm}^2 \text{ s sr}$$

(4) Convert to normal incidence flux:

$$j2 = \pi\, j1 = \sim 3 \times 1.5 \times 10^6 \text{ e/cm}^2 \text{ s} = 4.5 \times 10^6 \text{ e/cm}^2 \text{ s}$$

(5) Convert flux to current in the Teflon®:

$$I = 1.602 \times 10^{-19} \times 4.5 \times 10^6 = 0.72 \text{ pA/cm}^2$$

Figure 37—Simple Charging Example

According to Figure 8 and section 5.2.3.2.2 in this NASA Technical Handbook, the charging rate in this Teflon® sample exceeds the safe level of 0.1 pA/cm^2. Therefore, this sample is threatened by occasional discharges. More than 10 mil of aluminum shielding equivalent are required on top of this sample to reduce the charging rate in the Teflon® layer to below 0.1 pA/cm^2.

Note: The analysis in this section uses deposited flux of 0.1 pA/cm^2 as a criterion rather than incident flux of 0.1 pA/cm^2 as used in the rest of this NASA Technical Handbook. This is less conservative than the incident flux criterion. A flux of 0.1 pA/cm^2 in 10 hr accumulates 2 x 10^{14} e/m^2 in 10 hr, which will create an electric field of 2 x 10^6 V/m (ε_r =2) if all electrons stop in the material in accordance with the criterion used in this paragraph—assuming an incident flux of 0.1 pA/cm^2 is more conservative because not all electrons will be stopped in the material. The latter assumption is the better one unless the dielectric strength of the material in question is known to be high as in this example for Teflon®. See Bodeau (2010) which challenges the 10-hour accumulation time for highly resistive materials. The proper criterion for if discharges will happen is the breakdown threshold field rather than the critical flux. The electric field is calculated from the deposited flux and the proper charging time (Eq. 3).

C.3 DETAILED ANALYSIS

A proper analysis should be performed using the models and tools listed in Appendices A and B to determine charge deposition rates (fluxes and fluences). The analysis should determine if sufficient charge exists for breakdown (ESDs).

Detailed formulations, e.g., NUMIT and DICTAT, have been developed for determining the development of electric fields in irradiated insulators. In the end, for good insulators at high fluxes, the electric field builds up to and stabilizes at 10^5 and rarely to 10^6 V/cm (10^7-10^8 V/m).

The conductivity of the material is a critical parameter to assess breakdown fields and generally is not well known enough to provide meaningful calculations. For proper answers, one should know the conductivity under the expected irradiation, in-orbit operating temperature, and after exposure to vacuum, to perform a meaningful detailed analysis. Even then, predicting pulse amplitudes and rates is only an approximation.

As a matter of comparison, a computer code was used to replicate the previous simple example. The results were that the deposited electron flux in the Teflon® was computed to be about 40% of the result from the simple analysis. This shows that, for the test case, the simple analysis was conservative by a factor of 2.5. Although shown to be conservative as calculated for the case shown in Appendix C.2 of this NASA Technical Handbook, the simple analysis should always be treated with some suspicion.

Note: TIGER calculations have demonstrated that tantalum (a commonly used material for spot shields) backscatters some electrons at the surface, and thus the simple calculations above will lead to higher deposited electron flux than in the actual case (our one example had double the flux of the TIGER-calculated case). Other physics effects may also be present. Fortunately, this phenomenon is not significant for aluminum. The level of effect for copper and silver will be intermediate between aluminum and tantalum.

C.4 SPACECRAFT LEVEL ANALYSIS

A spacecraft level of analysis is used to predict the current density (flux) within the spacecraft interior. It can use radiation analysis tools modified as required to accomplish the task. Conventional radiation analyses inside a spacecraft use transport codes to carry out 3D tracking of energetic particles through the spacecraft walls to a specific target. The output of these codes is the radiation dose as a function of the detector material (usually Si). Several computer codes that use electron spectra and spacecraft geometry as inputs can also be used to determine internal fluxes or radiation dose at specific sites (see Appendix B). This is first done with only the walls and shelves in place. Once the isoflux contours are determined, the flux levels are compared to the critical flux level. If the predicted levels exceed the critical levels, then a box-level analysis is conducted. If the flux level inside the box still exceeds the critical flux level, then additional shielding or changes in placement to enhance shielding should be considered.

The criterion to be used for IESD is that the current (flux) should be less than 0.1 pA/cm^2 for any period of 10 hours. If this criterion is satisfied, there should be few problems with internal charging.

C.4.1 Dose-to-Fluence Approximation

To determine an approximate electron flux/fluence from a radiation transport code, a simple equivalence from dose (rad-Si) to electron fluence can be used if the dose has been already calculated or if it is easier to calculate dose. Dose and fluence are related by the equation (reference Wenaas, et al. [1979]); SD 71-770, The Effects of Radiation on the Outer Planets Grand Tour):

$$\text{Fluence (e/cm}^2) = 2.4 \times 10^7 \times \text{Dose (rad-Si)} \qquad \text{(Eq. 38)}$$

Although the actual conversion factor varies with energy, this equation is valid for electron energies from ~0.2 to 30 MeV. This is adequate for most internal charging assessments based on typical space environments and can be used for lower energies without loss of "back-of-the-envelope" accuracy already inherent in this method.

As the results from this simple conversion are typically conservative (it predicts greater electron fluence than actually exists), its use would lead to a conservative design and hence greater cost. Coakley (1987), for example, says that a 416 krad dose is equivalent to 2 x 10^{13} e/cm^2 fluence, or fluence (e/cm^2) = 5 x 10^7 x dose (rad-Si). This is within a factor of two of Eq. 38. Also, DICTAT uses fluence (e/cm^2) = 3.3 x 10^7 x dose (rad-Si).

APPENDIX D

TEST METHODS

D.1 PURPOSE

This Appendix highlights various test methods for charging assessment.

Tests that can be performed to validate some aspects of charging problems are described conceptually below. The focus here is largely on materials with limited descriptions of component, subsystem, and system tests. Details such as test levels, test conditions, instrumentation ranges, bakeout time, sample size, pass/fail criteria, etc., should be considered for any tests. Vacuum bakeout/aging of materials before testing is important because electrical properties, especially resistivity, quite often increase with aging in space as adsorbed water and other conductive contaminants depart because of outgassing.

D.2 ELECTRON BEAM ESD TESTS

Electron beam test facilities are to be used to test smaller elements of the spacecraft. This test can be used to determine whether a material sample or a part will arc in a given electron environment and can measure the size and rate of the resultant ESD, if any. Electron beam tests have the advantage that they are real: the electrons can be accelerated to energies that will penetrate and deposit charge more or less to the depth desired by the experimenter. They have the disadvantage that the beam is usually mono-energetic rather than a spectrum—the electrons initially will be deposited in a diffuse layer dependent on their energy, rather than distributed throughout the exposed material. Usually, the illuminated area is less than 10^3 cm^2 in size. The real area may not be testable, in which case scaling should be applied to the measured results to estimate the real threat. A typical test configuration in a vacuum chamber is shown in Figure 38, Typical Electron Beam Test Facility Setup.

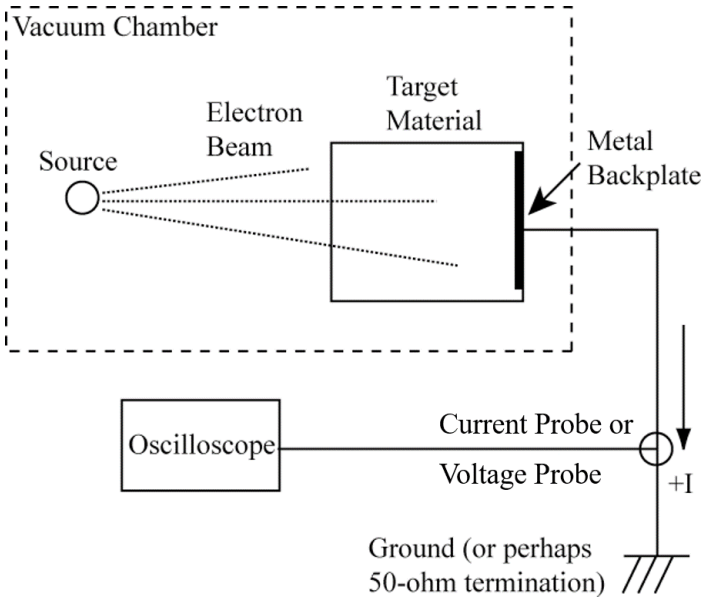

Figure 38—Typical Electron Beam Test Facility Setup

The electron source should have both the requisite energy (usually expressed in keV or MeV) and the requisite flux (expressed as a current density (pA/cm^2), or flux (e/cm^2 s)). (Note: 1 pA/cm^2 = 6.242 x 10^6 e/cm^2 s). The target material in Figure 38 shows a grounded backplate which may be ground through a termination (resistor). Some tests may involve a front metal plate, grounded, grounded through a load (e.g., 50 ohm), or ungrounded, to simulate the in-flight hardware more closely. In this example, the electrons, after deposition on or in the target material, may leak off to the backplate, or they may remain in the material if its resistivity is high. If they do not leak off to the backplate (harmlessly) fast enough, they continue accumulating until the electric field exceeds the dielectric strength of the material and an ESD occurs.

A current probe and oscilloscope are used to determine the current waveform of the ESD from the material. If a breakdown from the material to the metal backplate or to the other conductors in the vacuum chamber occurs, the current probe can measure the direct discharge current or the image charge movement of the backplate. From the waveform, the peak current, the pulse width, the slew rate (dI/dt), and the charge are calculated. If there is a 50-ohm termination or some other termination to mimic actual impedance, the voltage waveform can be measured through current and/or voltage probes and the power and energy in the discharge estimated. The frequency domain spectrum can be calculated through Fourier transform of the current (or voltage) pulse.

The best way to test a dielectric for IESD is to use an electron beam that penetrates to the middle of the thickness. First, dry the sample in vacuum (drying for a month is best; however, this may be accelerated via baking), then irradiate at 1 to 10 nA/cm^2 for several hours and monitor all conductors. A sample that does not arc after this test will be excellent in space.

Other diagnostics can be included such as a Rogowski coil to measure electrons blown off the front surface of the material to “space” (the chamber walls) or RF field sensors (EMC antennas and receivers) to measure the RF frequency spectrum of the radiated noise.

D.3 DIELECTRIC STRENGTH/BREAKDOWN VOLTAGE

This number can be used for ESD analyses to determine if the ESD can happen and/or to estimate the magnitude of the ESD. Usually, the dielectric strength (breakdown voltage) of a (dielectric) material is available in the published literature. Be aware that published breakdown voltages mean different things depending on the source such as the average breakdown voltage, the Weibull 63.2% likelihood breakdown voltage, or the breakdown inception voltage. For a large sample population, the cumulative fraction of events at or below a field $\boldsymbol{F}$ can approximate the probability of occurrence $\boldsymbol{F}$ using the three-parameter Weibull distribution, as shown in Eq. 39:

$$\boldsymbol{P(F) = 1 - \exp\left(-\left[\frac{F-F_s}{F_0-F_s}\right]^{\beta}\right)} \qquad \text{(Eq. 39)}$$

where, $\boldsymbol{F_0}$ is the characteristic field corresponding to a 63.2% probability of breakdown, $\boldsymbol{\beta}$ is the shape parameter, and $\boldsymbol{F_s}$ is the threshold breakdown field (reference Dissado and Fothergill [1992] and Chauvet and Laurent [1993]). Due to limited data or lack of apparent threshold breakdown field, the Weibull distribution is usually reduced to two parameters by setting $\boldsymbol{F_s}$ to zero. Other extreme value distributions have been used to estimate likelihoods of breakdowns based on experimental data; however, the Weibull distribution is the most prevalent. These analyses are typically presented with statistical confidence intervals. Typically, it is not explicitly stated on a materials data sheet or even test report what metric was used. For spacecraft charging applications, the most relevant measure is the breakdown inception voltage, i.e., the minimum voltage at which breakdown will occur in a material. Despite the fact that dc breakdown has been studied for decades, there is not yet a generally accepted physics-based theoretical model. The extensive structural disorder of most dielectrics together with underlying quantum mechanical effects preclude theoretical calculations of breakdown with exact solutions. Care should be taken when using empirical or statistical models to extrapolate experimental breakdown data. Even approximate models grounded in physics can alert one to extrapolations that may not be physically reasonable. Physics-based models such as those proposed by Crine (1989 and 2016) and Andersen, et al. (2015 and 2018) can cautiously be used to estimate breakdown strength beyond what can reasonably be verified by limited accelerated testing. Dielectric strength tests can be performed as illustrated in Figure 39, Testing for Breakdown Voltage. ASTM D3755, Standard Test Method for Dielectric Breakdown Voltage and Dielectric Strength of Solid Electrical Insulating Materials under Direct-Voltage Stress, is a standard test method for breakdown voltage. However, this standard was not designed for spacecraft applications and needs to be modified to be well-suited for space as it is sensitive to false positives, false negatives, and large uncertainties (reference Andersen [2018]). By design, such punch-through breakdown tests neglect partial discharge events which are more relevant for spacecraft charging (reference Frederickson, et al. [1986]). ASTM D3755 should be modified by testing in vacuum at appropriate temperature with continuous leakage current monitoring or other partial discharge detection rather than relying only on a current sensing element such as a breaker or fuse (reference Andersen, et al. [2015, 2017, 2018]). Normal precautions are to use mechanically sound and clean samples of the material under test. Generally, for any materials involved in internal charging studies, it is appropriate to have a vacuum bakeout to remove the adsorbed water and other contaminants and also test in a vacuum for best results. The test is

intended to measure the applied voltage until breakdown with a sufficient wait time. The result is the dielectric strength, which is often reported as V/mil of thickness. The result should also report the tested thickness: V/mil at thickness d.

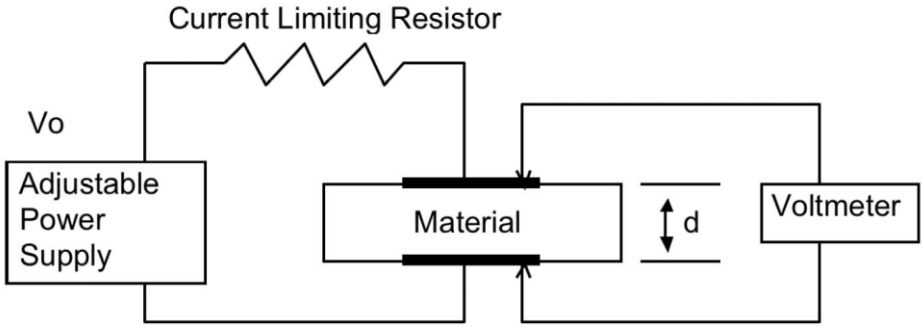

Figure 39—Testing for Breakdown Voltage

D.4 RESISTIVITY/CONDUCTIVITY DETERMINATION

Most space charging concerns relate to reducing the electric fields in and outside of materials. The design approach is to have conductive bleed paths from charge-capturing and storing materials to nearby conductive materials with differing potentials. The environments that cause the charging and the critical numeric values of electric fields of concern are discussed elsewhere in this NASA Technical Handbook. Calculating the resistances (resistivity/conductivity) of materials is the subject of this section.

There are two resistivities that are pertinent to the calculations: a bulk/volume resistivity and a resistivity called “surface resistivity.”

Volume conductivity and resistivity are reciprocals of each other. Rho (ρ, ohm m) = 1/sigma (σ, siemens per meter (S/m), mho/m, or 1/ohm m). The volume resistivity of a material is a useful parameter for internal charging assessments. Volume resistivity refers to the bulk resistance of a volume of material. Volume resistivity is determined in terms of the equations supporting Figure 40, Testing for Volume Resistivity. Material volume resistivity found in existing tables or the manufacturer’s data is typically a guaranteed lower bound and limited to $\leq 10^{15}$ ohm m. Note that these tabulated values are done in ambient condition at room temperatures with limited dwell time. All these factors tend to underestimate volume resistivity for spacecraft applications, often by many orders of magnitude (reference Dennison, et al. [2006] and Dekany, et al. [2013]). Volume resistivity can be measured in one of several ways as described in the following paragraphs. ASTM D257, Standard Test Methods for DC Resistance or Conductance of Insulating Materials, is a standard test method for dc resistance or conductance. For highly resistive materials, the dwell/wait time to reach equilibrium should be much longer than 60 seconds described in ASTM D257 as given in Appendix D.8 of this NASA Technical Handbook.

Figure 40 shows the concept of resistivity. The resistance from end to end of the 3D block of material is as follows:

$$R = \rho \times l/(h \times w) \quad \text{(Eq. 40)}$$

where:

R	=	resistance of the sample as measured from end to end (ohm)
ρ	=	volume resistivity (ohm m in SI units); sometimes called ρ_v (rho sub v)
l	=	length of sample (m)
w	=	width of sample (m)
h	=	height of sample (m)

therefore:

$$\rho = R \times (h \times w)/l \quad \text{(Eq. 41)}$$

Conductivity (σ) is the reciprocal of resistivity:

$$\sigma = 1/\rho \text{ (S/m or 1/ ohm m)} \quad \text{(Eq. 42)}$$

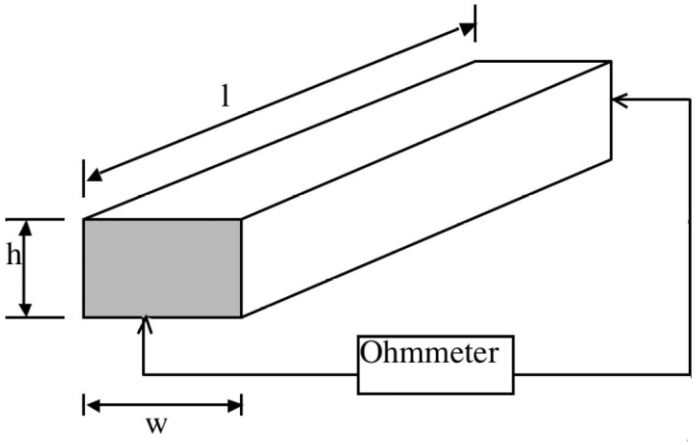

Figure 40—Testing for Volume Resistivity

There is another resistivity, surface resistivity, which is applicable to thin layers of material or surface coatings. Surface resistivity, ρ_s (rho sub s) is the resistance of a flat 2D square piece of material as measured from one edge to an opposite edge. It may also refer to a surface layer of conductivity on an insulator, which, if the surface has been contaminated by handling or processing, may differ significantly from the bulk resistivity. The resistance of a 2D surface measured in this manner will be:

$$R = \rho_s \times l/w \quad \text{(Eq. 43)}$$

where:

R	=	resistance of the sample as measured from end to end (ohm)
ρ_s	=	surface resistivity (properly “ohm” but often called “ohm per square”)
l	=	length of sample, with ground connections at the ends (m)
w	=	width of sample (m)

For a thin layer of homogeneous material without any surface contamination (absorption or adsorption), the bulk and surface resistivities have the following relation:

$$\rho = \rho_s \times h$$

For a square sample sheet (length equals width), it can be seen that the resistance from edge to edge will be the same value regardless of the size, so surface resistivity is often called “ohm per square,” although the proper unit is simply “ohm.”

Note that these equations only apply to homogenous materials. Non-homogeneous materials, such as conductively loaded insulators do not follow linear dimensional scaling rule. The resistivity (conductivity) changes abruptly at near percolation threshold.

D.5 SIMPLE VOLUME RESISTIVITY MEASUREMENT

Various difficulties occur when measuring high resistivities, such as higher resistance than can be measured by the ohmmeter, resistivity as a function of voltage stress, resistivity as a function of temperature (generally, more resistive when colder), resistivity modifications related to presence of absorbed moisture or surface contaminants, and surface resistivity leakage rather than current flow through the bulk of the material. Commercially available test devices, such as (1) the Hewlett-Packard Model 4329A high-resistance meter when used in conjunction with a Model 16008A Resistivity Cell (Hewlett-Packard Operating and Service Manual, 1983), or (2) the Keithley 6517B Electrometer in conjunction with Keithley 8009 Fixture, can account for some of these problems. That instrument combination can measure very high resistances, has several user-defined test voltages, and has guard rings to prevent surface leakage effects from contaminating the results. The person doing the test should still clean the contaminants on surface and bake out the test sample to get rid of moisture-caused conductivity. Testing versus temperature is important for cold situations (on the outside of the spacecraft) because resistance is significantly higher at cold space temperatures. For resistances above 10^{11} ohm, moisture bakeout and vacuum tests are necessary because moisture adsorption increases conductivity. Also, it may take time for vacuum to remove moisture or volatile contaminants as will occur during a space mission.

Measurements of resistivity that apply voltage to dielectrics using electrodes in direct contact with the sample will be dominated by the most conductive paths through the material. In homogenous materials, this may not be a significant effect. However, in materials that are a composite of conductive and insulative materials (e.g., carbon-loaded polymers), contact resistivity measurement methods may show resistivities low enough to avoid ESD but in fact exhibit ESD under an electron beam test. Contact measurements of resistivity determine how conductive a conductive network in a composite material can be. Hence, the contact resistivity measurements are not adequate proof that charging and discharging will not occur in orbit.

Exposure to radiation may increase conductivity (called RIC). That is, materials may have more conductivity than measured in a ground environment. The quantitative details of this phenomenon are too involved for this NASA Technical Handbook but in general should not be assumed to be significant help in the IESD situation (reference Gillespie [2013]).

D.6 ELECTRON BEAM RESISTIVITY TEST METHOD

This method has the advantage in that it measures the material in a vacuum and in response to an electron beam applying the voltage stress. With a metal front and backplate or only on backplate (or none at all), an electron beam is directed onto the front surface of a flat sample of the material as in Figure 41, Electron Beam Test for Resistivity. A non-contacting voltage probe is used to measure the potential on the front surface of the material. A picoammeter then measures the current flowing from the back surface to ground (reference Dennison, et al. [2006] and Dekany, et al. [2013]). The volume resistivity is calculated in the manner of Figure 40. Shielding is needed to avoid stray electron false data. In this method, the picoammeter readings will be dominated by the most conductive regions in a material while the peak front-surface potential readings will be dominated by the least conductive regions in a material. For the non-uniform materials, dividing front-surface voltage by picoammeter current mixes the characteristics of the two regions and therefore fails to characterize either properly. The proper resistance of the insulator parts of the composite should be established by monitoring the rate of voltage decay over time (from non-contacting voltage probe) that defines the electrical decay time constants and resistivity (see Appendix D.7 of this NASA Technical Handbook). Note that a composite that prevents ESD under an electron beam and appears to have moderate resistivity may inadvertently be too conductive in practice to prevent electrical shorts or leakage when used to insulate conductors. Electron beam test with non-contacting voltage probe measures how resistive a resistive part of a composite material can be.

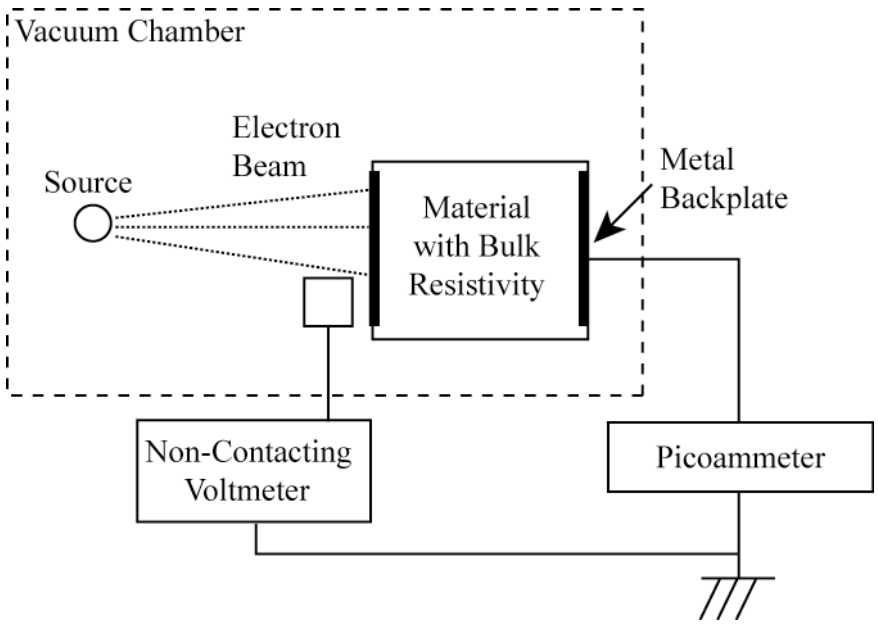

Figure 41—Electron Beam Test for Resistivity

D.7 NON-CONTACTING VOLTMETER RESISTIVITY TEST METHOD

This method, illustrated in Figure 42, Non-Contacting Voltage Decay Resistivity Test, assumes that the resistivity is a constant with respect to applied voltage stress. The method requires plating the

upper and lower surfaces of the material being tested to create a capacitor. The capacitance is determined and the capacitor charged. The power supply is disconnected. The voltage decay is monitored as a function of time as measured by a non-contacting voltmeter. The non-contacting voltmeter is necessary because most voltmeters have lower resistance than the test sample and would lead to incorrect measurements. The resistivity is determined by the equations given earlier and by making use of the voltage-decay versus time-curve given by the equations:

$$V = V_o \times e^{-(t/\tau)} \qquad \text{(Eq. 44)}$$

where:

t	=	time (s)
τ	=	R x C time constant (s)
R	=	resistance from top to bottom of the sample (ohm)
C	=	capacitance of the sample (F)

Note that some materials do not display the semi-log linear R-C circuit decay behavior assumed in Eq. 44 and show that time constant (τ) is varying with time (typically getting larger as the measurement time increases).

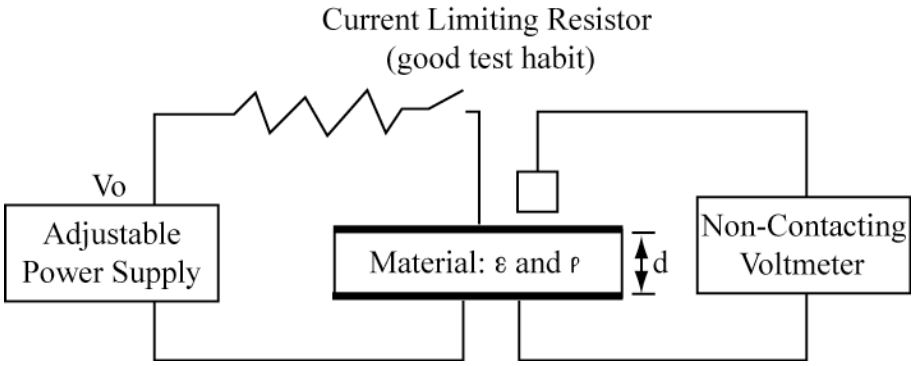

Figure 42—Non-Contacting Voltage Decay Resistivity Test

Problems with this method include the sample preparation (cleanliness, absorbed water, and temperature) and surface leakage around the edge; all should be properly considered. The test is recommended to be done in a vacuum chamber to reduce water absorption contamination of the sample. For non-homogenous materials, like conductive loaded insulators, the electrodes will not charge the bulk material since current will seek out the lower resistance paths in the material. In these cases, an electron beam, as shown in Figure 41, should be used to deposit the initial charge uniformly in the sample. The electron beam is then turned off and the voltage decay rate monitored.

Practicalities limit the maximum resistivities measurable with these conventional methods as described above. Ultimately, to measure very high resistivities, special techniques are necessary.

D.8 DIELECTRIC CONSTANT, TIME CONSTANT

The dielectric constant, ε_r, of a material can be determined experimentally, but it is often obtained from the manufacturer. However, the dielectric constant is frequency dependent, and time dependent under constant DC bias. Most manufacturer data are taken at power frequencies (50/60Hz) or at RF frequencies (MHz/GHz). Typically, the higher the frequency, the lower the dielectric constant. Internal charging is a very slow process. The dielectric constant can continuously increase over hours under constant voltage bias due to polarization effect (reference Adamec, et al., 1978). So electrical time constants derived from AC or high frequency testing will understate the actual time constant, hence the risk of reaching discharge thresholds.

From knowledge of permittivity ε and resistivity ρ, the material's relaxation time constant can be determined. One time constant example is the time for a capacitor-resistor combination's voltage to decay to *1/e* of its full value or about 37% of original voltage (see Figure 43, RC Time Constant).

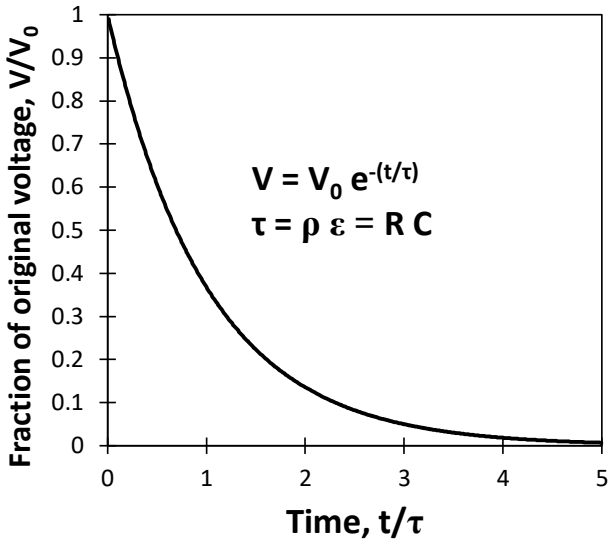

Figure 43—RC Time Constant

If a rectangular slab of material, as shown in Figure 44, Determining Material Time Constant, has metal electrodes on the top and bottom surfaces, it forms a capacitor, whose value is given by:

$$C = \varepsilon \cdot A / d \qquad \text{(Eq. 45)}$$

where:

- ε = permittivity of the material = ε_o x ε_r (F/m)
- ε_o = permittivity of free space = 8.85 x 10^{-12} F/m
- ε_r = dielectric constant of the material, usually between 2 and 10
- A = area of the sample = length x width (m^2)
- d = thickness, top to bottom (m)

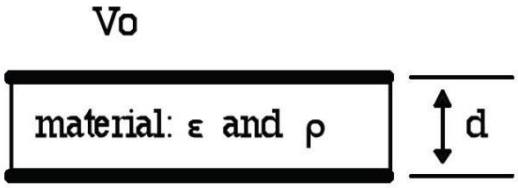

Figure 44—Determining Material Time Constant

If the units are the International System of Units (SI), the capacitance will be expressed in farad. Usually, capacitance related to space charging is expressed in pF because typical values for space charging are in this range.

The leakage resistance from top to bottom of the same rectangular slab is given by:

$$R = \rho\, d / A \qquad \text{(Eq. 46)}$$

where:

R = a resistor equivalent to the leakage resistance of the capacitor, computed from the resistivity by standard equations (ohm)

ρ = material's volume resistivity, often given in ohm m

If the units are consistent, the answer will be in ohm. For the geometry in Figure 44, it can be seen that the leakage time constant (τ) is:

$$\tau = R \times C = \rho \times \varepsilon \qquad \text{(Eq. 47)}$$

At five time constants, there is less than 1% of the original voltage; at 0.01 time constant, the voltage is still 99% of the original. A material time constant of 1 hour or less is desirable to leak off detrimental charges before excessive fields cause ESD breakdown in the material (reference Frederickson, et al. [1992]). The time constant of a good dielectric material (without radiation-induced conductivity) can be very long, weeks to months, even at room temperature.

Materials can be characterized by their time constants if both the dielectric constant and the resistivity are known. This is a theoretical description. Many high resistivity materials behave nonlinearly with applied voltage or applied radiation. Also, initial decay can be faster due to the fast change of permittivity (ε) called polarization. Thus, these concepts are introductory and approximate. For example, electron beam tests and parallel plate tests in vacuum have found that the charge bleed-off times obtained can be hundreds of hours.

D.9 V_{zap} TEST (MIL-STD-883-3, METHOD 3015.9 HUMAN BODY MODEL [HBM])

A V_{zap} test is a test of an electronic device's capability to withstand the effects of an electrical transient simulating fabrication handling. It is useful when attempting to decide whether a device can withstand an ESD transient. Figure 45, V_{zap} Test Configuration, shows a typical test configuration (MIL-STD-883-3, Environmental Test Methods for Microcircuits - Part 3: Test

Methods 3000-3999, Method 3015.9). The parameters are intended to represent the threat from an HBM.

The capacitor (C) in this layout (100±10% pF) is charged through 10^6<R1<10^7 ohm and then the power supply disconnected (switch S1). The capacitor is then discharged (through R2 = 1500 ohm) to the device under test (DUT), increasing the voltage until failure. Hardware is classified according to the highest test voltage step that passed without part failure: Class 0 (0-249 V), Class 1A (250-499 V), Class 1B (500-999 V), Class 1C (1000-1999 V), Class 2 (2000-3999 V), Class 3A (4000-7999 V), or Class 3B (>8000 V), depending on its damage threshold. (For example, if the damage threshold voltage is between 250 and 499 V, a part is classified to HBM Class 1A. In other words, HBM Class 1A part is guaranteed not to be damaged by capacitor voltage up to 249 V.) Note that the voltage described here is the voltage at the capacitor rather than the actual transient pulse voltage at DUT determined by the input impedance of the DUT relative to R2 (1500 ohm). Therefore, the component reported V_{zap} damage threshold cannot be used as the actual device damage threshold. For example, when the input impedance of the DUT is 50 ohm, 250 V at the capacitor (C) generates only ~ 8 V pulse at the DUT. Only 3.2% of the capacitor voltage and 0.1% of the stored energy is actually delivered to the device in this case (50 ohm DUT impedance).

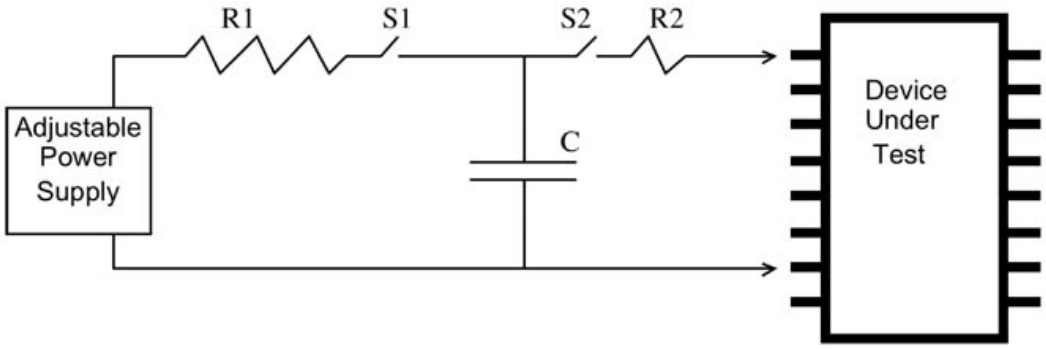

Figure 45—V_{zap} Test Configuration

Although providing some idea of the ESD sensitivity of the part, these broad test ranges may not be as precise as desired. HBM test is described here because device sensitivity information may exist from the manufacturer. For actual space discharge events, the values of C and R2 of the discharge system might be different from HBM. Therefore, if possible, it is recommended to test an electronic part with an equivalent circuit corresponding to actual space discharge (see section 6.3.2.4). Also, note that HBM test applies only three pulses at both polarities before moving to a higher voltage. When multiple discharges at near threshold voltage are expected in a mission, one should be careful to simply apply HBM class as the ESD sensitivity of parts.

Also, because the HBM test is assessing the risk of damage during handling outside of the circuits it is intended for, most of the pins are open circuit during the test. Spacecraft discharges occur after the parts are integrated into circuits, so the pins are connected to ground, voltage supplies, or other devices providing paths for the ESD pulse current to flow. Therefore, the damage threshold and extent of damage might be different between the two ESD test scenarios.

Results obtained by Trigonis (1981) for various parts, capacitor sizes, and series resistors (R2) are graphed in Figure 46, Typical Results for V_{zap} Test Showing Lines of Minimum Damage Threshold for Given Parameters (the Resistances of R2 in Figure 45). It illustrates how the damage threshold varies with each of the test parameters. Each point represents a different sample for the same part type subjected to a V_{zap} capacitor discharge at different voltages for various size capacitors. Both polarities are tested and are applied to the weakest pin pairs. The plotted lines show the least energy that damaged any part under any combination of the variables. One feature of the plot is the existence of a minimum damage voltage threshold for each device. This can be as low as 5 V for some newer devices. The second feature is a constant energy region at low capacitances (not obvious in this chart). The third feature is that the energy appears to go up for the lowest capacitor sizes; this may be an artifact of stray capacitance in the test fixture. It is appropriate to choose the lowest energy as the victim's sensitivity for analyses. It can be seen that, for these parts, the weakest component was damaged by 0.5 µJ. Therefore, based on these test results, an ESD needs to deliver at least 0.5 µJ to damage a part. Of course, having data for the actual parts in question is more desirable.

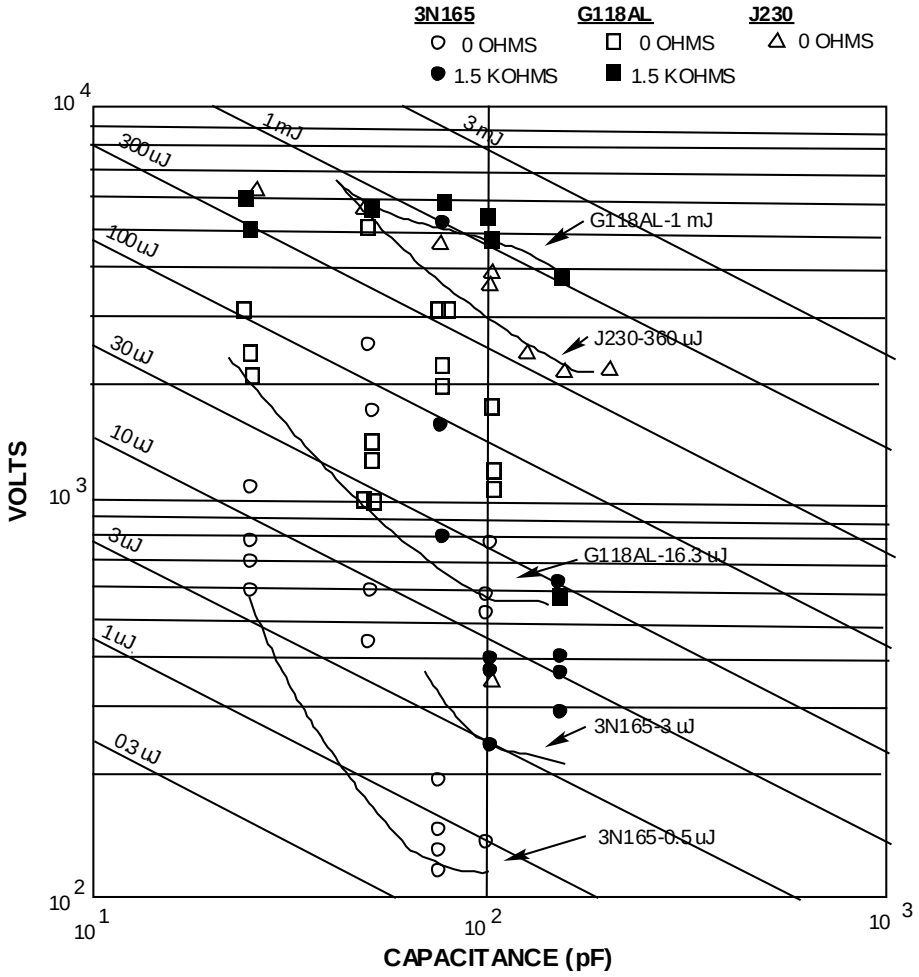

Figure 46—Typical Results for V_{zap} Test Showing Lines of Minimum Damage Threshold for Given Parameters (the Resistances of R2 in Figure 45)

Note: Diagonal lines are for constant energy: $E = 0.5\ C\ V^2$.

D.10 TRANSIENT SUSCEPTIBILITY TESTS

Transient susceptibility tests are very common in the EMC community. Transient injection is done by inductive or capacitive coupling as was shown in MIL-STD-461, Requirements for the Control of Electromagnetic Interference Characteristics of Subsystems and Equipment, for example. The difference between EMC and ESD is the width of the transient pulses: the EMC pulse is typically 10 µs wide, while an ESD pulse is on the order of 10 to 100 ns. A thorough and comprehensive test of a victim device would include varying the pulse width and then determining the voltage and energy threshold of susceptibility. The test should include all pins on the victim device that will encounter the threat, and both polarities of the transient. Testing should include when the input signal is in the high state, the low state, and/or transitioning states. Such a comprehensive characterization would involve more work than is usually done, but the analyst should understand that such test should cover all possible flight conditions.

There are two common sources for generating transient pulses for susceptibility testing. The first is the MIL-STD-1541A pulse source shown in Figure 47, MIL-STD-1541A Pulse Source for Transient Testing (repeated from section 6.3.1.1 in this NASA Technical Handbook). As stated there, this source provides a capacitive discharge with the amplitude set by the voltage used to charge the capacitor and also the electrode separation gap.

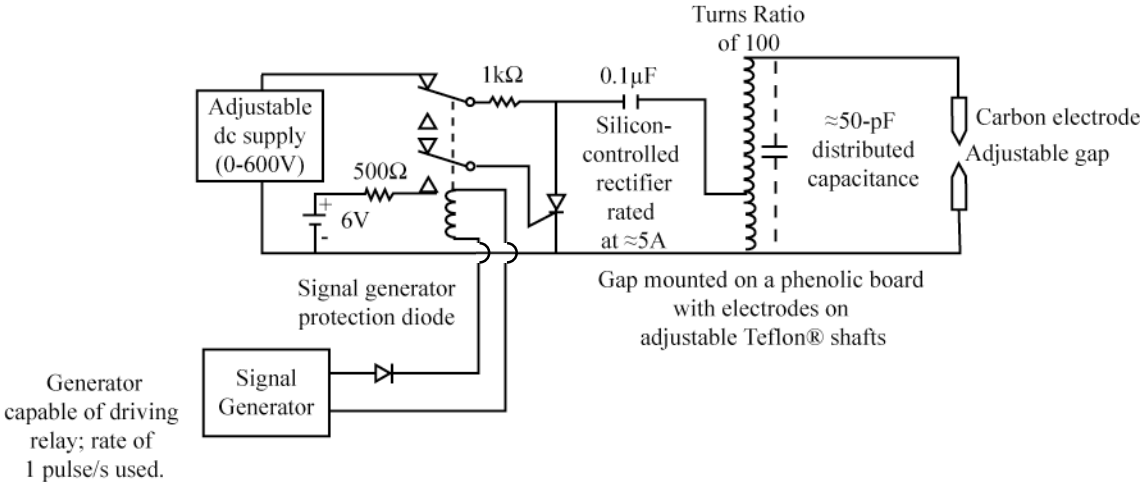

Note: Typical gap spacing, voltage, and energy levels.

Gap (mm)	**V_b** (kV)	**Energy** (µJ)
1	1.5	56
2.5	3.5	305
5.0	6.0	900
7.5	9.0	2000

Figure 47—MIL-STD-1541A Pulse Source for Transient Testing

The second source is a commercial human body discharge source (Schaeffner or Haefely, among others, supplies one such test device). These sources can be battery operated and also provide a capacitive discharge pulse. The charging voltage is variable so that the amplitude can be controlled. Transients from this source are fast (on the order of 150 ns) and the signal is very clean as opposed to the MIL-STD-1541A ESD transient source.

The state of the art is such that ESD test simulators should be improved to better simulate on-orbit ESD pulses. The reader should research for better sources.

D.11 COMPONENT/ASSEMBLY TESTING

Potentially susceptible components/assemblies should be tested for sensitivity to ESD. The component to be tested is to be mounted on a baseplate and functioning. Pulses are to be injected into the component and the performance of the device monitored for upsets. The pulses used are to cover the expected range of current amplitudes, voltages, and pulse durations. It is very important that the pulse device be electrically isolated from the component being tested and the monitoring equipment.

D.12 SURFACE CHARGING ESD TEST ENVIRONMENTS

Monoenergetic electron beam tests have been used conservatively to determine approximate surface charging threats of materials.

D.13 SYSTEM INTERNAL ESD TESTING

There is no convenient or cost-effective way to do a system-level internal ESD test.

APPENDIX E

VOYAGER SEMCAP ANALYSIS

E.1 PURPOSE

This Appendix provides an example of a detailed analysis of a spacecraft and the implications of space charging and resultant ESD events as illustrated by the discussion of design and testing of the Voyager spacecraft. To simulate the anticipated effects of arc discharges on Voyager, tests used a high-voltage-excited spark gap and a flat-plate capacitor with an arc gap to apply arcs on or near the spacecraft. The radiated fields from these sources were also approximated in SEMCAP (a circuit analysis tool using estimated ESD spark waveforms and stray circuit capacitances not part of the circuit design). Estimated induced voltages were then calculated at key locations using circuit analysis methods. (Note: Details are left out of this Appendix because SEMCAP was a very specialized software program of the 70s, which is no longer supported. There is currently no known Full Wave EMC Solver computer program with Finite Difference Time Domain/Finite Difference Frequency Domain EMC Analysis capability that roughly corresponds to SEMCAP.) Testing then measured induced voltages at those key locations with an oscilloscope. The observed data were compared to the predicted values to give a measure of accuracy of the computational tools. As can be seen below, there are enough unknown variables that the results would be expected to differ from reality. While SEMCAP is no longer supported, the mathematical formulas for inductive, capacitive and field-to-wire coupling that were embedded in SEMCAP are in many standard EMC texts and are still commonly used for ESD effects analyses. The limitations discussed below (underprediction bias and 20 dB uncertainty) would still apply if similar ESD source models are used. Similarly, those formulas are used to derive mutual capacitor and mutual inductor values for cross-talk analysis performed via LEM modeling. So LEM analysis would suffer similar inaccuracies with similar ESD source models.

The mean error between the predicted and measured results was -12 dB (under predicted) and the standard deviation was 20 dB (reference Whittlesey [1978]). Assuming these accuracy parameters to be applicable to predicted in-flight responses for Voyager, the spacecraft was considered to be immune to arc discharges below 20 mV on the basis of the SEMCAP analysis. Of course, for research applications, a mean offset of 12 dB and standard deviation of 20 dB sound very large. In spite of these estimated accuracies, the use of SEMCAP in this application caused numerous design changes believed to improve the arc discharge immunity of the Voyager spacecraft. Even though the flight Voyagers still suffered several arc discharge events in flight, the design changes resulting from SEMCAP (in conjunction with testing) significantly enhanced the spacecraft survivability and possibly prevented total failure at Jupiter.

The conclusion here is that even tools providing relatively indeterminate quantitative results can produce results useful for design understanding and possible design changes because they enforce a systematic approach to evaluating a spacecraft design for ESD.

APPENDIX F

SIMPLE APPROXIMATIONS: SPACECRAFT SURFACE CHARGING EQUATIONS

F.1 PURPOSE

This Appendix focuses on surface charging, whereas Appendix C addresses internal charging analyses.

The simple approximations discussed in this section are of a worst-case nature. If this analysis indicates differential potentials between non-circuit surface materials of less than 400 V, there should be no spacecraft discharge problems. If predicted potentials on materials exceed 400 V, the Nascap-2k code (see Appendix B.3.2 in this NASA Technical Handbook) is to be used.

Although the physics behind the spacecraft charging process is quite complex, the formulation can be expressed in very simple terms if a single Maxwell-Boltzmann distribution is assumed. The fundamental physical process for all spacecraft charging is that of current balance; at equilibrium, all currents sum to zero. The potential at which equilibrium is achieved is the potential of the surface with respect to the space plasma ground. In terms of the current (reference Garrett [1981]), the basic equation expressing this current balance for a given surface in an equilibrium situation is (refer to Figure 4):

$$I_E(V) - [I_I(V) + I_{SE}(V) + I_{SI}(V) + I_{BSE}(V) + I_{PH}(V) + I_B(V)] = I_T \qquad \text{(Eq. 48)}$$

where:

V	=	spacecraft surface potential relative to the space plasma (volt, V)
I_E	=	incident electron current to spacecraft surface (ampere, A)
I_I	=	incident ion current to spacecraft surface (A)
I_{SE}	=	secondary electron current due to I_E (A)
I_{SI}	=	secondary electron current due to I_I (A)
I_{BSE}	=	backscattered electron current due to I_E (A)
I_{PH}	=	photoelectron current (A)
I_B	=	active current sources such as charged particle beams or ion thrusters (A)
I_T	=	total current to spacecraft (at equilibrium, I_T =0) (A).

For a spherical body (spacecraft) and a single Maxwell-Boltzmann distribution (space plasma), the first-order current densities (the current divided by the area over which the current is collected, A/m^2) can be calculated (reference Garrett [1981]) using the following equations (appropriate for small conducting sphere at GEO):

Electrons

$$J_E = J_{E0} \exp(qV/kT_E) \qquad V<0 \text{ repelled} \qquad \text{(Eq. 49)}$$

$$J_E = J_{E0} [1 + (qV/kT_E)] \qquad V>0 \text{ attracted} \qquad \text{(Eq. 50)}$$

Ions

$$J_I = J_{I0} \exp(-qV/kT_I) \qquad V>0 \text{ repelled} \qquad \text{(Eq. 51)}$$

$$J_I = J_{I0} [1 - (qV/kT_I)] \qquad V<0 \text{ attracted} \qquad \text{(Eq. 52)}$$

where:

$$J_{E0} = (qN_E/2)(2kT_E/\pi m_E)^{1/2} \qquad \text{(Eq. 53)}$$
$$J_{I0} = (qN_I/2)(2kT_I/\pi m_I)^{1/2} \qquad \text{(Eq. 54)}$$

where:

- N_E = density of electrons (m^{-3})
- N_I = density of ions (m^{-3})
- T_E = temperature of electrons (Kelvin, K)
- T_I = temperature of ions (K)
- m_E = mass of electron (kg)
- m_I = mass of ions (kg)
- q = magnitude of the electronic charge, 1.6×10^{-19} Coulomb

Given these expressions and parameterizing the secondary and backscatter emissions, Eq. 48 can be reduced to an analytic expression in terms of the potential at a point. This model, called an analytic probe model, can be stated as follows:

$$A_E J_{E0} [1 - SE(V,T_E,N_E) - BSE(V,T_E,N_E)]\exp(qV/kT_E) - A_I J_{I0} [1 + SI(V,T_I,N_I)][1 - (qV/kT_I)] - A_{PH} J_{PH0} f(Xm) = I_T = 0 \qquad V<0 \qquad \text{(Eq. 55)}$$

where:

- A_E = electron collection area (m^2)
- J_{E0} = ambient electron current density (A/m^2)
- A_I = ion collection area (m^2)
- J_{I0} = ambient ion current density (A/m^2)
- A_{PH} = photoelectron emission area (m^2)
- J_{PH0} = saturation photoelectron current density (A/m^2)
- SE, SI, BSE = parameterization functions for secondary emission related to electrons and ions, and electron backscattering (unitless)
- $f(Xm)$ = attenuated solar flux as a function of altitude Xm of center of Sun above the surface of Earth as seen by spacecraft (unitless).

This equation is appropriate for a small (<10 m), uniformly conducting spacecraft at geosynchronous orbit in the absence of magnetic field effects. To solve the equation, V is varied until $I_T = 0$. Typical values of SI, SE, and BSE are 3, 0.4, and 0.2, respectively, for aluminum. For geosynchronous orbit, J_E/J_I is about 30 during a geomagnetic storm.

As discussed earlier (see Eq. 9), when the spacecraft is in eclipse (and ignoring secondary and backscattered terms), a simple proportionality between the spacecraft potential and the currents and temperature can be derived from Eq. 55:

$$V \sim -T_E \left[ln(J_{E0}/J_{I0}) + ln(A_E/A_I)\right] \quad \text{(Eq. 56)}$$

where:
V and T_E are in eV.

That is, to rough order in eclipse, the spacecraft potential is directly proportional to the plasma temperature expressed in eVs and to the natural log of the ratio of the electron and ion currents. Note, however, that secondary currents play a crucial role in actual calculations and T_E has to exceed some critical value (reference Garrett, et al. [1979]; Olsen [1983]; Lai and Della-Rose [2001]; Davis, et al. [2008]), usually of the order of 1000 eV, before charging will occur because secondary electron production can be greater than the ambient current for low enough T_E. Also, $ln(J_{E0}/J_{I0})$ often varies much more rapidly and by larger factors than T_E so that charging has been found often to be more related to changes in $ln(J_{E0}/J_{I0})$ than T_E (reference Garrett, et al. [1980a]).

APPENDIX G

DERIVATION OF RULE LIMITING OPEN CIRCUIT BOARD AREA

G.1 PURPOSE

This Appendix provides equations that describe the rationale for the internal charging design guideline in section 5.2.3.2.6 of this NASA Technical Handbook that limits open areas on a standard circuit board to less than 0.3 cm^2. The assumptions and resulting design guideline presented in this Appendix, however, have not been validated by test.

This derivation has been approached as a volumetric equation, i.e., the threat is developed on the basis that, when a surface area is dielectric, the circuit board under that dielectric is also a dielectric through to the bottom with no ground planes or traces to interrupt the storage of undesired energy in that volume. If there were a ground or ground-referenced plane at some depth, these calculations estimate a greater storage of energy than actually would be present.

The guideline additionally allows for the presence of ground and/or ground-referenced planes which reduces the level of concern. The energy of a capacitor of area A and discharge voltage V is:

$$E = 0.5\ C\ V^2 \qquad \text{(Eq. 57)}$$

$$C = \varepsilon_o\ \varepsilon_r\ A / d \qquad \text{(Eq. 58)}$$

where:

E	=	Energy (Joule, J)
C	=	Capacitance (farad, F)
V	=	Potential (volt, V)
$\varepsilon_o\ \varepsilon_r$	=	permittivity of the dielectric material (F/m)
d	=	thickness of the capacitor (m)
A	=	area (m^2).

The following calculation is based on a circuit board material with a relative dielectric constant of **4.7** and a 1 cm x 1 cm by ~1.5 mm (60 mil) thick patch with a 1500-V discharge voltage assuming dielectric strength of **1 x 10^6 V/m**. Also, all the energy stored in this circuit board is assumed to be transferred to an IC (victim) without any attenuation. (The allowed open circuit area will depend on the dielectric strength as well as the relative dielectric constant, the energy attenuation, and the IC's damage threshold energy.) This circuit board with the dimension described above contains about 2.5 x 10^{10} electrons. This quantity of electrons per square cm is the amount believed to be critical for internal discharges. The resultant calculated stored energy is about 3 µJ. The design guideline is based on protection of a victim with an assumed **1 µJ** damage sensitivity (and 100% energy transfer from a capacitor [source] to victim) so there should be a limit of approximately 0.3 cm^2 for area of an empty circuit board region.

If the potential of the discharge voltage is adjusted to be proportional to the thickness ($V = E_{th}\ d$), the results of the equations are combined:

$$E = 0.5\ (\varepsilon_o\ \varepsilon_r\ A / d)\ (E_{th}\ d)^2 \qquad \text{(Eq. 59)}$$

Or simplifying,

$$E = 0.5\ (\varepsilon_o\ \varepsilon_r\ A)\ E_{th}^2\ d \qquad \text{(Eq. 60)}$$

where:

E_{th} = dielectric strength (V/m) for the material in question.

The number of electrons implicit in this equation is the same, but the available energy to damage components is proportional to the thickness. If a ground plane (or power plane) is 8 mil below the dielectric surface, the stored energy will be less than a ground plane at 20 mil depth in proportion to the dielectric thickness which reduces the level of concern. The ground (or power) plane provides a nearby conductive medium to leak off charge during the charging process. During the discharge process, it provides a nearby location for the discharge to strike and is a much more robust victim than an IC.

A clarification of the rule is that it was based on an assumption that the material in question is approximately square. If it is a long, thin area, it is more difficult to concentrate the ESD energy in one pulse. Therefore, the applicable aspect ratio is 3:1. That is, the rule will permit a long patch of dielectric if one dimension is less than 0.3 cm (3 mm).

This effect is shown in Figure 48, Permissible Open Area of a Circuit Board Material versus Depth to a Ground Plane or Power Plane (Preferred) or Other Circuit Traces When Threshold Energy is 1 µJ and the Dielectric Constant is 4.7 (same as Figure 10 in section 5.2.3.2.6 of this NASA Technical Handbook) which also proposes a new rule for exposed dielectric areas on circuit boards. The design rule assumes a standard FR4 circuit board material of 60 mil (~1.5 mm) thickness (however, note all assumed parameters used in the derivation).

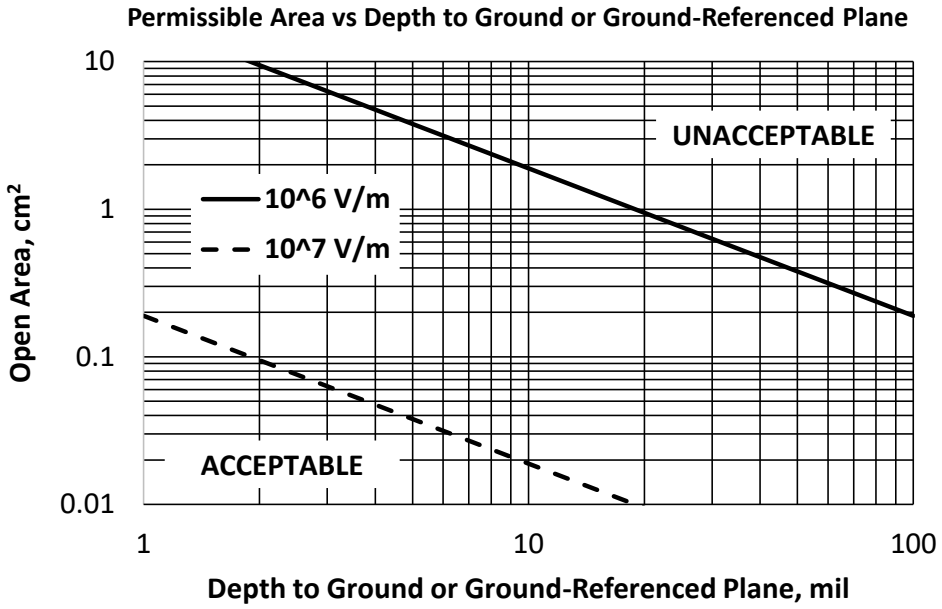

Figure 48—Permissible Open Area of a Circuit Board Material versus Depth to a Ground Plane or Power Plane (Preferred) or Other Circuit Traces When Threshold Energy is 1 µJ and the Dielectric Constant is 4.7

An experiment was performed to determine energy transfer from an area of circuit board metal to a victim wire (reference Leung, et al. [1983]). The energy transferred from a charged metal area of 1 cm^2 at breakdown to a nearby trace on the circuit board into a 50-ohm load was ~0.5 µJ, roughly one-fifth the amount calculated above for energy stored in a dielectric volume of the same 1 cm^2 surface area on the 60-mil thick dielectric. This might indicate a 20% energy transfer efficiency. It provides a ballpark validation of the analytic results derived above.

APPENDIX H

EXPANDED WORST-CASE GEOSYNCHRONOUS EARTH ENVIRONMENTS DESCRIPTIONS

H.1 PURPOSE

This Appendix provides the worst-case geosynchronous environment.

The worst-case geosynchronous environment descriptions in Table 16, Worst-Case Geosynchronous Environments, are actually several measured environments that caused the largest spacecraft charging events during those missions. They come from documented data measurements as referenced and are presented in a form that can be used in a double Maxwellian fit in a charging code such as Nascap-2k.

There are three environments (one from ATS-6 and two from SCATHA), each of which caused large potentials on the respective satellites. Thus, persons wishing to evaluate a satellite design more carefully should make three runs using all three environmental descriptions. Employing all three cases is suggested as the actual surface potentials computed for a specific design will depend not only on the environment but also on the spacecraft configuration, altitude control (spinning [SCATHA] or 3-axis stabilized [ATS-6]), and its surface materials. In this manner, the design of a satellite could be checked more thoroughly for charging effects in various worst-case environments.

Other estimates of a worst-case Earth geosynchronous environment are presented in Table 1 (section 4.2.2, using a single Maxwellian representation of the environment) and in Tables 9 and 10 (Appendix A.2.1). The latter, Appendix A.2.1, suggests a third approach: start with the average of the appropriate parameter and then increase it by one or more standard deviations, depending on the analyst’s design assumptions.

Table 16—Worst-Case Geosynchronous Environments

ELECTRONS		Deutsch* ATS-6	Mullen** SCATHA	Mullen*** SCATHA
Number density (ND) (cm^{-3})		1.22	0.9	3
Current density (J) (nA cm^{-2})		0.413	0.188	0.521
Energy density (ED) (eV cm^{-3})		2.93 X 10^4	9.60 X 10^3	2.40 X 10^4
Energy flux (EF) (eV cm^{-2} s^{-1} sr^{-1})		2.64 X 10^{13}	6.68 X 10^{12}	1.51 X 10^{13}
Number density for population 1 (N_1) (cm^{-3})	Average over all angles	0.0048	0.34	1.13
	Parallel	--	0.2	1.0
	Perpendicular	--	0.2	0.8
Temperature for population 1 (T_1) (keV)	Average over all angles	1.04	1.34	0.45
	Parallel	--	0.4	0.6
	Perpendicular	--	0.4	0.6
Number density for population 2 (N_2) (cm^{-3})	Average over all angles	1.22	0.56	1.87
	Parallel	--	0.6	1.4
	Perpendicular	--	2.3	1.9
Temperature for population 2 (T_2) (keV)	Average over all angles	16.08	10.55	8.27
	Parallel	--	24.0	25.1
	Perpendicular	--	24.8	26.1
Electron average temperature (T_{av}) (keV)		16.02	7.11	5.33
Electron root-mean-square temperature (T_{rms}) (keV)		16.09	8.94	7.31
IONS (PROTONS)		**Deutsch* ATS-6**	**Mullen** SCATHA**	**Mullen*** SCATHA**
Number density (ND) (cm^{-3})		0.245	2.3	3
Current density (J) (nA cm^{-2})		0.00254	0.0080	0.016
Energy density (ED) (eV cm^{-3})		1.04 X 10^4	1.90 X 10^4	3.70 X 10^4
Energy flux (EF) (eV cm^{-2} s^{-1} sr^{-1})		2.98 X 10^{11}	4.30 X 10^{11}	7.48 X 10^{11}
Number density for population 1 (N_1) (cm^{-3})	Average over all angles	0.0100	1.84	2.89
	Parallel	--	1.6	1.1
	Perpendicular	--	1.1	0.9
Temperature for population 1 (T_1) (keV)	Average over all angles	0.130	0.97	6.31
	Parallel	--	0.3	0.4
	Perpendicular	--	0.3	0.3
Number density for population 2 (N_2) (cm^{-3})	Average over all angles	0.235	0.46	0.11
	Parallel	--	0.6	1.7
	Perpendicular	--	1.3	1.6
Temperature for population 2 (T_2) (keV)	Average over all angles	29.6	23.63	59.06
	Parallel	--	26	24.7
	Perpendicular	--	28.2	25.6
Ion average temperature (T_{av}) (keV)		28.4	5.51	8.22
Ion root-mean-square temperature (T_{rms}) (keV)		29.5	13.5	11.8

Note: The SCATHA two-Maxwellian parameters are for fluxes parallel and perpendicular to the magnetic field and averaged over all angles.
Reference *Deutsch (1982) ** Mullen, Gussenhoven, and Garrett (1981a) *** Mullen and Gussenhoven (1983)

APPENDIX I

REFERENCES

I.1 PURPOSE

This Appendix provides references supporting the guidance in this NASA Technical Handbook. Latest issuances of referenced documents should be utilized unless specific versions are designated. Guidance in this NASA Technical Handbook does not supersede or waive existing guidance found in other Agency documentation. Conflicts between this NASA Technical Handbook and other documents are to be resolved by the delegated Technical Authority. Reference documents may be accessed from the NASA Technical Standards System at https://standards.nasa.gov or obtained directly from the Standards Developing Body, other document distributors, or the Office of Primary Responsibility for this NASA Technical Handbook.

These references are a sampling of the many possible information sources relevant to this NASA Technical Handbook. It is heavily colored by the principal authors' knowledge, experience, and prejudices and has left out many worthy references to keep it to a manageable size. The curious reader may dig deeper by following references in these documents. The specific sources referenced in the text are listed here as well. The various charging conference records themselves contain a wealth of technical papers.

I.2 GOVERNMENT DOCUMENTS

The latest issuances of cited documents apply unless specific versions are designated.

DoD

AFGL-TR-77-0288	Modeling of the Geosynchronous Orbit Plasma Environment-Part I
AFGL-TR-78-0304	Modeling of the Geosynchronous Plasma Environment Part 2, ATS-5 and ATS-6 Statistical Atlas
AFGL-TR-79-0015	Modeling of the Geosynchronous Orbit Plasma Environment - Part 3, ATS-5 and ATS-6 Pictorial Data Atlas
AFRL-VS-TR-20001578	6th Spacecraft Charging Technology Conference. 26-29 October 1998, Air Force Research Laboratory, Hanscom Air Force Base, Massachusetts. D.L. Cooke and S.T. Lai, compilers. This conference is documented on one or more CDs, one of which is contained in SEE Publication SEE/TP-2005-600 (Jody Minor, compiler, NASA MSFC). CD contains photo images of electronic files for the 1st through the 8th Spacecraft Charging Conferences.

AFWAL-TR-88-4143, Vol II	Design Guide: Designing and Building High Voltage Power Supplies, Materials Laboratory. Contains good design ideas.
MIL-STD-461	Requirements for the Control of Electromagnetic Interference Characteristics of Subsystems and Equipment. Various versions; version G is the latest as of 2015. Generally, a good EMC design will be helpful at mitigating space charging and ESD effects.
MIL-STD-883-3	Test Method Standard, Electrical Tests (Digital) for Microcircuits, Method 3015.9, Electrostatic Discharge Sensitivity Classification, 3 May 2018. This describes V_{zap} tests for measuring ESD threshold of electronic parts to the human body model for ESD.
MIL-STD-1541A (Cancelled)	**Electromagnetic Compatibility Requirements for Space Systems, 30 Dec. 1897. Cancelled in 2017. Appendix D.10 of this NASA Technical Handbook has a "Schematic Diagram of Arc Source" as copied from MIL-STD-1541A. The replacement documents (SMC-S-008, AIAA-S-121, and MIL-STD-464) of this standard no longer reference this arc source.**
MIL-STD-1686	Electrostatic Discharge Control Program for Protection of Electrical and Electronic Parts, Assemblies, and Equipment (Excluding Electrically Initiated Explosive Devices)
MIL-STD-1809	Space Environment for USAF Space Vehicles. This includes some electron spectra that can be used in the electron transport codes. It has good information that supplements Earth environmental information in this version of NASA-HDBK-4002. The LEO Aurora environment is based on this standard.
PL-TR-93-2027(I)	Proceedings of the Spacecraft Charging Technology Conference, 1989, Volume I. R.C. Olsen, Ed. 31 October – 3 November 1989, Naval Postgraduate School, Monterey, California. More detailed explanations of the space environment and its interactions with spacecraft.

NASA

NASA-CP-2004-213091	Spacecraft Charging Technology Conference, Minor, J.L., compiler. October 20-24, 2003, Marshall Space Flight Center, Huntsville, Alabama. More detailed explanations of the space environment and its interactions with spacecraft.
NASA-CP-2071	Spacecraft Charging Technology – 1978. (Also, AFGL-TR-79-0082.) October 31 – November 2, 1978. United States Air Force

	Academy, Colorado Springs, Colorado. More detailed explanations of the space environment and its interactions with spacecraft.
NASA-CP-2182	Spacecraft Charging Technology – 1980. (Also, AFGL-TR-81-0270.) November 12-14, 1980, United States Air Force Academy, Colorado Springs, Colorado. More detailed explanations of the space environment and its interactions with spacecraft.
NASA-CP-2359	Spacecraft Environmental Interactions Technology – 1983 (Also AFGL-TR-85-0018.) October 4-6, 1983, United States Air Force Academy, Colorado Springs, Colorado. More detailed explanations of the space environment and its interactions with spacecraft.
NASA-HDBK-4001	Electrical Grounding Architecture for Unmanned Spacecraft. This is a handy general document. Notice that the grounding diagrams show that the circuit grounds exit the boxes and apparently connect to a remote ground; this is a schematic and not a physical diagram. The grounds should be contained within the box for the EMC reason that it should not act as a radiator (antenna) of noise into or out of the box.
NASA-HDBK-4002	Avoiding Problems Caused by Spacecraft On-Orbit Internal Charging Effects. One of the two base documents for NASA-HDBK-4002A.
NASA-HDBK-4006	Low Earth Orbit Spacecraft Charging Design Handbook. This document is written by two of NASA's senior researchers in spacecraft charging, recognized experts on charging (and discharging) of solar arrays in space plasmas. It is a fine reference to have on your bookshelf for spacecraft charging. See also NASA-STD-4005.
NASA-HDBK-4007	Spacecraft High-Voltage Paschen and Corona Design Handbook.
NASA-RP-1354	Spacecraft Environments Interactions: Protecting Against the Effects of Spacecraft Charging.
NASA-RP-1375	Failures and Anomalies Attributed to Space Charging.
NASA-STD-4003A	Electrical Bonding for Nasa Launch Vehicles, Spacecraft, Payloads, and Flight Equipment.
NASA-STD-4005	Low Earth Orbit Spacecraft Charging Design Standard. The NASA standard for LEO charging, it gives mitigation techniques for LEO,

	some of which are also applicable to GEO and polar environments. See also NASA-HDBK-4006.
NASA-STD-4010	NASA Standard for Lightning Launch Commit Criteria for Space Flight.
NASA TMX-73537	Proceedings of the Spacecraft Charging Technology Conference (also AFGL-TR-77-0051), C.P Pike and R.R. Lovell, Eds., 27-29 October 1976, United States Air Force Academy, Colorado Springs, Colorado. More detailed explanations of the space environment and its interactions with spacecraft.
NASA/TP-2003-212287	Low Earth Orbit Spacecraft Charging Design Guidelines. See section 5.2.4.2 for added information.
NASA TP-2361 (1984)	Design Guidelines for Assessing and Controlling Spacecraft Charging Effects. One of two base documents for NASA-HDBK-4002A. Listed as a historical reference; some of the deleted sections can provide more background information and illustrations. Section 2.3 describes charge loss in a discharge. Section 3.1.2.3 describes retarding potentials on large portions of dielectrics.
NASA Form 4657	Change Request for a NASA Engineering Standard.

I.3 NON-GOVERNMENT DOCUMENTS

The latest issuances of cited documents apply unless specific versions are designated.

ASTM

ASTM D257	Standard Test Methods for DC Resistance or Conductance of Insulating Materials. Uses test methods appropriate for dielectric materials used in normal terrestrial applications. For measurement of highly resistive materials in space and cold temperatures, special measurement methods should be used. Current version is ASTM D257-14(2021)e1.

ASTM D3755	Standard Test Method for Dielectric Breakdown Voltage and Dielectric Strength of Solid Electrical Insulating Materials under Direct-Voltage Stress

European Cooperation for Space Standardization (ECSS)/European Handbooks

ECSS-20-06	Spacecraft Charging-Environment-induced Effects on the Electrostatic Behaviour of Space Systems. Unpublished draft that should be published because of its useful content. See ECSS-E-ST-20-06C below.
ECSS-E-ST-20-06C-Rev1. 2019a	Space Engineering, Spacecraft Charging Standard. 15 May 2019. This is a set of design rules but is far more than that. It contains the background physics and provides a wealth of space charging information, both scientifically and practically oriented. The standard is a very good educational reference. Sometimes, however, it is not explicit in that it may provide two or more answers to the same question (e.g., what environment to use).
ECSS-E-HB-20-06A. 2019b	Assessment of Space Worst Case Charging Handbook. 15 May 2019.

European Space Research and Technology Centre

SP-476	7th Spacecraft Charging Technology Conference; 2001: A Spacecraft Charging Odyssey. 23-27 April 2001, Noordwijk, The Netherlands

Japan Aerospace Exploration Agency (JAXA)

JERG-2-211A	Design Standard, Spacecraft Charging and Discharging. May 10, 2012.
SP-05-001E	9th Spacecraft Charging Technology Conference, Goka, Tateo, Compiler. 4-8 April 2005. Epochal Tsukuba, Tsukuba, Japan

Other

ANSI/AIAA S-115-2013	Low Earth Orbit Spacecraft Charging Design Standard Requirement and Associated Handbook. September 2013
AIAA S-111A-2014	Qualification and Quality Requirements for Space Solar Cells. 2014
AIAA S-112A-2013	Qualification and Quality Requirements for Electrical Components on Space Solar Panels. 2013

ISO 11221:2011	Space Systems – Space Solar Panels – Spacecraft Charging Induced Electrostatic Discharge Test Methods. August 2011
QinetiQ/KI/SPACE/ HB042617	Spacecraft Plasma Interaction Guidelines and Handbook. Another good reference for persons wishing further background on the subject.
SD 71-770	The Effects of Radiation on the Outer Planets Grand Tour (November 1971). Prepared for the Jet Propulsion Laboratory by Space Division, North American Rockwell. This old document may be difficult to find but is a good reference document.

I.4 OTHER REFERENCES

Adamec, V.; Calderwood, J.H. (1978). "Electrical conduction and polarisation phenomena in polymeric dielectrics at low fields." *J. Phys. D: Appl. Phys.* Vol. 11 pp. 781-800.

Agostinelli, S.; Allison, J.; Amako, K.; Apostolakis, J.; Araujo, H.; Arce, P.; Asai, M.; Axen, D.; Banerjee, S.; Barrand, G., Behner, F.; Bellagamba, L.; Boudreau, J.; Broglia, L.; Brunengo, A.; Burkhardt, H.; Chauvie S.; Chuma, J.; Chytracek, R.; Cooperman, G.; Cosmo, G.; Degtyarenko, P.; Dell'Acqua, A.; Depaola, G.; Dietrich, D.; Enami, R.; Feliciello, A.; Ferguson, C.; Fesefeldt, H.; Folger, G.; Foppiano, F.; Forti, A.; Garelli, S.; Giani, S.; Giannitrapani, R.; Gibin, D.; Gómez Cadenas, J.J.; González, I.; Gracia Abril, G.; Greeniaus, G.; Greineraf, W.; Grichinef, V.; Grossheim, A.; Guatelli, S.; Gumplinger, P.; Hamatsu, R.; Hashimoto, K.; Hasui, H.; Heikkinen, A.; Howard, A.; Ivanchenko, V.; Johnson, A.; Jones, F.W.; Kallenbach, J.; Kanaya, N.; Kawabata, M.; Kawabata, Y.; Kawaguti, M.; Kelner, S.; Kent, P.; Kimura, A.; Kodama, T.; Kokoulin, R.; Kossov, M.; Kurashige, H.; Lamanna, E.; Lampén, T.; Lara, V.; Lefebure, V.; Lei, F.; Liendl, M.; Lockman, W.; Longo, F.; Magni, S.; Maire, M.; Medernach, E.; Minamimoto, K.; Mora de Freitas, P. Morita, Y.; Murakami, K.; Nagamatu, M.; Nartallo, R.; Nieminen, P.; Nishimura, T.; Ohtsubo, K.; Okamura, M.; O'Neale, S.; Oohata, Y.; Paech, K.; Perl, J.; Pfeiffer, A.; Pia, M.G.; Ranjard, F.; Rybin, A.; S. Sadilov, S.; Di Salvoc E.; Santin, G.; Sasaki, T.; Savvas, N.; Sawada, Y.; Scherer, S.; Sei, S.; Sirotenko, V.; Smith, D.; Starkov, N.; Stoecker, H.; Sulkimo, J.; Takahata, M.; Tanaka, S.; Tcherniaev, E.; Safai Tehranig E.; Tropeano, M.; Truscott, P.; Uno, H.; Urban, L.; Urban P., Verderi, M.; Walkden, A.; Wander, W.; Weber, H.; Wellisch, J.P.; Wenaus, T.; Williams, D.C.; Wright, D.; Yamada, T.; Yoshida, H..; Zschiesche D. (2003)."Geant4-A Simulation Toolkit." *Nuclear Instruments and Methods in Physics Research.* Vol. A, No. 506, pp. 250-303.

Allison, J.; Amako, K; Apostolakis, J.; Araujo, H.; Arce Dubois, P.; Asai, M.; Barrand, G.; Capra, R.; Chauvie, S.; Chytracek, R.; Cirrone, G.A.P.; Cooperman, G.; Cosmo, G.; Cuttone, G.; Daquino, G.G.; Donszelmann, M.; Dressel, M.; Folger, G.; Foppiano, F.; Generowicz, J.; Grichine, V.; Guatelli, S.; Gumplinger, P.; Heikkinen, A.; Hrivnacova, I.; Howard, A.; Incerti, S.; Ivanchenko, V.; Johnson, T.; Jones, F.; Koi, T.; Kokoulin, R.; Kossov, M.; Kurashige, H.; Lara, V.; Larsson, S.; Lei, F.; Link, O.; Longo, F.; Maire, M.; Mantero, A.;

Mascialino, B.; McLaren, I.; Mendez Lorenzo, P.; Minamimoto. K.; Murakami, K.; Nieminen, P.; Pandola, L.; Parlati, S.; Peralta, L.; Perl, J.; Pfeiffer, A.; Pia, M.G.; Ribon, A.; Rodrigues, P.; Russo, G.; Sadilov, S.; Santin, G.; Sasaki, T.; Smith, D.; Starkov, N.; Tanaka, S.; Tcherniaev, E.; Tomé, B.; Trindade, A.; Truscott, P.; Urban, L.; Verderi, M.; Walkden, A.; Wellisch, J.P.; Williams, D.C., Wright, D.; Yoshida. H. (2006). "Geant4 Developments and Applications." *IEEE Transactions on Nuclear Science.* Vol. 53, No. 1, pp. 270-278.

Allison, J.; Amako, K.; Apostolakis, J.; Arce, P.; Asai, M.; Aso, T.; Bagli, E.; Bagulya, A.; Banerjee, S.; Barrand, G.; Beck, B.R.; Bogdanov, A.G.; Brandt, D.; Brown, J.M.C.; Burkhardt, H.; Canal, Ph.; Cano-Ott, D.; Chauvie, S.; Cho, K.; Cirrone, G.A.P.; Cooperman, G.; Cortés-Giraldo, M.A.; Cosmo, G.; Cuttone, G.; Depaola, G.; Desorgher, L.; Dong, X.; Dotti, A.; Elvira, V.D.; Folger, G.; Francis, Z.; Galoyan, A.; Garnier, L.; Gayer, M.; Genser, K.L.; Grichine, V.M.; Guatelli, S.; Guèye, P.; Gumplinger, P.; Howard, A.S.; Hřivnáčová, I.; Hwang, S.; Incerti, S.; Ivanchenko, A.; Ivanchenko, V.N.; Jones, F.W.; Jun, S.Y.; Kaitaniemi, P.; Karakatsanis, N.; Karamitros, M.; Kelsey, M.; Kimura, A.; Koi, T.; Kurashige, H.; Lechner, A.; Lee, S.B.; Longo, F.; Maire, M.; Mancusi, D.; Mantero, A.; Mendoza, E.; Morgan, B.; Murakami, K.; Nikitina, T.; Pandola, L.; Paprocki, P.; Perl, J.; Petrović, I.; Pia, M.G.; Pokorski, W.; Quesada, J.M.; Raine, M.; Reis, M.A.; Ribon, A.; Ristić Fira, A.; Romano, F.; Russo, G.; Santin, G.; Sasaki, T.; Sawkey, D.; Shin, J.I.; Strakovsky, I.I.; Taborda, A.; Tanaka, S.; Tomé, B.; Toshito, T.; Tran, H.N.; Truscott, P.R.; Urban, L.; Uzhinsky, V.; Verbeke, J.M.; Verderi, M.; Wendt, B.L.; Wenzel, H.; Wright, D.H.; Wright, D.M.; Yamashita, T.; Yarba, J.; Yoshida, H. (2016) "Recent developments in Geant4." *Nuclear Instruments and Methods in Physics Research Section A: Accelerators, Spectrometers, Detectors and Associated Equipment,* Vol. 835, 2016, pp. 186-225.

Amorim, E.; Payan, D.; Reulet, R.; Sarrail, D. (April 2005). *Electrostatic Discharges on a 1 m^2 Solar Array Coupon – Influence of the Energy Stored on Coverglass on Flashover Current.* Paper presented at the 9th Spacecraft Charging Technology Conference. Tsukuba, Japan. Plasma propagation speed: 0.7 - 1.1 x 10^4 m/s.

Andersen, A.; Dennison, J.R.; Sim, A.M.; Sim C. (2015). "Measurements of Endurance Time for Electrostatic Discharge of Spacecraft Materials: A Defect-Driven Dynamic Model." *IEEE Transactions on Plasma Science*. Vol. 43, No. 9, pp. 2941-2953.

Andersen, A.; Moser, K.; Dennison J.R. (2017). "Perspectives on the Distributions of ESD Breakdowns for Spacecraft Charging Applications." *IEEE Transactions on Plasma Science*. Vol. 45, No. 8, pp. 2031-2035.

Andersen, A. (2018). *The Role of Recoverable and Non-recoverable Defects in DC Electrical Aging of Highly Disordered Insulating Materials*. PhD Dissertation, Utah State University Department of Physics.

Anderson, P.C. (2012). " Characteristics of spacecraft charging in low Earth orbit." *Journal of Geophysical Research*. Vol. 117, A07308.

Baker, D.N.; Kanekal, S.G.; Hoxie, V.C.; Batiste, S.; Bolton, M.; Li, X.; Elkington, S.R.; Monk, S.; Reukauf, R.; Steg, S.; Westfall, J.; Belting, C.; Bolton, B.; Braun, D.; Cervelli, B.; Hubbell, K.; Kien, M.; Knappmiller, S.; Wade, S.; Lamprecht, B.; Stevens, K.; Wallace, J.; Yehle, A.; Spence, H.E.; Friedel, R. (2013). "The Relativistic Electron-Proton Telescope (REPT) Instrument on Board the Radiation Belt Storm Probes (RBSP) Spacecraft: Characterization of Earth's Radiation Belt High-Energy Particle Populations." *Space Science Reviews.* Vol. 179, No. 1-4, pp. 337-381.

Balcewicz, P.; Bodeau, J.M.; Frey, M.A.; Leung, P.L.; Mikkelson, E.J. (1998). "Environmental On-Orbit Anomaly Correlation Efforts at Hughes." *6th Spacecraft Charging Technology Conference Proceedings*. AFRL-VS-TR-20001578. pp. 227-230.

Beutier, T.; Delage, E.; Wouts, M.; Serres, O.; Peyrard, P.-F. (2003). *FASTRAD new tool for radiation prediction*. Proceedings of the 7th European Conference on Radiation and Its Effects on Components and Systems (RADECS). Noordwijk, The Netherlands.

Bever, R.S.; Staskus, J. (1981). "Tank Testing of a 2500 cm^2 Solar Panel." *Spacecraft Charging Technology Conference—1980*. NASA CP-2182, pp. 211-227. Supports cerium-doped solar array coverglass charging being lower than fused silica.

Bielajew, A.F.; Hirayama, H.; Nelson, W.R.; Rogers, D.W.O. (June 1994). *History, Overview and Recent Improvements of EGS4.* SLAC-PUB-6499 (NRC-PIRS-0436, KEK Internal 94-4). Paper presented at Radiation Transport Calculations Using the EGS4. Capri, Italy.

Blake, J.B.; Carranza, P.A.; Claudepierre, S.G.; Clemmons, J.H.; Crain, W.R.; Doutan, Y.; Fennel, J.F.; Fuentes, F.H.; Galvan, R.M.; George, J.S.; Henderson, M.G.; Lalic, M.; Lin, A.Y.; Looper, M.D.; Mabry D.J.; Mazur, J.E.; McCarthy, B.; Nguyen, C.Q.; O'Brien, T.P.; Perez, M.A.; Redding, M.T.; Roeder, J.L.; Salvaggio, D.J.; Sorensen, G.A.; Spence, H.E.; Yi, S.; Zakrzewski, M.P. (2013). "The *Magnetic Electron Ion Spectrometer* (MagEIS) Instruments Aboard the Radiation Belt Storm Probes (RBSP) Spacecraft." *Space Science Reviews.* Vol. 179, No. 1-4, pp. 383-421.

Bodeau, M. (2005). "Going Beyond Anomalies to Engineering Corrective Action, New IESD Guidelines Derived from a Root-Cause Investigation." Presented at the 2005 Space Environmental Effects Working Group, Aerospace Corp., El Segundo, CA. See also Balcewicz and others (1998).

Bodeau, M. (2010). "High Energy Electron Climatology that Supports Deep Charging Risk Assessment in GEO." AIAA 2010-1608, 48th AIAA Aerospace Sciences Meeting, Orlando, FL. A fine work with good concepts, explained and illustrated with actual space data and estimates of fluence accumulation versus material resistivity. He challenges the 0.1 pA/cm^2 and 10 hr flux integration guidelines.

Bodeau, M. (2012). "Current and Voltage Thresholds for Sustained Arcs in Power Systems." *IEEE Transactions on Plasma Science.* Vol. 40, No. 2, pp. 192-200.

Bodeau, M. (2013). "Test Approach to Assess Solar Array Diode Board Susceptibility to Sustained Arcing." *Journal of Spacecraft and Rockets.* Vol. 50, No. 6, pp. 1277-1287.

Bodeau, M. (2014). "Updated Current and Voltage Thresholds for Sustained Arcs in Power Systems." *IEEE Transactions on Plasma Science.* Vol. 42, No. 7, pp. 1917-1921.

Bodeau, M. (2015). "Observation of Sustained Arc Circuit Failure on Solar Array Backside in Low Earth Orbit." *IEEE Transactions on Plasma Science.* Vol. 43, No. 9, pp. 2961-2974.

Bogorad, A.L.; Deeter, M.P.; August K.A.; Doorley G.; Likar J.J.; Herschitz R. (2008). " Shielding Effectiveness and Closeout Methods for Composite Spacecraft Structural Panels." *IEEE Transactions on Electromagnetic Compatibility*. Vol. 50, No. 3, pp. 547-555.

Bogus, K.; Claassens, C.; Lechte, H. (1985). *Investigations and conclusions on the ECS solar array in-orbit power anomalies*. Proc. 18th IEEE Photovoltaic Specialists Conference, Las Vegas, USA, 21-25 October 1985, pp. 368-375. MARECS-A and ECS-1 experienced partial loss of power after five years on station. In-orbit tests identified the failure to be a short to panel structure of several sections of the array. This is one of the earliest known references to a flight failure analysis. The analysis resulted in a recommendation to resistively isolate the solar array structure from the spacecraft structure.

Boscher, D.M.; Bourdarie, S.A.; Friedel, R.H.W.; Belian, R.D. (2003). "Model for the Geostationary Electron Environment." *IEEE Transactions on Nuclear Science.* Vol. 50, No. 6, pp. 2278-2283.Brandhorst, H.; Rodiek, J.; Ferguson, D.; O'Neill, M. (2007). *Stretched Lens Array (SLA): A Proven and Affordable Solution to Spacecraft Charging in GEO*. Paper presented at the 10th Spacecraft Charging Technology Conference, Biarritz, France. This new concept design, based on the DS-1 spacecraft, eliminates many space charging problems that are present on normal solar arrays. It uses cylindrical Fresnel lenses, focusing light on 1-cm wide, triple junction cells (overall efficiency 27 percent), and over 1000-V differential voltage standoff adjacent cells. It is fully insulated and micrometeoroid-immune. Brandhorst also says that conductive coverglass (~10^9 ohm cm) is helpful; may be grounded or may be at the cell potential on an ITO surface.

Brunson, J.; Dennison, J.R. (June 2007). *Dependence of Resistivity in Low-Density Polyethylene on Space Environment Parameters*. Paper presented at the 10th Spacecraft Charging Technology Conference. Biarritz, France.

Carruth, Jr., M.R.; Schneider T.A.; McCollum, M.; Finckenor, M. (2001). *ISS and Space Environment Interactions without Operating Plasma Contactor*. AIAA-2001-401, Aerospace Sciences Meeting and Exhibit, 39th, Reno, Nevada, January 9-11.

Chauvet, C.; Laurent, C. (1993). "Weibull Statistics in Short-term Dielectric Breakdown of Thin Polyethylene Films." *IEEE Transactions on Electrical Insulation*. Vol. 28, No.1. pp. 18-29.

Chiu, Y.T.; Luhmann, J.G.; Ching, B.K.; Boucher, Jr, D.J. (1979). "An Equilibrium Model of Plasmaspheric Composition and Density." *Journal of Geophysical Research*. Vol. 84, No.A.3. pp. 909-916.

Chock, R.; Ferguson, D.C. (1997). *Environments WorkBench - An Official NASA Space Environments Tool.* Paper presented at the 32nd Intersociety Energy Conversion Engineering Conference. Washington, D.C. IECEC 97452, pp. 753-757.

Coakley, P. (1987). *Assessment of Internal ECEMP with Emphasis for Producing Interim Design Guidelines*. AFWL-TN-86-28, June 1987. This 63-page document was excellent in its day and still is a fine reference that should be on every ESD practitioner's bookshelf. The design numbers from that document are very similar to those of this NASA Technical Handbook.

Cooke, D.L. (1998). *Simulation of an Auroral Charging Anomaly on the DMSP Satellite*. AIAA-98-0385, 36th Aerospace Sciences Meeting and Exhibit, Reno, NV.

Crine, J.P.; Parpal, J.L.; Dang C. (1989). *A new approach to the electric aging of dielectrics*. Paper presented at the Conference on Electrical Insulation and Dielectric Phenomena (CEIDP), Pocono Manor, PA, pp. 161-167.

Crine, J.P. (2016). *Role of electrostriction on the electrical aging of polymers*. Paper presented at the 2016 IEEE International Conference on Solid Dielectrics (ICSD), New York City, NY, pp. 685-688.

Daly, E.J. (1988). "The Evaluation of Space Radiation Environments for ESA Projects." *ESA Journal.* Nov. 12, pp. 229-247.

Davis, S.; Stillwell, R.; Andiario, W.; Snyder, D.; Katz, I. (1999). *EOS-AM Solar Array Arc Mitigation Design*. SAE Technical Paper 1999-01-2582 presented at 34th Intersociety Energy Conversion Engineering Conference. Vancouver, British Columbia, Canada. IECEC-01-2582.

Davis, V.A.; Mandell, M.J.; Gardner, B.M.; Mikellides, I.G.; Neergaard Parker, L.; Cooke, D.L.; Minow, J. (2003). *Validation of Nascap-2k Spacecraft-Environment Interactions Calculations*. Paper presented at the 8th Spacecraft Charging Technology Conference. Huntsville, Alabama.

Davis, V.A.; Mandell, M.J.; Thomsen, M.F. (2008). "Representation of the Measured Geosynchronous Plasma Environment in Spacecraft Charging Calculations." *Journal of Geophysical Research. 113,* A10204, doi:10.1029/2008JA013116.

de Soria-Santacruz, M.; Garrett, H.B.; Evans, R.W.; Jun, I.; Kim, W.; Paranicas, C.; Drozdov, A. (2016). "An empirical model of the high-energy electron environment at Jupiter." *Journal of Geophysical Research: Space Physics*. 121, pp. 9732–9743, doi:10.1002/2016JA023059.

DeForest, S. (1973). “Electrostatic Potentials Developed by ATS-5.” *Photon and Particle Interactions with Surfaces in Space*, *Proceedings of the 6th ESLAU Symposium*, R.J.L. Grard, (Ed.), D. Reidel Publishing Company, pp. 263-276. Placed here to honor this historic paper written at the inception of awareness of space charging.

Dekany, J.; Sim, A.M.; Brunson, J.; Dennison, J.R. (2013). "Electron Transport Models and Precision Measurements with the Constant Voltage Conductivity Method." *IEEE Transactions on Plasma Science*. Vol. 41, No. 12, p. 12.

Dennison, J.R.; Brunson, J.; Swaminathan, P.; Green, N.W.; Frederickson, A.R. (posthumously). (October 2006). “Methods for High Resistivity Measurements Related to Spacecraft Charging.” *IEEE Transactions on Plasma Science.* Vol. 34, No. 5, pp. 2191-2203. This reference provides a good summary insight into problems of measuring high resistivities for space usage and proposed test methods appropriate to these needs.

Dennison, J.R (2015). "Dynamic Interplay Between Spacecraft Charging, Space Environment Interactions, and Evolving Materials." *IEEE Transactions on Plasma Science*. Vol. 43, No. 9, pp. 2933-2940.

Denton, M.H.; Thomsen M.F.; Jordanova V.K.; Henderson M.G.; Borovsky J.E.; Denton J.S.; Pitchford D.; Hartley D.P. (2015). “An empirical model of electron and ion fluxes derived from observations at geosynchronous orbit”, *Space Weather*, Vol 13, 233–249, doi:10.1002/2015SW001168.

Deutsch, M-J. (1982). “Worst Case Earth Charging Environment.” *Journal of Spacecraft and Rockets*. Vol 19, No. 5, pp. 473-477.

DeWitt, R.N.; Duston, D.P.; Hyder, A.K., Eds. (1994). *The Behavior of Systems in the Space Environment.* Doredecht, The Netherlands: Kluwer Academic Publishers. Additional reading for the space environment and interaction with spacecraft.

Dichter, B.K.; Galica, G.E.; McGarity, J.O.; Tsui, S.; Golightly, M.J.; Lopate, C.; Connell, J.J. (2015). “Specification, Design, and Calibration of the Space Weather Suite of Instruments on the NOAA GOES-R Program Spacecraft.” *IEEE Transactions on Nuclear Science.* Vol. 62, No. 6, pp. 2776-2783.

Dissado, L.A.; Fothergill, J.C. (1992). *Electrical Degradation and Breakdown in Polymers*. The Institution of Engineering and Technology, London, UK.

Dunbar, W.G. (1988). *Design Guide: Designing and Building High Voltage Power Supplies*, AFWAL-TL-88-4143, Vol. II, Wright Patterson Air Base, OH. This 333-page classic should be on everyone’s bookshelf. Dielectric strength considerations are discussed at length.

Evans, R.W.; Garrett, H.B.; Gabriel, S.; Whittlesey, A. (November 1989). *A Preliminary Spacecraft Charging Map for the Near Earth Environment*. Paper presented at the Spacecraft Charging Technology Conference. Naval Postgraduate School, Monterey, California. This original

reference paper was omitted from the conference proceedings. See Whittlesey and others (1992) for an alternate reference with the "wishbone" chart.

Evans, R.W.; Garrett, H.B. (November - December 2002). "Modeling Jupiter's Internal Electrostatic Discharge Environment." *Journal of Spacecraft and Rockets*. Vol. 39, No. 6, pp. 926-932.

Ferguson, D.C. (1998). "Plasma Effects on Spacecraft Then and Now! A Welcome to Participants", *6th Spacecraft Charging Technology Conference Proceedings.* AFRL-VS-TR-20001578. pp. 1-5.

Ferguson, D.C.; Hillard, G.B. (2004). "New NASA SEE LEO Spacecraft Charging Design Guidelines-How to Survive in LEO Rather than GEO." NASA-CP-2004-213091, *8th Spacecraft Charging Technology Conference, October 20-24. 2003*. NASA, Marshall Space Flight Center, Huntsville, AL.

Frederickson, A.R. (1974). *Radiation Induced Electrical Current and Voltage in Dielectric Structures.* AFRL-TR-74-05823. A reference for NUMIT.

Frederickson, A.R. (1983). "Electric Discharge Pulses in Irradiated Solid Dielectrics in Space." *IEEE Transactions on Electrical Insulation.* Vol. 18, pp. 337-349. A reference for NUMIT.

Frederickson, A.R.; Cotts, D.B.; Wall, J.A.; Bouquet, F.L. (1986). "Spacecraft Dielectric Material Properties and Spacecraft Charging." *AIAA Progress in Astronautics and Aeronautics*. Vol. 107. New York: AIAA Press. Contains dielectric properties data, especially relating to spacecraft charging. Worth obtaining and reading.

Frederickson, A.R.; Holeman, E.G.; Mullen, E.G. (December 1992). "Characteristics of Spontaneous Electrical Discharging of Various Insulators in Space Radiations." *IEEE Transactions on Nuclear Science.* Vol. 39, No. 6, pp. 1773-1982. This document is a description of the best-known attempt to quantify internal charging effects on orbit, by means of a well-thought-out experiment design. The results were not all that the investigators had hoped, but the data are excellent and very good conclusions can be reached from the data, in spite of the investigators' concerns.

Funsten, H.O; Skoug, R.M.; Guthrie, A.A.; MacDonald, E.A.; Baldonado, J.R.; Harper, R.W.; Henderson, K.C.; Kihara, K.H.; Lake, J.E.; Larsen, B.A.; Puckett, A.D.; Vigil, V.J.; Friedel, R.H.; Henderson, M.G.; Niehof, J.T.; Reeves, G.D.; Thomsen, M.F.; Hanley, J.J.; George, D.E.; Jahn, J.-M.; Cortinas, S.; De Los Santos, A.; Dunn, G.; Edlund, E.; Ferris, M.; Freeman, M.; Maple, M.; Nunez, C.; Taylor, T.; Toczynski, W.; Urdiales, C.; Spence, H.E.; Cravens, J.A.; Suther, L.L.; Chen, J. (2013). "Helium, Oxygen, Proton, and Electron (HOPE) Mass Spectrometer for the Radiation Belt Storm Probes Mission." *Space Science Reviews*. Vol. 179, No. 1-4, pp. 423-484.

Garrett, H.B. (1979). "Review of Quantitative Models of the 0 to 100 keV Near Earth Plasma." *Reviews of Geophysics*, 17, pp. 397-417.

Garrett, H.B. (November 1981). "The Charging of Spacecraft Surfaces." *Reviews of Geophysics and Space Physics.* Vol. 19, No. 4, pp. 577-616. A nice summary paper, with numerical examples and many illustrations. This and Whipple (1981) are two definitive papers on the subject, each covering slightly different aspects.

Garrett, H.B. (1999). *Guide to Modeling Earth's Trapped Radiation Environment*. Reston, Virginia: American Institute of Aeronautics and Astronautics Press. AIAA G-083-1999, ISBN 1-56347-349-6. 55 pages.

Garrett, H.B.; DeForest, S.E. (1979). "Analytical Simulation of the Geosynchronous Plasma Environment." *Planetary and Space Science*, 27, pp.1101-1109. This paper includes a useful model of the geosynchronous plasma environment that can be used to study local time variations and variations with geomagnetic activity.

Garrett, H.B.; Pike, C.P., Eds. (1980a). "Space Systems and Their Interactions with Earth's Space Environment." *Progress in Astronautics and Aeronautics.* 71. Additional reading for the space environment and interactions with spacecraft.

Garrett, H.B.; Schwank, D.C.; Higbie, P.R.; Baker, D.N. (1980b). "Comparison Between the 30-80 keV Electron Channels on ATS-6 and 1976-059A During Conjunction and Application to Spacecraft Charging Prediction." *Journal of Geophysical Research. 85,* pp.1155-1162.

Garrett, H.B.; Schwank, D.C.; DeForest, S.E. (1981a). "A Statistical Analysis of the Low Energy Geosynchronous Plasma Environment, Part I – Electrons." *Planetary and Space Science*. 29, pp. 1021-1044.

Garrett, H.B.; Schwank, D.C.; DeForest, S.E. (1981b). "A Statistical Analysis of the Low Energy Geosynchronous Plasma Environment, Part II – Ions." *Planetary and Space Science.* 29, pp. 1045-1060.

Garrett, H.B.; Whittlesey, A.C. (1996). *Spacecraft Charging, An Update.* Paper AIAA 96-0143 presented at the 34th Aerospace Sciences Meeting and Exhibit. Reno, Nevada. Paper also presented at 2000 IEEE International Conference on Plasma Science, Washington, D.C. A good narrative history of spacecraft charging effects.

Garrett, H.B.; Whittlesey, A.C. (2000). "Spacecraft Charging, An Update." *IEEE Transactions on Plasma Science.* Vol. 28, No. 6, pp. 2017-2028.

Garrett, H.B.; Hoffman, A. (December 2000). "Comparison of Spacecraft Charging Environments at the Earth, Jupiter, and Saturn." *IEEE Transactions on Plasma Science*. Vol. 28, No. 6, pp. 2048 - 2057.

Garrett, H.B.; Ratliff, J.M.; Evans, R.W. (October 2005). *Saturn Radiation (SATRAD) Model.* JPL Publication 05-9, The Jet Propulsion Laboratory, Pasadena, CA: California Institute of Technology, pp. 103. https://trs.jpl.nasa.gov/handle/2014/38302.

Garrett, H.B.; Minow, J.I. (2007). *Charged Particle Effects on Solar Sails - Final Report.* NASA Report ISPT-SS-06-101, Marshall Space Flight Center.

Garrett, H.B., and Whittlesey, A.C. (2011). *Guide to Mitigating Spacecraft Charging Effects*, JPL Space Science and Technology Series, J. H. Yuen, Editor-in-Chief, John Wiley and Sons, Inc., Hoboken, NJ, 221. (Book version of NASA-HDBK-4002A.)

Garrett, H.B.; Close, S. (2013). "Impact-Induced ESD and EMI/EMP Effects on Spacecraft—A Review." *IEEE Transactions on Plasma Science.* Vol. 41, No. 12, pp. 3545-3557.

Garrett, H.B.; Jun, I.; Evans, R.W.; Kim, W.; Brinza, D.E. (2017). "The Latest Jovian-Trapped Proton and Heavy Ion Models." *IEEE Transactions on Nuclear Science*. Vol. 64, No. 11 pp. 2802 – 2813.

Gillespie, J.C. (2013). *Measurement of The Temperature Dependence of Radiation Induced Conductivity in Polymeric Dielectrics*. Master's Thesis, Utah State University Department of Physics.

Ginet, G.P.; O'Brien, T.P.; Huston, S.L.; Johnston, W.R.; Guild, T.B.; Friedel, R.; Lindstrom, C.D.; Roth, C.J.; Whelan, P.; Quinn, R.A.; Madden, D.; Morley, S.; Su, Y.-J. (2013). "AE9, AP9 and SPM: New Models for Specifying the Trapped Energetic Particle and Space Plasma Environment." *Space Science Reviews.* Vol. 179, No.1-4, pp. 579-615.

Green, N.W.; Frederickson, A.R.; Dennison, J.R. (October 2006). "Experimentally Derived Resistivity for Dielectric Samples from the CRRES Internal Discharge Monitor." *IEEE Transactions on Plasma Science*. Vol. 34, No. 5, pp 1973-1978.

Green, N.W.; Dawson, S.F. (2015). *Electrostatic Discharge Testing of Carbon Composite Solar Array Panels for Use in the Jovian Environment*. Paper presented at the AIAA Space Conference and Exposition, Pasadena, CA, pp. 4558.

Green, N.W.; Kim, W.; Low, N.; Zhou, C.; Andersen, A.; Linton, T.; Martin, E.; Chinn, J.Z. (2019). "Electrostatic Discharges from Conductive Thermal Coatings." *IEEE Transactions on Plasma Science*. Vol. 47, No. 8, pp. 3759-3765.

Gruss, M. (2015). *Air Force Seeks Info on Space Weather Sensor.* [Online]. Available at https://spacenews.com/air-force-seeks-info-on-space-weather-sensor/.

Gussenhoven, M.S.; Mullen, E.G. (1983). "Geosynchronous Environment for Severe Spacecraft Charging." *Journal of Spacecraft and Rockets,* pp. 20-26.

Halbleib, J.A.; Kensick, R.P.; Melhorn, T.A.; Valdez, G.D.; Seltzer, S.M.; Berger, M.J. (November 1994). *ITS 3.0: Integrated TIGER Series of Coupled Electron/Photon Monte Carlo Transport Codes.* Sandia National Laboratories. The Radiation Safety Information Computational Center, Code Package CCC-467, Oak Ridge National Laboratory. Provides additional information on ITS.

Harel, M. (May 1982). *Galileo NASCAP Analysis Report.* JPL Interoffice Memorandum (IOM) 5137-82-62.

Hastings, D.; Garrett, H.B. (1996). *Spacecraft-Environment Interactions.* Atmospheric and Space Science Series, A.J. Dessler, Ed. Cambridge, England: Cambridge University Press. This is a college text on the subject with emphasis on a number of space environments and their effects on spacecraft.

Haymes, R.C. (1971). *Introduction to Space Science.* New York: John Wiley and Sons, Inc. Additional reading for the space environment and interaction with spacecraft. Though dated, it is a valuable source of scientific information on the general field of space physics.

Heidebrecht (1975). *SEMCAP Program Description, Version 7.4*. TRW.

Hernandez-Pellerano, A.; Iannello, C.J.; Garrett, H.B.; Ging, A.T.; Katz, I.; Keith, R.L.; Minow, J.I.; Willis, E.M.; Schneider, T.A.; Whittlesey, A.C.; Wollack, E.J.; Wright, K.H. (2014). *International Space Station (ISS) Plasma Contactor Unit (PCU) Utilization Plan Assessment Update*. NASA Technical Report TI-13-00869, NESC. A NASA panel was chartered to look at safety issues for astronauts out of the ISS on a space walk that involved being near possibly hazardous situations. The charter was to assess the hazard, and suggest mitigation methods.

Hewlett-Packard Operating and Service Manual for Model 4329A High-Resistance Meter (and Model 16008A Resistivity Cell) (November 1983). With 16008 Resistivity Cell, directly displays high values of resistivity (saves calculation effort).

Hewlett-Packard Operating Note for Model 16008A Resistivity Cell, undated.

Hoeber, C.F.; Robertson, E.A.; Katz, I.; Davis, V.A.; Snyder, D.B. (February 1998). *Solar Array Augmented Electrostatic Discharge in GEO.* AIAA paper 98-1401 presented at 17th International Communications Satellite Systems Conference and Exhibit. Yokohama, Japan. This earlier reference is very desirable because of the clarity of exposition (several of its graphics are used in this document), the wide variety of parameters studied, and the numerous physics derivations used in their attempts to explain both the on-orbit experiences and the ground test results, and specific design guidelines to mitigate problems in the future. Later researchers have improved on the contents of this paper in terms of additional test complexity, but it is very readable. The wise person will read later papers and get testing done by persons with recent test experience and knowledge.

Hosoda, S.; Muranaka, T.; Kuninaka, H.; Kim, J.; Hatta, S.; Kurahara, N.; Cho, M.; Ueda, H.; Koga, K.; Goka, T. (2008). "Laboratory Experiments for Code Verification of Multi-Utility Spacecraft Charging Analysis Tool (MUSCAT)." *IEEE Transactions on Plasma Science*. Vol. 36, No. 5, pp. 2350-2359.

Inguimbert, V.; Levy, L.; Boulay, F.; Sarrail, D.; Migliorero, G.; Mausli, P.A. (2007). *Study of Arc Propagation in Solar Array Drive Mechanisms*. Paper presented at the 10th Spacecraft

Charging Technology Conference, June 18-21, 2007. Biarritz, France. The authors note parameters of track spacing, housing insulation, direct line of sight between conductors, or intertrack insulation barrier height increase, and brush insulation as design parameters to consider.

Inouye, G.T. (1976). "Spacecraft Potentials in a Substorm Environment, in Spacecraft Charging by Magnetospheric Plasma." *Progress in Astronautics and Aeronautics.* Vol. 42. A. Rosen, Ed. pp. 103-120. Cambridge, Massachusetts: MIT Press.

Jordan, T. (1987-1998). "NOVICE: Radiation Transport Shielding Code." T. Jordan, Experimental and Mathematical Physics Consultants. Gaithersburg, MD.

Jun, I. (2006). Private communication.

Jursa, A.S., Ed. (1985). *Handbook of Geophysics and the Space Environment.* National Technical Information Services Document, Accession No. ADA 167000. Additional reading for the space environment and interaction with spacecraft. An excellent reference for Earth space plasma environments, as well as many other space environments.

Katz, I.; Parks, D.E.; Wang, S.; Wilson, A. (1977). "Dynamic Modeling of Spacecraft in a Collisionless Plasma." *Proceedings of the Spacecraft Charging Technology Conference.* NASA TMX-73537/AFGL-TR-77-0051, pp. 319-330.

Katz, I.; Cassidy, J.J.; Mandell, M.J.; Schnuelle, G.W.; Steen, P.G.; Roche, J.C. (1979). "The Capabilities of the NASA Charging Analyzer Program." *Spacecraft Charging Technology – 1978*. NASA CP-2071/AFGL-TR-79-0082, pp. 101-122.

Katz, I.; Davis, V.A.; Snyder, D. (1998). "Mechanism for Spacecraft Charging Initiated Destruction of Solar Arrays in GEO." *36th AIAA Aerospace Sciences Meeting and Exhibit.* AIAA-1998-1002. This is a seminal text in this area. Be sure to read this document from one of the key experts in the field.

Kawakita, S.; Kusawake, H.; Takahashi, M.; Maejima, H.; Kim, J.; Hosoda, S.; Cho, M.; Toyoda, K.; Nozaki, Y. (2004). "Sustained Arc Between Primary Power Cables of a Satellite." *2nd International Energy Conversion Engineering Conference*, Providence, RI, 16-19 August. Contains description of ADEOS-II satellite failure analysis. See also Maejima et al. (2004).

Kennel, C.F.; Petschek, H.E. (1966). "Limit on stably trapped particle fluxes." *J. Geophys. Res., 71*, pp. 1-28.

Kim, W.; Green, N.W.; Whittlesey, A.C.; Katz, I.; Jun, I. (2010). "Internal Electrostatic Discharge Testing on Spacecraft Cables," *11th Spacecraft Charging Technology Conference*.

Kim W.; Jun, I.; and Garrett, H.B. (2012). "NUMIT 2.0: the latest version of the JPL internal charging analysis code," *12th Spacecraft Charging Technology Conference*.

Kim, W.; Chinn, J.Z.; Katz, I.; Garrett, H.B.; Wong, K.F. (2017). "3-D NUMIT: A General 3-D Internal Charging Code," *IEEE Transactions on Plasma Science*, Vol. 45, pp. 2298-2302.

Khachen, W.; Suthar, J.; Stokes, A.; Dollinger, R.; Dunbar, W.G. (1993). "Aerospace-specific Design Guidelines for Electrical Insulation." *IEEE Transactions on Electrical Insulation*, Vol. 28, No. 5, pp. 876-886. Includes approximate dielectric strengths (electric field stress) for aerospace dielectrics. Dunbar's valuable experience is expressly mentioned in this paper.

Koons, H.C. (1981). "Aspect Dependence and Frequency Spectrum of Electrical Discharges on the P78-2 (SCATHA) Satellite." *Spacecraft Charging Technology-1980*. NASA CP-2182/AFGL-TR81-0270, pp. 478-492.

Lai, S.T.; Della-Rose, D.J. (2001). "Spacecraft Charging at Geosynchronous Altitudes: New Evidence for Existence of Critical Temperature." *Journal of Spacecraft and Rockets*. Vol. 38, p. 922.

Leach, R.D.; Alexander, M.B. (Ed.) (August 1995). *Failures and Anomalies Attributed to Spacecraft Charging.* NASA Reference Publication 1375. This document has a very good list of specific space incidents that have been attributed to ESDs in space. It does not discriminate between surface charging or internal charging, but that is usually difficult to determine or does not appear in public literature.

Leung, P.L.; Plamp, G.H.; Robinson, P.A., Jr. (1983). "Galileo Internal Electrostatic Discharge Program." *Spacecraft Environmental Interactions Technology 1983*. NASA CP-2359/AFGL-TR-85-0018, 1983, pp. 423-435. This paper, documented in the 1985 publication and presented at the 4th Spacecraft Charging Technology Conference, describes a very neat and clear test that measures the effect of line lengths and circuit board metal areas in the resultant ESD amplitude. It also measures the amplitude of ESD transients from electron beam charging on 50 ohm loads from various conductors.

Leung, P.; Whittlesey, A.C.; Garrett, H.B.; Robinson, P.A., Jr. (May-June 1986). "Environment-Induced Electrostatic Discharges as the Cause of Voyager 1 Power-on Resets." *Journal of Spacecraft and Rockets*. Vol. 23, No. 3. One of the first and best documented examples of IESD.

Leung, P.L.; Mikkelson, E. (2007). *Mitigation of the Internal Charging Threat Posed by Energetic Electrons using an Electrically Leaky Coating.* Paper presented at the 10th Spacecraft Charging Technology Conference, June 18-21, 2007. This is a very nice paper describing the "before" large electrostatic transients accumulated on traditional conformal coating and the far smaller ESD transients with use of their new coating. Leung claims thorough space qualification for this product, but it is company proprietary and not for sale (in response to an audience question).

Likar, J.J.; Bogorad, A. L.; Malko, T.R.; Goodzeit, N.E.; Galofaro, J.T.; Mandell, M.J. (2006). "Interaction of Charged Spacecraft with Electric Propulsion Plume: On Orbit Data and

Ground Test Results." *IEEE Transactions on Nuclear Science*, Vol. 53, No. 6, pp. 3602-3606.

Likar, J.J.; Lombardi, R.E.; Bogorad, A.L.; Herschitz, R. (2015a). "Surface Charging Considerations for Composite Materials Used in Spacecraft Applications," *IEEE Transactions on Plasma Science*. Vol. 43, No. 9, pp. 2901-2906.

Likar, J.J.; Bogorad, A.L.; August, K.; Lombardi, R.E.; Kannenberg, K.; Herschitz, R. (2015b). "Spacecraft Charging, Plume Interactions, and Space Radiation Design Considerations for All-Electric GEO Satellite Missions." *IEEE Transactions on Plasma Science*. Vol. 43, No. 9, pp. 3099-3108.

Lindstrom, C.D.; Aarested, J.; Ballenthin, J.O.; Barton, D.A.; Coombs, J.M.; Ignazio, J.; Johnston, W.R.; Kratochvil, S.; Love, J.; McIntire, D.; Quigley, S.; Roddy, P.; Selesnick, R.S.; Sibley, M.; Vera,A.; Wheelock, A.; Wu, S. (2018). "The Compact Environmental Anomaly Sensor Risk Reduction: A Pathfinder for Operational Energetic Charged Particle Sensors." *IEEE Transactions on Nuclear Science.* Vol. 65, No. 1, pp. 439-447.

Maejima, H.; Kawakita, S.; Kusawake, H.; Takahashi, M.; Goka, T.; Kurosaki, T.; Nakamura, M.; Toyoda, K.; Cho, M. (2004). "Investigation of Power System Failure of a LEO Satellite." AIAA 2004-5657. *2nd International Energy Conversion Engineering Conference*, Providence, RI, 16-19 August. Contains description of ADEOS-II satellite failure analysis. See also Kawakita, et al. (2004).

Mandell, M.J.; Davis, V.A.; Gardner, B.M.; Joneward, G. (2003). "Electron Collection by International Space Station Solar Arrays." *8th Spacecraft Charging Conference, Huntsville AL*.

Mandell, M.J.; Davis, V.A.; Gardner, B.M.; Mikellides, I.G.; Cooke, D.L.; Minor, J. (2006). "Nascap-2k—An Overview." *IEEE Transactions on Plasma Science.* 34, p. 2084.

Massaro, M.J.; Green, T.; Ling, D. (1977). "A Charging Model for Three-Axis Stabilized Spacecraft." *Proceedings of the Spacecraft Charging Conference*. AFGL-TR-77-0051/NASA TMX-73537. pp. 237-270.

Massaro, M.J.; Ling, D. (1979). "Spacecraft Charging Results for the DSCS III Spacecraft." *Spacecraft Charging Technology - 1978*. NASA CP-2071/AFGL-TR-79-0082. pp. 158-178.

Mikatarian, R.; Barsamian, H.; Kern, J.; Koontz, S.; Roussel, J.F. (October 2002). *Plasma Charging of the International Space Station*. Paper presented at the 53rd International Astronautical Congress, The World Space Congress. Houston, Texas.

Minow, J.I.; Blackwell, W.C.; Neergaard Parker, L.; Evans, S.W; Hardage, D.M.; Owens, J.K. (2000). "Charged Particle Environment Definition for NGST: L2 Plasma Environment Statistics." *Proceedings of SPIE 4013, UV, Optical, and IR Space Telescopes and Instruments VI*. pp. 942-953.

Minow, J.I.; Blackwell, W.C., Jr.; Diekmann, A. (January 2004a). *Plasma Environment and Models for L2*. AIAA Paper 2004-1079 presented at the 42nd AIAA Aerospace Sciences Meeting and Exhibit. Reno, Nevada.

Minow, J.I.; Altstatt, R.L.; Neergaard Parker, L. (September 28-29, 2004b). *Interplanetary Radiation and Internal Charging Environment Models for Solar Sails*. Paper presented at the Solar Sail Technology and Application Conference. Greenbelt, Maryland.

Minow, J.I.; Neergaard Parker, L.; Altstatt, R.L. (April 2005). *Radiation and Internal Charging Environments for Thin Dielectrics in Interplanetary Space*. Paper presented at the 9th Spacecraft Charging Technology Conference. Tsukuba, Japan.

Minow, J.I.; Neergaard Parker, L.; Parker, L.N.; Altstatt, R.L.; W. Skipworth, W. (2006). *Ion Flux Environments in Interplanetary Space*. AIAA Paper 2006-0473 presented at the 44th AIAA Aerospace Sciences Meeting and Exhibit. Reno, Nevada.

Minow, J.I.; Diekmann, A.M.; Blackwell, W.C., Jr. (January 2007). *Status of the L2 and Lunar Charged Particle Environment Models.* AIAA paper 2007-0910 presented at the 45th AIAA Aerospace Sciences Meeting and Exhibit. Reno, Nevada.

Minow, J.I.; Wright, Jr, K.H.; Chandler, M.O.; Coffey, V.N.; Craven, P.D.; Schneider, T.A.; Parker, L.N.; Ferguson, D.C; Koontz, S.L.; Alred, J.W. (September 2010). *Summary of 2006 to 2010 FPMU Measurements of International Space Station Frame Potential Variations*. Paper presented at the 11th Spacecraft Charging Technology Conference, Albuquerque NM.

Minow, J.I., et al. (2018). *International Space Station (ISS) Plasma Interaction Model (PIM) Independent Review*. NASA Engineering and Safety Center Technical Assessment Report, NESC-RP-16-01108.

Mohammadzadeh, A.; Evans, H.; Nieminen, P.; Daly, E.; Vuilleumier, P.; Buhler, P.; Eggel, C.; Hajdas, W.; Schlumpf, N.; Zehnder, A.; Schneider, J.; Fear, R. (2003). "The ESA Standard Radiation Environment Monitor Program First Results from PROBA-I and INTEGRAL." *IEEE Transactions on Nuclear Science.* Vol. 50, No. 6, pp. 2272-2277.

Morley, S.K.; Sullivan, J.P.; Carver, M.R.; Kippen, R.M.; Friedel, R.H.W.; Reeves, G.D.; Henderson, M.G. (2017). "Energetic Particle Data from the Global Positioning System Constellation." *Space Weather.* Vol. 15, pp. 283-289.

Mullen, E.G.; Gussenhoven M.S.; Garrett, H.B. (1981a). *A 'Worst Case' Spacecraft Charging Environment as Observed by SCATHA on 24 April 1979.* AFGL-TR-81-0231.

Mullen, E.G.; Hardy, D.A.; Garrett, H.B.; and Whipple, E.C. (1981b). "P78-2 SCATHA Environmental Data Atlas." *Spacecraft Charging Technology. 1980*. NASA CP-2182/AFGL-TR-81-0270.

Mullen, E.G.; Gussenhoven, M.S. (1983). *SCATHA Environmental Atlas.* AFGL-TR-83-0002.

Mullen, E.G.; Gussenhoven, M.S.; Hardy, D.A.; Aggson, T.A.; Ledley, B.G.; Whipple, E. (February 1986). "SCATHA Survey of High-Level Spacecraft Charging in Sunlight." *Journal of Geophysical Research.* Vol. 91, No. A2. pp. 1474-1490. Discussion of some physics to explain observed data. A good reference for actual data.

Muranaka, T.; Hosoda, S.; Kim, J.; Hatta, S.; Ikeda, K.; Hamanaga, T.; Cho, M.; Usui, H.; Ueda, H.; Koga, K.; Goka, T (October 2008). "Development of Multi-Utility Spacecraft Charging Analysis Tool (MUSCAT)." *IEEE Transactions on Plasma Science*. Vol. 36, No. 5, pp. 2336-2349,

Naidu, M.S.; Kamaraju, V. (2009). High Voltage Engineering, Fourth Edition McGraw-Hill. Townsend's criteria for breakdown is described in this book.

Neergaard P.L.; Minow, J.; McCollum, M.; Cooke, D.; Katz, I.; Mandell, M.; Davis, V.; Hilton, J. (April 2001). "Comparison of the NASCAP/GEO, POLAR, SEE Charging Handbook, and NASCAP-2K.1 Spacecraft Charging Codes." *Proceedings of the 7th Spacecraft Charging Technology Conference.* Noordwijk, The Netherlands.

Nelson, W.R.; Hirayama, H.; Rogers, D.W.O. (December 1985). *The EGS4 Code System.* SLAC-265. Stanford Linear Accelerator Center: Stanford University, Stanford, California.

O'Brien, T.P., (2014) *AE9/AP9 Guidance for Third-Party Developers*. Aerospace Technical Report 2014-01204, Aerospace Corporation.

O'Brien, T.P; Whelan, P. (2016) *Specifications for Radiation Effects Kernels for Use with AE9/AP9.* Aerospace Technical Report 2015-02436, Aerospace Corporation.

Olsen, R.C. (November/December 1981). "Modification of Spacecraft Potentials by Thermal Electron Emission on ATS-5." *Journal of Spacecraft and Rockets.* Vol 18, No. 6. pp 527-532 (AIAA 81-4348).

Olsen, R.C. (1983). "A Threshold Effect for Spacecraft Charging." *Journal of Geophysical Research.* pp. 493-499.

Olsen, R.C.; Whipple, E.C. (1977). *Active Experiments in Modifying Spacecraft Potential: Results from ATS-5 and ATS-6.* University of California: San Diego. NASA CR-159993.

Olsen, R.C.; McIlwain, C.E.; Whipple, E.C. (August 1981). "Observations of Differential Charging Effects on ATS 6." *Journal of Geophysical Research.* Vol. 86, No. A8. pp. 6809-6819.

Parker, E.N. (1963). *Interplanetary Dynamical Processes*. New York: Interscience.

Peck, E.D.; Randall, C.E.; Green, J.C.; Rodriguez, J.V.; Rodger, C.J. (2015). "POES MEPED differential flux retrievals and electron channel contamination correction." *Journal of Geophysical Research, Space Physics.* Vol. 120, pp. 4596-4612.

Pourrouquet, P.**;** Varotsou, A.; Sarie, L.; Thomas, J.-C.; Chatry, N.; Standarovski, D.; Rolland, G.; Barillot, C. (2016). *Comparative study between Monte-Carlo tools for space applications*. Proceedings of the 16th European Conference on Radiation and Its Effects on Components and Systems (RADECS). Bremen, Germany.

Purvis, C.K.; Bartlett, R.O. (1980). "Active Control of Spacecraft Charging." *Space Systems and Their Interactions with the Earth's Space Environment.* H.B. Garrett and C.P. Pike. New York: AIAA Press. pp. 299-317.

Purvis, C.K.; Garrett, H.B.; Whittlesey, A.C.; Stevens, N.J. (September 1984). *Design Guidelines for Assessing and Controlling Spacecraft Charging Effects*. NASA Technical Paper 2361. This document has been widely used by practitioners of this art (usually EMC engineers or radiation survivability engineers) since its publication in 1984. Its contents are limited to surface charging effects. The contents are valid to this day for that purpose. NASA TP-2361 contents have been incorporated into this NASA-STD-4002, Rev A, with heavy editing. Many of the original details, especially time-variant and multiple-case versions of suggested environments, have been simplified into single worst-case environments in NASA-HDBK-4002, Revision A. Some background material has not been transferred into this document, so the original may still be of interest.

Reeves, G.D.; Vandegriff, E.M.; Niehof, J.T.; Morley, S.K.; Cunningham, G.S.; Henderson, M.G.; Larsen, B.A. (2020). "Defining radiation belt enhancement events based on probability distributions." *Space Weather*, 18. https://doi.org/10.1029/2020SW002528.

Robinson, P.A., Jr.; Holman, A.B. (1977). "Pioneer Venus Spacecraft Charging Model." *Proceedings of the Spacecraft Charging Technology Conference.* AFGL-TR-77-0051/NASA TMX-73537. pp. 297-308.

Robinson, P.A., Jr., Ed. (1988). *Introduction to Spacecraft Environments and the Anomalies They Cause.* Pasadena, California: Jet Propulsion Laboratory.

Roche, J.C.; Purvis, C.P. (1979). "Comparisons of NASCAP Predictions with Experimental Data." *Spacecraft Charging Technology-1978*. NASA CP-2071/AFGL-TR-79-0082. pp. 144-157.

Rodgers, D.J.; Hunter, K.A.; Wrenn, G.L. (2004). *The FLUMIC Electron Environment Model.* Paper presented at the 8th Spacecraft Charging Technology Conference. Huntsville, Alabama, USA, 20-24 Oct 2003.

Rodgers, D.; Heynderickx, D.; Demol, J.; Hilgers, A. (2005). *Spacecraft Plasma Interaction Guidelines and Handbook*. QinetiQ/KI/SPACE/HB042617, Draft, 27 May 2005, Version 0.10. This is intended to be an advice book for practitioners of this subject and is planned to consist of both a text version and an on-line interactive version. It is well-worth reading but did not appear on the ESA space charging web site as of this writing. It is a companion document to SCSS-E-20-06.

Roederer, J.G. (1970). *Dynamics of Geomagnetically Trapped Radiation.* New York: Springer-Verlag.

Rubin, A.G.; Katz, I.; Mandell, M.; Schnuelle, G.G.; Steen, P. (1980). "A Three-Dimensional Spacecraft Charging Computer Code." *Space Systems and Their Interactions with Earth's Space Environment. Progress in Astronautics and Aeronaut*ics. Vol. 71. New York: AIAA Press. pp. 318-336.

Saiki, T.; Abe, K.; Miyake, H.; Tanaka, Y.; Maeno, T. (2015). *Space charge distribution measurements in insulating materials of commercially available enameled wire*. IEEE Conference on Electrical Insulation and Dielectric Phenomena (CEIDP), pp. 94-97.

Sauer, H. (1996). Private Communication.

Schnuelle, G.W.; Parks, D.E.; Katz, I.; Mandell, M.J.; Steen, P.G**.** (1979). "Charging analysis of the SCATHA satellite." *Spacecraft Charging Technology*-1978. NASA CP2071/AFGL TR-79-0087. pp. 123-143.

Seltzer, S.M. (1980). "SHIELDOSE: A Computer Code for Space-Shielding Radiation Dose Calculations." NBS Technical Note 1116, Washington, DC.

Shugg, W.T. (1995). *Handbook of Electrical and Electronic Insulating Materials*. IEEE Press, Second Edition. An excellent general reference for dielectric characteristics written by a leader in the field.

Sicard-Piet, A.; Bourdarie, S.; Boscher, D.; Friedel, R.H.W.; Thomsen, M.; Goka, T.; Matsumoto, H.; Koshiishi, H. (2008). "A New International Geostationary Electron Model: IGE-2006, from 1 keV to 5.2 MeV." *Space Weather.* Vol. 6, S07003, doi:10.1029/2007SW000368.

Sorensen, J.; Rodgers, D.J.; Ryden, K.A.; Latham, P.M.; Wrenn, G.L.; Levey, L.; Panabiere, G. (2000). "ESA's Tools for Internal Charging." IEEE Transactions on Nuclear Science, 47 (3) 491-497. A published reference for DICTAT.

Stassinopoulos, E.G. (March-April 1980). "The Geostationary Radiation Environment." *Journal of Spacecraft and Rockets.* Vol. 17, No. 2. pp. 145-152.

Stone, E.C.; Frandsen, A.M.; Mewaldt, R.A.; Christian, E.R.; Margolies, D.; Ormes, J.F.; Snow, F. (July 1998). "The Advanced Composition Explorer." *Space Science Reviews.* Vol. 86, pp. 1-22.

Stratton, J.M.; Harvey, R.J.; Heyler, G.A. (2013). "Mission Overview for the Radiation Belt Storm Probes Mission", *Space Science Reviews*. Vol. 179, pp. 29–57.

Sturman, J.C. (September 1981). *Development and Design of Three Monitoring Instruments for Spacecraft Charging.* NASA-TP-1800.

Thomsen, M.F.; Denton, M.H.; Lavraud, B.; Bodeau, M. (2007). "Statistics of Plasma Fluxes at Geosynchronous Orbit Over More than a Full Solar Cycle." *Space Weather.* 5, S03004, doi:10.1029/2006SW000257.

Tribble, A. (1995). *The Space Environment: Implications for Spacecraft Design*. Princeton, NJ: Princeton University Press. This provides additional reading about the space environment and interactions with the spacecraft environment.

Trigonis, A. (May 1981). JPL Part Evaluation Report Log 3647.

Vette, J.I. (November 1991). *The AE-8 Trapped Electron Model Environment*. NSSDC/WDC-A-R&S (91-24). National Space Science Data Center, Greenbelt, Maryland.

Vette, J.I.; Teague, M.J.; Sawyer, D.M.; Chan, K.W. (1979). "Modeling the Earth's Radiation Belts." *Solar-Terrestrial Prediction Proceedings*. Boulder, Colorado.

Wenaas, E.P.; Treadaway, M.J.; Flanagan, T.M.; Mallon, C.E.; Danson, B. (1979). "High-Energy Electron-Induced Discharges in Printed Circuit Boards." *IEEE Transactions on Nuclear Science*. NS-26. pp. 5152-5155.

Wertz, J.R.; Larsen, W.J., Eds. (1991). *Space Mission Analysis and Design.* Doredecht, The Netherlands: Kluwer Academic Publishers. This provides additional reading about the space environment and interactions with the spacecraft environment.

Westman, H.P., Ed. (1968). *Reference Data for Radio Engineers,* Fifth Edition. Howard Sams & Co., Inc., Indianapolis, Indiana.

Whipple, E.C. (1981). "Potentials of Surfaces in Space." *Reports on Progress in Physics*. Vol. 44, pp. 1197-1250. Nice summary paper. Emphasis is on total charging and not internal charging, but good for physics background. This and Garrett (1981) are the two definitive papers on that subject, each covering slightly different aspects.

Whittlesey, A.C. (June 1978). *Voyager Electrostatic Discharge Protection Program.* Paper presented at IEEE International Symposium on EMC, Atlanta, Georgia. pp 377-383.

Whittlesey, A.C.; Garrett, H.B.; Robinson, Jr, P.A. (1992). *The Satellite Space Charging Phenomenon, and Design and Test Considerations*. Paper presented at IEEE International EMC Symposium. Anaheim, California.

Wilkenfeld, J.M.; Harlacher, B.L.; Mathews, D. (April 1982). *Development of Electrical Test Procedures for Qualification of Spacecraft against EID, Volume 2: Review and Specification of Test Procedures*. NASA CR-165590. EID refers to electron-induced discharge, a term used in those days. A very good survey of spacecraft ESD test methodology as of 1982. Includes the methods used for several satellite systems, and provides a comparison and evaluation of their relative merits. This is a fundamental document for anyone in the spacecraft ESD test business.

Wilkinson, D.C. (March-April, 1994). "National Oceanic and Atmospheric Administration's Spacecraft Anomaly Database and Examples of Solar Activity Affecting Spacecraft." *Journal of Spacecraft and Rockets*. Vol. 31, No. 2, pp. 160-165. NOAA keeps a confidential

list of spacecraft anomalies that can be searched for space anomaly correlations but without revealing the specific spacecraft.

Wong, K.F.; Kim, W. (2016). *Deep Charging Requirement and Analysis Approach for EOR to GEO*. Paper presented at the Spacecraft Charging Technology Conference, ESTEC, Noordwijk, The Netherlands.

Wrenn, G.L. (May-June 1995). "Conclusive Evidence for Internal Dielectric Charging Anomalies on Geosynchronous Communications Spacecraft." *Journal of Spacecraft and Rockets*. Vol. 32, No. 3, pp. 514-520. Note that the author believes that there is still a need to convince people that internal charging is a real phenomenon, as recently as 1995.

Wright, K.H.; Swenson, C.M.; Thompson, D.C.; Barjatya, A.; Koontz, S.L.; Schneider, T.A.; Vaugh, J.A.; Minow, J.I.; Craven, P.D.; Coffey, V.N.; Parker, L.N.; Bui, T.H. (2008). "Charging of the International Space Station as Observed by the Floating Potential Measurement Unit: Initial Results". *IEEE Transactions on Plasma Science* 36, p. 2280.

I.5 PROCEEDINGS OF SPACECRAFT CHARGING TECHNOLOGY CONFERENCES

Proceedings of the Spacecraft Charging Technology Conferences are valuable resources. The proceedings are presented in this section in chronological order.

1. Pike, C.P; Lovell, R.R., Eds. *Proceedings of the Spacecraft Charging Technology Conference, 24 February 1977.* NASA TMX-73537, AFGL-TR-77-0051. October 27-29, 1976. United States Air Force Academy, Colorado Springs, Colorado.

2. NASA Lewis Research Center. *Spacecraft Charging Technology – 1978.* NASA Conference Publication 2071, AFGL-TR-79-0082. October 31 - November 2, 1978. United States Air Force Academy, Colorado Springs, Colorado.

3. Stevens, N.J.; Pike, C.P., Eds. *Spacecraft Charging Technology – 1980.* NASA Conference Publication 2182, AFGL-TR-81-0270. November 12-14, 1980. United States Air Force Academy, Colorado Springs, Colorado.

4. Air Force Geophysics Laboratory, Hanscom AFB, Massachusetts. *Spacecraft Environmental Interactions Technology – 1983.* NASA Conference Publication 2359, AFGL-TR-85-0018. October 4-6, 1983. United States Air Force Academy, Colorado Springs, Colorado.

5. Olsen, R.C. Ed. *Proceedings of the Spacecraft Charging Technology Conference, 1989, Volume I.* PL-TR-93-2027(I). October 31 – November 3, 1989. Naval Postgraduate School, Monterey, California.

6. Cooke, D.L.; Lai, S.T., Compilers. *6th Spacecraft Charging Technology Conference*. October 26-29, 1998. Air Force Research Laboratory, Hanscom Air Force Base, Massachusetts. This

conference is documented on one or more CDs, one of which is contained in SEE Publication # SEE/TP-2005-600 (compiled by Jody Minor of NASA MSFC) as distributed after the 8th Charging Conference. This CD contains photo images of electronic files for the 1st through the 8th Spacecraft Charging Technology Conferences.

7. Harris, R.A., Ed. *Spacecraft Charging Technology (2001: A Spacecraft Charging Odyssey), Proceedings of the Seventh International Conference.* ESA SP-476. April 23-27, 2001. Noordwijk, The Netherlands.

8. Minor, J.L., Compiler. *8th Spacecraft Charging Technology Conference*. NASA/CP-2004-213091. October 20-24, 2003. NASA, Marshall Space Flight Center, Huntsville, Alabama.

9. Goka, T. Compiler. *9th Spacecraft Charging Technology Conference.* JAXA SP-05-001E. April 4-8, 2005. Epochal Tsukuba, Tsukuba, Japan.

10. *Proceedings of the 10th Spacecraft Charging Technology Conference (SCTC-10).* June 18-21, 2007. Biarritz, France. Sponsored by ONERA, ESA, NASA, CNES. Biarritz, France. Available on CD.

11. *Proceedings of the 11th Spacecraft Charging Technology Conference.* September 20-24, 2010. Albuquerque, NM. Special Issue on Spacecraft Charging Technology 2012; *IEEE Transactions on Plasma Science*, Vol. 40, No. 2, pp. 138, February 2012.

12. *Proceedings of the 12th Spacecraft Charging Technology Conference.* May 14-18, 2012. Kitakyushu, Japan. Special Issue on Spacecraft Charging Technology 2013; *IEEE Transactions on Plasma Science*, Vol. 41, No. 12, pp. 3302, December 2013. DOI: 10.1109/TPS.2013.2290251.

13. *Proceedings of the 13th Spacecraft Charging Technology Conference.* June 23-27, 2014. Pasadena, CA. Special Issue on Spacecraft Charging Technology; *IEEE Transactions on Plasma Science*, Vol. 43, No. 9, pp. 2775, September 2015. DOI: 10.1109/TPS.2017.2728878.

14. *Proceedings of the 14th Spacecraft Charging Technology Conference.* April 04-08, 2016. ESA-ESTEC, Noordwijk, The Netherlands. Special Issue on Spacecraft Charging Technology; *IEEE Transactions on Plasma Science*, Vol. 45, No. 8, pp. 1842, August 2017.

15. *Proceedings of the 15th Spacecraft Charging Technology Conference (SCTC2018).* June 25-29, 2018. Kobe, Japan. Special Issue on Spacecraft Charging Technology; *IEEE Transactions on Plasma Science*, Vol. 47, No. 8, pp, 3915-3922, August 2019. DOI: 10.1109/TPS.2019.2901681.

APPENDIX J

INDEX

ACE spacecraft (A.1.2.1).....111
ACRs Anomalous Cosmic Rays (B.2.1).....140
Acronyms, Abbreviations, Symbols, and Definitions (3.).....15
ADEOS-II satellite (1., 3.1, I.4).....11, 16, 193
AE8/AP8 see Environment codes
Antenna
  Apertures (5.2.5.4).....80
  Feeds (5.2.5.4).....80
  Grounding (5.2.5.3).....80
  Reflector surfaces (5.2.5.5).....80
Applicable documents (2.) (Move to Appendix I.).....15
Arrays
  Antenna array elements (5.2.5.5).....80
  Solar arrays (See Solar array ESD design guidelines, 5.2.4).....69
ATS-5, ATS-6 (A.1.2.2).....112
Attitude control packages (5.2.5.7).....81
Backscatter emission (5.1.4.1, F.1).....50, 168
Bleed paths (5.2.1.9).....62
Bleed resistors/resistances (5.2.1.4).....55
Bonding (See also Grounding) (5.2.1.3).....53
  Cable and wiring shields (5.2.1.3.2).....54
Breakdown
  Field of dielectrics (4.1.5).....32
  Fluence/Flux (4.1.7).....34
  Flux (5.2.3.2.2).....67
  Voltage on surfaces (4.4.1).....43
  Voltage/dielectric strength of dielectrics (general) (4.1.5) (see also Dielectrics).....32
Breakdown E-Field (4.4.1, 4.4.2).....43, 45
Cable shielding (5.2.1.2, 5.2.1.3.2).....52, 54
Capacitance/voltage threat to circuits (D.9, Figure 46).....162, 164
CEASE environmental anomaly sensor (7.2).....102
Charge lost in discharges (minor to severe) (4.4.1, Table 2).....45
Charging codes (B.3).....144
  Multi-Utility Spacecraft Charging Analysis Tool (MUSCAT) (B.3.1).....144
  Nascap-2k and NASCAP family of charging codes (B.3.2).....144
  Spacecraft Plasma Interaction System (SPIS) (B.3.3).....145
  NUMIT (B.3.4).....145
  3-D IESD code, including 3-D NUMIT (B.3.5).....145
  DICTAT (B.3.6).....146
Charging threat regions

Aurora (A.3.4)....128
Earth ESD hazard regions (1., Figures 1 and 2)....10, 12
Earth (radiation belts, A.3.1, Figure 32)....127
Earth (comparison with Jupiter/Saturn, A.4.2)....132
Jupiter (A.4.2)....132
Saturn (A.4.2)....132
Solar wind (A.4.1)....129
Circuit board open circuit area threat (G.1)....171
Computer analysis codes, see Environment codes (B.1), Transport codes (B.2),
Charging codes (B.3), or specific acronym....136, 140, 144
Conductor, definition (3.2)....24
Contamination of material surfaces effects (5.1.4.1)....50
Conversion, rad to electron fluences (C.4.1)....152
CREME96 (B.2.1) see Transport codes....140
Critical charge (fluxes and fluences at breakdown) (4.1.7) (5.2.3.2.2)....34, 67
CRRES see Satellite data sources, Environment codes
CTS Communications Technology Satellite (5.2.1.7)....61
Damage threshold of integrated circuits, illustrative (D.9, Figure 46)....162, 164
Data sources see Satellite data sources
Debye length (3.2)....24
Default values for ESD parameters (See Rules of thumb)
Definitions (3.2)....23
Density, Materials (8.1, 8.2, Tables 7 and 8)....103-107
Deployed packages, bonding (5.2.5.8)....81
Deposited flux versus incident flux (C.2, Note)....150
Design guidelines, spacecraft (5.)....47
Design guidelines (5.2)....51
General (5.2.1)....52
Internal charging (5.2.3)....66
Solar arrays (5.2.4)....69
Special situations (5.2.5)....78
Surface charging (5.2.2)....64
DICTAT see Charging codes
Dielectric
Breakdown E-field general (4.1.5)....32
Breakdown E-field (4.4.2)....45
Breakdown Voltage (4.1.5)....32
Constant (8.1, Table 7)....103, 105
Definition (3.2)....24
Density (8.1, Table 7)....103, 105
Resistivity (8.1, Table 7)....103, 105
Strength (8.1, Table 7)....103, 105
Strength (D.3 general description)....155
Time constant (8.1, Table 7)....105
Time constant (8.1, Figure 24)....106

Time constant (D.8, defined, Figure 43).....161
Voids (see Voids in dielectrics)
Diodes
In series with solar array strings (5.2.4.3 d).....71
Receiver protection (5.2.5.4).....80
Discharge currents
Estimated in-space (6.2, Table 5).....87, 88
From various test sources (6.3.1, Table 6).....88
Test example waveform (6.3.2.6.1, Figure 23).....97, 98
Dose to fluence conversion factor (C.4.1).....152
Electric field
Breakdown for dielectrics (8.1, Table 7).....103, 105
Electron beam tests (D.2).....153
Electron fluence from dose conversion (C.4.1).....152
Electron flux limits (5.2.3.2.2).....67
Electron trajectory disturbances (5.2.5.12, Figure 19).....82
Electron spectra curves GEO (4.2, Figure 9).....37
Electrostatic field effects on particle trajectories (5.2.5.12, Figure 19).....82
Environments
Amplitude statistics for GEO, 2-MeV electrons (A.2.2.3, Figure 31, A.2.2.6).....124
Geosynchronous mean and standard deviation (A.2.1, Tables 9 and 10)..... 116-119
Spectrum (4.2, Figure 9, A.2.2.5).....36, 37, 125
Time history of substorm (A.2.1, Figure 26).....119, 120
Variance with time averaging interval (A.2.2.3).....124
Variation with local time (A.2.2.4).....125
Variation with longitude/L-shell (A.2.2.2).....121
Variation with solar cycle (A.2.2.1, Figures 27 and 28).....121, 122
Environment codes (Appendix B).....136
AE8/AP8 (B.1.1).....136
AE9/AP9/SPM (IRENE) (B.1.2).....136
CRRES (B.1.3).....137
FLUMIC (B.1.4).....137
GIRE/SATRAD (B.1.5).....137
Handbook of Geophysics and the Space Environment (B.1.6).....138
L2-CPE (B.1.7).....138
MIL-STD-1809 (USAF) (B.1.8).....138
Geosynchronous Plasma Model (B.1.9).....139
IRI (B.1.10).....139
Others (B.1.11).....139
ESD conductive (see Static-conductive)
ESD event magnitudes (4.4.1, Table 2).....43, 45
ESD radiated spectrum (6.3.2.1).....92
ESD sensitivity, parts (D.9, Figure 45, V_{zap} test configuration).....162, 163
ESD sensitivity, parts example Figure (D.9, Figure 46).....163, 164
ESD test current waveforms (6.3.2.6.1, Figure 23).....97, 98

Faraday Cage construction (5.2.1.2) 52
FASTRAD see Transport codes
Filter
  Signal circuits (5.2.1.7, 5.2.1.14, 5.2.3.2.3, 5.2.4.3 s) 61, 63, 67, 75
  Solar array power (5.2.4.3 r) 75
Floating (unreferenced)
  Circuits should be ground referenced (5.2.1.4) 55
  Forgotten conductors (5.2.1.9) 62
  Radiation spot shields should be grounded (5.2.1.6) 61
  Solar arrays (5.2.4.3 e) 72
Fluence units (4.2.1) 37
FLUMIC see Environment codes
Flux units (4.2.1) 37
GCRs Galactic Cosmic Rays (B.2.1) 140
Geant4 see Transport codes
GIRE (A.4.2, B.1.5) 134, 137
GIRE/SATRAD see also Environment codes
GOES see Satellite data sources
Grounding/bonding (See also Bonding, 5.2.1.3) 53
  Antenna parts (5.2.5.3-5.2.5.6) 80-81
  Conductive elements, referencing (5.2.3.2.1) 66
  Electrical/electronic grounds (5.2.1.3.3) 55
  Radiation spot (local) shields have to be grounded (5.2.1.6) 61
Guidelines for Writing Requirements
  Antenna elements (5.2.5.3) 80
  Antenna aperture covers (5.2.5.4) 80
  Antenna reflector surfaces (5.2.5.5) 80
  Antenna array floating (ungrounded) elements (5.2.5.5) 80
  Basic (5.) 47
  Bonding across flexible joints (5.2.1.3, 5.2.1.13) 53, 63
  Bonding of conductive structural elements (5.2.1.3) 53
  Bonding of conductive surface areas (5.2.1.3.1) 54
  Cable shield grounding (5.2.1.3.2) 54
  Deployed packages (5.2.5.8) 81
  Diode isolation of each solar array string (5.2.4.3 d) 71
  Faraday Cage shielding (5.2.1.2) 52
  Floating wires, traces, and unused connector pins (5.2.3.2.1) 66
  In charging threat region (5. b) 48
  Procedures for handling, assembly, inspection, and test (5.2.1.16) 64
  Quantitative resistance/resistivity for surface materials (5.2.2.2) 64
  Radiation spot (local) shield and floating metal grounding (5.2.1.6) 61
  Receiver and transmitter ESD immunity (5.2.5.6) 81
  Surface potentials, deliberate, (5.2.5.11) 82
  Thermal blanket metalized surfaces (5.2.5.1) 78
  Thermal blanket redundant bonding tabs (5.2.5.1) 78

Handbook of Geophysics and the Space Environment see Environment codes
Human body model, MIL-STD-883-3, ESD test (D.9) 162
IESD, Internal Electrostatic Discharge, defined (1., 4.1.2, Figure 6) 13, 30
IGE-2006 geosynchronous plasma environment model (A.2.1) 116
Incident flux versus deposited flux (C.2, Note) 150
Insulator, definition see Dielectric definition
Integrated circuit ESD damage threshold (D.9, Figure 46) 164
Internal charging and surface charging differences (1.) 10
Internal charging
  Definition (1., 4.1.2, Figure 6) 13, 30
  Hazard versus electron flux (4.1.7, Figure 8) 36
  Illustration (4.1.2, Figure 6) 30
Isolate solar array from spacecraft structure (5.2.4.3 t) 75
ITS TIGER see Transport codes
Jupiter Radiation Environment Model see Environment codes, GIRE
L2-CPE see Environment codes
LANL Los Alamos National Lab detectors see Satellite data sources
Lens ESD threat (5.1.1.3) 49
Longitude variation of environment (A.2.2.2, Figure 29) 123
Louvers, thermal control bonding (5.2.5.2) 79
Magnitudes of surface ESDs (minor, moderate, and severe) (4.4.1, Table 2) 43, 45
Margins (6.1) 85
Materials
  Acceptable surface coatings (5.2.1.5.1, Table 3) 56, 58
  Characteristics, conductors (8.2, Table 8) 106
  Characteristics, dielectrics (8.1, Table 7) 103, 105
  Paints and conformal coatings (5.2.1.10) 62
  Surface selection advice (5.2.1.5.1) 56
  Undesirable surface coatings (5.2.1.5.1, Table 4) 56, 59
MCNP/MCNP6 see Transport codes
MEO environment (A.1.2.6, A.3.1) 113, 126
Micrometeoroid ESD trigger (4.4.1 b) 44
MIL-STD-1541A ESD sparker (6.3.1.1) 89
  Parameters (6.3.1, Table 6) 89
  Schematic (6.3.1.1, Figure 20) 90
  Testing (D.10) 165
  Waveform (6.3.2.6.1 Figure 23) 98
MIL-STD-883-3 (V_{zap} or Human Body Model ESD test) (D.9) 162
MIL-STD-1809 (USAF) (B.1.8) 138
MUSCAT see Charging codes
NASA-TP-2361 (4.4, 5.2.4.3 t) 43, 75
NASCAP, NASCAP/GEO, NASCAP/LEO see Charging codes
Nascap-2k see Charging codes
Nonconductive surfaces (5.2.1.5.2) 60
NOVICE see Transport codes

NUMIT see Charging codes
Ohm per square, definition (3.2, D.4) 25, 157
Optics ESD threat see lens ESD threat
Orbit avoidance to avoid ESD problems (5.2.1.1) 52
OSR (5.2.1.5.1 a; the second “a”) 57
Packages, deployed, bonding (5.2.5.8) 81
Parts, ESD sensitivity (5.2.1.15) 63
Particle trajectory distortion by E-field (5.2.5.12, Figure 19) 83
Paschen discharge (5.2.4.3 f, g) 73
Penetration depth, electrons and protons chart (4.1.2, Figure 5) 29
PEO environment (A.3.2) 127
Photoelectron emission (5.1.4.1) 50
Plasma illustration (4.1.1, Figure 3) 26, 28
POLAR see Charging codes, Nascap-2k
Probability of occurrence, GOES-7E >2 MeV electrons (A.2.2.3, Figure 31) 124
Radiation spot (local) shields (have to be grounded) (5.2.1.6) 61
Radiation-induced conductivity (RIC) (4.1.4) 32
Radome (5.2.5.4) 80
Rad dose to electron fluence conversion (C.4.1) 152
Range of electron and proton penetration in aluminum (4.1.2, Figure 5) 29
Receivers (5.2.5.6) 81
References (Appendix I) 176
Resistance/resistivity
  Guidelines for surface ESD (5.2.2) 64
  Definition, see Surface resistivity and Volume resistivity
Resistive dielectrics (5.2.1.5) 55
Resistivity of materials (8.1, 8.2, Table 7, Table 8) 103, 105, 106
Resistivity change/variation causes (5.1.4.1) 50
Rotating joint grounding (5.2.1.3, 5.2.1.13) 53, 63
Rules of thumb
  Aluminum shielding thickness for ESD protection at GEO: 130 mil (4.1.7, 5.2.3.2.2) 34, 67
  Breakdown level of e/cm^2 in dielectric: 2.2 x 10^{11} (4.4.2) 45
  Breakdown fields between dielectric and conductor: 2 x 10^7 V/m (4.4.1 b) 43
  Breakdown voltage on dielectric surfaces to conductor: 400 V (4.4.1 a) 43
  Bulk resistivity acceptable over conductor: 10^{11} ohm cm (Knowledge Check 5.12) 84
  Capacitance to space of a spacecraft: 200 pF (4.4.3) 45
  Dielectric: >10^{10} ohms/square (surface) or >10^9 ohm cm (bulk) (3.2) 24
  Dielectric strength of good dielectrics: 2x10^7 V/m (4.1.5, 4.4.2) 33, 45
  E-field from layer of 2.2 x 10^{11} e/cm^2 when dielectric constant is 2: ~2x 10^7 V/m (4.4.2) 45
  ESD discharge magnitudes: ~0.5 µC - 10 µC (Table 2, 4.4.1) 45
  Maximum e/cm^2 in 10 hr period: 2 x 10^{10} (5.2.3.2.2) 67
  Maximum incident electron flux before breakdown: 0.1 pA/cm^2 (5.2.3.2.2) 67
  Maximum stopped electron flux before breakdown: 0.1 pA/cm^2 (C.2, Note) 150
  “Safe” E-field: <10^6 V/m (4.1.5) 33
  Static-conductive: <10^{10} ohms/square (surface) or <10^9 ohm cm (bulk) (3.2) 25

Surface resistivity acceptable if grounded: 10^9 ohm/square (Knowledge Check 5.13).....84
Velocity of propagation of solar array surface discharge: 0.7 - 1.1 x 10^4 m/s (Amorim) 182
SAMPEX see Satellite data sources
Satellite data sources (A.1.2) 111
ACE Spacecraft (A.1.2.1) 111
ATS-5, ATS-6 (A.1.2.2) 112
CRRES (A.1.2.3) 112
DMSP (A.1.2.4) 112
GOES (A.1.2.5) 113
Los Alamos detectors (A.1.2.6) 113
POES (A.1.2.7) 114
SAMPEX (A.1.2.8) 114
SCATHA (A.1.2.9) 114
Van Allen Probes (A.1.2.10) 115
Other data sources (A.1.2.11) 115
SATRAD (A.4.2) 134
SATRAD (GIRE/SATRAD) see also environment codes
SCATHA spacecraft (4.2.2, A.1.2.9, A.2.1, Table 9) 38, 114, 116, 118
SCOPE (1.) 10
Secondary electron emission (5.1.4.1) 50
Secondary emission ratios (5.2.1.5.3) 60
SEE Single Event Effects (B.2.1) 140
SEMCAP (4.5.2, E.1) 46, 167
SEPs Solar Energetic Particles (B.2.1) 140
Shielding, wire bundles, bonding (5.2.1.3.2) 54
SHIELDOSE see Transport codes
Slip ring, grounding through (5.2.1.3, 5.2.1.13) 54, 63
Snap-over (5.2.4.1 e) 70
SOHO spacecraft (A.4.1) 129
Solar array ESD arcing damage photos (5.2.4.2, Figure 11) 71
Solar array ESD design guidelines (5.2.4) 69
Solar array isolation from spacecraft structure (5.2.4.3 t) 75
Solar cycle, variation with (A.2.2.1) 121
Solar wind environment (A.4.1) 129
Spacecraft grounding and bonding system architecture (5.2.1.16) 64
Spacecraft test techniques (6.) 85
SPENVIS see Transport codes
SPICE (4.5.1) 46
SPIS see Charging codes
Spot shields, radiation, grounding essential (5.2.1.6) 61
Static-conductive (3.2) 25
Structural and other conducting items (4.1.4) 32
Sunspots (A.2.2.1) 121
Surface
Materials selection advice (5.2.1.5.1) 56

Nonconductive (5.2.1.5.2) 60
Resistivity (D.4) 157
Surface charging and internal charging differences/distinction (1.) 10
Surface charging
Definition (1., 4.1.2) 10, 29
Illustration (4.1.1, Figure 4) 27, 28
Surface ESD magnitudes (minor, moderate, and severe) (4.4.1, Table 2) 43, 45
Surface potentials, deliberate (5.2.5.11) 82
Surface resistivity
Definition, rules (D.4) 157
Usage (D.4) 157
Techniques (for bonding) (5.2.1.5.1, second list) 57
Temperature effects on resistivity (5.1.4.1, 5.2.1.5) 50, 55
Thermal blankets (design rules, 5.2.5.1) 78
Thermal blanket metalized surface has to be grounded (5.2.5.1) 78
Thermal control louver bonding (design rules, 5.2.5.2) 79
Thermistor example of ESD sensitive circuit (5.2.4.3 q) 75
TID Total Ionizing Dose (4.1.4) 32
TIGER see Transport codes, ITS
Time constant see Dielectric time constant
TP-2361 see NASA-TP-2361
Transmitters (5.2.5.6) 81
Transport codes (B.2) 139
CREME96 (B.2.1) 140
EGS4 (B.2.2) 140
Geant4 (B.2.3) 140
ITS (TIGER) (B.2.4) 141
MCNP/MCNP6 (B.2.5) 141
NOVICE (B.2.6) 142
FASTRAD (B.2.7) 142
SHIELDOSE (B.2.8) 142
SPENVIS (B.2.9) 142
TRIM (B.2.10) 143
Summary of transport code capabilities (B.2.11, Table 15) 143
TRACE spacecraft (A.4.1) 129
TRIM see Transport codes
Triple junction point (3.2) 26
Ulysses spacecraft (A.4.1) 129
Ungrounded materials size limit (5.2.3.2.1) 66
Ungrounded wires, maximum permissible length (5.2.3.2.1) 66
Velocity, electrons and protons in plasma (4.1.1) 27
Voids in dielectrics (5.2.4.3 f) (grouting air pockets) 73
Volume resistivity
Definition (D.4) 156
Usage (D.4) 156

V_{zap} test (D.9).....162
WIND spacecraft (A.4.1).....129
Wires, permissible ungrounded length (5.2.3.2.1).....66
Wiring and cable shields
  Bonding (5.2.1.3.2).....54
  External wiring/cabling (5.2.1.12).....63
  Separation/segregation (5.2.1.14).....63
Worst-case GEO charging environment (4.2, Figure 9).....36, 37
Worst-case GEO plasma charging environment (A.2.1, Tables 9 and 10).....116, 118, 119
Yohkoh spacecraft (A.4.1).....129